BALANCING OF FLEXIBLE ROTORS

AT LOW SPEED

BY

OKE, WASIU ADEYEMI

A Thesis Presented to the
DEANSHIP OF GRADUATE STUDIES

KING FAHD UNIVERSITY OF PETROLEUM & MINERALS

DHAHRAN, SAUDI ARABIA

In Partial Fulfillment of the
Requirements for the Degree of

MASTER OF SCIENCE

In

MECHANICAL ENGINEERING

DECEMBER 2011

KING FAHD UNIVERSITY OF PETROLEUM & MINERALS

DHAHRAN 31261, SAUDI ARABIA

DEANSHIP OF GRADUATE STUDIES

This thesis, written by Oke, Wasiu Adeyemi under the direction of his thesis advisor and approved by his thesis committee, has been presented to and accepted by the Dean of Graduate Studies, in partial fulfillment of the requirements for the degree of **MASTER OF SCIENCE IN MECHANICAL ENGINEERING**.

Thesis Committee

Dr. Yehia A. Khulief (Advisor)

Dr. Yagoub N. Al-Nassar (Member)

Dr. Mehmet Sunar (Member)

Dr. Amro M. Al- Qutub
Department Chairman

Dr. Salam A. Zummo
Dean of Graduate Studies

14/1/12

Date

DEDICATION

This Thesis work is dedicated to my parents, Mr. and Mrs. Koleoso Oke, my sisters and brothers and to my lovely wife.

ACKNOWLEDGEMENT

First and foremost, my gratitude goes to KFUPM administration for giving me the opportunity to finish my MS program at KFUPM. I am extremely grateful to my Advisor and Supervisor, prof. Yehia A. Khulief for his unquantifiable support, guidance and encouragement throughout my stay at KFUPM and the period of my research work. Indeed, I would like to express my gratitude to Dr. Yagoub N. Al-Nassar and Dr. Mehmet Sunar for their support and encouragement.

Furthermore, I should like to thank my colleagues and friends at KFUPM for their support. In the same way, I like to express my appreciation to my Mentor, Mr. Ogundiran Tayo for his continued support and encouragement. I am particularly thankful to my sister Mrs. Risikat Ibraheem, for her sincere caring and support throughout my journey so far. The author would as well like to thank his brothers and sisters for their undiluted support, patience and understanding. I also want to thank my parents for their motivation, in spite of being far away from them. Above all, I would like to express my heartfelt appreciation to my wife, Zainab, for her moral support, patience, and encouragement.

Ultimately, my gratitude goes to God Almighty, for giving me life, wisdom, knowledge and guiding me to success.

TABLE OF CONTENTS

Page

TITLE PAGE……..... i

APPROVAL PAGE..... ii

DEDICATION..... iii

ACKNOWLEDGEMENT…..... iv

TABLE OF CONTENTS……..... v

LIST OF TABLES..... viii

LIST OF FIGURES..... x

ABSTRACT (ENGLISH)……..... xiv

ABSTRACT (ARABIC) ……..……..……..... xv

CHAPTER 1 ……...…… 01

1.0 INTRODUCTION..... 01

1.1 General Background..... 01

1.2 Literature Review..... 03

1.3 The Current Status…….... 16

1.4 Objectives of the Present Study..... 17

CHAPTER 2 ……...…… 18

2.0 THEORY OF BALANCING FLEXIBLE ROTORS..... 18

2.1 Fundamental Methods for Balancing Flexible Rotors..... 20

2.2 Balance Quality and Balancing Trial Weight..... 42

CHAPTER 3 ……..…… 50

3.0 ROTOR FINITE ELEMENT MODEL FORMULATION..... 50

3.1 Elastodynamic Modeling of the Rotor..……..... 52

3.2 Generalized Coordinates..... 53

3.3 Kinetic Energy Expression……..... 56

3.4 Strain Energy Expression…….… 62

3.5 Equation of Motion of the Shaft Element…….. 67

3.6 The Finite Element Formulation……..… 68

3.7 Mass Unbalance ……. 79

3.8 Eigenvalue Formulation…….. 80

3.9 Mode Shape and Natural Frequency..... 82

CHAPTER 4 ……..…… 86

4.0 ROTORDYNAMIC ANALYSES USING ANSYS..... 86

4.1 Rotor Reference Frame and Bearing in ANSYS..... 87

4.2 Rotating Structures Modeling in ANSYS..... 92

4.3 ANSYS Modal Analysis..... 94

4.4 ANSYS Harmonic Response Analysis..... 96

4.5 Bode, Orbit and Nyquist Plots..... 99

CHAPTER 5 ……..…… 101

5.0 METHODOLOGY OF LOW-SPEED BALANCING OF FLEXIBLE ROTORS……..... 101

5.1 Theory of Low-Speed Balancing for Flexible Rotor..... 101

5.2 Low -Speed Balancing Procedure..... 114

5.3 Rotor-Bearing System Modeling..... 116

5.4 Computational Strategy..... 120

CHAPTER 6 ……..…… 122

6.0 RESULTS AND DISCUSSIONS……..... 122

6.1 Three-Disk Rotor with Rigid Bearings (1)..... 123

6.2 Three-Disk Rotor with Rigid Bearings (2)..... 147

6.3 Low-Speed vs. Two-Plane Balancing Methods……..... 150

6.4 Multi Stage Turbine with Rigid Bearings..... 160

6.5 Multi Stage Turbine with Elastic Bearings..... 180

6.6 Performance of Balanced Rotor at High Speeds Analysis……..... 205

CHAPTER 7 ……..…… 212

7.0 CONCLUSIONS AND RECOMMENDATIONS..... 212

APPENDIX..... 214

REFERENCES..... 215

VITA..... 220

LIST OF TABLES

Table		Page
2.1	Transducers Measurements at Several Speeds when Trial Weight is attached to the First Balancing Plane.....	37
2.2	Transducers Measurements at Several Speeds when Trial Weight is attached to the Second Balancing Plane.....	37
2.3	Balance Quality Grades for Various Groups of Representative Rigid Rotors (From ISO 1940/1).....	43
4.1	The Forces in Y and Z Directions.....	98
6.1.1	Natural Frequencies of the Three-Disk Rotor…….	126
6.1.2	Natural Frequencies from Different Researchers……..….....	126
6.1.3	Initial Responses at Balancing Speed……....	130
6.1.4	Trial Parameters, Amplitudes and Phases at each Measurement Point.	130
6.1.5	Correction Parameters and Final Amplitudes and Phases at each Measurement Point.....	130
6.1.6	Percentage Unbalance Reduction at Measurement Points……..	146
6.2.1	Initial Responses at Balancing Speed (2,000 rpm)…….....	148
6.2.2	Trial Parameters, Amplitudes and Phases at each Measurement Point.	148
6.2.3	Correction Parameters and Final Amplitudes and Phases at each Measurement Point.....	149
6.2.4	Percentage Unbalance Increment/Reduction at Measurement Points...	149
6.3.1	Initial Responses at Balancing Speed (2,000 rpm)……...	153
6.3.2	Trial Parameters, Amplitudes and Phases at each Measurement Point.	153
6.3.3	Correction Parameters and Final Amplitudes and Phases at each Measurement Point.....	153
6.3.4	Percentage Unbalance Reduction at Measurement Points……..	159
6.4.1	Natural Frequencies of Multi Stage Turbine...……..……..……	162
6.4.2	Initial Responses at Balancing Speed (2,000 rpm)……...	166
6.4.3	Trial Parameters, Amplitudes and Phases at each Measurement Point.	166

6.4.4 Correction Parameters and Final Amplitudes and Phases at each Measurement Point..... 166
6.4.5 Percentage Unbalance Reduction at Measurement Points…… 176
6.5.1 Natural Frequencies of Multi stage Turbine……. 182
6.5.2 Initial Responses at Balancing Speed (2,000 rpm)....…….... 186
6.5.3 Trial Parameters, Amplitudes and Phases at each Measurement Point. 186
6.5.4 Correction Parameters and Final Amplitudes and Phases at each Measurement Point..... 186
6.5.5 Percentage Unbalance Reduction at Measurement Points (Y-Direction) 201
6.5.6 Percentage Unbalance Reduction at Measurement Points (Z-Direction)..... 201
6.6.1 Percentage Increment in Residual Unbalance of Rotor…… 208

LIST OF FIGURES

Figure		Page
2.1	A Shaft-Elastic Rotor.....	19
2.2	Natural Modes of a Roll-Shaped Rotor (Bending Shape of a Roll at (a) 1st Critical Speed (b) 2nd Critical Speed (c) 3rd Critical Speed).....	19
2.3	Correction Mass Distribution.....	24
2.4	The First Three Bending Mode Shapes of Rotor …….....	24
2.5	Distribution of Weights in order to Correct First Mode Bending without Affecting earlier Balance Results.....	27
2.6	Distribution of Weights in order to Correct Second Mode Bending without Affecting earlier Balance Results.....	27
2.7	Distribution of Weights in order to Correct Third Mode Bending without Affecting earlier Balance Results.....	27
2.8	Flexible Shaft.....	29
2.9	Maximum Permissible Residual Unbalance, e_{per} (From ISO 1940/1)	45
3.1	Possible Types of Rotor.....	51
3.2	Complex Shapes Rotors.....	51
3.3	Flexible Rotor Component.....	54
3.4	Cross-Section of Rotational Angles.....	54
3.5	Generalized Coordinate of the Element.....	57
3.6	The Tapered Shaft Element……..…….....	69
3.7	Mass Unbalance.....	69
3.8	Campbell Diagram.....	84
3.9	Non-Circular (Elliptical) Modes with Asymmetric Bearing Stiffness……..……	84
4.1	Reference Frame (Rotating and Stationary).....	89
4.2	Relationship between Real/Imaginary Components and Amplitude/Phase Angle.....	98
4.3	Unbalance Forces……...……..…	98

5.1 Flexible Rotor……..…… 102
5.2 First and Second Normal Mode Shapes and ODS Versus Nodes Numbers for Three-Disk Rotor..... 117
5.3 Two Different Ways of Modeling Rotor..... 117
6.1.1 Three-Disk Rotor..... 123
6.1.2 Three-Disk Rotor Modeling..... 124
6.1.3 Unbalance Three-Disk Rotor..... 128
6.1.4 First and Second Normal Mode Shapes and ODS Versus Nodes Number..... 128
6.1.5 Three-Disk Rotor Mode Shapes Before and After Balancing.....…… 132
6.1.6 Unbalanced and Balanced Three-Disk Rotor Mode Shapes...……..... 135
6.1.7 Plot of Responses due to the Correction Parameters and Initial Responses at Balancing Speed at Three Measurement Points…..... 138
6.1.8 Amplitude Phase Plots (Y- Direction) at Speed above Operation Speed…… 139
6.1.9 Amplitude Phase Plots (Z- Direction) at Speed above Operation Speed…… 142
6.3.1 First and Second Normal Mode Shapes and ODS Versus Nodes Number..... 151
6.3.2 Amplitude Plots due to the Correction Parameters and Initial Responses at Balancing Speed for Two-Plane Balancing Method..... 155
6.3.3 Amplitude Plots due to the Correction Parameters and Initial Responses at Balancing Speed for Low-speed Balancing Method..... 156
6.3.4 Amplitude Plots due to the Correction Parameters and Initial Responses at Operation Speed for Two-Plane Balancing Method..... 157
6.3.5 Amplitude Plots due to the Correction Parameters and Initial Responses at Operation Speed for Low-Speed Balancing Method..... 158
6.4.1 Multi Stage Turbine..... 160
6.4.2 Multi Stage Turbine Modeling..... 161
6.4.3 Unbalance Multi Stage Turbine..... 163

6.4.4 First, Second and ODS Normal Mode Shapes Versus Nodes Numbers……..... 163
6.4.5 Multi Stage Turbine Mode Shapes Before and After Balancing……. 168
6.4.6 Amplitude Plots due to the Correction Parameters and Initial Responses at Balancing Speed..... 171
6.4.7 Amplitude-Phase Plot (Y-Direction) at Operation Speed..... 172
6.4.8 Amplitude Plots (Z-Direction) at Operation Speed at Three Measurement Points..... 175
6.4.9 Comparison between Orbit Plots from Normal, Unbalanced and Balanced Turbines at First Critical Speed..... 178
6.4.10 Comparison between Orbit Plots from Normal, Unbalanced and Balanced Turbine at Second Critical Speed..... 179
6.5.1 Multi Stage Turbine..... 180
6.5.2 Multi Stage Turbine Modeling..... 181
6.5.3 Unbalanced Multi Stage Turbine..... 183
6.5.4 First and Second Normal Mode Shapes and ODS of Turbine Versus Nodes Number..... 183
6.5.5 Multi Stage Turbine Mode Shapes Before and After Balancing..... 188
6.5.6 Multi Stage Turbine Unbalanced and Balanced Mode Shapes..... 190
6.5.7 Amplitude Plots due to the Correction Parameters and Initial Responses at Balancing Speed at Three Measurement Points..... 193
6.5.8 Amplitude-Phase Plots (Y-Direction) at Speed Above Operation Speed……..... 194
6.5.9 Amplitude-Phase Plots (Z-Direction) at Speed Above Operation Speed..... 197
6.5.10 Comparison Between Orbit Plots from Normal, Unbalance and Balanced Turbine at First Critical Speed..... 203
6.5.11 Comparison Between Orbit Plots from Normal, Unbalance and Balanced Turbine at Second Critical Speed..... 204
6.6.1 Amplitude Plots (Y- and Z-Directions) at a Speed of 21,000 rpm….. 206
6.6.2 Amplitude plots (Y- and Z-Directions) at a Speed of 13,690 rpm….. 207

6.6.3 Amplitude Plots (Y-Direction) at a Speed of 10,020 rpm…….…….. 210
6.6.4 Amplitude Plots (Z-Direction) at a Speed of 10,020 rpm…….…….. 211

THESIS ABSTRACT (ENGLISH)

NAME: OKE, WASIU ADEYEMI

TITLE: BALANCING OF FLEXIBLE ROTORS AT LOW SPEED

MAJOR: MECHANICAL ENGINEERING

DATE: **DECEMBER, 2011**

Mass imbalance is one of the most common problems encountered in rotating equipment. All rotating machinery have some degree of mass unbalance caused by a variety of reasons, some of which are related to design and manufacturing processes and others are developed during installation and operation. Eventually, balancing of rotors has become a necessary corrective technique that takes place several times during the machines' service life in order to bring the associated vibrations to some acceptable limit. It is well-known that prolonged exposure to the vibration results in damage and increased downtime of the machine.

The demand for high-speed light-weight machines has resulted in rotors which deform elastically during their operation. A rotor is normally regarded as flexible, when it operates close to or above its natural frequency. In this case, the problem of unbalance becomes more complicated due to interaction with the elastic deformations of the rotor, and thus calling for a special balancing procedure. The available methods of balancing flexible rotor are being done in high-speed balancing facilities and such facilities are operated by specialists, and are found only in some industrialized countries.

The objective of the present work is to devise a method for balancing flexible rotors at low speeds, thus avoiding the need to transport the rotor to a high-speed balancing faculty. The proposed method utilized the measured eigenvectors, eigenvalues and responses from the unbalanced rotor through modal and harmonic responses analyses at low speed to determine the correction parameters. The rotor modeling and analyses were carried out using ANSYS and MATLAB, and the method was tested numerically to validate its applicability.

MASTER OF SCIENCE DEGREE

KING FAHD UNIVERSITY OF PETROLEUM & MINERALS

Dhahran, Saudi Arabia

THESIS ABSTRACT (ARABIC)

الاسم: **أوك واسيو أديمي**

العنوان: **موازنه الدوارات المرنه في السرعات المنخفضه**

التخصص: **الهندسة الميكانيكية**

التاريخ: **صفر\1433**

يعتبر اختلال التوازن الكتلي أحد أكثر المشاكل شيوعا في الآلات الدوارة، حيث لا تخلو أيٌ من الآلات الدوارة على درجة ما من اختلال التوازن الكتلي و ذلك لأسباب متنوعة منها ما يتعلق بعمليتي التصميم و التصنيع ، وأسباب أخرى تنتج خلال عمليات التركيب و التشغيل. و لهذا فإعادة التوازن لهذه الآلات أصبح ضرورة من خلال تقنية التصحيح التي تتكرر على مدى العمر التشغيلي للآلة و ذلك من أجل خفض الاهتزازات الناتجة إلى الحد المقبول وفقا للمقننات الصناعية. ومن المسلم به أن تعرض الآلة للاهتزاز مدة طويلة يؤدي إلى عطبها و زيادة فترات توقفها عن العمل.

ولقد أدت متطلبات الوزن الخفيف و السرعات العالية إلى استحداث أعمدة دوارة أكثر عرضة للانحناء المرن أثناء التشغيل ، وبناء عليه فقد تم تصنيف الأعمدة الدوارة إلى نوعين: صلب (Rigid) و مرن (Flexible). فيعتبر الدوَار من النوع الصلب عند إمكانية تصحيح توازنه عند أي مستويين و بعد ذلك يستمر متوازناً عند أية سرعة حتى سرعة التشغيل القصوى. أما الدوار الذي لا ينطبق عليه التعريف السابق بسبب الانحناء المرن فيصنف بأنه مرن. أما من وجهة النظر الديناميكية، فتعرف الأجزاء الدوارة المرنة بأنها التي تدور على سرعات تفوق سرعاتها الحرجة ، وتعتبر عملية موازنة الدوار المرن أكثر تعقيداً ، حيث يقوم الدوار المرن و بشكل متواصل بتغيير شكله المرن كلما وصل لإحدى سرعاته الحرجة ، مما يستلزم إعادة موازنته في مستويين جديدين. وتعتمد الطرق الحالية لموازنة الأجزاء الدوارة عالية السرعة على دوران العمود عند سرعة التشغيل في معامل اتزان خاصة ، والتي توجد فقط في بعض البلدان الصناعية الكبرى.

ويهدف هذا البحث إلى إيجاد طريقة لموازنة الأعمدة المرنة عالية السرعة ، عند سرعات اتزان منخفضة، وذلك لتفادي تكلفة و تعقيد عملية الموازنة على السرعات العالية. وتعتمد الطريقة المستحدثة للاتزان على التحليل الموجي لخصائص العمود الدوَار(Analysis Modal) ، بالإضافة إلى المحاكاة الرقمية باستعمال الحاسب الآلي ، واستخدام برامج ANSYS وMATLAB. ولقد تم اختبار الطريقة المستحدثة بالمحاكاة الرقمية، وذلك للتثبت من جدواها وكفاءة تطبيقها.

درجة الماجستير في العلوم

جامعة الملك فهد للبترول و المعادن

الظهران المملكة العربية السعودية

CHAPTER 1

INTRODUCTION

1.1 General Background

Unbalance is the uneven distribution of weights of rotor about its rotating centerline. Rotating machinery accounts for the immense majority of the contemporary Machines. While the dynamic behavior of such machinery has always been important, the need for higher efficiency has resulted in the design of machines which are increasingly liable to vibration as the speed increases. In particular, the combined effect of lighter weight and higher speeds would result in the increased flexibility of rotors, thus complicating the problem of unbalance; which is one of the most important disturbing forces in rotating Machinery.

Rotor is the rotating part of mechanical and electrical machines. A rotor is normally regarded as flexible, when it operates close to or above its natural frequency. A level of unbalance that is tolerable at a low speed is intolerable at a higher speed. This is due to the fact that the centrifugal force being produced by the unbalance condition will be coupled with elastic deformation of the rotor. Any unbalance in a rotating system can have devastating effects on the system during the start-up, slow down or when operating at or near the critical frequency.

According to Wowk [36], there was only static balancing prior to 1850. During that time, the available rotating machines were steam engines, wagon wheel, rail wheels and slow-speed pumps. The centrifugal force in such early machines was negligible because speeds were slow (less than 600rpm). In the second half of the 19th century, there were electric motors running at speeds above 900rpm. At such higher speeds the centrifugal forces becomes significant and as speed increases the vibration level increases. Static balancing is the first type of mass balancing and the rotor to be balanced would be allowed to rotate on smooth and hard parallels roll with its shaft. The heavy spot would rotate to bottom then some material would be removed from the bottom by drilling or adding weight to the top. Patent No. 110259 is an early balancing machine. This patient was filed by a Canadian, Henry Martinson in 1870. Two concepts were introduced by this machine: spinning the rotor for balancing (dynamic balancing) and apply weight on a long rotor at both ends (two-plane balancing). The rotor was mounted on bearings that were supported with springs and the motion generated by unbalance was amplified and made very noticeable. In 1929 the vector methods were presented by T.C. Rathbone first and later presented in 1934 by E.L. Thearle. Cross-effect was considered by both methods and analytical methods were presented to compensate for it. The vector method of Thearle is being referred to as influence coefficient method of simultaneously balance in two planes nowadays. This served as the basis for multi-plane balancing of flexible rotor that utilizes the influence coefficient balancing. The bulk of balancing problems were solved with single plane balancing and approximately 70% of all balancing being done these days used this method. Those difficult balance problems that could not be solved by single plane methods are being solved through two-plane

balancing while multi-plane balancing is being utilized for flexible rotors or rotors that have exceptional requirements.

Nevertheless, in 1950s, when there was good instrumentation to measure phase and the field balancing of flexible rotors in place became really victorious.

It was reported by Yamamoto and Ishida [38] that the development of a balancing technique for flexible rotors became essential as a result of the arrival of high-speed rotating machines and the two representative theories were recommended: modal balancing that was recommended in 1950s and the influence coefficient method proposed in early 1960s and developed along with the evolution of computers. The influence coefficient method of balancing was described in 1982 by Rieger and by Rao in 1983 as the application of trial masses to the machine in order to determine the system influence coefficient experimentally [9]. Modal balancing method can be traced back to a 1929 paper by T.C. Rathbone [36]. The two main methods of high speed balancing of flexible rotors are the modal balancing and influence coefficient balancing recommended in 1960s and 1970s, while other methods of high speed balancing are based on these two methods [6, 33].

1.2 Literature Review

The primary cause of the significant disturbing force in rotating Machinery is unbalance. Noise, wear and high level vibrations would occur when a machine is not balanced correctly. Imbalance forces will occur when the rotor mass centre is being eccentric to the shaft centre of rotation and creates centrifugal forces which operate on the rotor mass [9]. In addition, unbalance is the uneven allocation of the weight of a rotor

about its rotating centerline. The primary indicator of unbalance is high vibration amplitude at the rotational speed. Generally, the causes of unbalance can be divided into two types [36]:

1.) Operational changes:

    Corrosion and erosion, deposit build-up, maintenance action that affect the mass distribution (e.g drilling, grinding, cleaning, changing bearings, etc), distortion due to thermally induced or gravitation, wear at the bearing or journal that changes the geometric axis of rotation.

2.) Less than perfect manufacturing:

    Keys and keyways, cracks, porosity (particularly in casting), eccentricity, distortion due to the relaxation of residual stresses (shaft bow), hollow places contain loose parts moving around (that is dirty, water, welding slag)

Besides, the causes of unbalance were further divided into four groups as follow [4]:

- Material faults: Non-homogeneous material density, blow-holes in cast components, irregular material thickness
- Manufacturing and assembly errors: Shrinking after soldering or welding, distortion from welding and casting errors, permanent deformation caused by relieved stress, stress errors caused by work procedures, stress as a result of uneven tightening of bolts or screws.
- Construction and drawing errors: Un-machined surfaces on the rotor, components not symmetric, variations in roundness and construction because of coarse tolerances.

- Faults during operation: Blade fracturing on turbine rotors, wear on grinding wheels, erosion and corrosion of the rotor, material build-up on impellers, displacement of rotor parts caused by centrifugal force, thermal deformation of hot-gas exhaust fans, general wear.

Rotor can be classified and balanced as either rigid or flexible rotor [9, 27, 36]. A rigid rotor is the one in which during the operation it does not bend by an amount enough to produce a considerable change in the centre of mass eccentricity from the axis of rotation. This implies that in practice, rigid rotors are those rotors operating well below their pin-pin critical speed. The rigid rotor unbalances include static, moment (couple), dynamic and quasi-static [7, 24, 27].

According to [9, 27], the process of balancing rigid rotor involved addition of weights to the machine at any two or more balance planes. Static and dynamic balancing methods are the two procedures through which the rigid rotor can be balanced. Static balance is the condition that does not depend on the assumed angular orientation of the rotor. It involved the relocation of the mass centre in one or more directions to a stipulated point in space through the rearrangement of mass within the system or the addition of mass at proper coordinate values. It reduces system motion in one plane only or the plane synchronous with rotation. In order to remove the static unbalance, the balance weights need to be added at each end of the machine to be able to produce additional vibration that would cancel the unbalance. In dynamic balancing, the masses of the members and a speed squared are the major parameters. The forcing function for dynamic balancing is generally due to the rotation of the system and is oriented in the radial direction. When the resultant of all centrifugal forces acting on the rotor system is

zero, and the centrifugal force does not give rise to any couple acting on the machine, the rotor is said to be dynamically balanced.

In order to balance the machine correctly, both static and dynamic balances must be achieved. Static balance would be obtained when the rotor does not come to rest at any favored angular orientation if it is placed on knife-edge supports. Therefore, there would not be net moment that can create rotation about the shaft axis as a result of gravity forces on the masses. The rotor is statically balanced automatically once it is dynamic balance is achieved. However, static balance could be obtained without dynamic balance. With rigid rotor balancing techniques, the rotor would balance to a stage that it would get to the desired speed without having problems.

Moreover, flexible rotor is one in which considerable bending occurs. It can be identified as the one that is operating near or above a critical speed or identified as the one that has high length-to-diameter ratios. The examples of flexible rotor mentioned by Wowk [36] include high-speed turbines, generators, multistage compressors, multistage pumps and paper-machine rolls. The correction process is not complicated for rigid or simple rotors with only one mass in which it can be done by simply adding one balancing weight to the rotor at the right angular orientation. In rigid rotor balancing, there are two possible modes of vibration to deal with. The first is lateral mode that is related to static unbalance in which the ends of the rotor would be thrown out in the same direction. The second one is conical mode that is connected with dynamic unbalance in which the ends of rotor would be thrown out in opposite direction to each other. However, there are an infinite number of modes associated with long flexible rotors and this make the balancing process more difficult. This is due to the fact that both the distribution of unbalance

forces along the length of the shaft and the shaft vibration mode shape would affect the positions at which balance weights required to be added to attain balance. The location of the correction plane for weight addition is very vital in flexible rotor balancing and above all, flexible rotors by and large require more than two planes for absolute balancing. Flexible rotor balancing is sometimes synonymous with high-speed balancing.

A study of the literatures on flexible rotor balancing is presented herein. The first part deals with balancing of flexible rotors at high speed while the second part involves low-speed balancing of flexible rotors. The first part is as follows:

Xu et al. [37] devised a rotor balancing method with no test run. The method used idea of influence coefficient method and the initial phase points (IPP) of Holospectrum. The information from the two sensors in one measuring plane was combined by IPP and this described the vibration states of the rotor totally in the measurement plane. The main different between these two methods is that the new method devised optimizes the correction masses directly without making use of the influence coefficient matrix. The genetic algorithm was used to optimize the correction masses in order to minimize residual vibrations at selected measurement locations and balancing speeds. The major procedures used include measuring the original vibrations and calculated the theoretic unbalance responses caused only by correction masses. These two were added together and the correction masses were obtained from the results through genetic algorithm.

In their work, the unbalance responses were calculated by using the transfer matrix method. The optimization idea of both the least-squares and weighted least-squares method were used on separate cases. It was reported that both simulation and experimental analyses were carried out and they concluded that the results from both

analyses showed that the residual vibration could be reduced by their method successfully.

Nevertheless, in Xu et al. [37] method of balancing flexible rotor, the likely speed at which unbalance responses could be calculated was not stated and gyroscopic effect was not considered.

Herbert [11] suggested in his work the method through which it could be determined whether the rotor in question needed high speed balancing or not. This considered the state of the rotor in terms of its flexibility and operating environment. He said there were many large turbine generators, with multiple rotors, that would pass through their shaft critical speeds but they could be balanced safely at low speed. He made it know that the environment would not affect the rotors that are very stiff in relation to their support structures and they are going to be operating as free-free beams. At lower speeds, the rigid body modes of *bounce* and *rock* would dominate and only at higher speeds the first true flexural mode could be excited. Also, the rotors that are going to be operated as a pinned-pinned beam are those rotors that were weak in relation to their support structures and the motions of the rotors would be dominated by their flexural modes. This kind of rotor required high-speed balance procedures if it operated at speeds close to or above its first flexural frequency. It was concluded that by merely computing the pinned-pinned natural frequency a speedy estimate would show whether it is required to balance the rotor at high or low speed. However, the method is only applicable to large, reasonable symmetric rotors in the power generation industry and its suitability to a wide range of rotors needed to be investigated.

Liu and Qu [26] presented a balancing method for rotor systems called the holo-balancing method. The method made use of conventional balancing methods of flexible rotor systems. In order to make the balancing process easier in this method, genetic algorithm (GA) optimization and computer simulation were used. The foundation of holo-balancing for a flexible rotor system was the transfer matrix. It was stated that the transfer matrix could be acquired by tracking one field balancing, a trial weight adding experiment, or by theoretical calculation. In their work, two mutually perpendicular proximity transducers were mounted on each bearing section to monitor the vibration. The matrix of three-dimensional holospectrum that provided the complete vibration information of a rotor in all bearing sections was obtained from the integration of all the first frequency ellipses. The transfer matrix of a unit trial weight was acquired for each correction plane. This was acquired from the initial and unbalance responses due to a unit trial weights applied to the correction planes. Correction masses and angles on each balancing plane were then obtained from these matrices. The GA and the computer simulation were utilized in turn to optimize the correction masses. The method was validated through the field balancing of 300 and 330MW turbo-generator units (using single and multi plane balancing methods). Hence, they concluded that the holo-balancing method decreases test number, increases precision and efficiency of field balancing. It is noted that all balancing processes were carried out at rated speed. Besides, they did not discuss the required number of balancing planes and measuring points for optimum balancing.

Kang et al. [13] employed the minimization of condition number of Hermitian matrix of influence coefficients to balance the rotor. The sensor locations and balancing

planes selected for the balancing procedure were utilized to acquire the condition number of this matrix. In order to simulate the balancing of flexible rotor-bearing systems under diverse arrangements of sensors and planes, finite element analysis was used. The situations in which sensors were fixed and correction planes were not and vice versa were considered. In their study, the influence of condition number on balancing accuracy and correction masses were used to search for the best sensor and balancing plane locations. The influence coefficient method that used the finite element analysis was employed to simulate the balancing procedures of several flexible rotor-bearing systems. The trial weight located at correction plane was utilized to create an excitation of the finite element model. Through this, they were able to acquire the unbalanced response and influence coefficient matrix. They discovered that among all the possible arrangements of sensors and balancing planes considered, the best balancing results (highest accuracy and lowest total correction mass) was provided by those whose condition number lies below a certain threshold. The sum of the required correction masses tends to decrease as the condition number decreases, and accuracy tends to increase. They stated that by trying to minimize the condition number of Hermitian matrix of influence coefficients earlier before balancing, the accuracy of the method could be improved and this could be done by searching for the optimal locations of measurement sensors and/or balancing planes. Thus, the quantities and locations of measurement sensors and balancing planes must be decided prior to simulating influence coefficient matrix of a real rotor-bearing system.

In each set of simulation they carried out, the number of sensors and balancing planes were equaled and all the influence coefficient matrices obtained from each set were square matrices. Also, in each case considered, different condition number which

described the quality of influence coefficient matrix was obtained. In addition, they performed the experimental verification by using the rotor kit (with four disks, four sensors and keyphasor) to verify their simulation results and the balancing accuracies were calculated.

It was concluded that their results shown that by choosing an influence coefficient matrix with a smaller condition number, a higher balancing accuracy could be achieved.

However, in their work, several sensors, correction planes and different speeds (which include speeds below and above the critical speed) were considered. The most advantageous number of sensors and correction planes that required was not mentioned. In addition, the range of speeds at which their approach can be used to achieve effective balancing of flexible rotor was not discussed.

Das et al. [7] also proposed an active vibration control scheme for controlling transverse vibration of a rotor shaft due to unbalance and increase the stability limit speed of the system. The method utilized electromagnetic exciters climbed on the stator at a plane usually away from the conventional support (bearings) locations around the rotor shaft. This was done in order to apply appropriate force of actuation over an air gap to control the transverse vibration. The locations far-away from discs were considered for the exciters to avoid interfering with the rotor operation in any way. The electromagnetic exciters were designed in a manner that allowed a set of exciters to develop radial control force. This set consists of four pairs of poles of electromagnet which were symmetrically placed around the circumference of the rotor. Nonetheless, it was explained that whenever rotor is vibrating at any instant during the operation, it would move away from a particular pair but closer to opposite pair of poles. If X is the axis of rotation, along Y

or Z direction, the control force to oppose shaft deflection would be attained by concurrently stepping down the current in the coil around the opposite pair (to which the rotor is nearer). Similarly, the current in the coil around the particular pair of poles (from which the rotor is farther) would be stepped up by equal amount from the steady bias current. In order to show the effectiveness of electromagnetic exciter in controlling the rotor unbalance, the numerical simulation was performed. Lalanne's rotor with two identical orthotropic bearings was considered and MATLAB 7 was employed to develop program that was utilized to find the results. They observed from the results obtained that by virtue of incorporating stiffness and damping effects, the exciters helped not only to reduce the unbalance response amplitude but also raised the stability limit speed of the rotor-shaft system. Hence, they concluded that their method is free from the difficulties of maintenance, wear and tear and power loss and there exist specific locations of the exciters for considerable reduction of response and increment of stability limit speed with comparatively low value of control current. Nevertheless, the method proposed by Das et al. [7] cannot be applied to majority of rotors because the space (for the location of electromagnetic exciters which need to be fixed for effective performance) will not be available in all rotors. The exciters will also constraint the bearing or disk movement where the shaft is not long or disks are closed together. Similarly, the implementation will be more expensive for multi-correction planes.

As for low-speed balancing of flexible rotors, few investigations were reported. Tan and Wang [33] stated in their work that at low speed by using influence coefficient method of balancing; the first n modal components of unbalance of a flexible rotor could be balanced without solving for the unbalance components. Their objective was to

propose a theory and method of low speed balancing for flexible rotors that could unify the theories for balancing flexible rotors (modal and influence coefficient methods that have been developed) and at the same time that would balance the flexible rotors at low speed and give the same acceptable result as that of high speed. They developed the relationships between the modal and influence coefficient methods of balancing flexible rotors and theory of low speed balancing of flexible rotor was then deducted from them.

In their theory, they made it known that in order to balance the shaft at low speed, there are going to be correction and measurement planes and correction weights. So, from the deflection due to initial unbalance and balance correction of the shaft the influence coefficient matrix due to correction vector could be obtained. However, they stated that in order to make the residual unbalance deflections of the shaft equal to zero through the balance correction, different methods for balancing flexible shaft could be applied and these include modal balancing and influence coefficient methods. This implied that at the measurement points the initial unbalance deflections of the shaft could be reduced to zero as a result of the effects of the balance correction through these methods.

Moreover, it was stated in [33] that if the rotor is balanced through the modal balancing the residual unbalance deflections of a flexible rotor could be very small in a range of speeds lower than the *nth* critical speed. Also, a group of balance corrections could be acquired if the influence coefficient method was to be used at a balancing speed to make the residual unbalance deflections equal to zero at measurement points on the shaft, when these corrections are applied to the rotor. Hence, in order to determine the corrections through the influence coefficient method, the conditions stated in their theory that needed to be met are as follow: the operation speed could be equal or greater than balancing

speed but should less than the next critical speed, the balancing speed should not equal to any critical speed, the number of correction and measurement planes must equal to order of critical speed that is just higher than the operating speed, determinant of modal component matrices corresponding to the correction planes and the measurement points on the shaft should not equal to zero, the rotor–bearing systems should be undamped or with linear proportional or small damping and the effect of run speeds on its natural properties should be very small that they can be disregarded. It was concluded that if the above conditions were met, by using the influence coefficient method in a single speed, multi-correction-plane and multi measurement point, the first n modal component of unbalance of a flexible rotor can be corrected at low speed. It is noted, however that their method did not consider the gyroscopic, rotational and shear deformation effects in their theory. Also, their maximum balance speed was operation speed which was automatically above the available critical speeds within the operation speed and this was no longer a low speed. Similarly, the theory was made for low speed balancing of long (uniform rotor without disk) or shaft that represented few flexible rotors being in used and they did not demonstrate the applicability of the method.

Liu [25] also introduced a method that could be used to balance a flexible rotor with no test runs at high speeds and the method was regarded as Low-Speed Holo-Balancing (LSHB). The LSHB principle was based on the holospectrum technique and it used the balancing speed that was less than first critical speed. There was a relation between his work and that of Tan and Wang [33] theoretically. However, his method was devised for high speed rotating machinery running at the speed between the first and second critical speed and initial phase points (IPP) were used to indicate unbalance

responses. His method utilized the information from more than one sensors and a three-dimensional holospectrum was constructed to illustrate the absolute vibration response of a rotor through a multi-sensor fusion. In his work, the experimental rotor rig was used and his aim was to correct the first two low modal unbalances. The balancing speed was set to the speed below the first critical speed. The operation speed was between the first and second critical speeds while damping effect was neglected. Four runs were carried out, the first two runs were to obtain initial responses at operation and balance speeds while the third run was to obtain the response due to trial weights (located at the equal angles) at two balancing planes. The last run was like third run but it was to obtain the response due to couple unbalance with trial weights located at the two balance planes but at different angles (180^0 apart). Five sensors (4 proximity and 1 phase probes) were utilized and the information from these sensors was used. The vibration responses were defined by constructing a three-dimensional holospectrum through a multi-sensor fusion. The correction weights and angles were then acquired. He stated in his conclusion that the method adopted was an extension of the traditional flexible rotor balancing method but it did not involve test runs at operation or critical speed during the balancing processes.

However, the method developed in [25] was limited to the rotors that are operating between the first and second critical speeds only and it was applied to symmetric rotor that is not common. Similarly, the gyroscopic effect and damping in the system were not considered.

In the long run, regarding all the works narrated, some approaches and theoretical formulations have been described. The procedures and practices defined are very

distinctive in their own nature and content. All the reported studies suggested methods that could simplify the balancing procedure and the cost of performing rotor balancing. Above all, these procedures have an inherent value. Some require longer time, costly equipment such as accelerometers, probes and other balancing components that are not listed in the researchers' procedures. Some also need to be done by professional while some techniques are not applicable to all rotors. In addition, majority of researchers' silent on the optimum number of correction plane, number of measurement plane and balancing speed for their methods. At the same time, some of these researchers did not consider the rotational inertia, shear deformation and gyroscopic effects that is vital in flexible rotor analysis. These and many more are the buried costs in all balancing practices that were not discussed. Hence, the need for a balancing system that reduces loss, downtime, training and the cost is crucial to company's managements.

1.3 The Current Status

The need to devise a low-speed balancing method for balancing high-speed rotors was recognized and addressed. Yet, very few investigations have been reported in the available literature. Flexible rotor balancing, in general, relies to a great extent on physical insight into modal nature of the unbalance response. In this regard, the insight into the elastodynamic behavior of rotors can be greatly aided by mathematical modeling. Although, the importance and utility of mathematical models were recognized and addressed by many investigators within the context of balancing multi-bearing rotor systems, they were not equally utilized in conjunction with devising low-speed methods for balancing high-speed flexible rotors. To date, there is no established systematic low-

speed scheme for balancing high-speed rotors. It was also noted that there is no high-speed balancing facility in the Kingdom, which stands in the forefront of turbomachinery users in the world.

1.4 Objectives of the Present Study

The objectives of this research work are:

1.) To devise a method for balancing flexible rotor at low speed

2.) To numerically test the developed technique in order to ascertain its validity.

In this regard, the hypothesis postulated by Tan and Wang [33] is extended to include rotary inertia, gyroscopic and shear effects. The developed method permits multi-disk multi-bearing rotor systems, by utilizing the powerful FEM discretization method. Moreover, the developed technique ensures that the balancing speed is well below the first critical speed; thus allowing high-speed flexible rotors to be balanced on traditional balancing machines; or open casing in balancing in the field.

The rotordynamics module in ANSYS will be used to model the rotor and perform the required analyses on it. MATLAB is then used for processing and manipulation of data and carrying out the numerical procedure for calculating the proper correction masses.

CHAPTER 2

THEORY OF BALANCING FLEXIBLE ROTORS

Several newly designed machines are equipped with flexible rotors. Examples of such machines include turbines, generators and pumps. Traditionally, the rotor is regarded as a plastic rotor if the change in unbalance is permanent whereas it is either body-elastic or shaft-elastic (Figure 2.1) if the unbalance decreases again as the speed decreases. Elastic-shaft rotor is a type of the rotor that operates either near to or beyond its critical speeds and distorts when approaching the critical speed. At the critical speed the deformation reaches its maximum and decreases again as the speed continues to increase. The rotor bends into a V-shape in the neighborhood of the first critical speed, S-shape near the second critical speed and W-shape in the vicinity of the third (Figure 2.2). Hence, these are at times referred to in balancing technology as a V-mode, S-mode and W-mode and these bending shapes associated with the critical speeds are called natural modes. In general, almost all rotating machine components which have a high service speed need to be balanced. The industries where machines need balancing include [4]:

1.) Mechanical and electrical machine construction:

Steam and gas turbines, compressors, pump rotors, gearbox components, electric motor and generator armatures, fast rotating components of transport systems.

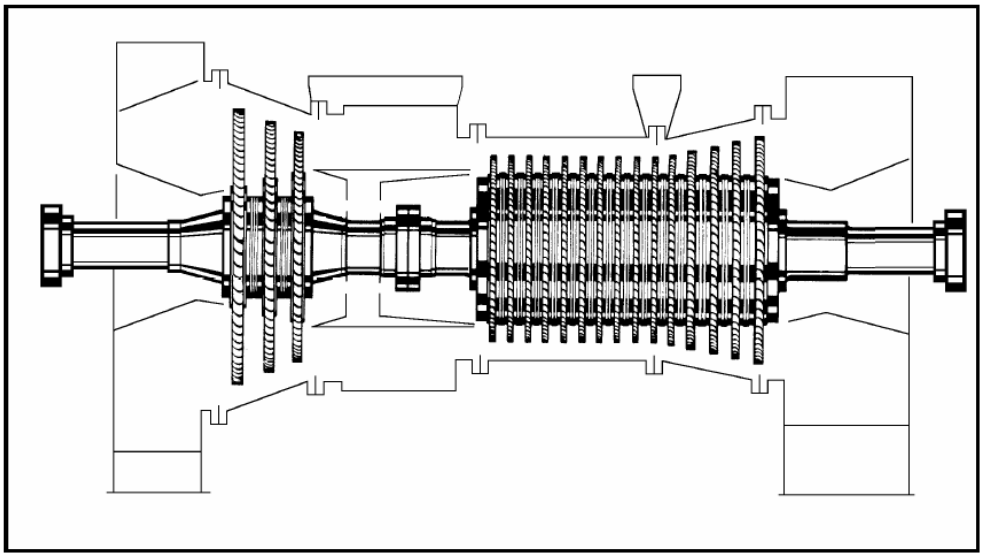

FIGURE 2.1: A Shaft-Elastic Rotor [4]

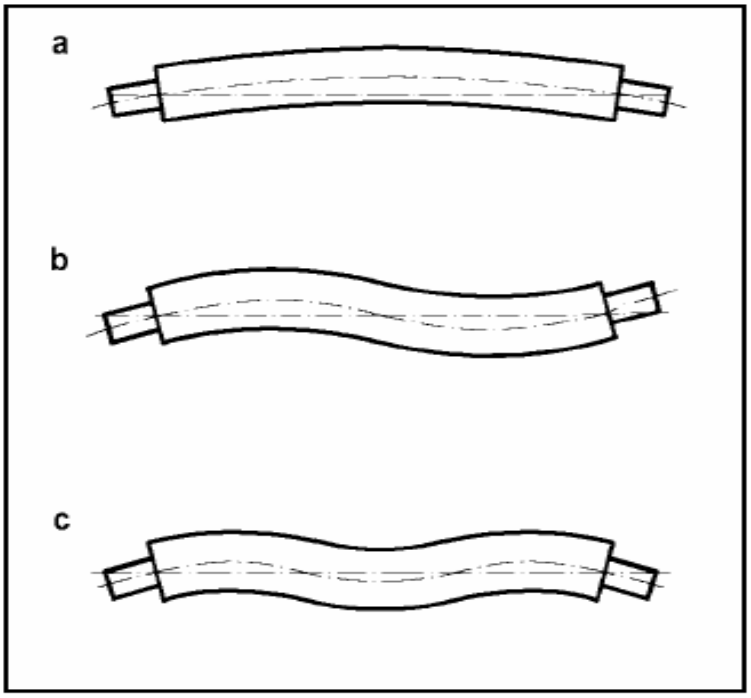

FIGURE 2.2: Natural Modes of a Roll-Shaped Rotor (Bending Shape of a Roll at (a) 1st Critical Speed (b) 2nd Critical Speed (c) 3rd Critical Speed) [4]

2.) Machine tool and fixture construction:

Cutting wheels, grinding discs and wheels, gears, drive assemblies, fast rotating equipment in turning and milling machines.

3.) Chemical industry, food industry and other material processing plants:

Centrifuges, stirring apparatus or agitators, pumps, fans, beaters or hammer mills, textile and winder spindles.

4.) Vehicles and other powered machine construction:

Crankshafts, flywheels, clutches, impellers, gearbox components, drive shafts, wheels, wheel sets, tires.

In this chapter, the fundamental methods of balancing flexible rotor are discussed with a brief outline of their mathematical background. In addition, the guidelines for selecting the balancing trail weights will be presented.

2.1 Fundamental Methods for balancing flexible Rotors

A flexible rotor has an infinite number of potential modes of vibration related to the system, whereas the rigid rotor has only two possible modes of vibration. Each vibration mode of the rotor is associated with a particular frequency. Therefore, it is imperative to balance flexible rotors not only for the first two possible modes of vibration (static and dynamic imbalances) but also for all elastic modes of vibration up to the maximum running speed of the machine.

There are several methods that can be used to balance the flexible rotor which include [36]: Influence-coefficient method; Modal balancing; Multi-plane, multispeed balancing; Low-speed, rigid rotor balancing; Low-speed, flexible balancing; Static-

coupling method and Single-plane balancing of components and manufacturing tolerance control.

In general, the two fundamental methods used to balance the flexible rotors include modal and influence coefficient balancing. They required high speeds with several numbers of trial runs. However, it should be noted that flexible rotor balancing is greatly depends on the prior experience with related rotors and is not simply methodized to be commonly applicable. Also, flexible rotors are costly and the speeds can make them hazardous. Due to these reasons, the flexible rotor balancing should not be attempted without a tutor [36].

In this section, the modal balancing and influence coefficient methods and their equations will be presented.

2.1.1 Modal Balancing Method

The modal method of balancing is the method in which weights are placed at precise axial location to cancel out critical speed bending. A different set of weight is determined and applied for each mode shape while the earlier rigid rotor balance done at lower speed would not be altered [36]. Modal balancing is a progressive, step by step technique through which the modal components of unbalance are acquired experimentally and corrected in succession, commencing from the first mode by fastening to the shaft the appropriate correction masses in order to reduce modal components of the residual unbalance to approximately zero [33]. The inherent assumptions of modal balancing include neglecting the effect of system damping, lateral anisotropy and gyroscopic forces [6]. Whenever balance weight is to be positioned, its

axial location should be chosen close to the anti-node in the mode shape because this is the area where the applied weight forces will have the greatest effect on straightening the shaft [9].

In order to balance the rotor through modal balancing, firstly, the vibrations (amplitude and phase angle relative to some reference position on the shaft) of machine are to be measured usually at places very close to the location of bearings.

The machine static unbalance is precisely corrected at the first critical speed since this is the speed that the machine is mainly sensitive to this kind of unbalance. Thus, to eliminate the vibration related to the static unbalance the balance weight will be attached to the rotor at balancing plane and machine needs to be operated to a speed close to the first critical speed when measurements are to be made. Then, the magnitude and angular position are to be determined as it was done initially, taking into consideration of the appropriate phase lag angle and machine sensitive to unbalance.

Also, the machine will operate close to the second critical speed of the machine in order to balance the second vibration mode and machine is sensitive to dynamic unbalance at this speed. Measure the vibration of the system and compute the needed magnitudes and phase angles of the balance weights as done in balancing first mode from the knowledge of the phase lag angle for the machine second critical speed and experience of the sensitivity of the machine to balance weight addition. Then, through the location of the anti-nodes of the mode shape concern the axial location of the balance weight is determined.

Since some flexible rotor machines operate close to or above n^{th} $(n = 3,4,.....)$ critical speed, it becomes a must to balance the rotor up to third critical speed if $n = 3$ for

instance. If the rotor is operating close to third critical speed and in order to correct vibrations the balance weight is added to the anti-node at the centre only, this will upset the static balance and at first critical speed the level of vibration will increase. Hence, it is crucial to add some mass at the centre of the rotor together with an equal amount 180^o around the rotor, half at each end of the machine so that static balance will not be upset. This means that to be able to balance third critical speed, three planes are needed for the balance weights addition and are usually positioned close to the anti-nodes of the third mode of vibration. This process is also applicable to the balancing of machines with any number of critical speeds. In addition, concerning the machines that operate with very flexible bearing, it is advisable to balance the rigid body modes before starting the flexural modes (Figure 2.3). In this case, correction is made at a number of balance planes equal to the number of flexural mode under consideration plus two more planes. These are needed for successive balancing of flexural modes in order to ensure that previous rigid body balance is not upset. This method is referred to as $n+2$ plane balancing method [4, 9, 23] (see Figure 2.3). Some general mode shapes and likely weight placements are as shown in Figure 2.4.

Regarding the overhung rotor, before the rotor is assemble on the machine the shaft must be balanced in isolation and the second balancing will then be done with attention focus on the rotor. Also, it is generally desirable to balance them as independent units if the machines consist of two or more shafts coupled together [9].

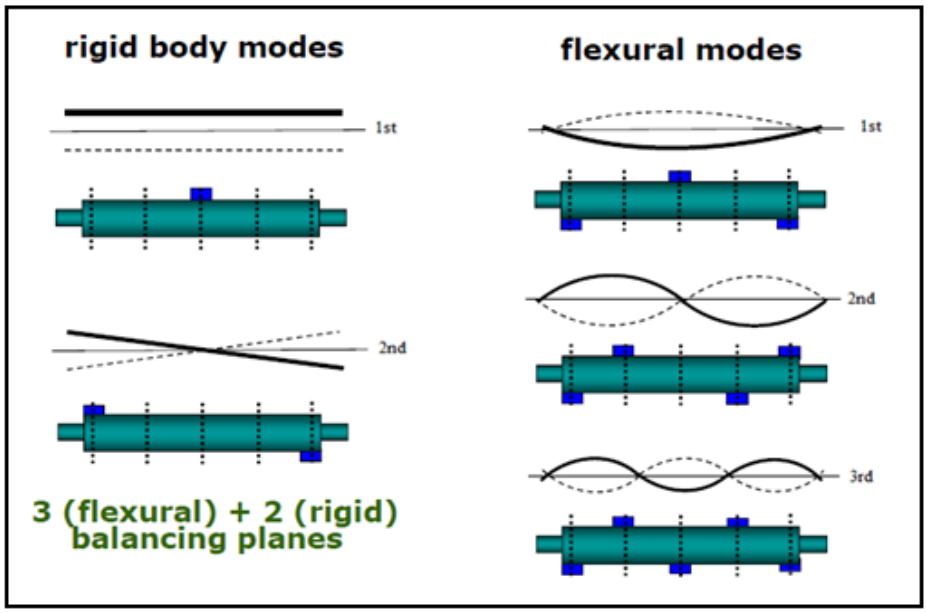

FIGURE 2.3: Correction Mass Distribution [9, 23]

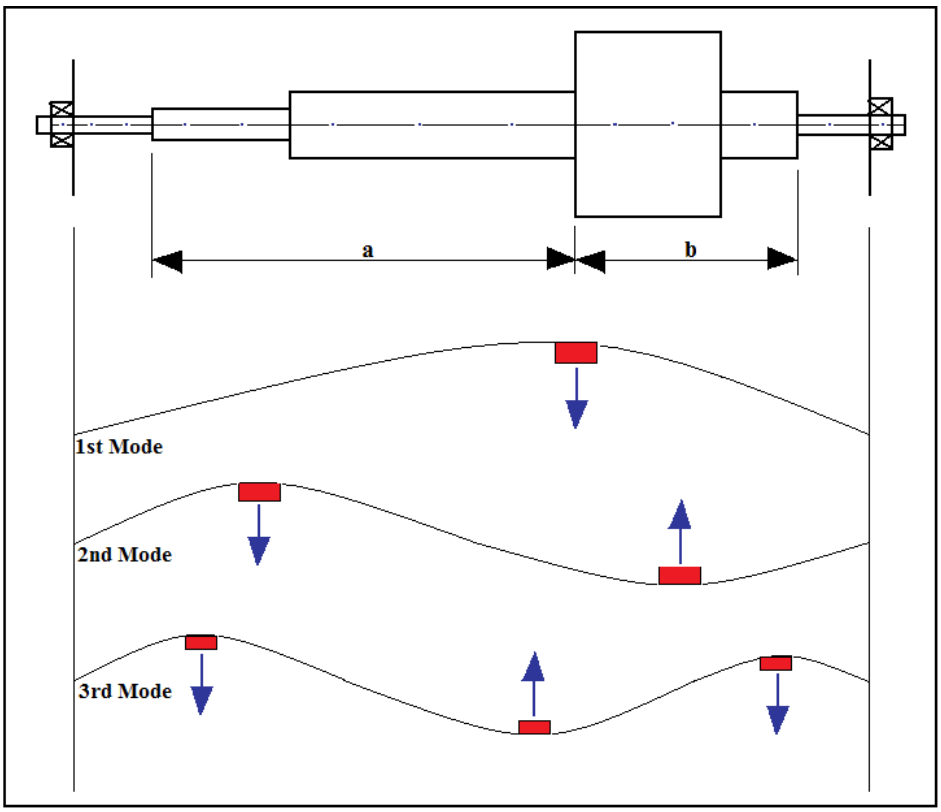

FIGURE 2.4: The First Three Bending Mode Shapes of Rotor [36]

However, the procedures that have been utilized to perform the modal balancing are usually classified as either n or $n+2$ plane modal balancing [6, 38]. The common procedures of modal method of balancing include [36]:

1.) Balancing the rotor at low speed as a rigid rotor first to correct gross unbalances. Two weights will be placed on the rotor outboard near the end planes.
2.) If balancing was to be done on a high speed facility, rotor needs to be mounted on bearings that are similar in stiffness to the site conditions but if the balancing is to be done in its original place, this requirement is not compulsory.
3.) Operate the rotor to a speed approaching the first critical speed and measure the vibration.
4.) Stop the rotor and toward the middle of the rotor attach the trial weight. Since any single weight placement will damage the previous balance achieved as a rigid rotor and to prevent this, the trial weight should be distributed as shown in the Figure 2.5 (for symmetric rotor). In case of unsymmetrical rotor shown in Figure 2.4 the compensating weights in the end planes should be adjusted by the lever rule based on the location of the centre weight. For instance, the left W_L and right W_R compensating weights can be computed as

$$W_L = W\frac{b}{a+b},\ W_R = W\frac{a}{a+b} \tag{2.1}$$

Apart from this, the compensation weight set can be measured on the balancing machine rather than calculating it.
5.) Operate the rotor again to the same speed as the original run in step 3 and measure the vibration.

6.) Using the standard single plane vector calculation to calculate the correction weight. If needed be, trim balance as essential until the first critical speed can be safely traversed.

7.) Operate the rotor to a safe speed approaching the second critical speed and measure the vibration again.

8.) Stop the rotor and attach the trial weight set as shown in the Figure 2.6. This weight set is devised to decrease second mode bending with no damage to the previous balance results at the first critical speed and as a rigid rotor. This weight set is applicable to a symmetrical rotor.

9.) Operate the rotor again to the same speed used in step 7 and measure the vibration.

10.) Using the standard single plane vector calculation again to calculate the correction weight. Also, if demanded, trim balance as required until the second critical speed can be safely traversed.

11.) Operate the rotor again to a safe speed approaching the third critical speed and measure the vibration.

12.) Stop the rotor and attach the trial weight set as shown in the Figure 2.7. This weight set is meant to change mainly third critical speed bending and maintain the previous balance improvements. This weight set is also applicable to a symmetrical rotor.

Regarding unsymmetrical rotors, the amount in the end planes require to be adjusted based on the locations of the central weights and sensible leverage.

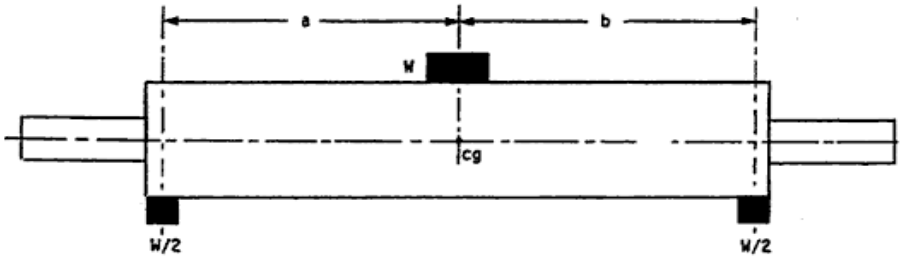

FIGURE 2.5: Distribution of Weights in order to Correct First Mode Bending without Affecting earlier Balance Results [36]

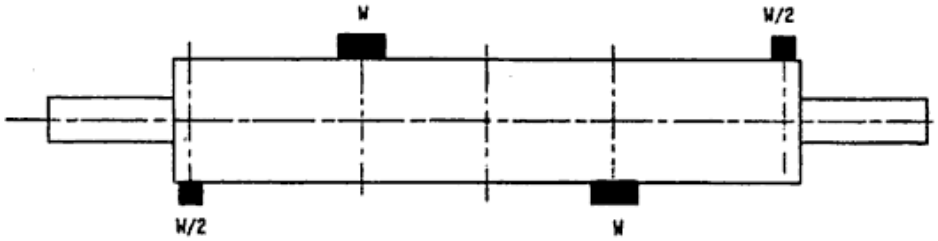

Figure 2.6: Distribution of Weights in order to Correct Second Mode Bending without Affecting earlier Balance Results [36]

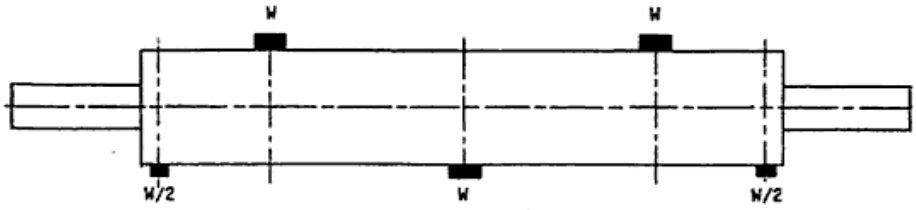

FIGURE 2.7: Distribution of Weights in order to Correct Third Mode Bending without Affecting earlier Previous Balance Results [36]

Although, during a low speed run as a rigid rotor the end corrections can also be measured on balancing machine.

13.) Operate the rotor again to the same speed used in step 11 and measure the vibration.

14.) Using the standard single plane vector calculation again to calculate the correction weight and if required, trim balance as compulsory until the third critical speed can be safely crossed.

15.) Repeat the procedure for higher modes until the final service speed is attained. Each succeeding weight set should be carefully chosen so that the previous balance will not be disturbed.

16.) The final balancing will be done at the rotor's service speed with the correction weight placed in the end planes only.

It is noteworthy to mention that the relative locations and amount of weight sets shown in Figures 2.5, 2.6 and 2.7 are only for symmetrical rotors while axially unsymmetrical correction planes are needed for unsymmetrical rotors, and the weights may require to be adjusted to acquire the correct couples. In case that all weights cannot be placed at the same radius, to attain equivalent centrifugal force effects, further adjustments need to be carried out.

In addition, some knowledge regarding the deflection is fundamental to the modal method of balancing [8, 23, 36]. Therefore, it is most valuable to have numerous proximity probes along the rotor to measure deflection or to have some other means of measuring (like shaft riders or a laser vibrometer) to obtain this information. In order to be able to balance up to the n^{th} critical speed the modal balancing method needs an

additional correction plane for each higher mode. Normally, the flexible rotor balancing needs $n+2$ correction planes, where the latter two are used at the start to correct the rigid rotor vibration.

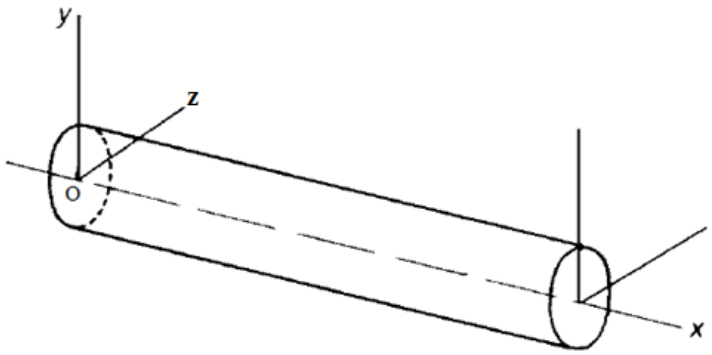

FIGURE 2.8: Flexible Shaft

Furthermore, the most common case of distributed unbalance may be expanded in terms of the modal eccentricity components in terms of the mode shapes. The amplitude response of these modes can then be obtained according to the responses to the modal components. These components are acquired be expanding the eccentricity in terms of the modal functions. Hence, the unbalance components are reduced gradually from lower mode in modal balancing method [38]. In this context, the theoretical basis of the method is highlighted. The equation of motion of the beam element (Figure 2.8) in y-direction is given as

$$\rho A(x)\frac{\partial^2 y}{\partial t^2}+\frac{\partial^2}{\partial x^2}\left(EI(x)\frac{\partial^2 y}{\partial x^2}\right)=F(x,t) \tag{2.2}$$

$$m(x)\ddot{y}(x,t)+\frac{\partial^2}{\partial x^2}\left(EI(x)y''(x,t)\right)=F(x,t) \tag{2.3}$$

where $m(x)$, $EI(x)$ and $F(x,t)$ are mass per unit length, flexural rigidity and external force.

When balance correction is added to a rotating unbalance shaft, the external force (centrifugal inertial force) in Eq. (2.3) will consist of forces caused by both the unbalance and balance correction [33]. Hence, Eq. (2.3) will become

$$m(x)\ddot{y}(x,t)+\frac{\partial^2}{\partial x^2}\left(EI(x)y''(x,t)\right)=\Omega^2 e^{j\Omega t}\left[m(x)a(x)+m_c(x)r_c(x)\right] \tag{2.4}$$

In which Ω, $a(x)$, $m_c(x)$ and $r_c(x)$ are rotational speed of shaft, shaft eccentricity, correction mass and radius of correction mass from centre of the shaft. If $y(x,t)$ is defined as

$$y(x,t)=\sum_{i=1}^{\infty}\beta_i(t)\phi_i(x) \tag{2.5}$$

Then

$$\left.\begin{aligned}\ddot{y}(x,t)&=\sum_{i=1}^{\infty}\ddot{\beta}_i\phi_i(x)\\ y''(x,t)&=\sum_{i=1}^{\infty}\beta_i(t)\phi_i''(x)\end{aligned}\right\} \tag{2.6}$$

Upon substituting Eq. (2.6) in Eq. (2.4) we have

$$m(x)\sum_{i=1}^{\infty}\ddot{\beta}_i\phi_i(x)+\frac{\partial^2}{\partial x^2}\left(EI(x)\sum_{i=1}^{\infty}\beta_i(t)\phi_i''(x)\right)=\Omega^2 e^{j\Omega t}\left[m(x)a(x)+m_c(x)r_c(x)\right] \tag{2.7}$$

If Eq. (2.7) is multiply by $\phi_i(x)$ and then integrate over the entire length of the shaft, then

$$\begin{aligned}&\int_0^l \ddot{\beta}_i m(x){\phi_i}^2(x)dx+\int_0^l \beta_i(t)EI(x)\{\phi_i''(x)\}^2(x)dx=\Omega^2 e^{j\Omega t}\left[\int_0^l \phi_i(x)m(x)a(x)dx+\right.\\ &\left.\int_0^l \phi_i(x)m_c(x)r_c(x)dx\right]\end{aligned} \tag{2.8}$$

However, for the orthogonality condition of a continuous rotor

$$\int_0^l m(x)\phi_i(x)\phi_j(x)dx = \begin{cases} 0 & (i \neq j) \\ \overline{m} & (i = j) \end{cases}, \ \overline{m}_i \text{ is modal mass or constant}$$

Hence,

$$\left.\begin{aligned} \int_0^l m(x)\phi_i{}^2(x)dx &= \overline{m}_i \\ \int_0^l EI(x)\{\phi_i''(x)\}^2(x)dx &= k_i \end{aligned}\right\} \tag{2.9}$$

For which $\overline{m}_i$ and k_i are modal or generalized mass and stiffness. When the Eq. (2.9) is substituted into Eq. (2.8), the following will be obtained

$$\ddot{\beta}_i + \omega_i{}^2\beta_i(t) = \frac{1}{\overline{m}_i}\Omega^2 e^{j\Omega t}\left[\int_0^l m(x)a(x)\phi_i(x)dx + \int_0^l m_c(x)r_c(x)\phi_i(x)dx\right] \tag{2.10}$$

Hence, from Eq. (2.10) [23]

$$\int_0^l m_c(x)r_c(x)\phi_i(x)dx = -\int_0^l m(x)a(x)\phi_i(x)dx = -U_i \tag{2.11}$$

in which U_i is modal unbalance and for the n plane modal balancing,

$$m_c(x)r_c(x) = \sum_{j=1}^{n} u_j\delta(x - x_j) \tag{2.12}$$

When Eq. (2.12) is put into Eq. (2.11), it becomes

$$\int_0^l m_c(x)r_c(x)\phi_i(x)dx = \sum_{j=1}^{n} u_j\phi_i(x_j) = -U_i \quad for \ \ i, j = 1,2,....,n \tag{2.13}$$

Generally, regarding the balancing of n modes, a simultaneous solution is needed for correction in n balancing planes, requiring analysis in the xy and xz planes, which implies that one needs to deal with planar components algebraically rather than with single resultant modal corrections [10].

So, if for instance, $n=3$, modal unbalances U_1, U_2 and U_3 are known and they are in the same xy plane, then the simultaneous equations for balancing the first 3 modes from Eq. (2.13) with correction planes 1, 2 and 3 are

First critical speed $(csp=1)$

$$\begin{aligned} u_1\phi_1(x_1)+u_2\phi_1(x_2)+u_3\phi_1(x_3) &= -U_1 \\ u_1\phi_2(x_1)+u_2\phi_2(x_2)+u_3\phi_2(x_3) &= 0 \\ u_1\phi_3(x_1)+u_2\phi_3(x_2)+u_3\phi_3(x_3) &= 0 \end{aligned} \tag{2.14a}$$

Second critical speed $(csp=2)$

$$\begin{aligned} u_1\phi_1(x_1)+u_2\phi_1(x_2)+u_3\phi_1(x_3) &= 0 \\ u_1\phi_2(x_1)+u_2\phi_2(x_2)+u_3\phi_2(x_3) &= -U_2 \\ u_1\phi_3(x_1)+u_2\phi_3(x_2)+u_3\phi_3(x_3) &= 0 \end{aligned} \tag{2.14b}$$

Third critical speed $(csp=3)$

$$\begin{aligned} u_1\phi_1(x_1)+u_2\phi_1(x_2)+u_3\phi_1(x_3) &= 0 \\ u_1\phi_2(x_1)+u_2\phi_2(x_2)+u_3\phi_2(x_3) &= 0 \\ u_1\phi_3(x_1)+u_2\phi_3(x_2)+u_3\phi_3(x_3) &= -U_3 \end{aligned} \tag{2.14c}$$

Then, u_1, u_2 and u_3 can be solved for in the Eq. (2.14). Hence, the three unbalances needed to be added to the three balancing planes can be obtained as follows;

$$u_i = \sum_{j=1}^{n} u_i \Big|_{csp=j,\, u\phi=u_i\phi_j}, \quad i,n=1,2,3 \tag{2.15}$$

Since it is complicated to establish U_1, U_2, U_3 practically, they can be determined by trial and error [38]. This can be done by attaching the correction weight m_{11} to the rotor first balancing plane and operate it at a speed close to first critical speed, the correction weight value will be vary after each run until the first mode vibration decreases to

acceptable level. Also, the two correction weights m_{12} and m_{22} will be attached again to the rotor in order to balance the second mode and the rotor will be run at a speed close to second critical speed. The value of these weights will be adjusted after each run until the second mode was decreased. When, the second mode is balanced, the three correction weights m_{13}, m_{23} and m_{33} will attached to the rotor at balancing planes and operate the rotor to a speed close to third critical speed. Varying each of these weights after each run until the third mode is decreased. Then, the total correction weight at first, second and third balancing planes will be $m_{11} + m_{12} + m_{13}$, $m_{22} + m_{23}$ and m_{33}.

However, as the number of modes to be balanced rises up, the balancing planes needed also increase, equivalent to the number of modes to be balanced. No plane should be selected at a node [10].

The advantages of modal balancing method include [6, 23, 27]:

- It has excellent sensitivity at high speeds and at highest speeds the number of sensitivity runs is reduced.
- Balancing of a specific mode is allowed without affecting earlier balanced modes (lower modes).
- It can be completely empirical procedure.

Similarly, its disadvantages are [6, 23]

- It needs substantial operator insight/precise prior knowledge of rotor dynamics
- Unrealistic assumptions of planar mode shapes may not be suitable for system with considerable damping or bearing cross coupling effects.
- Sensitive to measurement error

- It requires a highly skilled operator
- It does not easily lend itself to production applications

2.1.2 Influence Coefficients Method

In a situation whereby a system has large damping or if a system has some rotors connected to each other such as in steam turbine generator system, the characteristic modes will not become visible obviously, influence coefficient method of balancing is then employed [38]. Influence coefficient method of balancing is defined as data processing technique to minimize rotor's vibration to an acceptable value according to a appropriate criterion [33]. It is also a method that makes use of either weighted least-square or least-least square method to solve over-determined linear equation system in order to obtain the correction masses [37]. The method is shortcoming is that a huge amount of test runs are required to obtain not only the original vibration data but also the data of trial weights in multiple correction planes at different speeds [25]. The method assumes that the rotor response is a linear function of the unbalance [6, 25, 36]. It is a standard and extensively used method for field balancing in industrial applications. It needs no much knowledge of the rotation system and the balancing operation is easy to carry out on a computer. Due to the inaccuracy of the sensors and nonlinearity of the rotor-bearing system, certain errors are generated [13].

In order to determine the influence coefficients of the system experimentally, this method involves the application of trial masses to the machine. These will then be used to calculate the exact magnitudes and the positions of the balance correction weights when the initial imbalance vibration has been documented. It is noteworthy to mention that

more influence coefficients may be needed depending on the vibration mode to be balanced. The influence coefficient matrix must be square and invertible; otherwise an optimization process is needed [9]. However, the influence-coefficient method of balancing is described as an extension of two-plane balancing methods by adding correction planes, speeds and measurement points and there are no restrictions to the number of correction planes or to the number of speeds at which measurements are to be acquired. Influence-coefficient method can be applied to both flexible and rigid rotors, as well as multi-baring rotors. It shortcoming is that it must be carried out with a computer due to the extensive matrix computations [36]. This method is an empirical method that adds trial weights at selected balance planes and assumes that the rotor response is a linear function of unbalance. This can be linear written as a system of equations [9, 36]

$$\{V\} = [A]\ \{U\} \tag{2.15}$$

where $V, A \text{ and } U$ are vibration amplitude and phase, influence coefficients matrix and unbalance.

The equations are going to be generated by making many rotor runs as the trial weights are moved from one correction plane to the other. The weight set that will be selected mathematically must be the one that will produce the minimum vibration at all measurement points. This can be computed for one speed or with at least square fit for many speeds. There must be as many trial runs at least as there are measurement locations [9, 33, 36]. In order to achieve better balancing, additional data with more trial runs at different speeds can be combined statically. The common procedure for the influence coefficient method can be highlighted as follows [36]:

1.) There should be q correction planes, n transducers to measure vibration and k speeds. It will then be $p = kn$ opportunities to obtain data while the balancing speeds include $S_1, S_2, ..., S_k$

2.) Carry out an initial run to measure the vibration at each transducer for each speed one after the other in the original condition. Let the vibration amplitude, and phase at each transducer be represented by W_{no}^{k}, where superscript k refers to kth speed and the subscripts n and o refer to the nth transducer and original condition.

3.) Attach the trial weight m_1 to the rotor in correction plane 1. Its radius is r_1 and phase angle is ϕ_1.

4.) Run the rotor again and measure the vibration (due to adding m_1 in correction plane 1) at each transducer n for each speeds k one after the other. The following tabulated measurements shown in Table 2.1 will be achieved: W_{n1}^{k}

5.) Remove the trial weight m_1 from plane 1 and attach the trial weight m_2 (the same trial weight as m_1 or a different one) in correction plane 2. This is going to have radius of r_2 and phase angle location of ϕ_2.

TABLE 2.1: Transducers Measurements at Several Speeds when Trial Weight is attached to the First Balancing Plane

First Plane				
Transducer Number	**Speed Number**			
	1	2	…	k
1	W_{11}^{1}	W_{11}^{2}	…	W_{11}^{k}
2	W_{21}^{1}	W_{21}^{2}	…	W_{21}^{k}
⋮	⋮	⋮	…	⋮
n	W_{n1}^{1}	W_{n1}^{2}	…	W_{n1}^{k}

TABLE 2.2: Transducers Measurements at Several Speeds when Trial Weight is attached to the Second Balancing Plane

Second Plane				
Transducer Number	**Speed Number**			
	1	2	…	k
1	W_{12}^{1}	W_{12}^{2}	…	W_{12}^{k}
2	W_{22}^{1}	W_{22}^{2}	…	W_{22}^{k}
⋮	⋮	⋮	…	⋮
n	W_{n2}^{1}	W_{n2}^{2}	…	W_{n2}^{k}

6.) Run the rotor again and measure the vibration that will occur due to the addition of m_2 in correction plane 2 at each transducer n for each speed k one after the other. The following measurements shown in Table 2.2 will be acquired: W_{n2}^{k}

7.) Repeat the steps 5 and 6 for all the available correction planes for $x = 3,4,....,q$ .The measurements W_{nx}^{k} as that of step 4 and 6 will be obtained for each x .

8.) Compute the influence coefficients as follows

$$a_{nj}^{k} = \frac{W_{nj}^{k} - W_{no}^{k}}{m_j r_j e^{i\phi_j}} \tag{2.16}$$

where $j = 1,2,3.....,q$, $m_j r_j e^{i\phi j}$ is trial weight and m_j , r_j and $e^{i\phi_j}$ ($i = \sqrt{-1}$) are its mass, its radius and its phase angle.

If the trial weight is arbitrarily selected as the zero angle location, then $e^{0} = 1$.

9.) Construct the influence coefficient matrix with elements obtained in step 8:

$$\left.\begin{matrix} a_{11}^{1} & a_{12}^{1} & \cdots & a_{1q}^{1} \\ a_{21}^{1} & a_{22}^{1} & \cdots & a_{2q}^{1} \\ \vdots & \vdots & \cdots & \vdots \\ a_{n1}^{1} & a_{n2}^{1} & \cdots & a_{nq}^{1} \end{matrix}\right\} \Rightarrow a_{n1}^{1} \quad a_{n2}^{1} \quad \cdots \quad a_{nq}^{1}$$

$$\left.\begin{matrix} a_{11}^{2} & a_{12}^{2} & \cdots & a_{1q}^{2} \\ a_{21}^{2} & a_{22}^{2} & \cdots & a_{2q}^{2} \\ \vdots & \vdots & \cdots & \vdots \\ a_{n1}^{2} & a_{n2}^{2} & \cdots & a_{nq}^{2} \end{matrix}\right\} \Rightarrow a_{n1}^{2} \quad a_{n2}^{2} \quad \cdots \quad a_{nq}^{2}$$

$$\vdots$$

$$\vdots$$

$$\left.\begin{matrix} a_{11}^{k} & a_{12}^{k} & \cdots & a_{1q}^{k} \\ a_{21}^{k} & a_{22}^{k} & \cdots & a_{2q}^{k} \\ \vdots & \vdots & \cdots & \vdots \\ a_{n1}^{k} & a_{n2}^{k} & \cdots & a_{nq}^{k} \end{matrix}\right\} \Rightarrow a_{n1}^{k} \quad a_{n2}^{k} \quad \cdots \quad a_{nq}^{k}$$

Then,

$$[A]=\begin{bmatrix} a_{n1}^{1} & a_{n2}^{1} & \cdots & a_{nq}^{1} \\ a_{n1}^{2} & a_{n2}^{2} & \cdots & a_{nq}^{2} \\ \vdots & \vdots & \cdots & \vdots \\ a_{n1}^{k} & a_{n2}^{k} & \cdots & a_{nq}^{k} \end{bmatrix} \tag{2.17}$$

10.) The influence coefficient matrix $[A]$ must be square and non-singular matrix so that it can be inverted to $[A]^{-1}$. In order to achieve these requirements, p must equal to q or the number of data points must equal the number of correction planes. If balancing was carried out at a single speed (k=1), $p=n$ and the number of transducers must equal to the number of correction planes. The data set should be modified to make $p=q$ if the data obtained is more than required. This can be done by eliminating part of the data or additional data is preserved and least squares fit is applied generally to the speeds to achieve an optimum balance.

11.) Calculate the vector of correction weights, $\{U\}$ given as [6, 9, 33, 36]

$$\{U\}=-[A]^{-1}\ \{W\} \tag{2.18}$$

$$\{U\}=\begin{bmatrix} U_1 & U_2 & \cdots & U_q \end{bmatrix}^T$$

$$\{W\}=\begin{bmatrix} W_{10}^{1} & W_{20}^{1} & \cdots & W_{n0}^{1} & W_{10}^{2} & W_{20}^{2} & \cdots & W_{n0}^{2} & W_{10}^{3} & \cdots & \cdots & W_{n0}^{k} \end{bmatrix}^T$$

It can be seen in this method that the number of transducers can be reduced if more balancing speeds are to be used. It is advisable to use more than one balancing speed to apply the statistical averaging method and eliminate some measurement inaccuracies [36].

However, if the Eq. (2.16) is used as it is, the unit of elements of a_{nj}^{k} in $[A]$ will be the inverse of unit of trial weight employed (such as g^{-1}, kg^{-1} and so on). Since, two values would be obtained from each complex element U_i in $\{U\}$ in which $i = 1,2,.....,q$, then, the unit of the first value (τ_i) may be gm, kgm or any other unit of mass and radius while the second one (θ_i) will be the unit of angle in radian or degree. Therefore, for U_i, its τ_i will contain both value of correction mass and its radius of application $(m_i r_i)$ while its θ_i will be the angle at which the correction value should be applied at the balancing plane i. Then, the below equation will need to be solved to obtain the correction mass and its radius

$$\tau_i = m_i r_i \tag{2.19}$$

Here, two methods may be used to solve Eq. (2.19) but the first one is better:

1.) assumed reasonable r_i and obtain m_i

2.) assumed reasonable m_i and obtain r_i

It is imperative to know that the assumption of r_i is better to be based on the statement made by [36] that the best place where weights can be placed is where they can be captured by centrifugal force .

Similarly, all these can be avoided if the Eq. (2.16) was reformed by omitting r_j so that we have

$$a_{nj}^{k} = \frac{W_{nj}^{k} - W_{no}^{k}}{m_j e^{i\phi_j}} \tag{2.20}$$

and this will make the unit of a_{nj}^{k} in $[A]$ to be any of the following $g^{-1}m, kg^{-1}m$ or others and the unit of τ_i in U_i will be g, kg or any other unit of mass while that of θ_i will remain either radian or degree. So, $m_i \equiv \tau_i$ and r_i equals the r_j used during the trial processes.

The advantages of this method include [6, 36]:

- It is applicable to both rigid and flexible rotors
- It is readily computerized and automated
- For any number of vibration sensors it provides least-squares minimization of data.
- In case of measurement error, data manipulation have been developed for compensation
- It requires less or no insight into the physical bending modes of the rotating system

The disadvantages are [6, 36]:

- The influence coefficient is rather a mechanical method and is prone to produce less than satisfactory results initially if insensitive measurement points or correction planes were chosen
- A large number of runs is needed to be able to obtain rotor sensitivity data at highest balancing speed, It must be done on the computer because of the lengthy matrix computations
- It may even diverge temporarily before converging to a smoother running condition

- It requires large amount of test runs

2.2 Balance Quality and Balancing Trial Weight

2.2.1 Balance Quality Requirements

Balancing quality grades provide a guideline for the acceptable residual unbalance for different types of rotating machines. Several organizations provide recommended balance quality grades standards, which include the following organizations: ASA STD-1975 (ISO standard 1940/1), MIL-STD-167-1 (1974) and API standards [8, 12, 29]. The generally accepted reference for selecting rigid rotor balance quality is the International Standard ISO 1940/1. It has been paralleled approved by GERMAN Standards as VDI2060, the American National Standards Institute, ANSI, as S2.19-1975 and BRITISH Standards as BS 6861 [12].

Generally, the larger the rotor mass or the slower the rotor speed, the greater the unbalance that can be tolerated [8]. The balance quality grades (G) is based on the experience of related rotor in different groups shown in Figure 2.9. The various available groups are as shown in the Table 2.3. The ISO specification pertains to the whole rotor (total of all balance planes). In order to use this standard balance quality, the following steps need to be taken [12]:

1.) The balance quality grade "G number" should be selected from Table 2.3

2.) Determine the permissible residual specific unbalance value e_{per} from the Figure 2.9 for the rotor's maximum speed and the selected "G Number" in step 1.

TABLE 2.3: Balance Quality Grades for Various Groups of Representative Rigid Rotors

(From ISO 1940/1) [12]

Balance Quality Grade	**Product of the Relationship** $(e_{per} \times \omega)$ (1) (2) mm/s	**Rotor Types-General Examples**
G 4000	4000	Crankshaft/drives(3) of rigidly mounted slow marine diesel engines with uneven number of cylinders(4)
G 1600	1600	Crankshaft/drives of rigidly mounted large two-cycle engines
G 630	630	Crankshaft/drives of rigidly mounted large four-cycle engines Crankshaft/drives of elastically mounted marine diesel engines
G 250	250	Crankshaft/drives of rigidly mounted fast four-cylinder diesel engines(4)
G 100	100	Crankshaft/drives of fast diesel engines with six or more cylinders(4) Complete engines (gasoline or diesel) for cars, trucks and locomotives(5)
G 40	40	Car wheels, wheel rims, wheel sets, drive shafts Crankshaft/drives of elastically mounted fast four-cycle engines with six or more cylinders(4) Crankshaft/drives of engines of cars, trucks and locomotives
G 16	16	Drive shafts (propeller shafts, cardan shafts) with special requirements Parts of crushing machines Parts of agricultural machinery Individual components of engines (gasoline or diesel) for cars, trucks and locomotives Crankshaft/drives of engines with six or more cylinders under special requirements
G 6.3	6.3	Parts of plant machines Marine main turbine gears (merchant service) Centrifuge drums Paper machinery rolls; print rolls Fans Assembled aircraft gas turbine rotors Flywheels Pump impellers Machine-tool and general machinery parts Medium and large electric armatures (of electric motors having at least 80mm shaft height) without special requirements Small electric armatures, often mass produced, in vibration insensitive applications and/or with vibration-isolating mountings

		Individual components of engines under special requirements
G 2.5	2.5	Gas and steam turbines, including marine main turbines (merchant service) Rigid turbo-generator rotors Computer memory drums and discs Turbo-compressors Machines-tools drives Medium and large electric armatures with special requirements Small electric armatures not qualifying for one or both of the conditions specified for small electric armatures of balance quality grade G 6.3
G 1	1	Tape recorder and phonograph (gramophone) drives Grinding-machine drives Small electric armatures with special requirements
G 0.4	0.4	Spindles, discs and armatures of precision grinders Gyroscopes

1) $\omega = 2\pi n/60 \approx n/10$, if n is measured in revolutions per minute and ω in radians per second.

2) For allocating the permissible residual unbalance to correction planes, refer to "Allocation of U_{per} to correction Planes."

3) A crankshaft/drive is an assembly which includes a crankshaft, flywheel, clutch, pulley, vibration damper, rotating portion of connecting rod, etc.

4) For the purposes of this part of ISO 1940/1, slow diesel engines are those with a piston velocity of less than 9m/s; fast diesel engines are those with a piston velocity of greater than 9m/s.

5) In complete engines, the rotor mass comprises the sum of all masses belonging to the crankshaft/drive described in note 3 above.

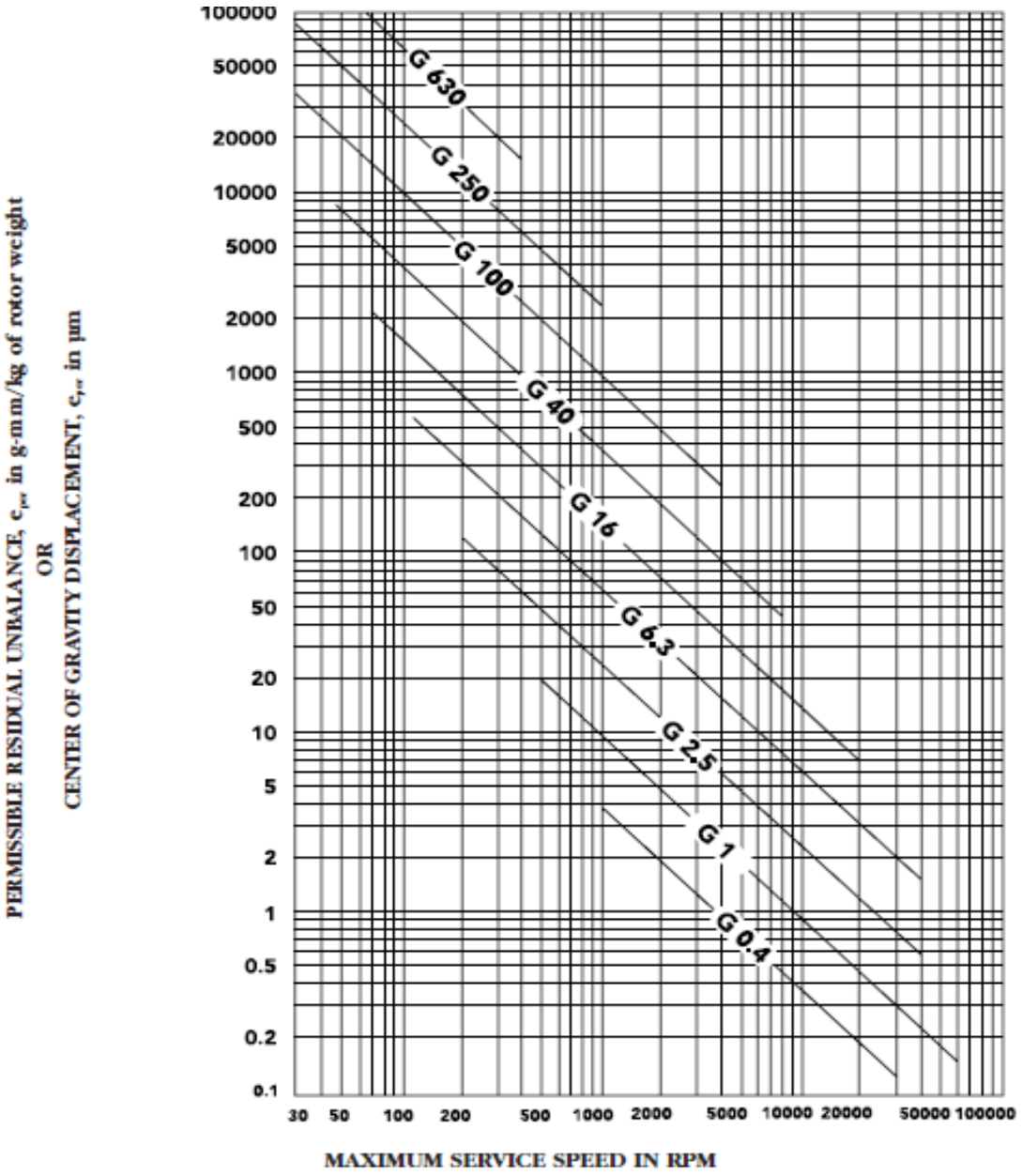

FIGURE 2.9: Maximum Permissible Residual Unbalance, e_{per} (From ISO 1940/1) [12]

3.) Multiply rotor weight by the e_{per} obtained in step 2 to acquire the permissible residual unbalance U_{per}.

4.) Base on the rotor configuration; allocate U_{per} to the balancing correction planes.

The "G Number" is constant for rotors of the same type and is the product of specific unbalance and the angular velocity of the rotor at maximum operating speed, that is [12]

$$G = e * \omega \tag{2.21}$$

This is based on the fact that identical rotors geometrically running at the equal speed will have similar stresses in the rotor and its bearings. The quality grades are separated by a factor 2.5 and to be able to suit special requirements the G numbers of midway value may be utilized.

2.2.2 Permissible Residual Unbalance and Trial Weight

The permissible residual unbalance U_{per} is a function of G number, maximum service speed of rotation and rotor weight. It can be determined as follows [4, 12]

$$U_{per} = e_{per} * m \tag{2.22}$$

where e_{per} and m are permissible residual specific unbalance and rotor mass.

Also, for flexible rotor, the permitted maximum residual unbalance for a rotor or in a correction plane can be obtained from Eq. (2.22).

However, the use of Figure 2.9 to obtain U_{per} in Eq. (2.22) can be avoided and the following equations can be used to obtain U_{per} [12]

$$U_{per}(g-mm) = 9549 \times G \times \frac{W}{N} \quad (W \ \ in \ \ kg) \tag{2.23}$$

$G =$ Balance quality grade from Table 2.3, $W =$ Rotor weight and $N =$ Maximum service (RPM). In addition, from some balancing machine manufacturers a slide rule that calculates U_{per} is also available.

Besides, a trial or test weight is to be added temporarily at each selected correction plane of the rotor during the balancing processes to determine the relationship between unbalance and vibration. The trial weight w_t for the flexible rotor can also be obtained as follow [29]:

$$w_t = \frac{12700 \times m_r}{N \times R} \quad (g) \tag{2.24}$$

Whereby $m_r =$ Mass of rotor (kg), $N =$ Maximum operating speed (rpm) and $R =$ radius of balancing plane (mm)

This trial weight should not be too large to the extent that it will cause damage due to unnecessary vibration but should be large enough to produce sufficient amplitude change. The universal criteria being in used is to select a trial weight that will produce a force of 10% of the rotor weight [36]. Therefore, the additional dynamic load as a result of trial weight due to this criterion will not more than 10% of the static load and this is absolutely safe. Although, an additional dynamic load up to 50% is also acceptable for short runs. The equation for calculating the trial weight w_t due to 10% criteria for flexible rotor is given as [36]:

$$w_t = \frac{56375 \times w_r}{N^2 \times R} \times 28.35 \quad (g) \tag{2.25}$$

in which $w_r = \text{Static weight of rotor}\,(lbf)$, $N = \text{Speed of rotor}\,(rpm)$ and $R = \text{Radius of}$ trial weight (in). The above equation is too conservative for rigid rotor, hence, the trial weight for rigid rotor can be calculated from the equation and the value obtain can be increased until the sufficient change is produced [36].

As a general rule, a trial weight should be selected that will cause a 30% change in amplitude or a 30-degree shift in the reference mark location. Changes of this magnitude will ensure that accurate results are obtained. A common practice used in selecting the trial weight, is selecting a mass that will produce a force *F* equal to 10% of the rotor weight on the supporting bearings, then, the resulting imbalance w_t is given by

$$w_t = \frac{91.19 \times F}{N^2} \quad (kg.m) \tag{2.26}$$

$$F = \frac{w_r}{Nb} 10\% \quad (N)$$

where w_r, N and Nb are weight of rotor, rotor operation speed and number of bearing that rotor contained respectively.

Moreover, since the trial weight needs to be large enough to cause an obvious, measurable change (> 25% in amplitude and/or 30° in angle) in the unbalance value, it is recommended that a diversity of trial weights be prepared since the actual mass cannot be determined in advance. Hence, the mass of the trial weight can also be obtained by using the following "rule-of-thumb" if there has been no previous experience with the rotor but this should be used with caution and it is not a rigid rule [4, 36]

$$w_t = 30 \times \frac{w_r}{R} \quad (g) \tag{2.27}$$

where w_t, w_r *and* R are mass of trial weight (g), mass of rotor (kg) and radius of trial weight (mm) respectively. A trial weight greater than the one calculated from the above formula may be essential in the case of heavy and slow-running machines while for machines with a lower dynamic stiffness or in the case of high-speed machines, a considerably smaller trial weight may be enough.

In order to find out if the trial weight is sufficient or if the mass should be changed, the simplest way is to carry out a test run. However, instead of removal by drilling or grinding it is simpler for the trial weight and correction weights to be effected by the addition of mass to the rotor. Apart from the fact that weight addition is more precise, weight removal should only be utilized when weight addition is impossible, e.g. for reasons of safety [4].

CHAPTER 3

ROTOR FINITE ELEMENT MODEL FORMULATION

In this chapter, the elastodynamic model of the rotor-bearing system with multi-disk arrangement is presented. The finite element model will be augmented with mass unbalance and material damping. This finite element model is required to develop the mathematical procedure of the low-speed balancing scheme.

It always becomes imperative to know quantitatively the natural frequencies, vibration modes and response to unbalance excitations in the design of a practical rotor. FEM is one of the methods being used for this purpose. FEM is the discretization method of a continuous structure. It has been utilized effectively in design and analysis of practical rotors with a complex and irregular shapes. The rotor bearing system is divided into three components which include shaft, disc and bearing. Each of these divisions need to be modeled in order to formulate its equation of motion and the general equations of motion will then be acquired from those formulations.

The analysis of a continuous rotor is based on the theory of beam lateral vibrations. The Bernoulli-Euler beam theory is the most basic in this regard and the derivation of the equations of motion of a simple continuous rotor based on this theory. These equations represent correctly the motion of slender rotor. However, the effect of rotary inertia and shear deformation occur when the wavelength of vibration mode

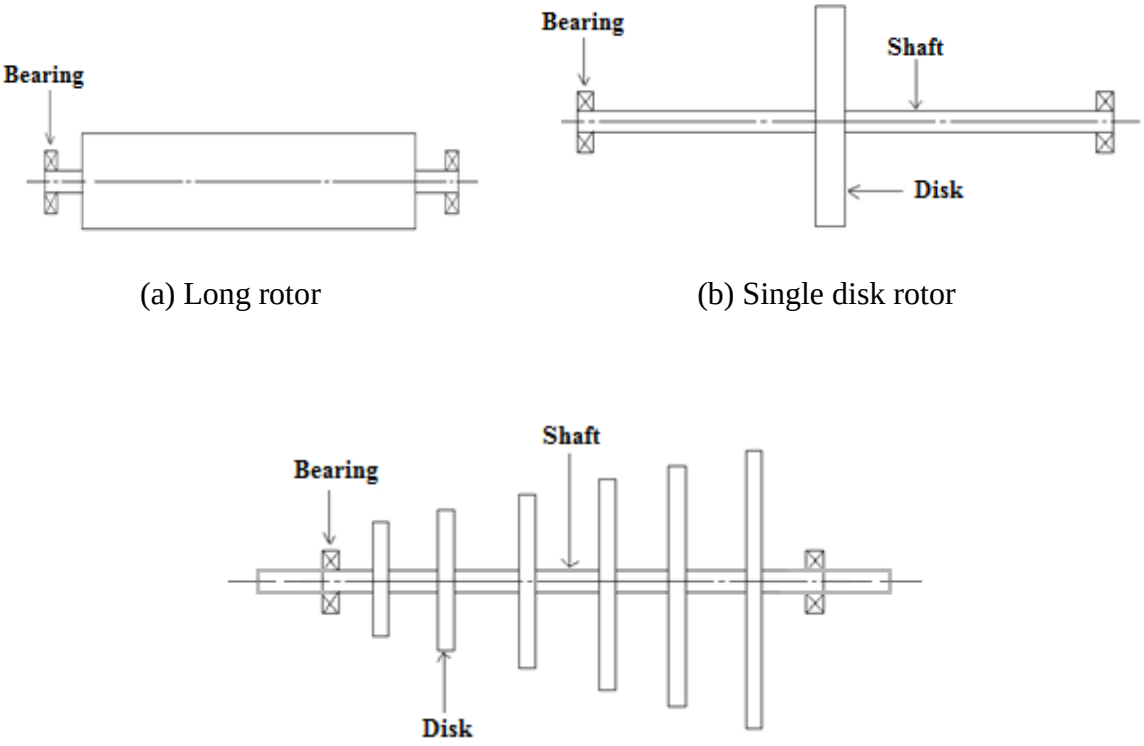

(a) Long rotor

(b) Single disk rotor

(c) Multi disk rotor

FIGURE 3.1: Possible Types of Rotor

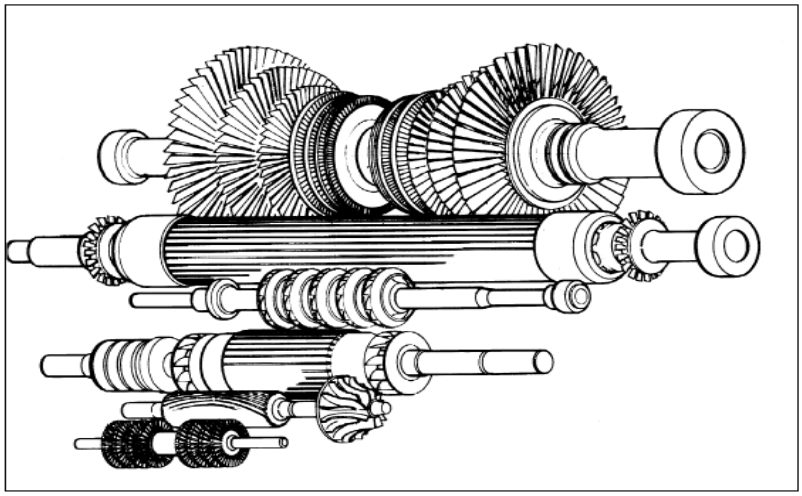

FIGURE 3.2: Complex Rotor Shapes [4]

relative to the beam thickness becomes small. The Timoshenko beam is the beam model that takes these two effects into consideration. Similarly, in rotor analysis these two effects will surface in

addition to gyroscopic moment when the ratio of the diameter to the length increases [38].

However, in modeling, rotors are often model by circular shaft elements with four nodal degrees of freedom. Similarly, the disk can be modeled as either rigid or flexible disk [28]. The rotor can be long type, contain one or more disk as shown in the Figure 3.1 while the examples of more complex shape rotors are as shown in Figure 3.2.

3.1 Elastodynamic Modeling of the Rotor

The FEM elastodynamic model of the rotor-bearing system presented in this chapter is based on the work of Khulief and Mohiuddin [14, 15, 16, 17, 19]. The model is extended to account for unbalance, which can be placed at any desired location on the rotor. Material damping is also added to this rotor model.

The basic elements of the rotor, in general, are the shaft, the disk, and the bearings. For realistic dynamic analysis of rotors, the following important features need to be accounted for in the derived dynamic model:

- Shear and rotary inertia effects
- Gyroscopic effects, which couple the rotational motions in two perpendicular directions.
- The variable shaft geometry; e.g. tapered, stepped, solid, as well as hollow shaft sections.

- Type of bearings; e.g. rigid, isotropic, orthotropic, etc.
- Internal damping and fluid dynamic effects.

In this chapter, the general assumptions are stated, the kinetic and potential energies are obtained, and the general equations of motion are derived using the Lagrangean approach. The elastic component of the rotor to be analyzed is shown in Figure 3.3. The rotor length L is rotating at a speed of $\dot{\theta}(t)$. Two reference frames are used to describe the system motion; the first is the fixed reference frame $R_o(X\ Y\ Z)$, and the second is a rotating reference frame $R(x\ y\ z)$. The *X*-axis and *x*-axis are collinear and coincident with the rotor's centerline. The two reference frames are phased out by an angle θ. In addition, the following assumptions are considered:

1. The material of the rotor is elastic, homogeneous and isotropic.
2. Plane cross sections, initially perpendicular to the neutral axis of the rotor, remain plane put no longer perpendicular to the neutral axis during bending.
3. The deflection of the rotor is produced by displacement of points of its centerline.
4. The axial deformation of the rotor is small and can be neglected.
5. The shaft is flexible, while disks are treated as rigid.

3.2 Generalized Coordinates

For completeness, the model derivation will be briefly presented here; thus arriving at the final rotor equations with unbalance to be employed in the formulation of the low-speed balancing scheme.

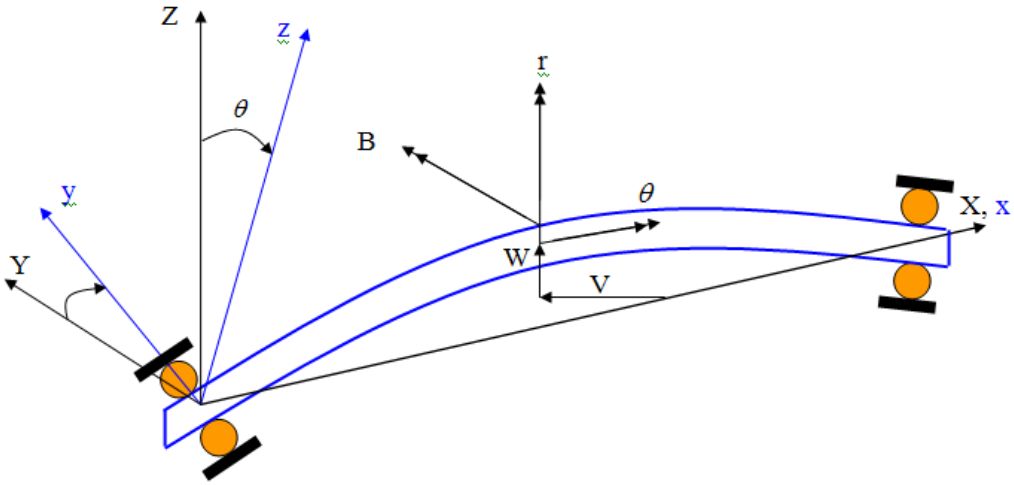

FIGURE 3.3: Flexible Rotor Component

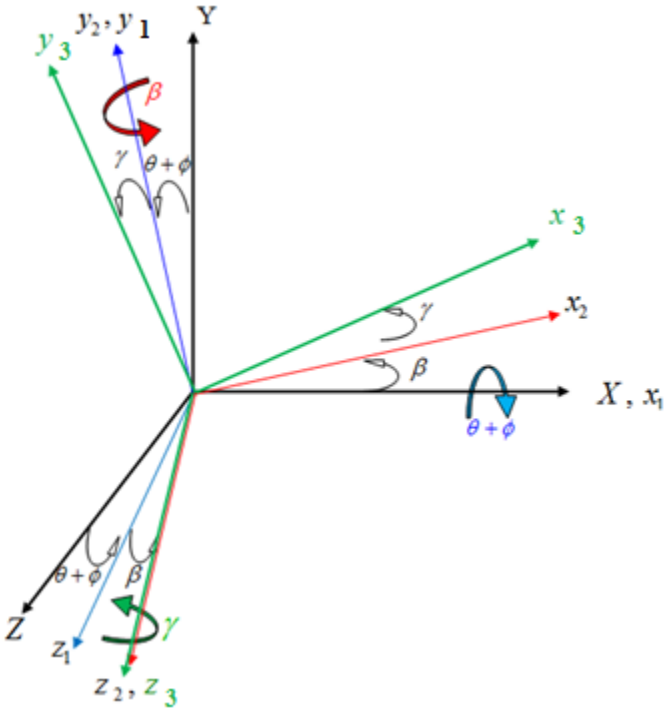

FIGURE 3.4: Cross-Section Rotational Angles [17]

The finite element method is used to model the rotor shaft. Let XYZ be a global Cartesian coordinate system with its origin fixed to the undeformed shaft element.

The $x_i y_i z_i$ $(i = 1,2,3)$ is a local Cartesian coordinate system after the deformation of the element. The local coordinate system $x_i y_i z_i$ is related to the global coordinate system XYZ by a set of rotations ϕ , β and γ. To achieve the orientation of any cross-section of the shaft element, one first rotates it by an angle $(\theta + \phi)$ about the $X - axis$, then by an angle β about the new *y-axis* (denoted by y_1), and finally by an angle γ about the final *z-axis* (denoted by z_2), as shown in Figure 3.4. The instantaneous angular velocity vector $\overline{\omega}$ of the $x\ y\ z$ frame may be expressed as

$$\overline{\omega} = (\dot{\theta} + \dot{\phi})\hat{I} + (\dot{\beta})\hat{j}_1 + (\dot{\gamma})\hat{k}_1 \tag{3.1}$$

Where $I, \hat{j}_1$ *and* $\hat{k}_1$ are unit vectors along the I, y_1 *and* z_1 axes, respectively. The term $\dot{\theta}$ is the constant angular velocity of the rotary table. Transforming Eq. (3.1) into $X\ Y\ Z$ coordinate leads to the following expression:

$$\begin{aligned}\overline{\omega} = (\dot{\theta} + \dot{\phi})\hat{I} + \dot{\beta}[\cos(\theta + \phi)\hat{J} + \sin(\theta + \phi)\hat{K}] \\ + \dot{\gamma}[-\sin\beta\hat{I} - \sin(\theta + \phi)\cos(\beta)\hat{J} + \cos\beta\cos(\theta + \phi)\hat{K}]\end{aligned} \tag{0.2}$$

Assuming β and γ are so small deformations. Therefore, according to the linear theory of elasticity, the following substitutions have been made in equation (0.2):

$$\cos\beta = \cos\gamma = 1$$
$$\sin\beta = \beta \quad and \quad \sin\gamma = \gamma$$

Equation (3.2) can be rewritten as:

$$\begin{aligned}\bar{\omega} &= \left(\dot{\theta}+\dot{\phi}\right)\hat{I} + \dot{\theta}_y\left[\cos\left(\theta+\phi\right)\hat{J} + \sin\left(\theta+\phi\right)\hat{K}\right] \\ &+ \dot{\theta}_z\left[-\theta_y\hat{I} - \sin\left(\theta+\phi\right)\hat{J} + \cos\left(\theta+\phi\right)\hat{K}\right] \\ &= \left(\dot{\theta}+\dot{\phi}-\dot{\gamma}\,\beta\right)\hat{I} + \left[\dot{\beta}\cos\left(\theta+\phi\right) - \dot{\gamma}\sin\left(\theta+\phi\right)\right]\hat{J} \\ &+ \left[\dot{\beta}\sin\left(\theta+\phi\right) + \dot{\gamma}\cos\left(\theta+\phi\right)\right]\hat{K}\end{aligned} \tag{3.3}$$

or

$$\bar{\omega} = \begin{Bmatrix}\omega_x \\ \omega_y \\ \omega_z\end{Bmatrix} = \begin{Bmatrix}\dot{\theta}+\dot{\phi}-\dot{\gamma}\,\beta \\ \dot{\beta}\cos\left(\theta+\phi\right) - \dot{\gamma}\sin\left(\theta+\phi\right) \\ \dot{\beta}\sin\left(\theta+\phi\right) + \dot{\gamma}\cos\left(\theta+\phi\right)\end{Bmatrix} \tag{3.4}$$

3.3 Kinetic Energy Expression

Referring to Figure 3.5, consider an arbitrary point p^i on the undeformed shaft element. With respect to $X^i\ Y^i\ Z^i$ coordinate system, point p^i is defined by the vector $\bar{r}_0$. Point p^i is then transformed into point p in the deformed state of the element. The location of p with respect to $X^i\ Y^i\ Z^i$ coordinate system is given by the vector $\bar{r}$. The global position of point p is defined by vector $\bar{r}_p$.

$$\bar{r}_p = \bar{R} + \bar{r} \tag{3.5}$$

where $\bar{R}$ defines the location of the origin of the $X^i\ Y^i\ Z^i$ coordinate system with respect to global coordinate system $X\ Y\ Z$. The vector $\bar{r}$ can be represented as

$$\bar{r} = \bar{r}_0 + \bar{u} \tag{3.6}$$

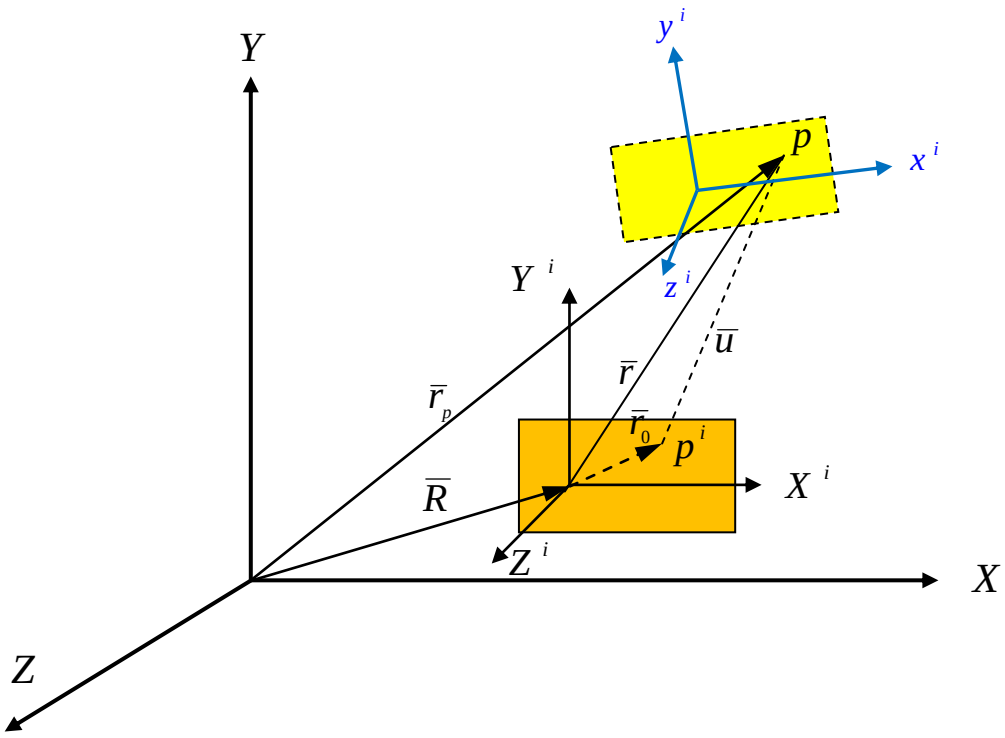

FIGURE 3.5: Generalized Coordinate of the Element [17]

Therefore, the position vector $\bar{r}_p$ of point *p* can be written as

$$\bar{r}_p = \bar{R} + \bar{r}_0 + \bar{u} \tag{3.7}$$

where $\bar{u}$ represents the deformation vector of point p^i. Differentiating $\bar{r}_p$ with respect to time yields the velocity of point p as

$$\begin{aligned} \frac{d\bar{r}_p}{dt} &= \dot{\bar{r}}_p + \bar{\omega} \times \bar{r}_p \\ &= \dot{\bar{r}}_p + [\tilde{\omega}]\{r_p\} \end{aligned} \tag{3.8}$$

where (·) denotes differentiation with respect to time and the skew symmetric matrix $[\tilde{\omega}]$ is given by

$$[\tilde{\omega}] = \begin{bmatrix} 0 & -\omega_z & \omega_y \\ \omega_z & 0 & -\omega_x \\ -\omega_y & \omega_x & 0 \end{bmatrix}$$

Using the finite element discretization method, the vector $\bar{u}$ can be written as

$$\bar{u} = \{u\} = [N_v]\{e\} \tag{3.9}$$

where $\{e\}$ is the vector containing the nodal coordinates and $[N_v]$ is the translation shape function. There is no change in the magnitude of $\bar{R}$ and $\bar{r}_0$ when the element deforms. Therefore the rate of change of magnitude of the position vector $\bar{r}_p$ is given by:

$$\{\dot{r}_p\} = \{\dot{u}\} = [N_v]\{\dot{e}\} \tag{3.10}$$

Substituting equation (3.10)(3.10) in equation (3.8), we get

$$\frac{d\bar{r}_p}{dt} = [N_v]\{\dot{e}\} + [\tilde{\omega}]\{r_p\}$$
$$= [N_v \quad \tilde{\omega}]\begin{Bmatrix} \dot{e} \\ r_p \end{Bmatrix}$$

The kinetic energy of the element is obtained by integrating the kinetic energy of the infinitesimal volume at point *p* over the volume *V*

$$KE = \frac{1}{2}\int_V \mu \left\{\frac{dr_p}{dt}\right\}^T \left\{\frac{dr_p}{dt}\right\}$$
$$= \frac{1}{2}\int_V \mu \begin{bmatrix} \dot{e}^T & r_p{}^T \end{bmatrix} \begin{Bmatrix} N_v{}^T \\ \tilde{\omega}^T \end{Bmatrix} [N_v \quad \tilde{\omega}] \begin{Bmatrix} \dot{e} \\ r_p \end{Bmatrix} dV$$

$$= \frac{1}{2}\int_V \mu [\ \{\dot{e}\}^T [N_v]^T [N_v]\{\dot{e}\} + \{\dot{e}\}^T [N_v]^T [\tilde{\omega}]\{r_p\}$$
$$+ \{r_p\}^T [\tilde{\omega}]^T [N_v]\{\dot{e}\} + \{r_p\}^T [\tilde{\omega}]^T [\tilde{\omega}]\{r_p\}\ ] dV \qquad (3.11)$$

where μ is the mass density of the element. The first term in equation (3.11)(3.11) gives the kinetic energy due to translation; the second and third terms are identically zero if moments of inertia are calculated with respect to center of mass of the element. The last term gives kinetic energy due to rotation that includes gyroscopic moments. To evaluate the last term, one can utilize the following expression:

$$[\tilde{\omega}]^T [\tilde{\omega}] = \begin{bmatrix} \omega_z^2 + \omega_y^2 & -\omega_x\omega_y & -\omega_z\omega_x \\ -\omega_x\omega_y & \omega_z^2 + \omega_x^2 & -\omega_y\omega_z \\ -\omega_x\omega_z & -\omega_y\omega_z & \omega_y^2 + \omega_x^2 \end{bmatrix} \qquad (3.12)$$

Therefore,

$$\textbf{The term:}\quad \frac{1}{2}\int_V \mu\{r_p\}^T\,[\tilde{\omega}]^T\,[\tilde{\omega}]\{r_p\}dV = \frac{1}{2}\int_0^l \mu\left(I_x\omega_x^2 + I_y\omega_y^2 + I_z\omega_z^2\right)dx \tag{3.13}$$

Substituting equation (3.12) in equation (3.13)(, we obtain

$$\begin{aligned}\int_V \mu\{r_p\}^T\,[\tilde{\omega}]^T\,[\tilde{\omega}]\{r_p\}dV = \int_0^l \mu\Big\{ & I_x\left(\dot{\theta}+\dot{\phi}-\dot{\gamma}\,\dot{\beta}\right)^2 \\ & + I_y\left(\dot{\beta}\cos(\theta+\varphi)-\dot{\gamma}\sin(\theta+\varphi)\right)^2 + I_z\left(\dot{\beta}\sin(\theta+\varphi)+\dot{\gamma}\cos(\theta+\varphi)\right)^2\Big\}dx\end{aligned} \tag{3.14}$$

Equation (3.14) can be written in the form

$$\begin{aligned}\frac{1}{2}\int_V \mu\{r_p\}^T\,[\tilde{\omega}]^T\,[\tilde{\omega}]\{r_p\}dV &= \frac{1}{2}I_p\left(\dot{\theta}^2+\dot{\varphi}^2\right)dx + \int_0^l I_p\,\dot{\theta}\dot{\varphi}dx \\ &\quad - \int_0^l I_p\left(\dot{\theta}+\dot{\phi}\right)\dot{\gamma}\,\beta\,dx + \frac{1}{2}\int_0^l I_D\left(\dot{\beta}^2+\dot{\gamma}^2\right)dx\end{aligned} \tag{3.15}$$

or simply

$$\begin{aligned}\frac{1}{2}\int_V \mu\{r_p\}^T\,[\tilde{\omega}]^T\,[\tilde{\omega}]\{r_p\}dV &= \frac{1}{2}\int_0^l I_p\,\dot{\theta}^2dx + \frac{1}{2}\int_0^l I_p\,\dot{\varphi}^T\,\dot{\varphi}dx \\ &\quad + \int_0^l I_p\,\dot{\theta}\dot{\varphi}dx - \int_0^l I_p\left(\dot{\theta}+\dot{\phi}\right)\dot{\gamma}^T\,\beta\,dx + \int_0^l I_D\begin{Bmatrix}\dot{\beta}\\ \dot{\gamma}\end{Bmatrix}^T\begin{Bmatrix}\dot{\beta}\\ \dot{\gamma}\end{Bmatrix}dx\end{aligned} \tag{3.16}$$

where

$$\mu I_y = \mu I_z = I_D \quad \text{and} \quad \mu I_x = I_p$$

One can express the following variables as:

$$\begin{aligned}\varphi &= \left[N_\varphi\right]\{e\}, \qquad \dot{\varphi} = \left[N_\varphi\right]\{\dot{e}\} \\ \beta &= \left[N_\beta\right]\{e\}, \qquad \dot{\beta} = \left[N_\beta\right]\{\dot{e}\} \\ \gamma &= \left[N_\gamma\right]\{e\}, \qquad \dot{\gamma} = \left[N_\gamma\right]\{\dot{e}\}\end{aligned} \tag{3.17}$$

where

$\left[N_{\varphi}\right] \equiv$ torsional shape function, $[N_{\beta}]$ *and* $[N_{\gamma}] \equiv$ rotational shape function

Therefore, equation (3.16) becomes

$$\begin{aligned}\frac{1}{2}\int_V \mu\left\{r_p\right\}^T\left[\tilde{\omega}\right]^T\left[\tilde{\omega}\right]\left\{r_p\right\}dV &= \frac{1}{2}\int_0^l I_p\,\dot{\theta}^2\,dx + \frac{1}{2}\int_0^l \left\{\dot{e}\right\}^T\left[N_{\varphi}\right]^T I_p\left[N_{\varphi}\right]\left\{\dot{e}\right\}dx \\ &+ \int_0^l I_p\,\dot{\theta}\dot{\varphi}\,dx - \int_0^l \left\{\dot{e}\right\}^T\left[N_{\gamma}\right]^T I_p\,\dot{\theta}\left[N_{\beta}\right]\{e\}dx \\ &- \int_0^l \left\{\dot{e}\right\}^T\left[N_{\gamma}\right]^T I_p\,\dot{\theta}\left[N_{\beta}\right]\{e\}\left[N_{\varphi}\right]\left\{\dot{e}\right\}dx \\ &+ \frac{1}{2}\int_0^l \left\{\dot{e}\right\}^T\begin{bmatrix}N_{\beta}\\ N_{\gamma}\end{bmatrix}^T I_D\begin{bmatrix}N_{\beta}\\ N_{\gamma}\end{bmatrix}\left\{\dot{e}\right\}dx\end{aligned} \tag{3.18}$$

The term $\int_0^l I_p\,\dot{\theta}\dot{\varphi}dx$ gives the inertia coupling between rigid body coordinates and elastic coordinates.

For constant $\dot{\theta}$ this term has no contribution to the equation of motion of the rotor. Neglecting this term and introducing the following expressions:

$$\int_0^l I_p\,dx = C_1$$

$$\int_0^l I_p\left[N_{\varphi}\right]^T\left[N_{\varphi}\right]dx = \left[M_{\varphi}\right]$$

$$\int_0^l I_p\left[N_{\gamma}\right]^T\left[N_{\beta}\right]dx = \left[G_1\right]$$

$$\int_0^l I_p\left[N_{\gamma}\right]^T\left[N_{\beta}\right]\{e\}\left[N_{\varphi}\right]dx = \left[M_e\right]$$

and

$$\int_0^l I_D\begin{bmatrix}N_{\beta}\\ N_{\gamma}\end{bmatrix}^T\begin{bmatrix}N_{\beta}\\ N_{\gamma}\end{bmatrix}dx = \left[M_r\right]$$

Equation (3.18) reduces to

$$\frac{1}{2}\int_V \mu\{r_p\}^T[\tilde{\omega}]^T[\tilde{\omega}]\{r_p\}dV = \frac{1}{2}C_1\dot{\theta}^2 + \frac{1}{2}\{\dot{e}\}^T[M_o]\{\dot{e}\} - \dot{\theta}\{\dot{e}\}^T[G_1]\{e\} - \{\dot{e}\}^T[M_e]\{\dot{e}\} + \frac{1}{2}\{\dot{e}\}^T[M_r]\{\dot{e}\} \tag{3.19}$$

Hence, the kinetic energy of the shaft element given by Equation (3.11) can be written as

$$\begin{aligned} T &= \frac{1}{2}\{\dot{e}\}^T[M_t]\{\dot{e}\} + \frac{1}{2}C_1\dot{\theta}^2 + \frac{1}{2}\{\dot{e}\}^T[M_o]\{\dot{e}\} - \dot{\theta}\{\dot{e}\}^T[G_1]\{e\} \\ &\quad - \{\dot{e}\}^T[M_e]\{\dot{e}\} + \frac{1}{2}\{\dot{e}\}^T[M_r]\{\dot{e}\} \\ &= \frac{1}{2}\{\dot{e}\}^T[M]\{\dot{e}\} + \frac{1}{2}C_1\dot{\theta}^2 - \dot{\theta}\{\dot{e}\}^T[G_1]\{e\} \end{aligned} \tag{3.20}$$

where $\dot{\theta}$ denotes the rigid body rotation and $[M]$ is the augmented mass matrix, as given by

$$[M] = [M_t] + [M_r] + [M_\varphi] - 2[M_e] \tag{3.21}$$

3.4 Strain Energy Expression

Since the axial deformation is neglected, a typical cross-section of the shaft located at a distance x from the left end, in a deformed state, is described by the translations $v(x, t)$ and $w(x, t)$ in the Y- and Z-directions and small rotations $\varphi(x, t)$, $\beta(x, t)$, and $\gamma(x, t)$ about X, j_2, and k axes, respectively. The two translations (v, w) consist of a contribution (v_b, w_b) due to bending and a contribution (v_s, w_s) due to shear deformations. These may be written as

$$\begin{aligned} v(x, t) &= v_b(x, t) + v_s(x, t) \\ w(x, t) &= w_b(x, t) + w_s(x, t) \end{aligned} \tag{3.22}$$

The rotations (β, γ) are related to bending deformations (v_b, w_b) by the following expressions:

$$\beta(x, t) = -\frac{\partial w_b(x, t)}{\partial x}$$
$$\gamma(x, t) = \frac{\partial v_b(x, t)}{\partial x} \tag{3.23}$$

The strain energy expression is

$$U_1 = \frac{1}{2}\int_V \varepsilon' \sigma \, dV \tag{3.24}$$

where ε is the strain due to bending, which can be expressed as

$$\varepsilon = -y\frac{\partial^2 v_b^*}{\partial x^2} - z\frac{\partial^2 w_b^*}{\partial x^2} \tag{3.25}$$

Recalling the stress-strain relationship $\sigma = E\varepsilon$, one can write the strain energy in the form

$$U_1 = \frac{E}{2}\int_V \varepsilon' \varepsilon \, dV = \frac{E}{2}\int_V \varepsilon^2 \, dV \tag{3.26}$$

Using Eq. (3.25) into Eq. (3.26), one gets

$$\begin{aligned} U_1 &= \frac{E}{2}\int_0^l \int_A \left(-y\frac{\partial^2 v_b^*}{\partial x^2} - z\frac{\partial^2 w_b^*}{\partial x^2}\right)^2 dA\, dx \\ &= \int_0^l \int_A \left[y^2\left(\frac{\partial^2 v_b^*}{\partial x^2}\right)^2 + z^2\left(\frac{\partial^2 w_b^*}{\partial x^2}\right)^2 + 2yz\frac{\partial^2 v_b^*}{\partial x^2}\frac{\partial^2 w_b^*}{\partial x^2}\right] dA\, dx \end{aligned} \tag{3.27}$$

Because of symmetry the integral corresponding to the third term in Eq. (3.27) is zero. We have designated the following:

$$I_z = \int_A y^2 \, dA \qquad \text{and} \qquad I_y = \int_A z^2 \, dA \tag{3.28}$$

Therefore, the strain energy due to bending is given by

$$U_1 = \frac{E}{2}\int_0^l \left[I_z \left(\frac{\partial^2 v_b^*}{\partial x^2} \right)^2 + I_y \left(\frac{\partial^2 w_b^*}{\partial x^2} \right)^2 \right] d\,x \tag{3.29}$$

The shear strain in X-Z plane is

$$v_{xz} = \frac{\partial v}{\partial z} + \frac{\partial w_s}{\partial x} = \frac{\partial w^*}{\partial x} - \frac{\partial w_b^*}{\partial x} \tag{3.30}$$

Similarly, shear strain in X-Y plane is

$$v_{xy} = \frac{\partial v^*}{\partial x} - \frac{\partial v_b^*}{\partial x} \tag{3.31}$$

Now, the strain energy due to shear deformation is given by

$$U_2 = \int_V \left(\tau_{xy} v_{xy} + \tau_{xz} v_{xz} \right) dV \tag{3.32}$$

The shear stress τ_{xy} corresponding to a given shear force varies over the cross-section. It follows that the corresponding shear strain will also vary over the cross-section. This variation can be accounted for by introducing the shear correction factor κ, which depends upon the shape of the cross-section, such that

$$\tau_{xy} = \kappa G v_{xy} \quad and \quad \tau_{xz} = \kappa G v_{xz} \tag{3.33}$$

For an isotropic material the shear modulus G is given by

$$G = \frac{E}{2(1+v)} \tag{3.34}$$

where v is Poisson's ratio. The shear correction factor κ is given for solid circular cross-section as

$$\kappa = \frac{6(1+v)}{7+6v} \tag{3.35}$$

and for hollow circular cross-section by

$$\kappa = \frac{6(1+\nu)\left(1+\varsigma^2\right)^2}{(7+6\nu)\left(1+\varsigma^2\right)^2 + (20+12\nu)\varsigma^2} \tag{3.36}$$

where ς is the ratio of inner radius to the outer radius. Therefore, Eq. (3.32) can be expressed in the form

$$\begin{aligned} U_2 &= \frac{1}{2}\int_V \kappa G\left(v_{xy}^2 + v_{xz}^2\right) \\ &= \frac{1}{2}\int_0^l \kappa G\, A(x)\left[\left(\frac{\partial v^*}{\partial x} - \frac{\partial v_b^*}{\partial x}\right)^2 + \left(\frac{\partial w^*}{\partial x} - \frac{\partial w_b^*}{\partial x}\right)^2\right] dx \end{aligned} \tag{3.37}$$

Expressing the strain energies as a function of *v* and *w* components of displacement in R_0(XYZ) using

$$\begin{aligned} v^* &= v\cos\theta - w\sin\theta \\ w^* &= v\sin\theta + w\sin\theta \end{aligned} \tag{3.38}$$

we get

$$\begin{aligned} U_1 = \frac{E}{2}\int_0^l I_z \Bigg[&\left(\cos\theta\,\frac{\partial^2 v_b}{\partial x^2} - \sin\theta\,\frac{\partial^2 w_b}{\partial x^2}\right)^2 \\ &+ I_y\left(\cos\theta\,\frac{\partial^2 w_b}{\partial x^2} + \sin\theta\,\frac{\partial^2 v_b}{\partial x^2}\right)^2\Bigg] dx \end{aligned} \tag{3.39}$$

Since the shaft is symmetric ($I_y = I_z = I$), the strain energy due to bending becomes

$$\begin{aligned} U_1 &= \frac{E}{2}\int_0^l I(x)\left[\left(\frac{\partial^2 v_b}{\partial x}\right)^2 + \left(\frac{\partial^2 w_b}{\partial x}\right)^2\right] dx \\ &= \frac{E}{2}\int_0^l I(x)\left[\left(\frac{\partial \gamma}{\partial x}\right)^2 + \left(\frac{\partial \beta}{\partial x}\right)^2\right] dx \end{aligned} \tag{3.40}$$

Similarly the strain energy due to shear becomes

$$U_2 = \frac{1}{2}\int_0^l \kappa G\, A(x)\left[\left(\frac{\partial^2 v_s}{\partial x^2}\right)^2 + \left(\frac{\partial^2 w_s}{\partial x^2}\right)^2\right] d\,x \tag{3.41}$$

Also, the strain energy due to torsion is given by

$$U_3 = \frac{1}{2}\int_0^l G\, J\left(\frac{\partial \varphi}{\partial x}\right)^2 d\,x \tag{3.42}$$

Therefore, the total strain energy of the rotor shaft is

$$\begin{aligned} U = {} & \frac{1}{2}\int_0^l E\, I\,(x)\left[\left(\frac{\partial \gamma}{\partial x}\right)^2 + \left(\frac{\partial \beta}{\partial x}\right)^2\right] d\,x \\ & + \frac{1}{2}\int_0^l \kappa G\, A(x)\left[\left(\frac{\partial v_2}{\partial x}\right)^2 + \left(\frac{\partial 2_2}{\partial x}\right)^2\right] d\,x + \frac{1}{2}\int_0^l G\, J\left(\frac{\partial \varphi}{\partial x}\right)^2 d\,x \end{aligned} \tag{3.43}$$

After substituting Eq. (3.22) and Eq. (3.23) into Eq. (3.43), one gets

$$\begin{aligned} U = {} & \frac{1}{2}\int_0^l E\, I\left\{\left(\frac{\partial \beta}{\partial x}\right)^2 + \left(\frac{\partial \gamma}{\partial x}\right)^2\right\} d\,x \\ & + \frac{1}{2}\int_0^l \kappa G\, A\left\{\left(\frac{\partial v}{\partial x} - \gamma\right)^2 + \left(\frac{\partial w}{\partial x} - \beta\right)^2\right\} d\,x + \frac{1}{2}\int_0^l G\, J\left(\frac{\partial \varphi}{\partial x}\right)^2 d\,x \end{aligned} \tag{3.44}$$

Eq. (3.44) can be written in matrix form as

$$[U] = \frac{1}{2}\{e\}^T \,|\, K \,|\, \{e\} \tag{3.45}$$

where $|K|$ is the augmented stiffness matrix given by

$$[K] = [K_e] + [K_s] + [K_\varphi] \tag{3.46}$$

where $[K_e]$ = elastic stiffness matrix, $[K_s]$ = shear stiffness matrix, and

$[K_\varphi]$ = torsional stiffness matrix

3.5 Equation of Motion of the Shaft Element

The equation of motion of the element can be derived using Lagrange's equation, which can be mathematically written as

$$\frac{d}{dt}\left(\frac{\partial L}{\partial q}\right) - \frac{\partial L}{\partial q} = Q \tag{3.47}$$

where

$L = T - U$ = Lagrangean function, q = generalized coordinates and Q = vector of generalized forces

Substituting L in the above equation, the equations of motion are obtained as

$$C_1 \ddot{\theta} = Q \tag{3.48}$$

where C_1 is as defined in Eq. (3.19) and

$$|M|\{\ddot{e}\} - \dot{\theta}\left(|G_1|^T - |G_1|\right)\{\dot{e}\} + [K]\{e\} = Q \tag{3.49}$$

Denoting

$$[G_1] - [G_1]^T = [G]$$

Then, Eq. (3.49) becomes

$$[M]\{\ddot{e}\} + \dot{\theta}[G]\{\dot{e}\} + [K] = Q \tag{3.50}$$

where $[M]$ = augmented mass matrix, $[G]$ = gyroscopic matrix and

$[K]$ = augmented stiffness matrix

3.6 The Finite Element Formulation

The rotor configuration can be defined by a properly generated mesh of finite shaft elements. The disk and bearing properties are added at respective nodes. In this formulation the general shaft element is considered as linearly tapered.

A straight shaft element would be a special case of the tapered one, yet allowing for modeling the tapered segments of any rotor. A linearly tapered shaft element of circular cross-section has its radius varying linearly with length, so that area and moment of inertia are second and fourth order functions of axial position, respectively. Combination of unequal shaft elements are permitted by the model developed in this study. The element consists of two nodes and each node has five degrees of freedom; two transverse displacements (v, w), two bending rotations (β, γ) and a torsional rotation (φ).

A typical axial cross-section of a linearly tapered finite element is shown in Figure 3.6. It is assumed that the cross-sectional properties in a given element are continuous functions of axial position. It is also assumed that the element cross-section has two planes of symmetry X-Z and X-Y.

Each end of the element is associated with an inner and outer radius, denoted by r and R, with the subscripts k and j referring to the left end ($x = 0$) and right end ($x = l$) of the element, respectively. Defining a non-dimensional position coordinate ξ equal to the ratio x/l, the inner and outer radii may be expressed as

$$\begin{aligned} r &= r_k (1 - \xi) + r_j \xi \\ R &= R_k (1 - \xi) + R_j \xi \end{aligned} \tag{3.51}$$

Representing the ratios of inner and outer radii on each end as ρ and α, which are equal to r_j / r_k and R_j / R_k, respectively, allows Eq. (3.51) to be rewritten as

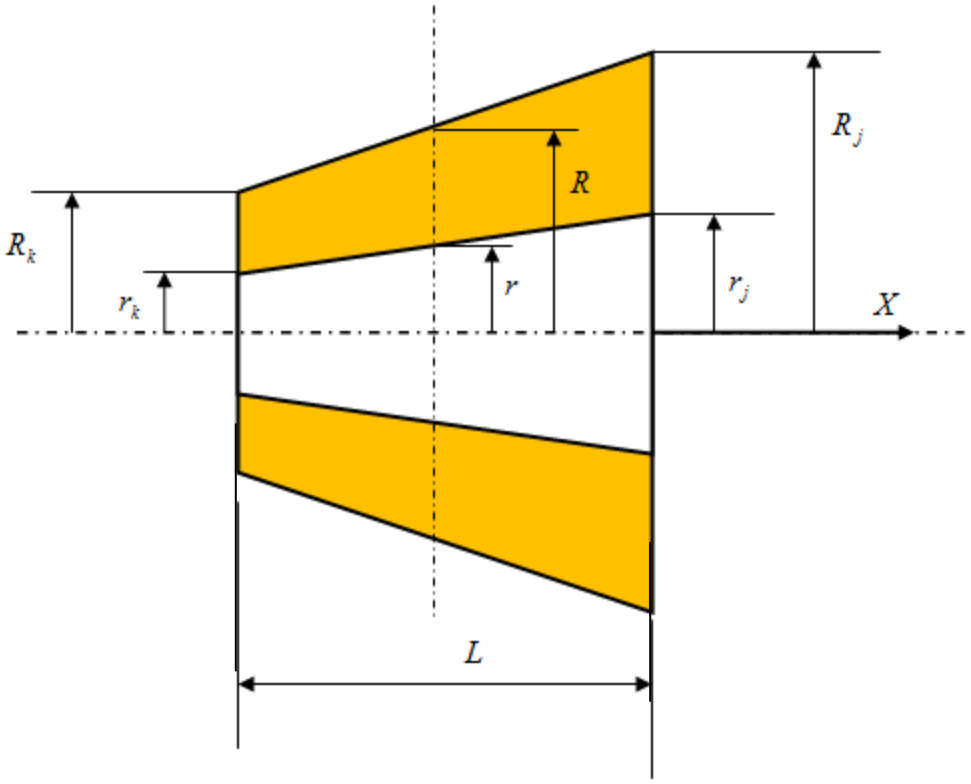

FIGURE 3.6: The Tapered Shaft Element [16]

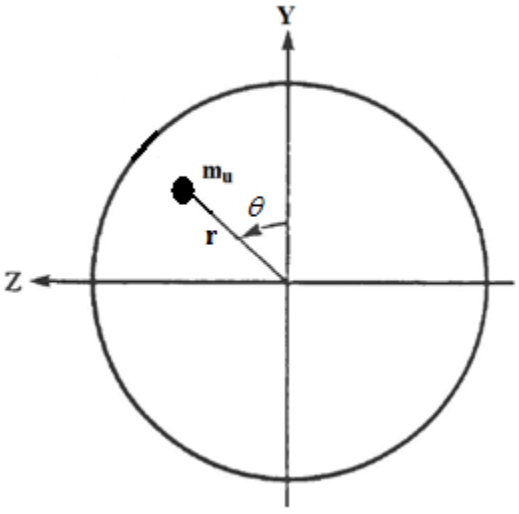

FIGURE 3.7: Mass Unbalance

$$r = r_k \left(1 + (\rho - 1)\xi \right)$$
$$R = R_k \left(1 + (\alpha - 1)\xi \right) \tag{3.52}$$

Using Eq. (3.52) in the cross-sectional area expression results in the following second order polynomial expression:

$$A = \pi\left(R^2 - r^2 \right) = A_k \left[1 + \alpha_1 \xi + \alpha_2 \xi^2 \right] \tag{3.53}$$

where the following coefficients are introduced:

$$A_k = \pi\left(R_k^2 - r_k^2 \right)$$
$$\alpha_1 = 2\left[R_k^2 (\alpha - 1) - r_k^2 (\rho - 1) \right] \Big/ \left(R_k^2 - r_k^2 \right)$$
$$\alpha_2 = 2\left[R_k^2 (\alpha - 1)^2 - r_k^2 (\rho - 1)^2 \right] \Big/ \left(R_k^2 - r_k^2 \right)$$

Similarly for cross-sectional inertia, the use of Eq. (3.52) results in a fourth order polynomial expression

$$I = \pi \left(R^4 - r^4 \right) \Big/ 4 = I_k \left[1 + \delta_1 \xi + \delta_2 \xi^2 + \delta_3 \xi^3 + \delta_4 \xi^4 \right] \tag{3.54}$$

where the coefficients are given by

$$I_k = \pi \left(R_k^4 - r_k^4 \right) \Big/ 4$$
$$\delta_1 = 4\left[R_k^4 (\alpha - 1) - r_k^4 (\rho - 1) \right] \Big/ \left(R_k^4 - r_k^4 \right)$$
$$\delta_2 = 6\left[R_k^4 (\alpha - 1)^2 - r_k^4 (\rho - 1)^2 \right] \Big/ \left(R_k^4 - r_k^4 \right)$$
$$\delta_3 = 4\left[R_k^4 (\alpha - 1)^3 - r_k^4 (\rho - 1)^3 \right] \Big/ \left(R_k^4 - r_k^4 \right)$$
$$\delta_4 = \left[R_k^4 (\alpha - 1)^4 - r_k^4 (\rho - 1)^4 \right] \Big/ \left(R_k^4 - r_k^4 \right)$$

The translational deformation of an arbitrary point internal to the element can be represented as

$$\begin{Bmatrix} v(x,t) \\ w(x,t) \end{Bmatrix} = \begin{bmatrix} N_{v_1} & 0 & 0 & N_{v_2} & 0 & N_{v_3} & 0 & 0 & N_{v_4} & 0 \\ 0 & N_{v_1} & -N_{v_1} & 0 & 0 & 0 & N_{v_3} & -N_{v_4} & 0 & 0 \end{bmatrix} \{ e(t) \}$$
$$= \left[N_v (x) \right] \{ e(t) \} = \begin{bmatrix} N_{vv}(x) \\ N_{vw}(x) \end{bmatrix} \{ e(t) \} \tag{3.55}$$

The rotation of a typical cross-section of the element is represented by

$$\begin{Bmatrix}\beta(x,t)\\ \gamma(x,t)\end{Bmatrix}=\begin{bmatrix}N_{v1} & 0 & 0 & N_{v2} & 0 & N_{v3} & 0 & 0 & N_{v4} & 0\\ 0 & N_{v1} & -N_{v2} & 0 & 0 & 0 & N_{v3} & -N_{v4} & 0 & 0\end{bmatrix}\{e(t)\}$$
$$=[N_{\beta}(x)]\{e(t)\}=\begin{bmatrix}N_{\beta\beta}(x)\\ N_{\beta\gamma}(x)\end{bmatrix}\{e(t)\} \qquad (3.56)$$

The torsional displacement of a typical cross-section of the element is approximated by

$$\{\varphi(x,t)\}=\begin{bmatrix}0 & 0 & 0 & 0 & N_{\varphi_1} & 0 & 0 & 0 & 0 & N_{\varphi_2}\end{bmatrix}\{e(t)\}=\begin{bmatrix}N_{\varphi}(x)\end{bmatrix}\{e(t)\} \qquad (3.57)$$

The individual shape functions N_{v_i} where $i=1,2,3,4;$ represent static displacement modes associated with unit displacement of one of the end point coordinates with all other coordinates constrained to zero. N_{β_i} where $i=1,2,3,4;$ represent static rotation shape functions associated with unit displacements of one of the endpoint coordinates with all other coordinates constrained to zero. N_{φ_i} where $i=1,2;$ represent static torsion shape functions associated with unit displacement of one of the endpoint coordinate with all other coordinates constrained to zero. The individual shape functions are as

$$
\begin{aligned}
N_{v_1} &= \frac{1}{1+\Phi}\left[\,1-3\xi^2+2\xi^3+\Phi(1-\xi)\,\right]\\
N_{v_2} &= \frac{1}{1+\Phi}\left[\,\xi-2\xi^2+\xi^3+\frac{\Phi}{2}\left(\xi-\xi^2\right)\right]\\
N_{v_3} &= \frac{1}{1+\Phi}\left[\,3\xi^2-2\xi^3+\Phi(\xi)\,\right]\\
N_{v_4} &= \frac{1}{1+\Phi}\left[\,-\xi^2+\xi^3+\frac{\Phi}{2}\left(-\xi+\xi^2\right)\right]\\
N_{\beta_1} &= \frac{6}{l(1+\Phi)}\left[\,\xi^2-\xi\,\right]\\
N_{\beta_2} &= \frac{1}{1+\Phi}\left[\,1-4\xi+3\xi^2+\Phi(1-\xi)\,\right]\\
N_{\beta_3} &= \frac{6}{l(1+\Phi)}\left[-\xi^2+\xi\,\right]\\
N_{\beta_4} &= \frac{1}{1+\Phi}\left[\,3\xi^2-2\xi+\Phi\xi\,\right]\\
N_{\varphi_1} &= 1-\xi\\
N_{\varphi_2} &= \xi
\end{aligned}
\tag{3.58}
$$

where

$$\xi = \frac{x}{l} \tag{3.59}$$

and

$$\Phi = \frac{12EI}{\kappa AGl^2} \tag{3.60}$$

The parameter Φ is known as the shear deformation parameter (the ratio between bending stiffness and shear stiffness), E is the modulus of elasticity, I is the second moment of the cross-sectional area, A is the cross-sectional area of the shaft element, G is the shear modulus, l is the element length, and κ is the shear correction factor depending on the

shape of the cross-section. The shear correction factor κ is given by Eq. (3.35) and Eq. (3.36).

3.6.1 The Rotor Shaft

The strain energy expression of a rotating tapered shaft element of length l, in the matrix form is given by

$$(U) = \frac{1}{2}\{e\}^T [K]\{e\} \tag{3.61}$$

The matrix [K] is the augmented stiffness matrix given by

$$[K] = \left[K_e\right] + \left[K_s\right] + \left[K_\varphi\right] \tag{3.62}$$

where

$$[K_e] = \int_0^t [B_e]^T EI[B_e]dx \equiv Elastic\ \ stiffness\ \ matrix \tag{3.63}$$

$$[K_s] = \int_0^t [B_s]^T kGA\ [B_s]dx \equiv Shear\ \ stiffness\ \ matrix \tag{3.64}$$

$$[K_\varphi] = \int_0^t [B_\varphi]^T GJ\ \ [B_\varphi]dx \equiv Torsional\ \ stiffness\ \ matrix \tag{3.65}$$

The curvature k and the shear strain v_{xy} within the element are expressed as

$$\kappa = \frac{\partial \gamma}{\partial x} = \left[B_e\right]\{e\} \tag{3.66}$$

$$v_{xy} = \frac{\partial v}{\partial x} - \gamma = \left[B_s\right]\{e\} \tag{3.67}$$

where

$$\left[B_{\varphi} \right] = \frac{\partial}{\partial x} \left[N_{\varphi} \right] \tag{3.68}$$

$$\left[B_{e} \right] = \frac{\partial}{\partial x} \left[N_{\beta} \right] \tag{3.69}$$

$$\left[B_{s} \right] = \frac{\partial}{\partial x} \left[N_{v} \right] - \left[N_{\beta} \right] \tag{3.70}$$

Carrying out the integration of Eq. (3.16), the elastic stiffness matrix [K_e] is obtained with nonzero entries as presented in [14]. The explicit expression for the element shear stiffness matrix [K_s] is obtained by carrying out the integration of Eq. (3.17). The shear stiffness matrix [K_s] is obtained with nonzero entries as presented in [14]. Similarly, the torsional stiffness matrix [K_φ] is established by evaluating the integral of Eq. (3.18). The nonzero entries of torsional stiffness matrix [K_φ] are presented in [14].

The kinetic energy of a rotating tapered shaft element of length l in matrix form is given by

$$T = \frac{1}{2} \left\{ \dot{e} \right\}^{T} [M] \left\{ \dot{e} \right\} + \frac{1}{2} C_1 \dot{\theta}^2 - \dot{\theta} \left\{ \dot{e} \right\}^{T} \left[G_1 \right] \left\{ \dot{e} \right\} \tag{3.71}$$

The matrix [M] is the composite mass matrix given by

$$[M] = \left[M_t \right] + \left[M_r \right] + \left[M_{\varphi} \right] - 2 \left[M_e \right] \tag{3.72}$$

This is known as the consistent mass matrix because it is formulated from the same shape functions $\left[N_v \right]$, $\left[N_{\beta} \right]$, and $\left[N_{\varphi} \right]$ that are used to formulate the stiffness matrix. The matrix [M_e] gives the coupling between torsional and transverse vibration and is time dependent. It is neglected for eigenvalue analysis as eigenvalue is system inherent property and is independent of time. The components of the mass matrix are

$$\left[M_t \right] = \int_0^l \left[N_v \right]^T \mu A \left[N_v \right] dx = \text{ translational mass matrix} \tag{3.73}$$

$$\left[M_r \right] = \int_0^l \left[N_\beta \right]^T I_D \left[N_\beta \right] dx = \text{rotary inertia mass matrix} \tag{3.74}$$

$$\left[M_\varphi \right] = \int_0^l \left[N_\varphi \right]^T I_p \left[N_\varphi \right] dx = \text{ torsional mass matrix} \tag{3.75}$$

The explicit expressions for the element translational mass matrix [M_t], the rotary inertia mass matrix [M_r] and the element torsional mass matrix [M_φ] are obtained by carrying out the integration of Eqs (3.40), (3.41), and (3.42), respectively. The nonzero entries of [M_t], [M_r], and [M_φ] are presented in [14], in that order.

The gyroscopic matrix [G] is given by

$$[G] = \left[G_1 \right] - \left[G_1 \right]^T \tag{3.76}$$

where constant rotating speed [G_1] can be calculated by

$$\left[G_1 \right] = \int_0^l \left[N_{\beta\gamma} \right]^T I_p \left[N_{\beta\beta} \right] dx \tag{3.77}$$

The explicit expressions for the elemental gyroscopic mass matrix [G] are obtained by integrating Eq. (3.77), and then substituting it into Eq. (3.76). The nonzero entries of [G] are presented in [14].

3.6.2 The Material Damping

The material damping of the rotor shaft can be accommodated. The effects of hysteretic and viscous forms of internal damping for a cylindrical element can be

included by assuming a constitutive relationship between axial stress and the axial strain in the form

$$\sigma_x = E\left\{\frac{\varepsilon_x}{\sqrt{1+\eta_h^2}} + \left(\eta_v + \frac{\eta_h}{\sqrt{1+\eta_h^2}}\right)\dot{\varepsilon}_x\right\} \tag{3.78}$$

where σ_x is the axial stress, ε_x is the axial strain, $\dot{\varepsilon}_x$ is the time rate of change of the axial strain and E is the modulus of elasticity. η_v and η_h denote the viscous damping factor and the loss factor due to hysteretic damping for the rotating shaft material, respectively.

After expressing the potential energy and the dissipation function in terms of the bending stiffness matrix, and accounting for shear and torsional deformations, the final form of the potential energy is given by

$$\begin{aligned} U = {} & \frac{1}{2}\frac{1+\eta_h}{\sqrt{1+\eta_h^2}}\{e\}^T\left[K\right]\{e\} \\ & + \frac{1}{2}\left(\eta_v\Omega + \frac{\eta_h}{\sqrt{1+\eta_h^2}}\right)\{e\}^T\left[N\right]\left[K\right]\{e\} \end{aligned} \tag{3.79}$$

where $\Omega =$ Rotational speed and the dissipation function for the shaft finite element is given by

$$D = \frac{1}{2}\eta_v\{\dot{e}\}^T\left[K\right]\{e\} \tag{3.80}$$

3.6.3 The Disk

The disk is assumed to be rigid and is solely characterized by its kinetic energy. The expression for kinetic energy of the disk can be derived using the procedure followed for the shaft element. Let *v* and *w* designate the coordinates of the center of mass 'O' of the disk in X^i, Y^i, Z^i coordinate system. The disk deforms in the $y - z$ plane.

The expression for the kinetic energy of the disk can be derived as

$$T^d = \frac{1}{2} m^d \left(\dot{v}^2 + \dot{w}^2\right) + \frac{1}{2} I_D \left(\dot{\beta}^2 + \dot{\gamma}^2\right) + \frac{1}{2} I_p \left(\dot{\theta}^2 + \dot{\varphi}^2\right) + I_p \dot{\theta}\dot{\varphi} - I_p \left(\dot{\theta} + \dot{\varphi}\right)\dot{\gamma}\beta \tag{3.81}$$

Similar to Eq. (3.20), Eq. (3.81) can be written in matrix form as

$$T^d = \frac{1}{2} \left\{ \dot{e}^d \right\}^T \left[M^d \right] \left\{ \dot{e}^d \right\} + \frac{1}{2} I_p \dot{\theta}^2 - \dot{\theta} \left\{ \dot{e}^d \right\}^T \left[G_1^d \right] \left\{ e^d \right\} \tag{3.82}$$

where $\{e^d\}$ is the vector containing the nodal coordinates of the disk and

$$\left[M^d \right] = \left[M_t^d \right] + \left[M_r^d \right] + \left[M_\varphi^d \right] - 2\left[M_e^d \right] \tag{3.83}$$

The constituent matrices of Eq. (3.83) are

$$\left[M_t^d \right] = \begin{bmatrix} m^d & 0 & 0 & 0 & 0 \\ 0 & m^d & 0 & 0 & 0 \\ 0 & 0 & 0 & 0 & 0 \\ 0 & 0 & 0 & 0 & 0 \\ 0 & 0 & 0 & 0 & 0 \end{bmatrix}, \quad \left[M_r^d \right] = \begin{bmatrix} 0 & 0 & 0 & 0 & 0 \\ 0 & 0 & 0 & 0 & 0 \\ 0 & 0 & I_D^d & 0 & 0 \\ 0 & 0 & 0 & I_D^d & 0 \\ 0 & 0 & 0 & 0 & 0 \end{bmatrix} \tag{3.84}$$

$$\left[M_\varphi^e \right] = \begin{bmatrix} 0 & 0 & 0 & 0 & 0 \\ 0 & 0 & 0 & 0 & 0 \\ 0 & 0 & 0 & 0 & 0 \\ 0 & 0 & 0 & 0 & 0 \\ 0 & 0 & 0 & 0 & I_p^d \end{bmatrix}, \quad \left[M_e^d \right] = \begin{bmatrix} 0 & 0 & 0 & 0 & 0 \\ 0 & 0 & 0 & 0 & 0 \\ 0 & 0 & 0 & 0 & 0 \\ 0 & 0 & \beta & 0 & 0 \\ 0 & 0 & 0 & 0 & 0 \end{bmatrix} \tag{3.85}$$

and

$$\left[G_1^d \right] = \begin{bmatrix} 0 & 0 & 0 & 0 & 0 \\ 0 & 0 & 0 & 0 & 0 \\ 0 & 0 & 0 & I_p^d & 0 \\ 0 & 0 & 0 & 0 & 0 \\ 0 & 0 & 0 & 0 & 0 \end{bmatrix} \tag{3.86}$$

Applying Lagrange's equation, the equation of motion of the rigid disk is derived as

$$\left[M^d \right] \left\{ \ddot{e}^d \right\} + \dot{\theta} \left[G^d \right] \left\{ \dot{e}^d \right\} = Q^d \tag{3.87}$$

where Q^d is the generalized force for the disk and $\left[G^d \right] = \left[G_1^d \right] - \left[G_1^d \right]^T$

3.6.4 The Bearings

The stiffness and damping terms are assumed to be known. The virtual work δW of the forces acting on the shaft can be written as

$$\begin{aligned} \delta W = & -K_{yy} v \delta v - K_{yz} w \delta v - K_{zz} w \delta w - K_{zy} v \delta w \\ & - C_{yy} \dot{v} \delta v - C_{yz} \dot{w} \delta v - C_{zz} \dot{w} \delta w - C_{zy} \dot{v} \delta w \end{aligned} \tag{3.88}$$

$$\delta W = F_v \delta v + F_w \delta w \tag{3.89}$$

where F_v and F_w are the components of the generalized force. In matrix form Eqs (3.88) and (3.89) can be written as

$$\begin{Bmatrix} F_v \\ F_w \end{Bmatrix} = - \begin{bmatrix} K_{yy} & K_{yz} \\ K_{zy} & K_{zz} \end{bmatrix} \begin{Bmatrix} v \\ w \end{Bmatrix} = \begin{bmatrix} C_{yy} & C_{yz} \\ C_{zy} & C_{zz} \end{bmatrix} \begin{Bmatrix} \dot{v} \\ \dot{w} \end{Bmatrix} \tag{3.90}$$

Similarly, Eq. (3.90) can be expressed in matrix form as

$$\left[C^b \right] \left\{ \dot{e}^b \right\} + \left[K^b \right] \left\{ e^b \right\} = \left\{ Q^b \right\} \tag{3.91}$$

where

$$\left[K^b\right] = \begin{bmatrix} K_{yy} & K_{yz} \\ K_{zy} & K_{zz} \end{bmatrix} \quad \text{and} \quad \left[C^b\right] = \begin{bmatrix} C_{yy} & C_{yz} \\ C_{zy} & C_{zz} \end{bmatrix} \tag{3.92}$$

$\{Q^b\} =$ Generalized force for the bearing

3.7 Mass Unbalance

The influences of numerous mass unbalances that are acting concurrently were considered here. For the mass unbalance located at $t = 0$ at an angular position θ with respect to $Y - axis$ (Figure 3.7), the unbalance force can be described as in [22] at node j as

$$\{\{F_U\}_D\}_j = m_u r\omega^2 \begin{bmatrix} \sin(\omega t + \theta) \\ \cos(\omega t + \theta) \\ 0 \\ 0 \\ 0 \end{bmatrix} \tag{3.93}$$

Hence, Eq. (3.93) can be expressed further as

$$\{Q^u\}_j = m_u r\omega^2 \begin{bmatrix} \sin(\omega t)\cos\theta \\ -\sin(\omega t)\sin\theta \\ 0 \\ 0 \\ 0 \end{bmatrix} + m_u r\omega^2 \begin{bmatrix} \cos(\omega t)\sin\theta \\ \cos(\omega t)\cos\theta \\ 0 \\ 0 \\ 0 \end{bmatrix} \tag{3.94}$$

$$\{Q^u\}_j = m_u r\omega^2 [\cos\theta \quad -\sin\theta \quad 0 \quad 0]^T \sin(\omega t) + m_u r\omega^2 [\sin\theta \quad \cos\theta \quad 0 \quad 0]^T \cos(\omega t)$$

$$\{Q^u\}_j = \{q_1^d\}_j \sin(\omega t) + \{q_2^d\}_j \cos(\omega t) \tag{3.95}$$

$$\{q_1^d\}_j = m_u r\omega^2 [\sin\theta \quad \cos\theta \quad 0 \quad 0]^T \tag{3.96}$$

$$\{q_2^d\}_j = m_u r\omega^2 [\cos\theta \quad -\sin\theta \quad 0 \quad 0]^T \tag{3.97}$$

where m_u and r are the unbalance mass and eccentricity (the distance of unbalance from the geometry centre of the shaft).

Hence, the Q^d in Eq. (3.87) will become equal to the Q^u in Eq. (3.95) when the disk contained unbalance force.

3.8 The Eigenvalue Formulation

Now, the equation of motion of a rotor bearing system can be written in the assembled general form as [34]

$$[\bar{M}]\{\ddot{e}\}+[\bar{C}]\{\dot{e}\}+[\bar{K}]\{e\}=\{Q\} \tag{3.98}$$

This is an augmented equation of motion of the rotor bearing system that will be utilized in formulation the low-speed balancing scheme. For modal analysis, the free vibrational equation of motion of a rotor bearing system in Eq. (3.98) will then be

$$[\bar{M}]\{\ddot{e}\}+[\bar{C}]\{\dot{e}\}+[\bar{K}]\{e\}=\{0\} \tag{3.99}$$

with

$$[\bar{M}]=\left[M^{e}\right]+\left[M^{d}\right]$$

$$[\bar{C}]=\left[G^{e}\right]+\left[C^{b}\right]+\left[G^{d}\right]-\eta_v[K]$$

$$[\bar{K}]=\frac{1+\eta_h}{\sqrt{1+\eta_h^2}}\left[K^{e}\right]+\left(\eta_v\Omega+\frac{\eta_h}{\sqrt{1+\eta_h^2}}\right)[N]\left[K^{e}\right]+\left[K^{b}\right]$$

where

$\left[M^{e}\right]=$ inertial matrix of the shaft, $\left[M^{d}\right]=$ inertial matrix of the disk,

$\left[G^{e}\right]=$ gyroscopic matrix of the shaft, $\left[G^{d}\right]=$ gyroscopic matrix of the disk,

$\left[C^b \right]$ = damping matrix of the bearing, $\left[K^e \right]$ = stiffness matrix of the shaft,

$\left[K^b \right]$ = stiffness matrix of the bearing, $\{e\}$ = nodal deformation vector,

$\{Q\}$ = Vector of generalized forces

These constituent matrices are highly banded in nature. The matrix [M] is symmetric, whereas [G^e] and [G^d] are skew-symmetric. The matrix [K] is symmetric when the bearings are rigid or when they have stiffness coefficients in the principal directions. The matrix [C] is skew symmetric only when the bearing is undamped ($C_{yy} = C_{zz} = C_{yz} = C_{zy} = 0$). If the bearings are damped, the matrix [C] is a non-symmetric real matrix.

The solution of Eq. (3.99) may be obtained by representing it in the following state space form:

$$\begin{bmatrix} [0] & -[M] \\ [M] & [C] \end{bmatrix} \begin{Bmatrix} \{\ddot{e}\} \\ \{\dot{e}\} \end{Bmatrix} + \begin{bmatrix} [M] & [0] \\ [0] & [K] \end{bmatrix} \begin{Bmatrix} \{\dot{e}\} \\ \{e\} \end{Bmatrix} = \begin{Bmatrix} 0 \end{Bmatrix} \tag{3.100}$$

Or, simply as

$$[E]\{\dot{y}\} + [F]\{y\} = \{0\} \tag{3.101}$$

in which

$$\{v\} = \begin{Bmatrix} \dot{e} \\ e \end{Bmatrix} \tag{3.102}$$

The matrices [E] and [F] are highly banded. If the bearing is undamped then the matrix [E] is skew-symmetric. The matrix [F] is symmetric when the bearings are isotropic with ($K_{yz} = K_{zy} = 0$). If the bearings are damped or orthotropic or both then nothing can be said about the symmetry or skew-symmetry of the matrices [E] and [F]. Thus, the type

of bearings used in the rotor-bearing system play an important role in selecting a numerical strategy to solve the equation of motion.

3.9 Mode shape and Natural Frequency

The natural frequencies, mode shapes and other characteristics of the rotor bearing system can be obtained from the solution of Eq. (3.98) and this equation can be solved analytically or numerically.

Caughey and O'Kelly [5] in their work made it know that the undamped linear dynamic systems possess normal modes (classical normal modes) and in each normal mode the different parts of the system pass through their maximum or minimum positions at the same time. Generally, regarding damped systems, in a normal mode of oscillation the various parts of the system do not pass through their maximum or minimum position at the same time. Hence, they concluded that:

1.) The damped natural frequency of the highest mode is often less than or equal to the undamped frequency in a linear dynamic system with weak damping, regardless of what form of damping matrix is utilized.
2.) The damped natural frequency of the lowest mode may be higher than the corresponding undamped frequency, depending on the selection of damping matrix and the mode separation.
3.) The damped natural frequencies are always less than or equal to the corresponding undamped frequencies in a system with classical normal modes.

Similarly, Swanson et al. [32] stated in their work, that when the shaft is not rotating the structural modes are planar but they become circular when the shaft starts

rotating, and split into forward and backward modes. As the speed increases the forward modes increase in frequency while the backward modes decrease in frequency. The distribution of mass and diametral mass moment of inertia and the shape of the corresponding mode shape will determine how much the mode changes. There is a critical speed every time the rotor speed passes through with a forward whirling damped natural frequency unless the bearings have high damping. However, the modes have mixed forwards and backwards motion in some cases. They made it clear that several real machines do not have equaled bearing/mount stiffness in all directions. The support structure is normally asymmetric in case of rolling element bearings whereas both the support and the bearing can be asymmetric fluid-film bearings. As a result of these, there are three main effects [32]:

1.) Firstly, there will be additional frequency separation between the pairs of modes as shown in the Figure 3.8

2.) In the second, the orbits traced out by points on the rotor will not be circular again but become elliptical (Figure 3.9). The picture remains much the same if otherwise. This second effect applies to fluid-film bearings. Their stiffness and damping characteristics are strong function of shaft speed. In addition, the fluid-film bearings have cross-coupling between the vertical and horizontal axes. In the vertical axis a force will produce a displacement in the horizontal axis and vice-versa.

    Hence, the neat generalization that forward whirl increases with speed and backward whirl decreases with speed is likely to be changed for these bearings. It is possible for a forward mode to really appear to decrease with speed, and/or a

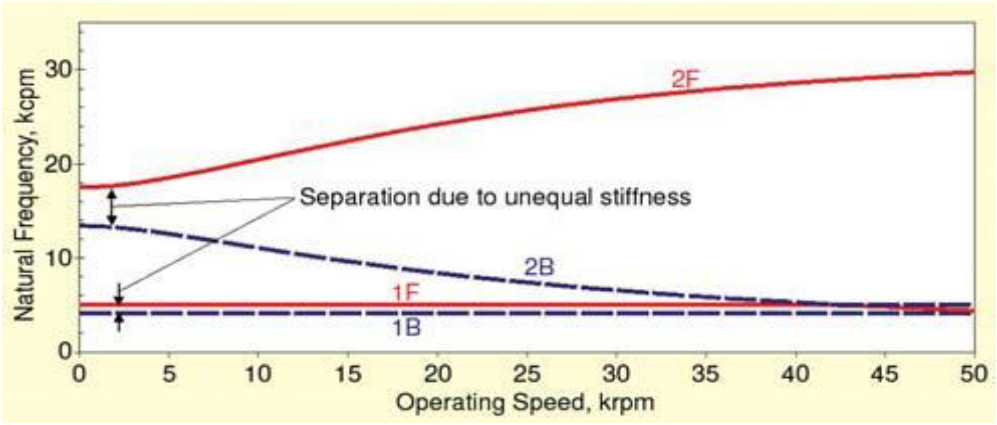

FIGURE 3.8: Campbell Diagram [9]

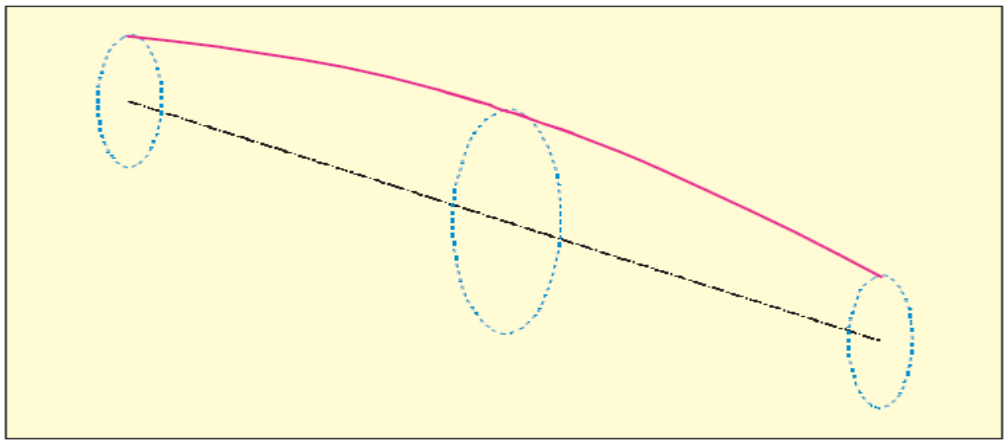

FIGURE 3.9: Non-Circular (Elliptical) Modes with Asymmetric Bearing Stiffness [9]

backward mode increase with speed depending on the rotor and bearing characteristics and how the bearing change with speed.

3.) Since rotating machinery is hardly ever proportionally damped and the modes are usually complex rather than real, the phase angle between various points on the shaft is often not 0° or 180°, as is commonly seen in lightly damped structural modes.

Besides, the gyroscopic moment increases a forward critical speed but decreases the backward critical speed. This divides the critical speed into two values. Nevertheless, the effect of gyroscopic moment will not become visible considerably in slender uniform shaft with no disk and natural frequency does not change very much. Also, the tensions raises the critical speeds while the compression lowers them in case of axial force [38].

CHAPTER 4

ROTORDYNAMIC ANALYSIS USING ANSYS

Rotordynamics is described as the study of vibrational behavior in axially symmetric rotating structures [31]. Characteristic inertia effects are being developed by engines, motors, disk drives and turbines and this effect can be analyzed to decrease the possibility of failure and improve the design. Such as in a gas turbine engine, at higher rotational speeds, the inertia effects of the rotating parts must be constantly represented in order to precisely envisage the rotor behavior.

The gyroscopic moment initiated by the precession motion of the vibrating rotor as it spins is a vital part of the inertia effects. The gyroscopic moment acting on the rotor becomes seriously significant as spin velocity increases. At the design level, failure to account for these effects can lead to bearing and/or support structure damage [31]. In a situation whereby there is either an overhung rotor (so that any force causes a substantial slope of the shaft at the rotor) or where the rotor is operating at high speeds, the gyroscopic effects tend to be mainly important [9]. An important factor in enhancing the stability of a vibrating rotor include accounting for bearing stiffness and support structure flexibility, and then understanding the resulting damping behavior.

The rotordynamic features such as gyroscopic effects and bearing support flexibility can be integrated into the standard Finite Element Analysis (FEA) modal,

harmonic and transient analysis procedures found in ANSYS. When this is done, one can analyze and determine the design integrity of rotating equipment [31].

Similarly, the result obtained from ANSYS can be processed further to find out the critical parameters. The rotor critical speed and its stability can be determined by using the Campbell plots. The rotor's forward and backward whirl can be envisaged in such a way the critical factors and the areas of concern can be established.

Hence, the balancing of flexible rotors at low speed that this work is all about was simulated in ANSYS 12.1 and in this chapter those necessary areas that needed for a successful simulation were discussed.

4.1 Rotor Reference Frame and Bearing in ANSYS

ANSYS has two types of reference frame: rotating and stationary frames (shown in the Figure 4.1). Inertial forces and moments are observed when a structure is rotating. In order to express these quantities correctly, either a stationary reference frame: global Cartesian ($OZXY$) or a rotating reference frame that is attached to the structure ($O'Z'X'Y'$) can be chosen. The rotating frame applies the Coriolis effect to the following structural element types: BEAM188, BEAM189, MASS21, SHELL181, PLANE182, PLANE183, SOLID185, SOLID186 and others. Both Coriolis and spin softening effect contribute to the gyroscopic in a rotating reference frame. ANSYS applies spin-softening by default for dynamic analyses but it can be deactivated. Rotating frame of reference is primarily applicable in the field of flexible body dynamics generally where the structure has no stationary parts and the whole structure is rotating. Hence, only Coriolis force will

be considered for this kind of analyses. It should be noted here that in the dynamics equations expressed in a rotating reference frame, gyroscopic effect will not be added. The results that are going to be acquired in the rotating reference frame may not compare well with stationary reference frame results if the structure contains a part with large inertia (for instance, large disk) [2, 21]. The displacement field will be computed by ANSYS with respect to the coordinate system attached to the structure and rotating with it at specified angular velocity. In rotating structure analysis, the following analysis types support the use of rotating reference frame: Static, Modal, Transient and Harmonic.

The gyroscopic damping matrix will be activated when the stationary reference frame is adopted in the following structural elements: BEAM4, BEAM188, BEAM189, MASS21, SOLID272, SOLID273, PIPE16, PIPE288, SHELL63, SHELL181 and others. Although, the gyroscopic damping matrix generated is valid only for a linear analysis. In addition, in stationary reference frame, the rotating structure must be axisymetric about the axis of rotation [2, 21]. ANSYS computes the displacement field with respect to the global coordinate system in this type of the frame. The areas primarily where stationary frame of reference is applicable is in the field of rotordynamic where a rotor (rotating structure) is modeled along with a stationary support structure. The example of such application includes gas turbine engine rotor-stator assembly or an electric turbo generator, where the rotor spins inside a specially designed housing. Also, in rotating structure analysis the following analysis types support the use of stationary reference frame: Modal, Transient and Harmonic except Static.

However, ANSYS recommended that the modal analysis of rotor should be done in stationary reference frame. The **CORIOLIS** command is used for analyzing in either a

rotating or a stationary reference frame but performs differently according to the designated *RefFrame* value which can be either OFF or ON. If *RefFrame* = OFF the frame under consideration is rotating reference frame and vice versa. Hence, all the simulations carried out to achieve the objectives of this work were done in stationary reference frame.

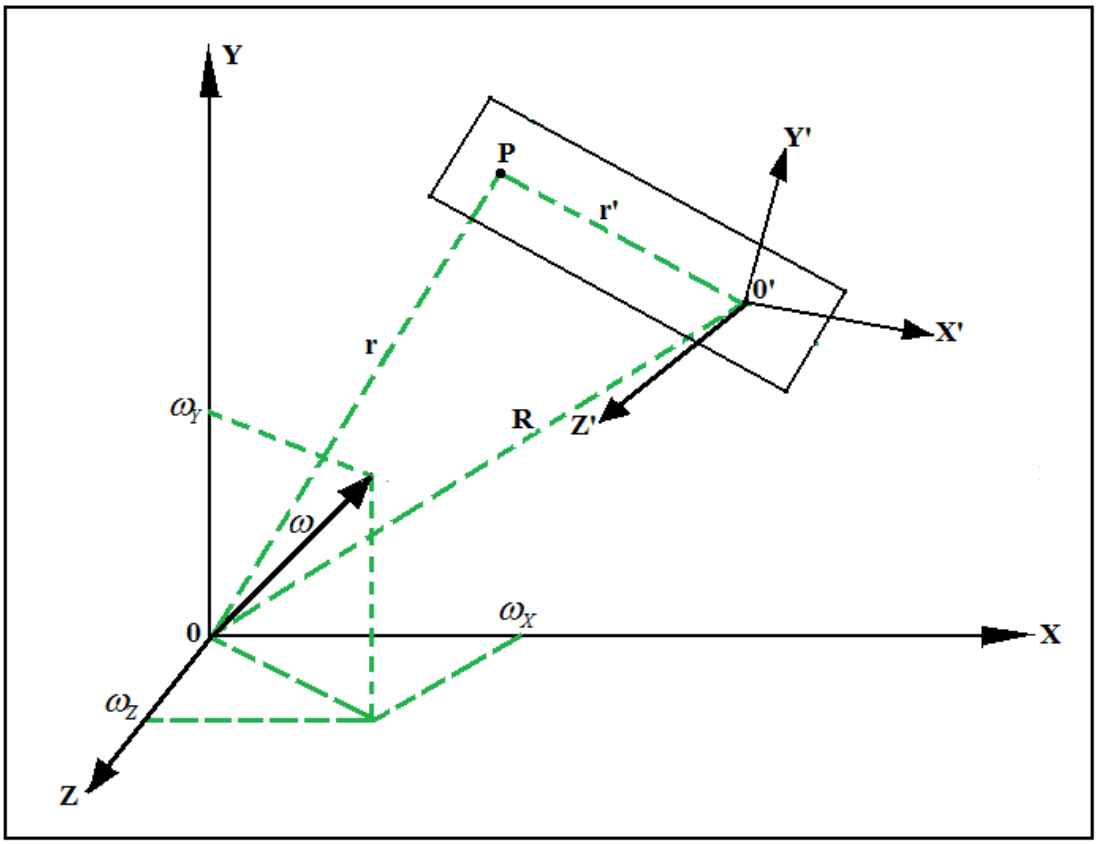

FIGURE 4.1: Reference Frame (Rotating and Stationary)

Furthermore, all the equations dealt with regarding the rotor bearing system in Chapter 3 that finally lead to the equation of motion were taking care in the ANSYS and the dynamic equation incorporating the effect of rotation. The matrix $[G]$ in the equation of motion is a damping matrix contribution due to the rotation of the structure. Usually,

in a rotating reference frame $[G]$ is called Coriolis matrix and gyroscopic matrix in a stationary reference frame. Coriolis forces and damping matrices are available for the elements listed under the rotating reference frame in the section 4.1 above or in the CORIOLIS command documentation. Nevertheless, the effect of spin softening modifies the apparent rigidity of the structure in both Coriolis matrix for dynamic analysis and a Coriolis force for quasi-static analyses [2].

Similarly, in the stationary reference frame, gyroscopic matrix is provided. If a structure is spinning around an axis say ϕ, then a reaction moment will appear if a rotation about an axis perpendicular to ϕ was applied to the structure. This moment is referred to as gyroscopic moment. Its axis is perpendicular to both the spinning axis ϕ and the applied rotation axis. Hence, gyroscopic effect is the coupling rotational degrees of freedom which are perpendicular to the spinning axis.

If the spinning axis was considered to be along Z, then

- The spinning velocity (input using the OMEGA or CMOMEGA commands) is $\omega_z = \dot{\theta}_z$
- The displacements perpendicular to the spin axis are u_y and u_x
- The corresponding rotations are θ_y and θ_x, and the angular velocities are $\dot{\theta}_y$ and $\dot{\theta}_x$

The gyroscopic finite element matrix is calculated from the kinetic energy due to the inertia forces. The kinetic energy for lumped mass and beam element is detailed in kinetic energy for the gyroscopic matrix calculation of lumped mass and legacy beam element. However, both mass and beam are supposed to be axisymmetric around the

spinning axis. Regarding lumped mass, the spinning axis is along one of the principal axis of inertia whereas for the beam it is along the length.

Moreover, the beam element is considered as an infinite number of lumped masses then, the gyroscopic kinetic energy of the element can be acquired by integrating the gyroscopic matrix for lump mass along the length of the beam. Gyroscopic matrix is deduced from the element shape functions. However, the gyroscopic matrices are available for the elements listed under stationary reference frame in the section 4.1 or in the CORIOLIS command documentation.

The rotating damping matrix $[B]$ in a stationary reference frame is a non-symmetric matrix that will modify the apparent stiffness of the structure. Regarding the elements that generate a gyroscopic matrix, the rotating damping matrices are available for them.

Besides, in ANSYS, bearings are usually represented by a single MATRIX27 or multiple COMBIN14 but due to the invention of COMBIN214 element, the radial stiffness and damping in vertical, horizontal planes and cross coupled terms can be specified by a single element. The bearing damping and stiffness can be a function of rotor speed, that is $C_f = C_f(\omega)$ and $K_f = K_f(\omega)$.

In this work, both COMBIN14 and COMBIN214 elements were used separately on a rotor and when their results were compared, they gave the same results. So, the two were used on different occasions.

4.2 Rotating Structures Modeling in ANSYS

The lumped mass approach has being used traditionally to model rotating structures. This approach utilizes the centre of mass to compute the effects of rotation on attached or proximal components. Regarding this approach, its main restraint is the inaccurate approximation of both the location and the distribution of the mass and inertias, along with the resulting imprecision in the calculation of internal forces and stresses in the components themselves. The finite element (FE) method used in ANSYS offers a pretty approach to modeling a rotordynamic system. Despite the fact that it may require more computational resources compared to standard analyses, it has the following advantages [31]:

- A large range of elements supporting gyroscopic effects
- The ability of solid element meshes to account for the flexibility of the disk as well as the possible coupling between disk and shaft vibrations.
- Perfect modeling of the mass and inertia
- The use of the CAD geometry when meshing in solid elements
- The ability to include stationary parts within the full model or as substructures.

Moreover, in general, a rotating structure consists of stationary parts, rotating parts, and bearings which link the rotating parts to the stationary parts and/or the ground. When the model is constructed to separate and define these parts, the understanding of the relationships between them always becomes easier.

All rotating parts must be axisymmetric. The elements that are going to be used for the rotating parts of the model must support gyroscopic effects such as those listed in the

section 4.1 or they can be obtained from CORIOLIS command documentation where those elements for which the gyroscopic matrix is available are listed.

When bearings are to be modeled, either a spring/damper element COMBIN14, a general stiffness/damping matrix MATRIX27, a bearing element COMBI214, or a multipoint constraint element MPC184 can be used.

In rotordynamic analysis, there is no different in defining material properties from the way it is being done in any other analysis.

The OMEGA or CMOMEGA command is needed to be used to define the rotational velocity. In a situation where by there are stationary parts and/or several rotating parts having different rotational velocities, CMOMEGA command is required otherwise OMEGA command should be used. In order to take into account the gyroscopic effect in all rotating parts as well as the rotating damping effect, the CORIOLIS command should be used. The ANSYS meshing commands is required to mesh the parts and some areas may need more detailed meshing and/or specialized considerations.

The solution phase of a rotordynamic analysis sticks to standard ANSYS conventions and it should be remembered that the gyroscopic matrices (as well as perhaps the bearing matrices) may not be symmetric. In this phase, modal, harmonic and transient analyses can be performed. If numerous modal analyses were performed, it allows one to review the stability and acquire critical speeds from the Campbell diagrams. The harmonic analysis permits one to calculate the response to synchronous (for example, unbalance) or asynchronous excitations [31]. Also, the transient analysis allows one to study the response of the structure under transient loads (for example, a 1G shock) or analyze the startup or stop effects on a rotating spool and the related

components. In addition, in a typical rotordynamic analysis, prestress can be a significant factor, so, it can be included in the modal, transient, or harmonic analysis.

Besides, when results are to be reviewed, the general postprocessor (POST1) and the time-history postprocessor (POST26) should be used. In higher version of ANSYS 12, specific commands are available in POST1 for Campbell diagram analysis (PLCAMP, PRCAMP), animation of the response (ANHARM) and orbits visualization and printout (PLORB, PRORB). In other version up to ANSYS 12.0, these commands are not available in POST1, they need to be invoked. Unfortunately, the ANSYS 12.1 used for this work did not contain these specific commands in POST1 all the commands employed were invoked when the needs arose.

4.3 ANSYS Modal Analysis

Modal analysis is a method that can be used to determine the vibration characteristics (natural frequencies and mode shapes) of a structure or machine component while design is going on. It also acts as a gate way for more detailed analyses such as harmonic response, transient dynamic and spectrum analyses [3]. Natural frequencies and mode shapes are important parameters in system design for dynamic loading conditions. During the modal analysis any nonlinearity which include plasticity and contact (gap) elements are neglected if existed in the system being analysed. ANSYS has quite a number of mode extraction/eigensolver methods from which the one that matched the system under consideration will be chosen. The available mode extraction methods or eigensolvers include Block Lancoz (default), PCG Lancoz, Reduced, Unsymmetric, Damped, QR Damped and Supernode.

The Damped and QR damped allow the damping to be added to the system model. All mode extraction methods can be used for most applications except Unsymmetric, Damped and QR Damped that were made for special applications [3].

QR Damped is faster and achieves better calculation efficiency than Damped method. In modal coordinate, the QR Damped uses reduced modal damped matrix to calculate complex damped frequencies. In rotordynamic analysis, both Damped and QR Damped eigensolvers are pertinent but before the selection of any of them, the following should be considered [31]:

- if further analyses such as harmonic, transient or modal superposition analysis is to be performed, it is advisable to use QR Damped because Damp eigensolver does not support modal superposition methods.
- The QR Damped eigensolver solves a reduced system of equation while Damp eigensolver solves the full system equation. QR Damped is more efficient than the Damp eigensolver computationally and it is limited to the cases where damping (viscous, material, etc) is not critical.

Hence, Damp eigensolver is proposed when solid elements are utilized for the rotating part of the structure and rotating damping is included.

When QR Damped is used to solve the problem, the results to be listed will consist of many parts, the three important parts include: mode number, complex frequency (Hz) and the natural frequency (Hz). The real part of complex frequency shows the damping of a particular frequency as well as its stability. The negative real part indicates the mode is stable otherwise it is not. The complex part of the complex frequency represents the damped frequency. Damping ratio is the ratio between the real

part and the complex frequency modulus (also referred to as norm of the complex frequency).

It is imperative to know that the gyroscopic effect will creates damping matrix but it does not dissipate energy if there is no damping in a rotating structure and all the real parts of its complex frequencies will be zeros. Similarly, if the damping is so significant that it represses the frequency or if the complex frequency corresponds to a rigid body mode, the complex part will be zero.

4.4 ANSYS Harmonic Response Analysis

The harmonic response analysis gives the capability to envisage the sustained dynamic behavior of the systems and will allow the investigator to know if the designs or systems will effectively overcome fatigue, resonance and other dangerous effects of forced vibrations [3]. The harmonic response analysis is also a method that can be utilized to determine the steady-state response of a linear structure to loads that varying sinusoidally (harmonically) with time. The aim of harmonic analysis is to compute the system's response at numerous frequencies and acquire a graph of some response quantity (displacements) versus frequency which can then be used for further analyses. Harmonic analysis will compute the steady state forced vibration only while the transient vibrations that usually occur at earlier time of excitation will be neglected.

4.4.1 Applying Loads on the Model

By definition, harmonic analysis presumes that any applied load varies harmonically (sinusoidally) with time. The amplitude, the phase angle, and the forcing frequency range are the three pieces of information that generally needed as shown in the Figure 4.2 in order to fully specify the harmonic load. The *amplitude* is the maximum value of the load, which needs to be specified through the commands. The *phase angle* is a measure of the time by which the load lags (or leads) a frame of reference. It is the angle measured from the real axis on the complex plane shown in Figure 4.2. The only situation in which the phase angle is needed is if there were multiple loads that are out of phase with each other. The real and imaginary components of the out-of-phase loads should be specified using the *VALUE* and *VALUE2* fields of the appropriate displacement and force commands since phase angle cannot be specified directly. Figure 4.2 shows how to calculate the real and imaginary components. Pressures and other surface and body loads can only be specified with a phase angle of 0^o (no imaginary component) with the following exceptions: nonzero imaginary components of pressures can be applied using the SURF153 and SURF154 elements in a full harmonic response analysis, or using a mode superposition harmonic response analysis if the mode-extraction method is Block Lanczos, PCG Lanczos, or Supernode commands.

The *forcing frequency range* is the frequency range of the harmonic load (in cycles/time). It is specified afterwards as a load step option with the HARFQ command.

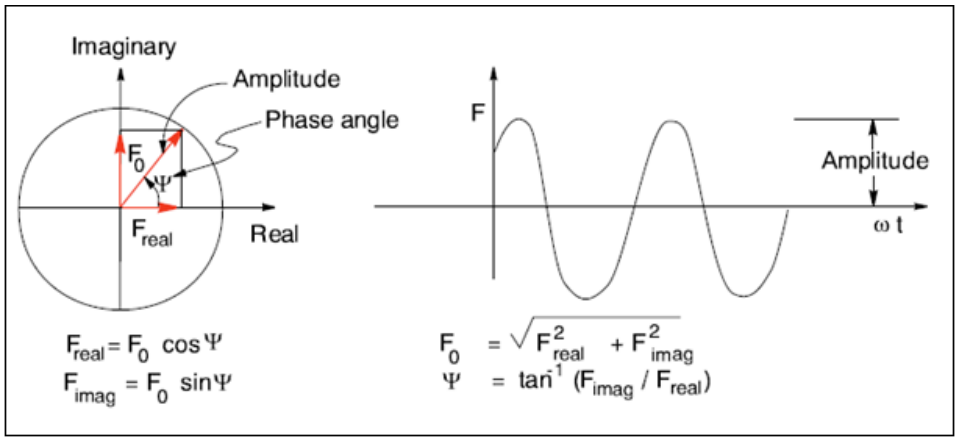

FIGURE 4.2: Relationship between Real/Imaginary Components and Amplitude/Phase Angle [2, 3]

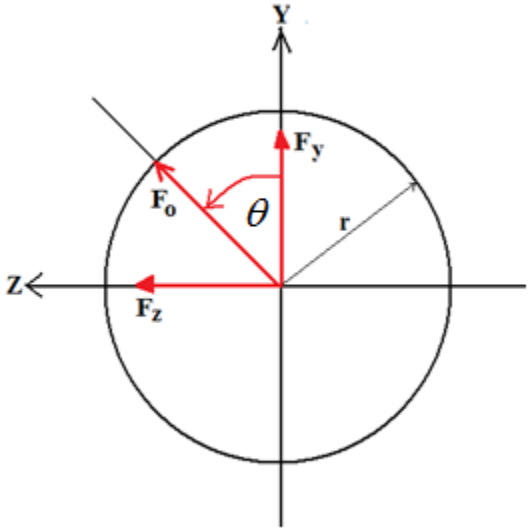

FIGURE 4.3: Unbalance Forces

TABLE 4.1: The Forces in Y and Z Directions

Force	Real (VALUE)	Imaginary (VALUE2)
FY	$F_0 \cos\theta$	$-F_0 \sin\theta$
FZ	$-F_0 \sin\theta$	$-F_0 \cos\theta$

4.4.2 Harmonic Analysis due to Unbalance or General Rotating Asynchronous Forces

Some forces may rotate synchronously (for example, unbalance) or asynchronously with the structure. In such cases, the SYNCHRO command is use to update the amplitude of the rotational velocity vector with the frequency of excitation at each frequency step of the harmonic analysis. Forces are defined as static (**F**) based on the Figure 4.3 as shown in the Table 4.1 where X is the assumed spin axis. F_0 is the amplitude of the force. In case of unbalance, the amplitude is equal to the mass times the distance (radius) of the unbalance mass to the spin axis. That is [2, 31];

$$F_0 = mr$$

α is the phase of the force, needed only when several such forces, each with a different relative phase, are defined. If the forces are caused by an unbalance mass, multiplication of the amplitude of the static forces (**F**) by the square of the spin velocity is unnecessary. ANSYS performs the calculation automatically at each frequency step [2].

4.5 Bode, Nyquist and Orbit Plots

There are numerous ways of showing frequency response data and these including Bode plots (amplitude-phase plots) and Nyquist plots (polar plots). The Bode plot made up of two parts which include the amplitude versus frequency and the phase versus frequency. This plot can be made for different section or node along the rotor through the POST26 command from harmonic response analyses.

Similarly, Nyquist Plot is also a way of displaying frequency responses of linear systems. It shows both amplitude and phase angle on a single plot, using frequency as a parameter in the plot. The plots have properties that permit one to see whether a system is stable or unstable and it will take some mathematical development to see that, but it is the most useful property of Nyquist plots. In order to create a Nyquist plot, the imaginary part will be on the vertical axis of a plot while the real part will be on the horizontal axis.

Besides, the steady state trajectory of a node positioned on the spin axis is called orbit which is an ellipse. Elliptical orbit is applicable only to the nodes on the rotational velocity axis. After modal or harmonic analysis, the characteristics of the orbits can be printed out [31]. The orbit can be acquired for a particular damped frequency after a complex modal analysis or for a specific excitation frequency after harmonic analysis. The orbit plot can be made at different speed through POST1 command. The orbit plot command applies only to some elements like BEAM4, BEAM188, BEAM189, PIPE16, PIPE288, PIPE265, REINF264 and REINF265 [2]. The command will not work when the system is stationary that is, if its operation speed is zero.

CHAPTER 5

METHODOLOGY OF LOW-SPEED BALANCING OF FLEXIBLE ROTORS

The methodology developed for low-speed balancing of high-speed flexible rotors is based on a revised hypotheses as that postulated by Tan and Wang [33]. The developed methodology accounts for the rotor's rotary inertia, gyroscopic and shear effects, which were not considered by the Euler-Bernoulli formulation presented in [33]. Moreover, the developed scheme adopts a FEM approach, thus allowing for handling any complicated rotor configuration; including multi-disk, multi- bearing, tapered shaft segments; etc. In this context, both modal and influence coefficient methods of balancing were adopted. Mode shapes are used to determine the proper balancing planes. Balancing is carried out at a speed well below the first critical speed.

5.1 Theory of Low-Speed Balancing For Flexible Rotor

The analysis in this part proceeds along a parallel line to the formulation presented in [33]. For an isotropic flexible shaft, the coordinate system *Oxys* is attached to the rotor as shown in the Figure 5.1. The deflection of the shaft can be expressed in this coordinate system as

$$z(s) = x(s) + iy(s) \tag{5.1}$$

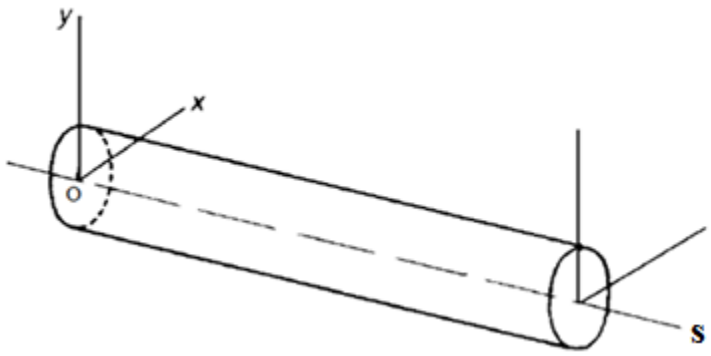

FIGURE 5.1: Flexible Rotor

The components of the shaft deflection in $x-s$ and $y-s$ planes are $x(s)$ and $y(s)$ in that order. The unbalance in the shaft would create centrifugal inertia forces $F(s)$ acting on the shaft. The differential equation of the shaft deflection is given by Equation (3.98), which can be written as

$$[\overline{M}]\{\ddot{z}\} + [\overline{C}]\{\dot{z}\} + [\overline{K}]\{z\} = \{F\} \tag{5.2}$$

where

$$[\overline{M}] = [M^e] + [M^d]$$
$$[\overline{C}] = [G^e] + [C^b] + [G^d] - \eta_V [K]$$
$$[\overline{K}] = \frac{1+\eta_h}{\sqrt{1+\eta^2{}_h}}[K^e] + \left(\eta_V \Omega + \frac{1+\eta_h}{\sqrt{1+\eta^2{}_h}}\right)[N][K^e] + [K^b]$$

and

$[M^e]$ = inertial matrix of the shaft, $[M^d]$ = inertial matrix of the disk,

$[G^e]$ = gyroscopic matrix of the shaft, $[G^d]$ = gyroscopic matrix of the disk,

$[K] = [\bar{K}]$ Augmented stiffness matrix or composite element stiffness matrix of the shaft,

$[C^b] =$ damping matrix of the bearing, $[K^e] =$ stiffness matrix of the shaft,

$\left[K^b \right] =$ stiffness matrix of the bearing, $\{z\} =$ nodal deformation vector,

$\{F\} =$ Vector of generalized forces, $\eta_v =$ Viscous damping factor,

$\Omega =$ Rotational speed, $\eta_h =$ Loss factor due to hysteretic damping for the rotating shaft material

Each of this matrices and vectors are defined and explained in the Chapter 3.

However, if $m(s)$ is mass per unit length at any point s (where $0 < s < L$), L is the length of the shaft and Ω is the rotational speed of the shaft. The characteristic modal functions ($\phi_{1(s)}, \phi_{2(s)}, \ldots.$) of the shaft and corresponding natural frequencies ($\omega_1, \omega_2 \ldots\ldots$) can be determined if the support and boundary conditions of the shaft are known. Here, the natural frequencies ω_j and mode shapes $\phi_{j(s)}$ refer to the *jth* principal mode. Utilizing the orthogonality condition, one gets

$$\int_0^L m(s)\phi_{j(s)}\phi_{i(s)} ds = \begin{Bmatrix} H_j & i = j \\ 0 & i \neq j \end{Bmatrix} \tag{5.3}$$

where H_j is the *jth* modal mass. Now, the distribution of unbalance on the shaft $u(s)$ can be expressed in terms of the orthogonal principal modes as

$$u(s) = \sum_{j=1}^{\infty} c_j m(s)\phi_{j(s)} ds \tag{5.4}$$

where c_j is the coefficient of the modal component of unbalance. Also, due to orthogonality conditions given in the Eq. (5.3), we can have

$$c_j = \frac{1}{H_j}\int_0^L m(s)\phi_{j(s)}ds \tag{5.5}$$

In order to balance the shaft at low speed, the following corrections are needed:

P = correction planes at $s = s_p$, $p = 1,2,.....,P$.

m_p = Correction mass in each plane at $s = s_p$ attached at a radius r_p and angle θ_p

If the balance correction at plane P is $U_p = m_p r_p e^{i\theta_p}$, then total balancing corrections can be written as

$$U(s) = \sum_{p=1}^{P} U_p \delta(s - s_p) \tag{5.6}$$

where $\delta(s - s_p)$ is the Dirac delta function. However, Eq. (5.6) can further be expressed by utilizing Eq. (5.3) as

$$U(s) = \sum_{j=1}^{\infty} d_j m(s)\phi_j(s) \tag{5.7}$$

where

$$d_j = \frac{1}{H_j}\sum_{p=1}^{P} U_p \phi_j(s_p) \tag{5.8}$$

Hence, if Eq. (5.8) is substituted into Eq. (5.7), we obtain

$$U(s) = \sum_{j=1}^{\infty} m(s)\phi_j(s)\frac{1}{H_j}\sum_{p=1}^{P} U_p \phi_j(s_p) \tag{5.9}$$

Now, due to unbalance and balance correction on the shaft, the centrifugal force $F(s)$ consists of forces created by both unbalance $u(s)$ and balance correction $U(s)$. Accordingly, one can write

$$F(s) = \Omega^2 u(s) + \Omega^2 U(s) = \Omega^2 \sum_{j=1}^{\infty} m(s)\phi_j(s)\left[c_j + \frac{1}{H_j} \sum_{p=1}^{P} U_p \phi_j(s_p) \right] \quad (5.10)$$

Similarly, if the damping part of Eq. (5.2) is temporarily set to zero, and assumed the solution of the equation to be harmonic as $z = z(s)e^{i\Omega t}$ *and* $F = F(s)e^{i\Omega t}$. The Eq. (5.2) will become

$$\begin{aligned} &-\Omega^2[\overline{M}]\{z(s)\} + [\overline{K}]\{z(s)\} = \{F(s)\} \\ &\left[[\overline{K}] - \Omega^2[\overline{M}]\right]\{z(s)\} = \{F(s)\} \end{aligned} \quad (5.11)$$

or

$$\begin{aligned} &(k - \Omega^2 m(s))z(s) = F(s) \\ &z(s)m(s)(\omega^2 - \Omega^2) = F(s) \\ &z(s)(\omega^2 - \Omega^2) = (m(s))^{-1} F(s) \end{aligned} \quad (5.12)$$

If we substitute Eq. (5.10) into Eq. (5.12), one gets

$$\begin{aligned} z(s)(\omega_j{}^2 - \Omega^2) &= \Omega^2 \sum_{j=1}^{\infty} \phi_j(s)\left[c_j + \frac{1}{H_j} \sum_{p=1}^{P} U_p \phi_j(s_p) \right] \\ z(s) &= \sum_{j=1}^{\infty} \frac{\Omega^2}{(\omega_j{}^2 - \Omega^2)}\left[c_j + \frac{1}{H_j} \sum_{p=1}^{P} U_p \phi_j(s_p) \right]\phi_j(s) \\ z(s) &= \sum_{j=1}^{\infty} w_j \phi_j(s) \end{aligned} \quad (5.13)$$

where

$$w_j = \sum_{j=1}^{\infty} \frac{\Omega^2}{(\omega_j{}^2 - \Omega^2)}\left[c_j + \frac{1}{H_j} \sum_{p=1}^{P} U_p \phi_j(s_p) \right] \quad (5.14)$$

The constant coefficients w_j are referred to as *jth* modal components of the deflection of the shaft.

If we define

$$\eta_j = \Omega / \omega_j \quad (5.15)$$

Upon substituting Eq. (5.15) into Eq. (5.13), we can have

$$z(s)=\sum_{j=1}^{\infty}\frac{\eta_j^{\,2}}{(1-\eta_j^{\,2})}\left[c_j+\frac{1}{H_j}\sum_{p=1}^{P}U_p\phi_j(s_p)\right]\phi_j(s) \tag{5.16}$$

When there is a damping distribution that is proportional to either mass, stiffness or both, or small, in the shaft-bearing system, we can have

$$z(s)=\sum_{j=1}^{\infty}\frac{\eta_j^{\,2}}{(1-\eta_j^{\,2}+i(2D_j\eta_j)}\left[c_j+\frac{1}{H_j}\sum_{p=1}^{P}U_p\phi_j(s_p)\right]\phi_j(s) \tag{5.17}$$

where D_j is modal damping coefficient.

Furthermore, the balance correction vector $\{\hat{U}\}$ can be expressed as

$$\{\hat{U}\}=\{U_1,U_{2,}.....,U_p\}^T \tag{5.18}$$

and the subvectors of the principal modes as

$$\{\Psi_{Pj}\}=\{\phi_j(s_1)\quad\phi_j(s_2)\quad\cdots\quad\phi_j(s_p)\}^T \tag{5.19}$$

in which $s_1,s_2,.....s_p$ are the locations of correction planes on the shaft.

Therefore, Q measurements of the unbalance responses of the shaft can be taken at $s=s_q$ for $q=p+1,p+2,.....,p+Q$. Now, the measurement vector $\{Z\}$ is defined as

$$\{Z\}=\{z(s_{p+1})\quad z(s_{p+2})\quad\cdots\quad z(s_{p+Q})\}^T \tag{5.20}$$

and the subvectors of the principal modes as

$$\{\Psi_{Qj}\}=\{\phi_j(s_{p+1})\quad\phi_j(s_{p+2})\quad\cdots\quad\phi_j(s_{p+Q})\}^T \tag{5.21}$$

If Eq. (5.20) is combined with Eq. (5.16), one obtains

$$\{Z\}=\sum_{j=1}^{\infty}\frac{\eta_j^{\,2}}{1-\eta_j^{\,2}}\left[c_j+\frac{1}{H_j}\{\Psi_{Pj}\}^T\{\hat{U}\}\right]\{\Psi_{Qj}\} \tag{5.22}$$

If we use $\{Z_0\}$ to represent the shaft deflections caused by the initial unbalance $u(s)$ before the balancing correction is applied to the shaft, then

$$\{Z_0\} = \sum_{j=1}^{\infty} \frac{\eta_j^{\,2}}{1-\eta_j^{\,2}} c_j \{\Psi_{Qj}\} \tag{5.23}$$

Also, if we consider the influence coefficient method in which the influence coefficient a_{ik} is defined as the response function of point $s = s_i$ due to a unit correction, $U_k = 1$ in the correction plane $s = s_k$. If we set for $1 \le k \le p$

$$c_j = 0\,, \qquad U_p = \begin{Bmatrix} 1 & for\ p = k \\ 0 & for\ p \neq k \end{Bmatrix}$$

in Eq. (5.16). Then, it will become

$$a_{ik} = \sum_{j=1}^{\infty} \frac{\eta_j^{\,2}}{1-\eta_j^{\,2}} \frac{1}{H_j} \phi_j(s_k)\phi_j(s_i) \tag{5.24}$$

Hence, the influence coefficient matrix $[A]$ can be defined for the measurement vector $\{Z\}$ and correction vector $\{\hat{U}\}$ based on Eq. (5.24) as

$$[A] = \begin{bmatrix} a_{p+1,1} & a_{p+1,2} & \cdots & a_{p+1,P} \\ a_{p+2,1} & a_{p+2,2} & \cdots & a_{p+2,P} \\ \vdots & \vdots & & \vdots \\ a_{p+Q,1} & a_{p+Q,2} & \cdots & a_{p+Q,P} \end{bmatrix} = \sum_{j=1}^{\infty} \frac{\eta_j^{\,2}}{1-\eta_j^{\,2}} \frac{1}{H_j} \{\Psi_{Qj}\}\{\Psi_{Pj}\}^T \tag{5.25}$$

However, if we expand the Eq. (5.22) and substitute Eq. (5.15) and Eq. (5.25), thereafter, we will have

$$\{Z\} = \sum_{j=1}^{\infty} \frac{\eta_j^{\,2}}{1-\eta_j^{\,2}} c_j \{\Psi_{Qj}\} + \sum_{j=1}^{\infty} \frac{\eta_j^{\,2}}{1-\eta_j^{\,2}} \frac{1}{H_j} \{\Psi_{Qj}\}\{\Psi_{Pj}\}^T \{\hat{U}\} = \{Z_0\} + [A]\{\hat{U}\} \tag{5.26}$$

In order to make the residual unbalance deflections of the shaft equal to zero by applying the balance correction $\hat{U}$, different methods of balancing flexible shaft can be realized from Eq.(5.22) and Eq. (5.26) in that order. In the first instance, if in Eq. (5.22), we set

$$c_j + \frac{1}{H_j}\{\Psi_{Pj}\}^T\{\hat{U}\} = 0, \quad j = 1,2,..... \tag{5.27}$$

the Eq. (5.22) will become equal to zero. That is, $\{Z\} = \{0\}$. In this case, the modal components of unbalance are corrected in a progressive, gradually and this approach is referred to as modal balancing method.

Similarly, in Eq. (5.26), if

$$\{Z_0\} + [A]\{\hat{U}\} = \{0\} \tag{5.28}$$

we will have $\{Z\} = \{0\}$. Here, the initial unbalance deflections of the shaft at all measurement points are reduced to zero. This is due to the effect of the balance correction $\{\hat{U}\}$ as determined by the influence coefficient matrix $[A]$. This approach is termed as influence coefficient balancing method.

According to Eq. (5.22), Eq. (5.25) and Eq. (5.26), the two major types of flexible rotor balancing (modal and influence coefficient balancing) are related. However, Eq. (5.22) can be referred to as the unified expression of the modal balancing and influence coefficient techniques. It also represents the relations of the deflections of the shaft to the initial unbalance, to the balance correction and to the natural properties of the shaft.

Furthermore, let us introduce α_j and β_j to designate the following:

$$\alpha_j = \frac{\eta_j^{\,2}}{(1-\eta_j^{\,2})}, \quad \beta_j = \frac{\eta_j^{\,2}}{(1-\eta_j^{\,2} + i(2D_j\eta_j)} \qquad for\ j = 1,2,..... \tag{5.29}$$

where α_j and β_j are the *jth* undamped and damped dynamic amplifying coefficients in that order. So, if we substitute Eq. (5.29a) and Eq. (5.29b) in Eq. (5.16) and Eq. (5.17), respectively, we get

$$z(s) = \sum_{j=1}^{\infty} \alpha_j \left[c_j + \frac{1}{H_j} \sum_{p=1}^{P} U_p \phi_j(s_p) \right] \phi_j(s) \tag{5.30}$$

$$z(s) = \sum_{j=1}^{\infty} \beta_j \left[c_j + \frac{1}{H_j} \sum_{p=1}^{P} U_p \phi_j(s_p) \right] \phi_j(s) \tag{5.31}$$

Thus, the balance correction $\{\hat{U}\}$ which satisfies Eq. (5.28) can be defined as

$$\begin{aligned} [A]\{\hat{U}\} &= -\{Z_0\} \\ \{\hat{U}\} &= -[A]^{-1}\{Z_0\} \end{aligned} \tag{5.32}$$

In this case, when the Eq. (5.32) is solved, the corrections $\{\hat{U}\}$ will generally depend on the balancing speed. If we consider the expression for the Eq. (5.32a) from Eq. (5.26) along with Eq. (5.29a), the equation will become

$$\sum_{j=1}^{\infty} \alpha_j \frac{1}{H_j} \{\Psi_{Qj}\}\{\Psi_{Pj}\}^T \{\hat{U}\} = -\sum_{j=1}^{\infty} \alpha_j c_j \{\Psi_{Qj}\} \tag{5.33}$$

In addition, if we assume that the *nth* critical speed of the rotor that is higher than the operating speed is ω_n, then the following expressions can be obtained

$$[\Phi_{Pn}] = \begin{bmatrix} \Psi_{P1} & \Psi_{P2} & \cdots & [\Psi_{Pn}] \end{bmatrix}, \; \Phi_{Qn} = [\Psi_{Q1} \quad \Psi_{Q2} \quad \cdots \quad \Psi_{Qn}], \; \{\hat{C}\} = \{\hat{c}_1 \quad \hat{c}_2 \quad \cdots \quad \hat{c}_n\}^T \tag{5.34}$$

$$diag(\alpha_j) = \begin{bmatrix} \alpha_1 & 0 & 0 & 0 \\ 0 & \alpha_2 & 0 & 0 \\ 0 & 0 & \ddots & 0 \\ 0 & 0 & 0 & \alpha_n \end{bmatrix}, \quad diag\left(\frac{1}{H_j}\right) = \begin{bmatrix} \frac{1}{H_1} & 0 & 0 & 0 \\ 0 & \frac{1}{H_2} & 0 & 0 \\ 0 & 0 & \ddots & 0 \\ 0 & 0 & 0 & \frac{1}{H_n} \end{bmatrix} \tag{5.35}$$

where $H_j \equiv jth$ modal mass, $\alpha_j \equiv \frac{\eta_j^{\,2}}{1-\eta_j^{\,2}}$, $\eta_j \equiv \Omega/\omega_j$, $\{\hat{C}\} \equiv$ unbalance components and $[\Phi_{Pn}]$ and $[\Phi_{Qn}] \equiv$ modal component matrices corresponding to the correction planes and the measurement points on the shaft, respectively. One can rewrite Eq. (5.33) in the following expanded form:

$$\left(\sum_{j=1}^{n}\alpha_j\frac{1}{H_j}\{\Psi_{Qj}\}\{\Psi_{Pj}\}^T+\sum_{j=n+1}^{\infty}\alpha_j\frac{1}{H_j}\{\Psi_{Qj}\}\{\Psi_{Pj}\}^T\right)\{\hat{U}\}=-\left(\sum_{j=1}^{n}\alpha_j c_j\{\Psi_{Qj}\}+\sum_{j=n+1}^{\infty}\alpha_j c_j\{\Psi_{Qj}\}\right) \quad (5.36)$$

Upon substituting Eq. (5.34) and Eq. (5.35) into this Eq. (5.36), we obtain

$$\left[[\Phi_{Qn}]diag(\alpha_j)diag\left(\frac{1}{H_j}\right)[\Phi_{Pn}]^T+\sum_{j=n+1}^{\infty}\alpha_j\frac{1}{H_j}\{\Psi_{Qj}\}\{\Psi_{Pj}\}^T\right]\{\hat{U}\}= -\left[[\Phi_{Qn}]diag(\alpha_j)\{C\}+\sum_{j=n+1}^{\infty}\alpha_j c_j\{\Psi_{Qj}\}\right] \quad (5.37)$$

Noting that Ω , Ω_{op} and ω_n are balancing speed, operating speed and nth critical speed while ω_{n+1} is the $(n+1)th$ critical speed of rotor and n is the order of the critical speed that is just higher than the operating speed. Since operating speed of the rotor is lower than its nth critical speed, then for the corrections $\{\hat{U}\}$ to be determined by Eq. (5.32) and Eq. (5.27), the following conditions needed to be met:

$$\Omega \le \Omega_{op} < \omega_n, \quad \Omega_{op} << \omega_{n+1} \quad (5.38)$$

The operation speed of the rotor is much lower than its $(n+1)th$ critical speed, if the condition in Eq. (5.38) is met, we will have

$$\eta_j << 1, \ \alpha_j << 1, \qquad j = n+1, n+2, ... \quad (5.39)$$

Then, the summation on the both sides of Eq. (5.37) can be neglected. So, Eq. (5.37) can be reduced to

$$\left[[\Phi_{Qn}]diag(\alpha_j)diag\left(\frac{1}{H_j}\right)[\Phi_{Pn}]^T\right]\{\hat{U}\} = -\left[[\Phi_{Qn}]diag(\alpha_j)\{C\}\right] \qquad (5.40)$$

then the other conditions are

$$\eta_j \neq 1,\ j = 1,2,.....,n \qquad (5.41)$$

$$P = Q = n \qquad (5.42)$$

$$\det([\Phi_{Qn}]) \neq 0, \qquad \det([\Phi_{Pn}]) \neq 0 \qquad (5.43)$$

The $diag(\alpha_j)$ will not be singular if and only if the condition in Eq. (5.41) is met. Similarly, the modal component matrices $[\Phi_{Qn}]$ and $[\Phi_{Pn}]$ will be square and nonsingular if the conditions in Eq. (5.42) and Eq. (5.43) are met. When all these conditions are met, Eq. (5.40) becomes

$$\{\hat{U}\} = -\left[diag\left(\frac{1}{H_j}\right)[\Phi_{Pn}]^T\right]^{-1}\{C\} \qquad (5.44)$$

Since all the terms in the Eq. (5.44) are constants and independent of balancing speed, then, the balancing correction $\{\hat{U}\}$ is a constant vector. Hence, due to the fact that Eq. (5.32) and Eq. (5.40) have the same solutions, balancing correction defined by Eq. (5.44) is the solution of Eq. (5.32) that represents the influence coefficient balancing.

In addition, to be able to ascertain whether the solution $\{\hat{U}\}$ defined by the Eq. (5.44) will satisfy the equation of modal balancing or not, the Eq. (5.44) can be expressed as

$$\left[diag\left(\frac{1}{H_j} \right) [\Phi_{Pn}]^T \right] \{\hat{U}\} + \{C\} = \{0\} \tag{5.45}$$

or

$$\left(\frac{1}{H_j} \right) \{\Psi_{Pn}\}^T \{\hat{U}\} + c_j = \{0\}, \qquad j = 1,2,.....,n \tag{5.46}$$

If Eq. (5.46) is compared with Eq. (5.27), it can be seen that the Eq. (5.46) is exactly the equation of modal balancing for the first n principal modes. Thus, it can be concluded that when the conditions in the equations (5.38), (5.41), (5.42) and (5.43) are satisfied, the balancing correction $\{\hat{U}\}$ acquired by using the influence coefficient method and solving Eq. (5.32), is equivalently given by Eq. (5.44). Therefore, at any speed that is lower than or equal to the operation speed, the first n modal components of unbalance can be balanced. In other words, the calculated correction masses at the low balancing speed (a convenient speed below the first critical rotor speed) are sufficient to balance the rotor, which should stay balanced at any other higher operating speed.

It should be noted that the unbalance components $c_j\,(j = 1,2,....,n)$ are not required to be known. Besides, the above analysis can also be made for rotor-bearing system with linear proportional damping. By considering the Eq. (5.31) and Eq. (5.32), we can obtain

$$\begin{aligned} \left[[\Phi_{Qn}] diag(\beta_j) diag\left(\frac{1}{H_j} \right) [\Phi_{Pn}]^T + \sum_{j=n+1}^{\infty} \beta_j \frac{1}{H_j} \{\Psi_{Qj}\} \{\Psi_{Pj}\}^T \right] \{\hat{U}\} = \\ - \left[[\Phi_{Qn}] diag(\beta_j) \{C\} + \sum_{j=n+1}^{\infty} \beta_j c_j \{\Psi_{Qj}\} \right] \end{aligned} \tag{5.47}$$

When the conditions in the equations (5.38), (5.41), (5.42) and (5.43) are met, Eq. (5.47) becomes

$$\left[[\Phi_{Qn}] diag(\beta_j) diag\left(\frac{1}{H_j}\right) [\Phi_{Pn}]^T \right] \{\hat{U}\} = -\left[[\Phi_{Qn}] diag(\beta_j) \{C\} \right] \tag{5.48}$$

Similarly, the solution of Eq. (5.48) is given by

$$\{\hat{U}\} = -\left[[\Phi_{Pn}]^T diag\left(\frac{1}{H_j}\right) \right]^{-1} \{C\} \tag{5.49}$$

Equation (5.49) satisfies the modal balancing equation,

$$\left(\frac{1}{H_j}\right) \{\Psi_{Pn}\}^T \{\hat{U}\} + c_j = \{0\}, \qquad j = 1,2,.....,n \tag{5.50}$$

Nevertheless, for the linear proportional damping systems, Eq. (5.49) and Eq. (5.50) reveal that when the aforementioned conditions are fulfilled, the balancing correction $\{\hat{U}\}$ that satisfies the equations of modal balancing is independent of both balancing speed and damping of the rotor-bearing system. Finally, if the above conditions were met, by using the influence coefficient method at a single balancing speed, multi-correction-plane and multi measurement point, the first n modal component of unbalance of a flexible rotor can be corrected at low speed. In the next section, the procedure of implementation is described.

5.2 Low-Speed Balancing Procedure

In the case of actual filed applications, mode shapes and operational deflection shapes (ODS) of the rotor are to be acquired using experimental and operational modal analysis, respectively. However, the developed low-speed balancing scheme can be implemented numerically using the equations derived in Section 5.1 for the case of numerical testing of the method. The procedure listed hereunder is same for either case; regardless of the means of obtaining the modal characteristics of the rotor.

1.) Determine the operation speed Ω_{op} of the rotor

2.) Determine how many number of critical speed $(\omega_1, \omega_2, ...\omega_{n-1})$ that are below the operation speed and let their total number be N_c. The next critical speed ω_n that is above the operation speed will also need to be determined. Then, the total number of critical speed will then be $N = N_c + 1$ (Modal analysis may be required here). For example, if $N_c = 2$ then, $N = 3$.

3.) Carry out the harmonic response analysis on unbalance rotor at operation speed and construct the normal mode shapes (as in Figure 5.2) for the first N critical speeds obtained from step 2. Then, obtain the measurement points Q (represented by $M_1, M_2, ..., M_N$) and balancing planes P (represented by $S_1, S_2, ..., S_N$) from the figure as shown in Figure 5.2. It should be noted that none of the selected point should be allowed to fall on the node. However, the selected balancing planes should close to antinodes. It should be noted here that if $N_c = 2$ for instance, it means that the rotor operating speed is above the second critical speed but less than third. Then, $N = 3$ and in order to be able to have mode shape

for 3rd critical speeds, the operation speed will be assumed to be 3rd critical speeds. Its operation deflection shape (ODS) will then be used in that capacity. The normal mode shapes corresponding to three (N) critical speeds of the rotor modeled using *model B* (Figure 5.3) are shown in Figure 5.2

4.) Use the first condition (Eq. (5.43)) in section 5.1 to choose the balancing speed Ω (in this work, it is always less than first critical speed) and ensure thereafter that conditions in Eq. (5.44) and Eq. (5.46) are satisfied.

5.) Take and record the initial measurement vector of unbalance $\{Z_0\}$ (at both operation and balancing speeds) at N measurement points obtained from step 3.

6.) Carry out the balancing procedure using the influence coefficient method (as described in section 2.1.2) by using one balancing speed Ω and one run for each of the correction planes obtained in step 3. Measured the response/deflection (amplitude) of the rotor shaft accordingly at number of measuring points obtained from step 3 also (detail in section 2.1.2).

7.) Determine the influence coefficient matrix $[A]$ from results obtain in steps 5 and 6 as described in section 2.1.2 (using Eq. (2.20))

8.) Then, determine the required balancing correction vector $\{\hat{U}\}$ from Eq. (2.18) in section 2.1.2

9.) Use the result obtained in step 8 as required balancing corrections for the rotor

10.) Test runs the rotor at both balancing and operating speeds

11.) If the measured residual vibration is higher than the selected severity criteria, then any of the following measures can be applied:

- Any of the correction parameters (weight, radius and phase), preferably phase(s) can be adjusted and repeat the balancing again from step 6. This approach is encouraged if it was convinced that the measurement and correction planes selected were correct.
- The balancing and measurement planes can be adjusted if necessary.

5.3 Rotor-Bearing System Modeling

The ANSYS 12.1 was used to model and carry out all the analysis involved in this work. The stationary reference frame was considered in this work based on ANSYS advice in order to obtain reliable results. However, the two ways considered through which rotor could be modeled are as shown in the Figure 5.3. The *model B* in Figure 5.3 was considered for the rotor modeling throughout this work. This model is better than the second one in the sense that there is opportunity to have required number of correction planes and locate the correction weights at any desired part of the geometry of the rotor. All these are not available in the *model A* where all disks have been converted to concentrated load. The natural frequencies to be obtained from *model B* are higher than those from *model A.* However, from the sensitivity graph only the disk radius would impact critical speeds, bearing stiffness would not have an influence on critical speed and the first critical speed is more sensitive to the radius than the second one [34]. Therefore, *model B* is very important because the *model A* did not use the exact disk geometry and due to that fact the effect of the radius of the disk on the natural frequency has been reduced if not eliminated.

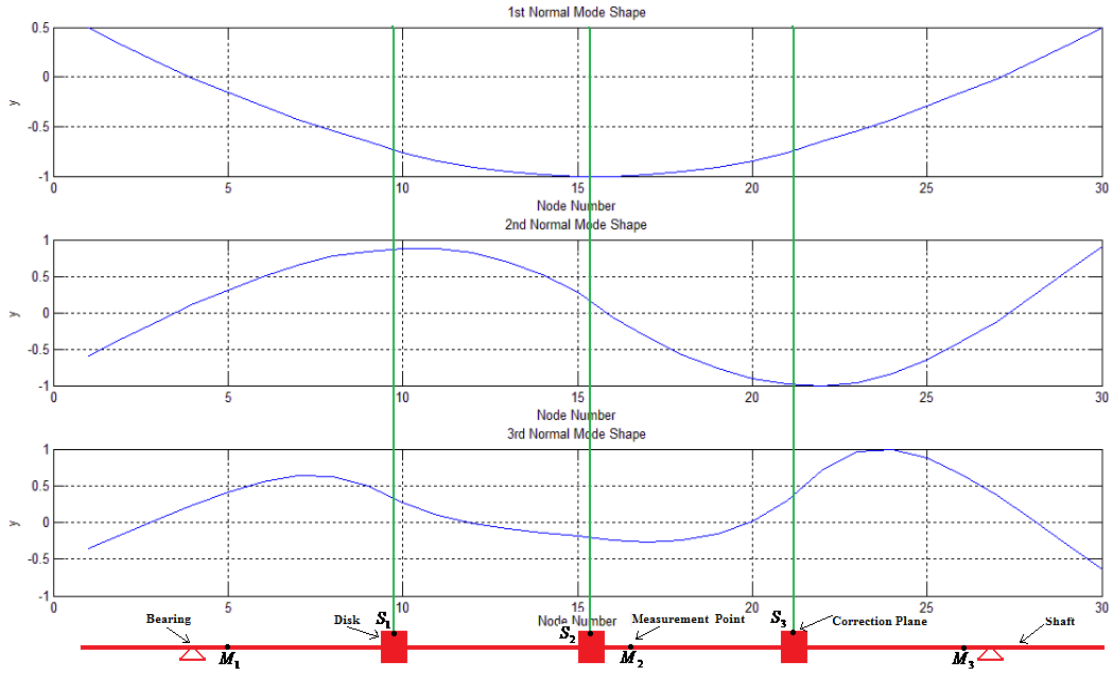

FIGURE 5.2: First and Second Normal Mode Shapes and ODS Versus Nodes Numbers for Three-Disk Rotor

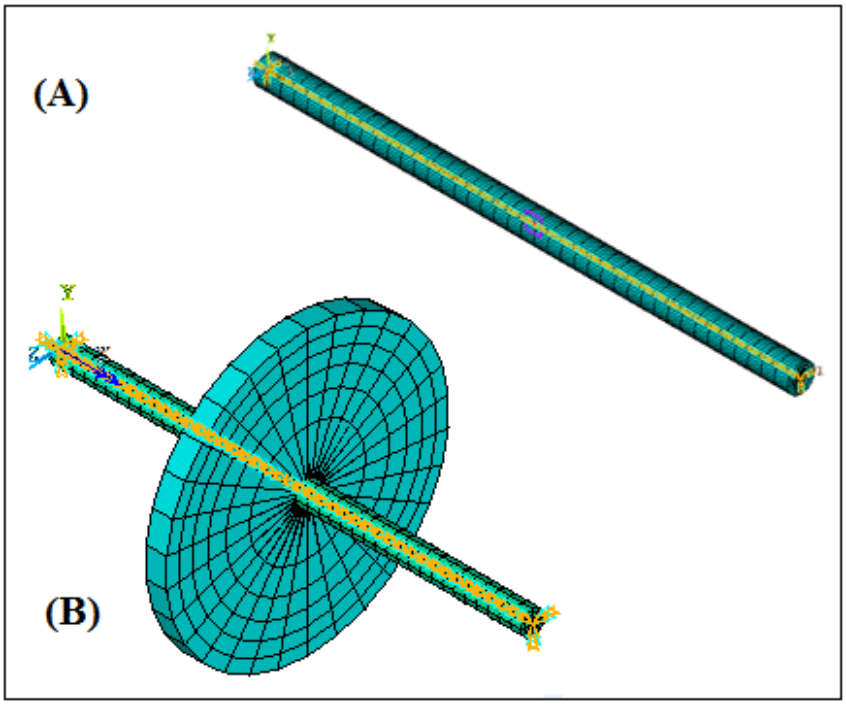

FIGURE 5.3: Two Different Ways of Modeling Rotor (A) Disk was considered as concentrated load on the shaft (B) Actual geometry of disk was considered with shaft

The BEAM188 and COMBIN214 elements were used in this work throughout for modeling entire rotor and bearings. At earlier stage, COMBIN14 was considered but COMBIN214 was later adopted due to its capability. BEAM188 was adopted because it allow one to use beam sections (SOLID and TUBE) to make diameters of both uniform and non-uniform rotor and this minimize the number of nodes to be dealt with. The sections involve in the model can be divided along the circumference and radius as much as possible. All the elements and nodes numbers that are going to be created due to these divisions will only be available to ANSYS program not to the user. Above all, ANSYS recommends the use of this element being a current-technology element. It based on Timoshenko beam theory which includes shear-deformation effects and it can be utilized for analyzing slender to moderately stubby/thick beam structures. BEAM188 has six or seven degrees of freedom at each node which include translations in the x, y, and z directions and rotations about the x, y, and z directions. A seventh degree of freedom (warping magnitude) is optional. This element is well-suited for different applications that include linear, large rotation, and/or large strain nonlinear. The elements support both consistent and lumped mass matrices. Consistent mass matrix is used by default and to use lumped mass matrix, it needs to be activated through LUMPM command.

It is noted that COMBIN214 has longitudinal as well as cross-coupling capability in 2-D applications. It is a tension-compression element with up to two degrees of freedom at each node (translations in any two nodal directions (x, y, or z)). It has two nodes plus one optional orientation node. No bending or torsion is considered. The element need to be defined by two nodes and it has stiffness characteristics K_{11} K_{22}, K_{12} and K_{21} and damping characteristics C_{11}, C_{22}, C_{12} and C_{21}. The unit of stiffness coefficient

is Force/Length while that of damping coefficient is Force×Time/Length. These characteristics can only be defined through the command. More information regarding the COMBIN214 is provided in the Appendix.

Furthermore, ANSYS parametric Design Language (APDL) was also considered in this work and everything regarding rotor under consideration which include geometry, meshing, adding gyroscopic matrix, material properties, boundary conditions and other required parameters for both modeling, modal and harmonic response analyses were carried out from APDL. APDL make the complex rotor shapes modeling and analyses easier to tackle; although programming code knowledge is highly the backbone for this approach.

Ultimately, QR Damped eigensolver was employed in modal Analysis for this work because of its capability as stated in Chapter 4. In both Modal analysis and harmonic response analyses, CORIOLIS command took care of gyroscopic effect. Also, stepped loading and SYNCHRO command (to indicate that the force on the model is due to unbalance) were also considered during harmonic analysis. The Modal analysis generates the rotor eigenvalues and their corresponding mode shapes. Thereafter, the unbalance was created on the rotor and harmonic responses analysis at operation speed was performed on the unbalance rotor in order to obtain the mode shapes. These mode shapes will be used to make the normal mode shape plot from which the appropriate correction planes and measurement points would be selected.

5.4 Computational Strategy

The developed low speed balancing scheme of flexible rotors described in the section 5.1 in conjunction with chapter 4 was adopted in this work. Moreover, all the measuring points considered for low speed balancing of flexible rotor in this work were points close

to bearing not bearing locations, as normally adopted in industry. However, this places no limitation on the method, as it is only mandated by the numerical model. This procedure would make it possible to select any number of measurement planes needed. Although, the bearing locations were the measurement points used for the two-plane balancing method because it is applicable to only rotor that has merely two bearings. The two-plane balancing method, as presented in Wowk [36] will be used for comparison purposes.

For data processing, Eq. (2.23) to Eq. (2.27) in section 2.2.2 have been written in MATLAB code, and are utilized to determine trial weights, while quality grade G was considered to be 6.3 (from Table 2.3). One of the trial weights among those calculated from these equations would be picked. Any trial weight selected was tested to see if it was capable of producing measurable response that would provide noticeable difference from that caused by initial unbalance. In addition, the correction radii are taken to be the outer radii of the rotor's disks, as commonly adopted in the literatures.

Once all the required measurement planes, correction planes and balancing speed were obtained, then the balancing operation proceeds as follows:

- First and foremost, the harmonic response analysis is performed to obtain the initial responses of rotor at the measurement points due to the unbalance both at operation and balancing speeds. The influence coefficient method of balancing

rotor would then follow by placing trial masses at the selected correction planes one after the other and carry out the harmonic response analysis at balancing speed. The measured responses at selected measuring points, together with the trial parameters (weights, radii and angles) and the initial responses at balancing speed are used to obtain the actual correction parameters.

- The influence coefficient matrix would be acquired through the Eq. (2.16) or Eq. (2.20) and corrections parameters (weights, radii and angles if Eq. (2.16) is used or weights and angles if Eq. (2.20) is used) are obtained through Eq. (2.18). These equations are programmed and solved using MATLAB.
- The trial parameters, initial responses at balance speed, and responses due to each trial weight in the course of balancing processes obtained from ANSYS harmonic response analyses are inserted into either Eq. (2.16) or Eq. (2.20). This results in the required matrix for Eq. (2.18), required to calculate the correction parameter at each correction plane.
- The acquired correction parameters are then be tested using ANSYS; both at balancing and operation speeds. These final responses after correction are compared to the initial responses of the unbalanced rotor to check the effectiveness of the balancing developed balancing scheme. If the results are not satisfactory, the process could be repeated (i.e. trim balancing session) is performed to arrive at the acceptable level of the residual unbalance.

CHAPTER 6

RESULTS AND DISCUSSIONS

In this chapter, the revised theory of low-speed balancing of flexible rotors developed in chapter 5 is applied to some case studies. The objective is to demostrate the applicability and verify the validity of the low-balancing scheme. The first case study considers a three-disk rotor, which represents a benchmark solution. The second case study represents a large-scale turbine rotor, resembling an actual industrial rotor system.

However, regarding rigid bearings, stiffness value mostly used in literatues range from 1.0E7N/m and above. In this work, the stiffness value used for rigid bearing is 1.0E8 N/m that is a representative stiffness value for the oil film in a journal bearing [30]. Steel is the material considered in this work and it is noted that it has a small damping factor η_v. The major function of damping in the system is to reduce responses and since the objective of this work is to balance the rotor, material damping was not considered. Therefore, η_v and loss factor due to hysteretic η_h were not used. If we can balance the rotor without considered these parameters, then the system will remain balanced or even more when they are considered thereafter. So, considering these parameters in our simulations when balancing is going on is not required.

6.1 Three-Disk Rotor with Rigid Bearings (1)

The Kikuchi's three-disk rotor of total mass $51.8kg$ [20] shown in Figure 6.1.1 on rigid bearings was considered here. The rotor dimensions, disk that contained unbalance and angle at which unbalance was located were as stated in Kikuchi's work. In this work, the rotor contains unbalance of 1.75E-3kg.m (at radius of 0.07m) at an angle of 0^0 on the right side of the middle disk and it is operating at a speed of 13,440 rpm, which is above the rotor's second critical speed. The bearings are rigid and they are isotropic with stiffness given by $K = 1.0E8N/m$. The objective is to balance this high-speed flexible rotor at low speed.

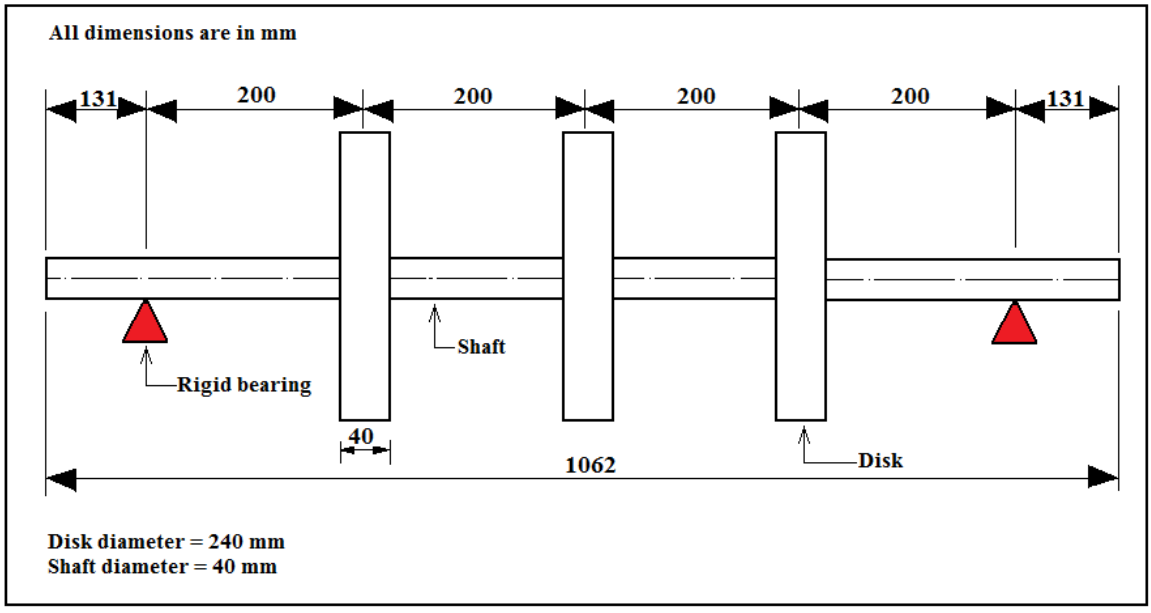

FIGURE 6.1.1: Three-Disk Rotor [20]

6.1.1Rotor Modeling

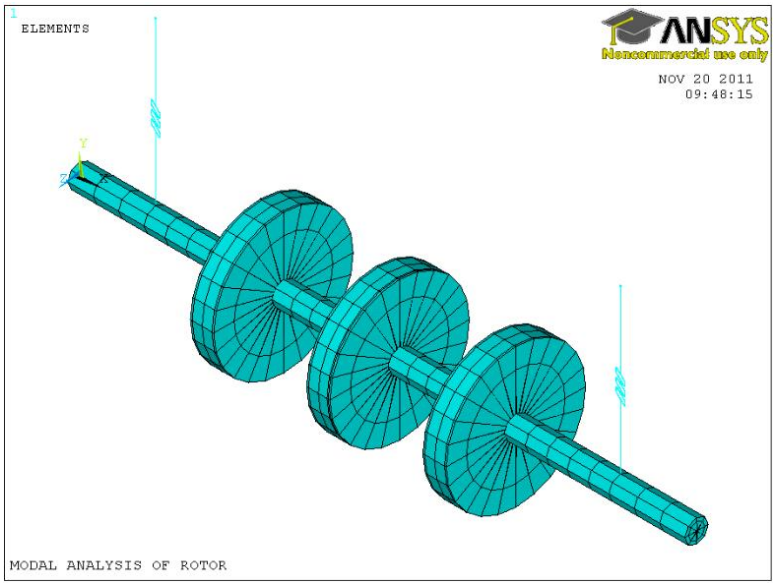

(a)Isometric View

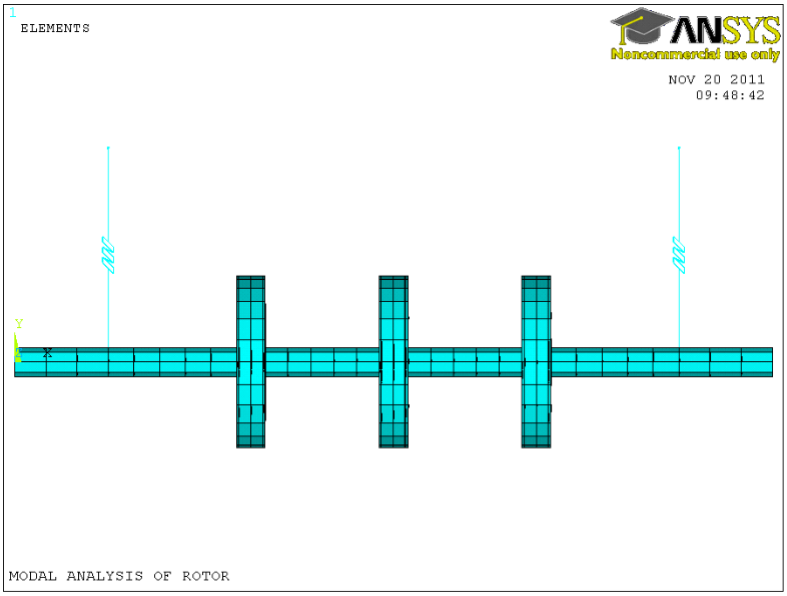

(b) Front View

FIGURE 6.1.2: Three-Disk Rotor Modeling

6.1.2 Modal Analysis of the rotor

The modal analysis was carried out on the above model at its operation speed and the first three natural frequencies of the system are listed in Table 6.1.1. The natural frequencies of this rotor were determined and reported by two other researchers. A comparison of such with results obtained by present work is tabulated in Table 6.1.2. It is observed that the first natural frequency obtained by the present model agrees with that of the Katsuaki [20], who first studied this rotor. The results obtained are higher than those obtained in Ref. [1], which is expected because the FEM used in ANSYS with consistent mass formulation is known to overestimate natural frequencies. Yet, they are known to be more accurate than those obtained using lumped mass models. Nevertheless, it is apparent that the solution of [1] has appreciably underestimated the natural frequencies.

6.1.3 Rotor Balancing

6.1.3.1 Operation Conditions

1.) The natural frequencies recorded above indicate that the rotor is operating between the second critical speed (185.34 Hz or 11,120.4 rpm) and third critical speed (392.03 Hz or 23,521.8 rpm).

2.) The operating speed Ω_{op} is 224 Hz (13,440 rpm)

TABLE 6.1.1: Natural Frequencies of the Three-Disk Rotor

Mode Number	Damped Frequency (Hz)		Undamped Frequency (HZ)
	Real	Complex	
1	0	43.43	48.695
	0	-43.43	
2	0	54.187	48.695
	0	-54.187	
3	0	163.15	185.34
	0	-163.15	
4	0	207.36	185.34
	0	-207.36	
5	0	342.69	392.03
	0	-342.69	
6	0	418.44	392.03
	0	-418.44	

TABLE 6.1.2: Natural Frequencies from Different Researchers

Natural Frequency (Hz)		
Ref. [20]	Ref. [1]	Present Work
48.7	42.8780	48.695
Not available	170.319	185.34
Not available	361.624	392.03

6.1.3.2 Mode Shapes from Harmonic Response Analysis

Based on the available parameters, the unbalance was created on the rotor as shown in Figure 6.1.3 and the harmonic response analysis was performed on the unbalanced rotor at operation speed (13,440 rpm).The mode shape corresponding to each critical speed were then obtained. Since the rotor is operating above the second critical speed, only the first and second natural mode shapes are needed. The rotor's operational deflection shape (ODS) is used to serve as mode shape of 3rd critical speed. The normal mode shapes shown in the Figure 6.1.4 are plotted, while the correction planes and measurement points are selected as shown in the Figure 6.1.4.

6.1.3.3 Low Speed Balancing Conditions

In order to satisfy the conditions required for low-speed balancing procedures described in section 5.2, the following parameters were used:

1.) Balancing speed Ω is 2,000 rpm which is well below the first critical speed.
2.) Since rotor is operating above the second critical speed, then $N = 3$ and three correction planes plus three measurement points are required.
3.) The three correction planes are S_1, S_2 and S_3 and the three measurement points are M_1, M_2 and M_3 which are located as shown in Figure 6.1.4.

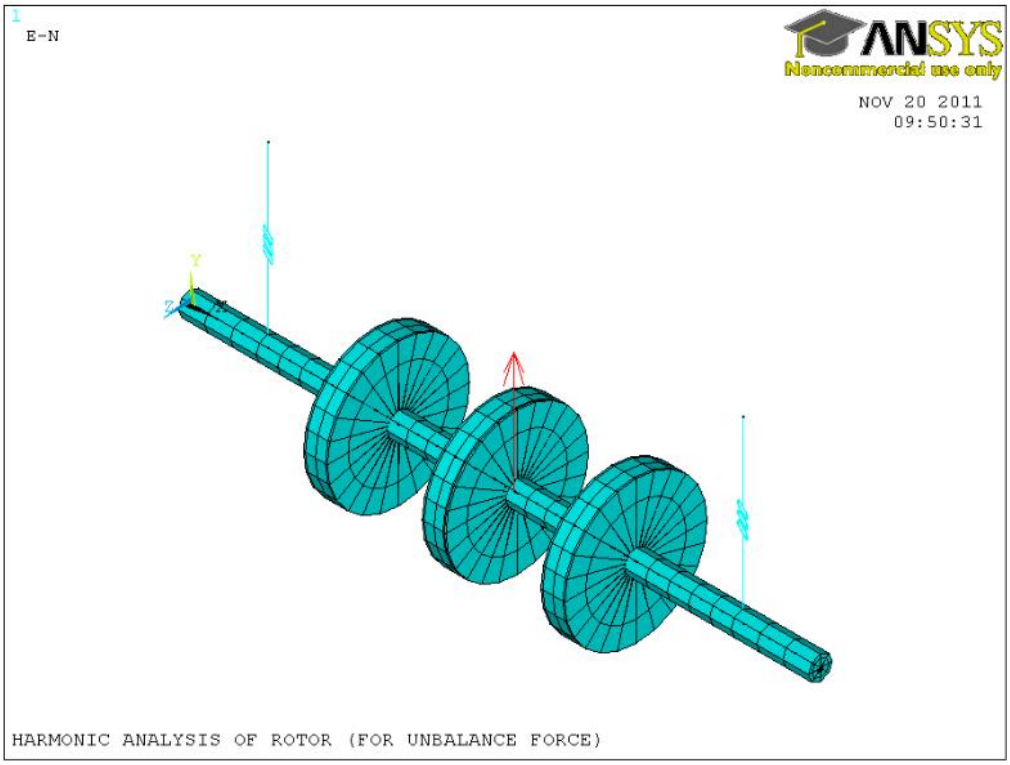

FIGURE 6.1.3: Unbalance Three-Disk Rotor

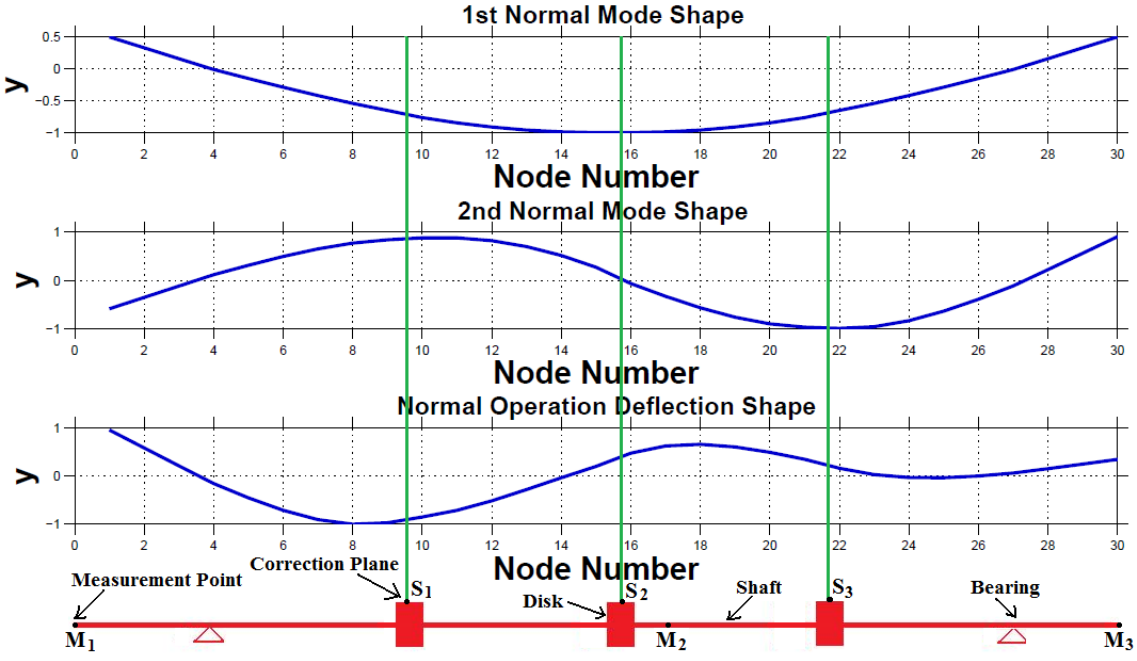

FIGURE 6.1.4: First and Second Normal Mode Shapes and ODS Versus Nodes Number

6.1.3.4 Low Speed Rotor Balancing Processes

6.1.3.4.1 Initial Responses depicted at measurement points

The Harmonic analysis was carried out for the unbalance rotor shown in the Figure 6.1.3 at speed (14,040 rpm) which is above the operation speed (13,440 rpm) and at balancing speeds in order to obtain the initial responses. The initial responses at the three measurement points (three nodes) are then acquired. The initial responses at balancing speed are shown in Table 6.1.3.

Now, having obtained the initial responses of the rotor, the balancing operation proceeds by adding trial weights to the unbalanced rotor at the selected correction planes, one after the other. Several trial sessions are carried out using the low-speed balancing procedure described in section 5.2 at balancing speed. In this context, we have tested four different sets of trial weights. The results obtained from the four different trials sessions are summarized in the Table 6.1.4.

6.1.4: Results

In this section, the correction parameters are determined by utilizing the data in Tables 6.1.3 and 6.1.4 together with the equation of the low-speed balancing procedure described in section 5.2. The balanced rotor (i.e. after adding correction masses) is tested at both balancing and operation speeds as well as at a speed above the operation speed. The acquired correction parameters and the responses at measurement points when each of the correction parameters was applied to the rotor at balancing speed are shown in the Table 6.1.5.

TABLE 6.1.3: Initial Responses at Balancing Speed (2,000 rpm)

Initial Measuremets					
Measurement Point 1 (Node 1)		Measurement Point 2 (Node 17)		Measurement Point 3 (Node 30)	
Max Amplitude	Phase (Deg.)	Max Amplitude	Phase (Deg.)	Max Amplitude	Phase (Deg.)
2.19E-05	180	4.49E-05	0	2.22E-05	180

TABLE 6.1.4: Trial Parameters, Amplitudes and Phases at each Measurement Point

Trial S/N	Trial Parameters							Measurements Due to Trial Parametrs					
								Measurement Point 1		Measurement Point 2		Measurement Point 3	
	Correction Planes		Mass (kg)	Radius r (m)	mr (kg.m)	Angle (Deg.)		Max Amplitude (m)	Phase (Deg.)	Max Amplitude (m)	Phase (Deg.)	Max Amplitude (m)	Phase (Deg.)
1	1	Node 71	0.010	0.12	1.20E-03	0		3.39E-05	180	6.61E-05	0	3.23E-05	180
	2	Node 74	0.008	0.12	9.60E-04	0		3.40E-05	180	6.95E-05	0	3.43E-05	180
	3	Node 78	0.015	0.12	1.80E-03	0		3.71E-05	180	7.80E-05	0	4.01E-05	180
2	1	Node 71	0.010	0.12	1.20E-03	10		3.37E-05	176.471	6.59E-05	-3.20336	3.22E-05	176.875
	2	Node 74	0.008	0.12	9.60E-04	170		1.02E-05	168.127	2.11E-05	-11.643	1.05E-05	168.457
	3	Node 78	0.015	0.12	1.80E-03	120		1.94E-05	137.479	4.03E-05	-45.3799	2.04E-05	130.393
3	1	Node 71	0.010	0.12	1.20E-03	5		3.38E-05	178.234	6.60E-05	-1.60	3.23E-05	178.436
	2	Node 74	0.008	0.12	9.60E-04	170		1.02E-05	168.127	2.11E-05	-11.64	1.05E-05	168.457
	3	Node 78	0.015	0.12	1.80E-03	180		6.74E-06	180	1.18E-05	-5.80E-07	4.25E-06	180
4	1	Node 10	0.010	0.12	1.20E-03	10		3.37E-05	176.471	6.59E-05	-3.20336	3.22E-05	176.875
	2	Node 16	0.008	0.12	9.60E-04	200		1.13E-05	-158.563	2.34E-05	21.07	1.16E-05	-159.094
	3	Node 21	0.015	0.12	1.80E-03	150		1.16E-05	139.157	2.32E-05	-45.6612	1.12E-05	126.564

TABLE 6.1.5: Correction Parameters and Final Amplitudes and Phases at each Measurement Point

Trial S/N	Calculated Correction Parameters				Final Measurement (Residual Unbalance)					
					Measurement Point 1		Measurement Point 2		Measurement Point3	
	Masses (kg)	Angles (Deg.)	mr (kg.m)		Max Amplitude (m)	Phase (Deg.)	Max Amplitude (m)	Phase (Deg.)	Max Amplitude (m)	Phase (Deg.)
1	0.0011	0	1.32E-04		3.36E-08	180	6.14E-08	-1.58E-04	3.07E-08	180
	0.0150	180	1.80E-03							
	0.0005	180	6.00E-05							
2	0.0011	20.0205	1.32E-04		8.89E-06	103.53	1.80E-05	-76.0295	8.94E-06	104.44
	0.0150	160.0018	1.80E-03							
	0.0005	59.9669	6.00E-05							
3	0.0011	10.0309	1.32E-04		8.10E-06	99.811	1.64E-05	-8.02E+01	8.07E-06	99.8551
	0.0150	160.0025	1.80E-03							
	0.0005	179.9573	6.00E-05							
4	0.0011	20.0077	1.32E-04		1.48E-05	-111.938	3.00E-05	68.0036	1.48E-05	-112.154
	0.0150	-139.998	1.80E-03							
	0.0005	119.9291	6.00E-05							

It is noted that, when the four sets of correction parameters (in Table 6.1.5) were applied to the rotor one after the other, the rotor was balanced not only at balancing speed but also at operation speed. The amplitude-phase plot of the initial responses due to unbalance and final responses acquired when rotor was balanced using the 1st and 3rd correction parameters at both balancing and operation speeds are shown, for each measurement point in subsection 6.1.4.2.

Accordingly, it is concluded from Figures 6.1.7 to 6.1.9 that the rotor could be balanced at low speed (a speed less than the first critical speed).

6.1.4 .1 3D Plots of Critical Mode shapes of the Rotor

Since rotor is operating above second critical speed, the 3D plots of the first two critical mode shapes of the rotor at operation speed (before and after balancing) are shown in the Figure 6.1.5. It is imperative to know that these mode shapes are obtained through the harmonic analysis at excitation frequency equivalent or close to each of the two critical speeds of normal rotor. The figures show the difference in rotor mode shapes before and after balancing.

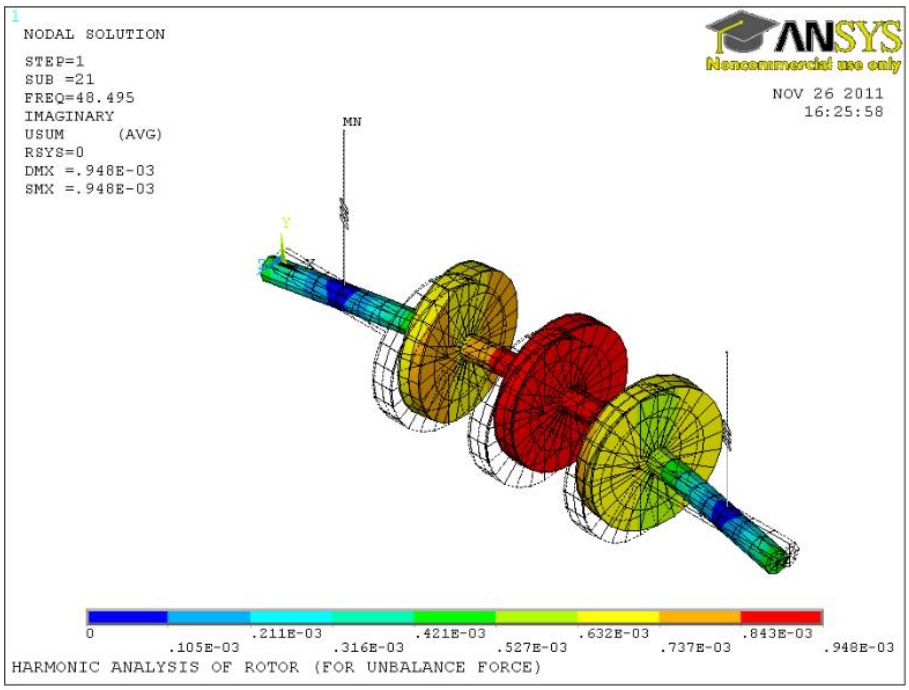

(a1): First critical mode Shape at excitation frequency of 48.495Hz before balancing

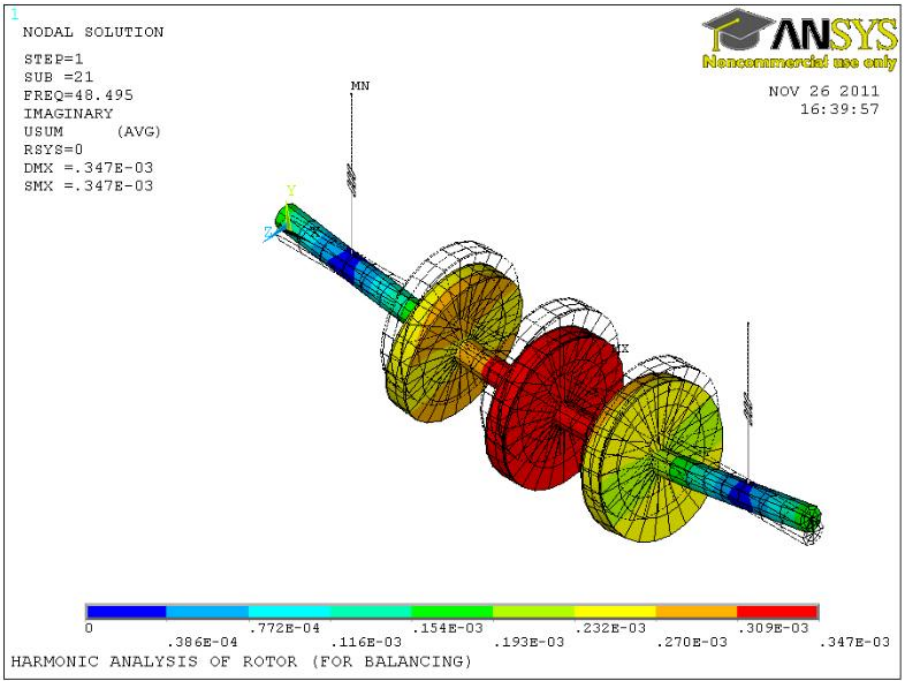

(a2): First critical mode shape at excitation frequency of 48.495Hz after balancing

FIGURE 6.1.5 (a): Three-Disk Rotor Mode Shapes Before and After Balancing

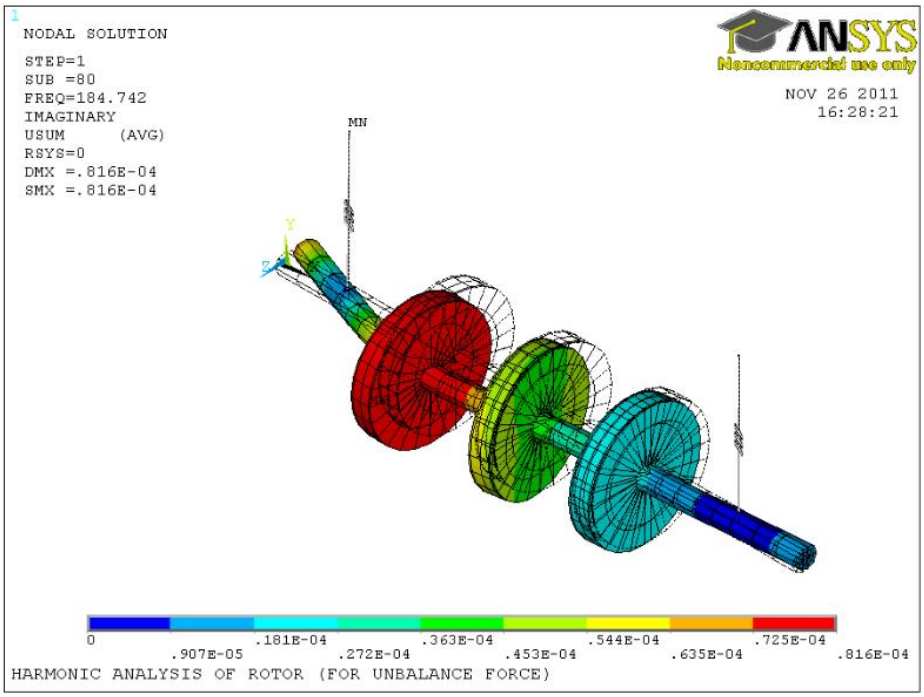

(b1): Second critical mode shape at excitation frequency of 184.742Hz before balancing

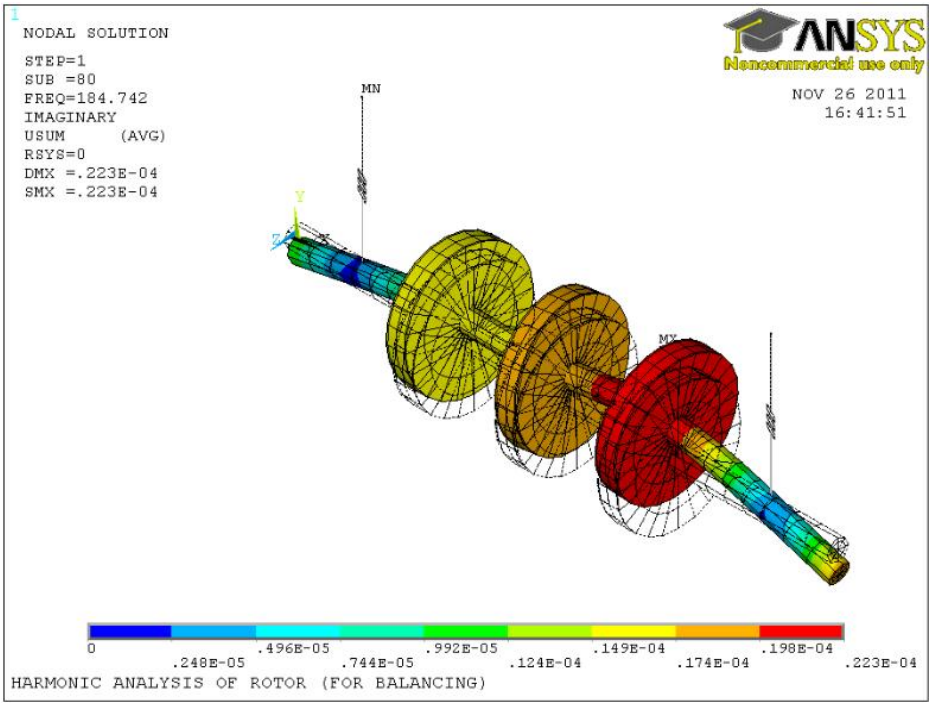

(b2): Second critical mode shape at excitation frequency of 184.742Hz after balancing

FIGURE 6.1.5 (b): Three-Disk Rotor Mode Shapes Before and After Balancing

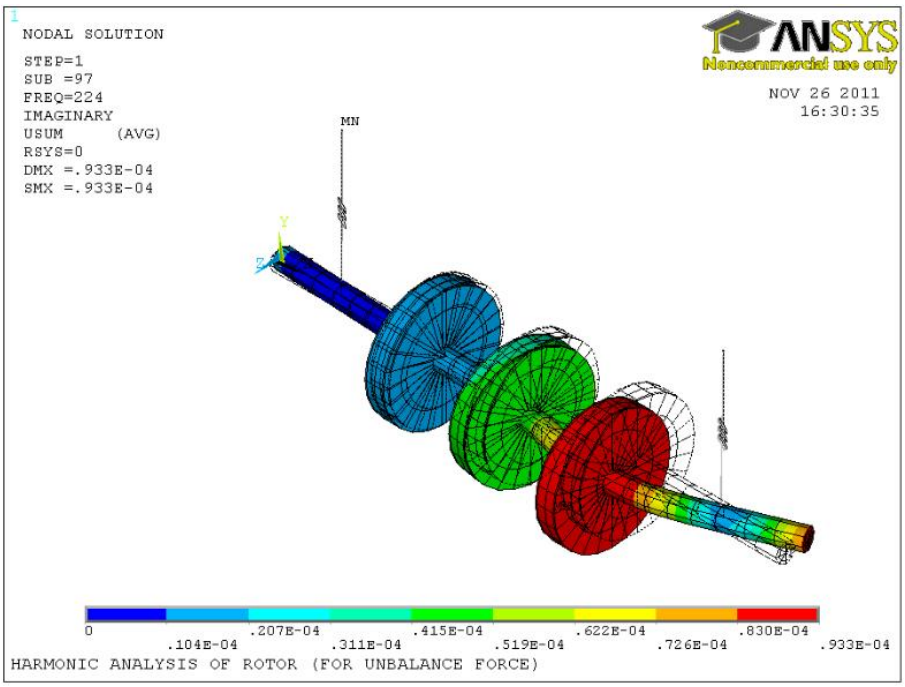

(c1): Operation deflection shape at excitation frequency of 224Hz before balancing

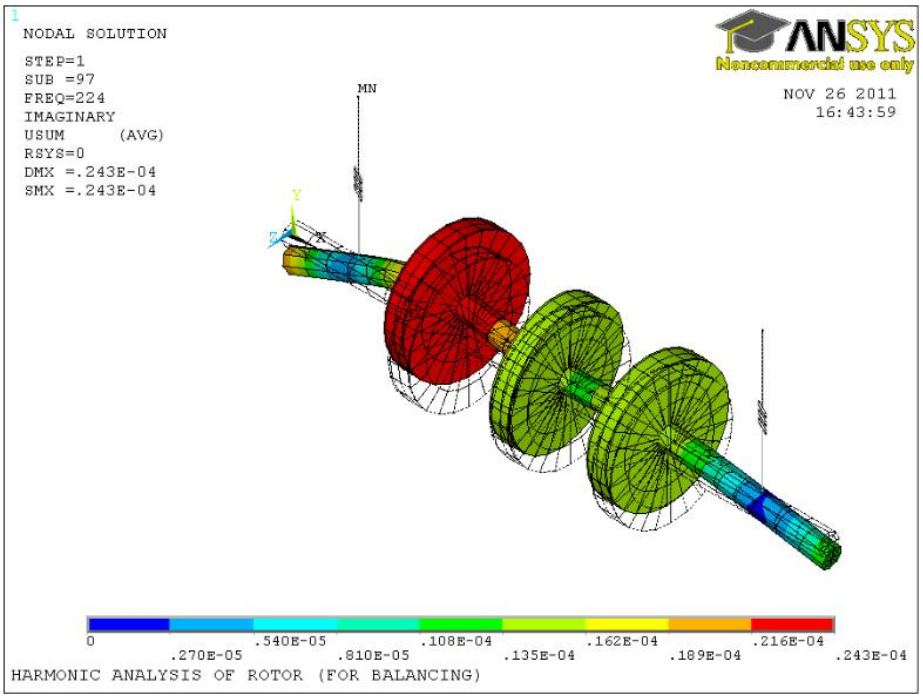

(c2): Operation deflection shape at excitation frequency of 224Hz after balancing

FIGURE 6.1.5 (c): Three-Disk Rotor Mode Shapes Before and After Balancing

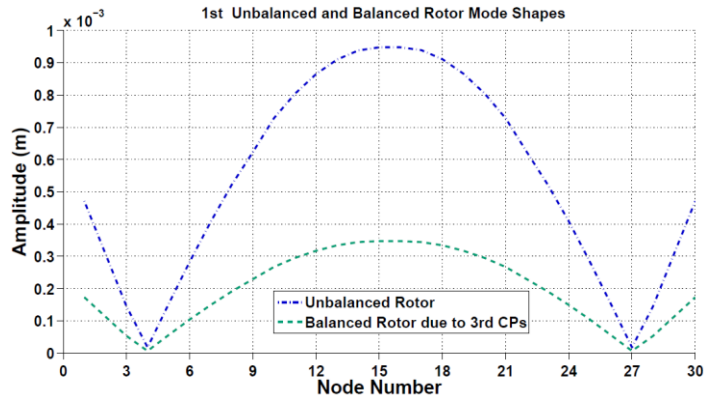

(a) First Mode

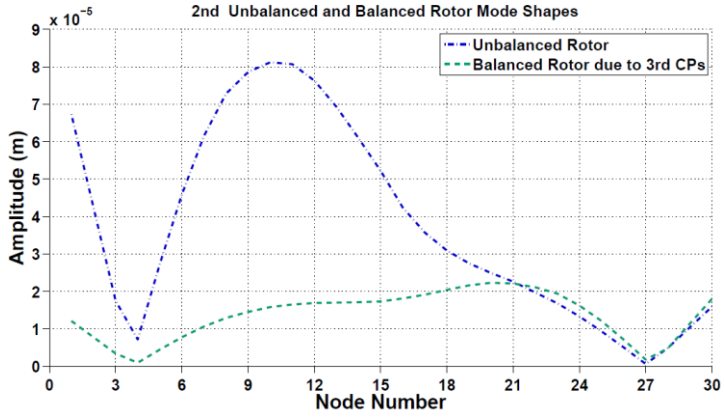

(b) Second Mode

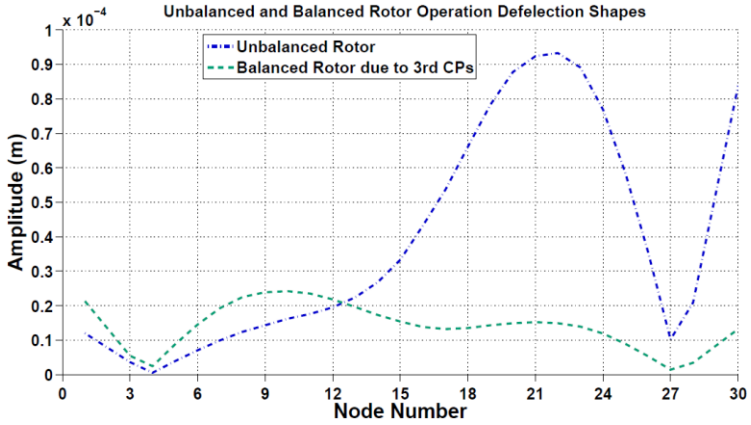

(c) Operation Deflection Shape (OPDS)

FIGURE 6.1.6: Unbalanced and Balanced Three-Disk Rotor Mode Shapes

Similarly, despite the fact that the differences in mode shapes are shown in three-diemnsional configuration in Figure 6.1.5 for unbalanced and balanced rotor, these differences were corroborated further in Figure 6.1.6 (a, b and c). Both Figures 6.1.5 and 6.1.6 are obtained by using USUM. It can been seen in these figures that modes of the rotor have been reduced drastically after the rotor was balanced.

6.1.4.2 Amplitude–phase plot (Bode Plot)

When the correction parameters (in Table 6.1.5) are applied to the rotor one after the other during the test-run at balancing and operation speeds as well as speed above the operation speed, the amplitude phase plots are made from the responses obtained. The amplitude-phase plot is made up of two parts, which include the amplitude versus frequency and the phase versus frequency. These are shown in the Figures 6.1.7 to 6.1.9 for all measurement points. Such figures demonstrate clearly how the low-speed balancing scheme reduced the initial unbalance to an acceptable level; as explained hereunder.

The Figures 6.1.7 shows the rotor responses at three measuring points; before and after balancing. It can be seen that at all measuring points, the final responses are decreased drastically when compared to initial response at balancing speed. Also, Figures 6.1.8 and 6.1.9 show the rotor responses (in y and z directions) at all measuring points when it is being tested at a speed above its operation speed. The initial responses that have been obtained from unbalanced rotor were plotted against the responses of balanced rotor. The vertical dashed line indicates the actual rotor operation speed.

Rotor was run to a speed above its operation speed in order to observe how far the balanced rotor will be able to maintain its balanced state. This test becomes necessary; as precautionary measure to check the likelihood that the rotor speed may drift above the operating speed, due to some unexpected operating circumstances. This test will allow one to know the safe speed that needs to be considered during all modes of operation without compromising the balancing conditions.

(1)Amplitude in Y- Direction at Balancing Speed

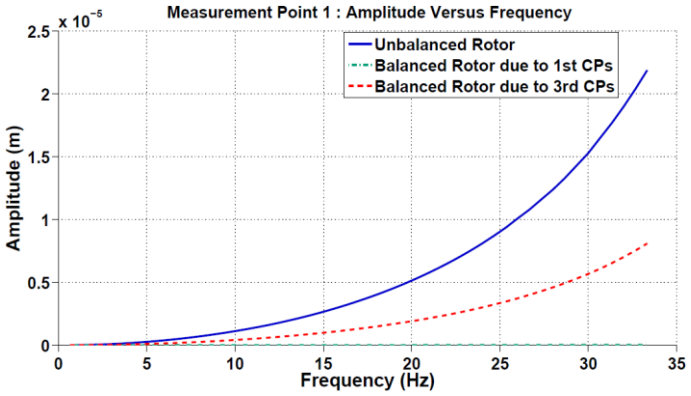

(a)Measurement point 1

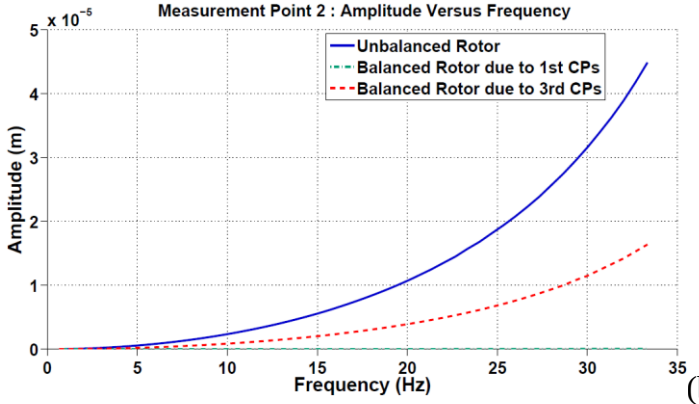

(b) Measurement point 2

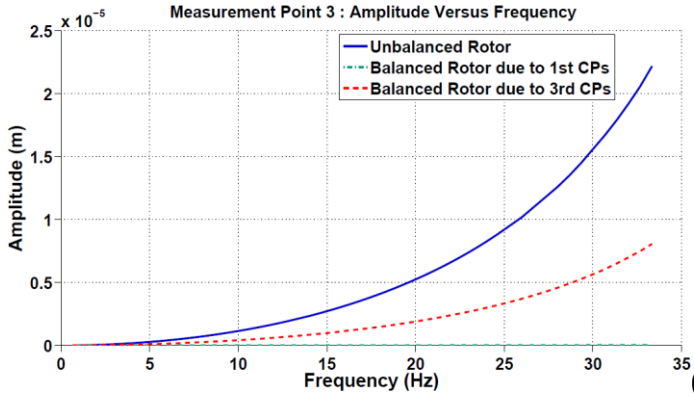

(c) Measurement point 3

FIGURE 6.1.7: Plot of Responses due to the Correction Parameters and Initial Responses at Balancing Speed at Three Measurement Points

(2)Amplitude-phase Plots in Y- Direction at Speed above the Operation Speed

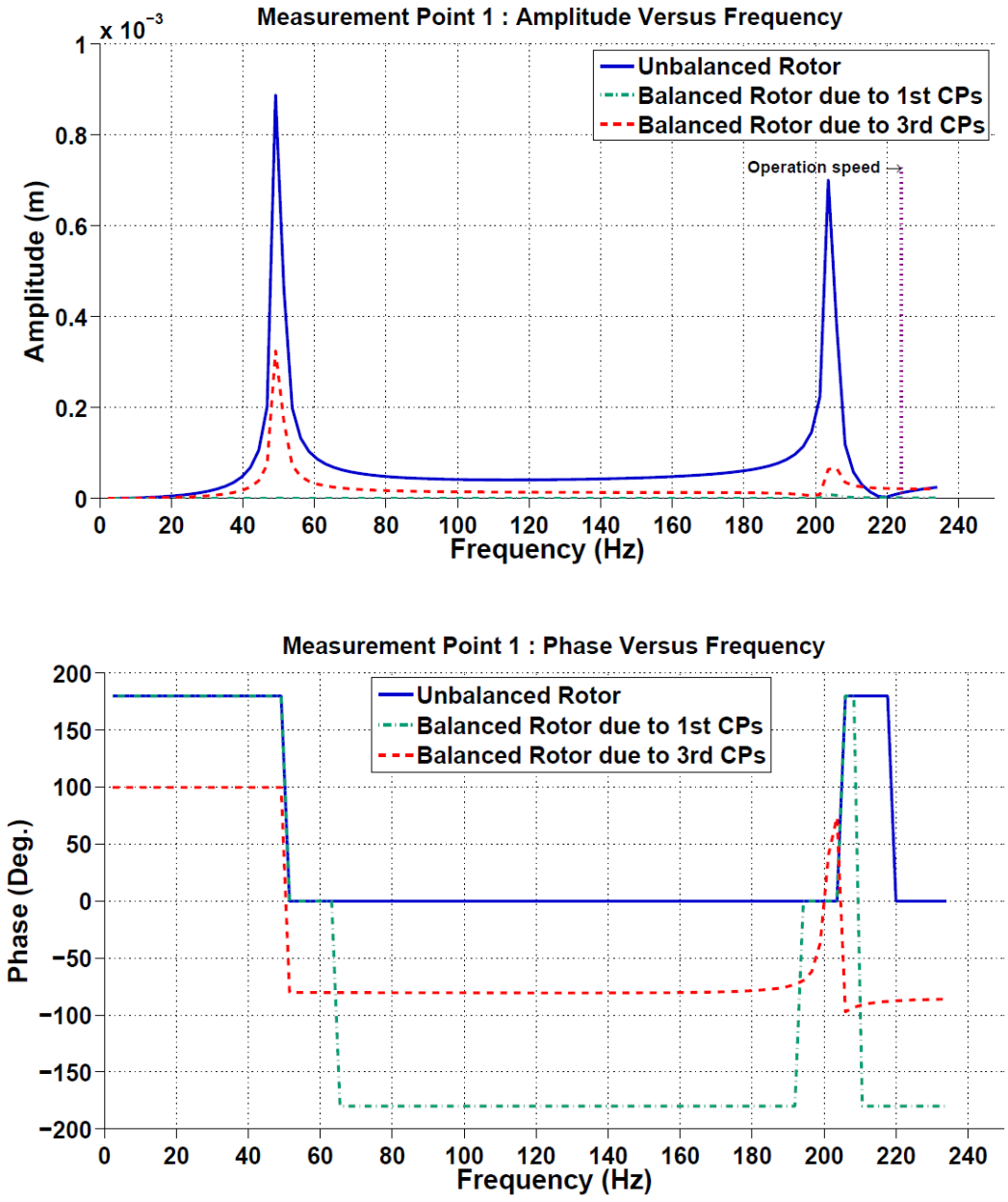

FIGURE 6.1.8: Amplitude Phase Plots (Y-Direction) at Speed above Operation Speed: at ***Measurement Point 1***

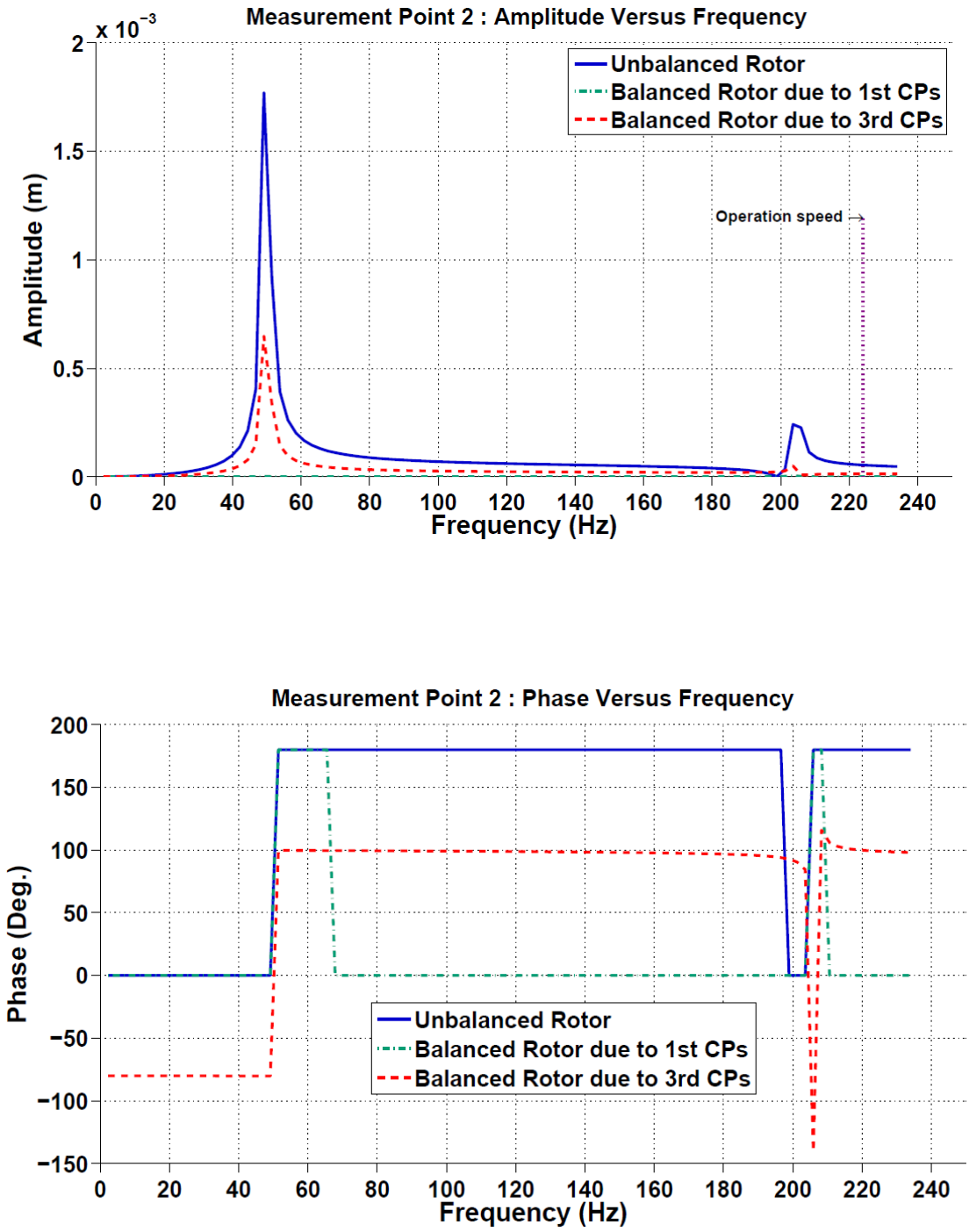

FIGURE 6.1.8: Amplitude Phase Plots (Y-Direction) at Speed above Operation Speed: at ***Measurement Point 2***

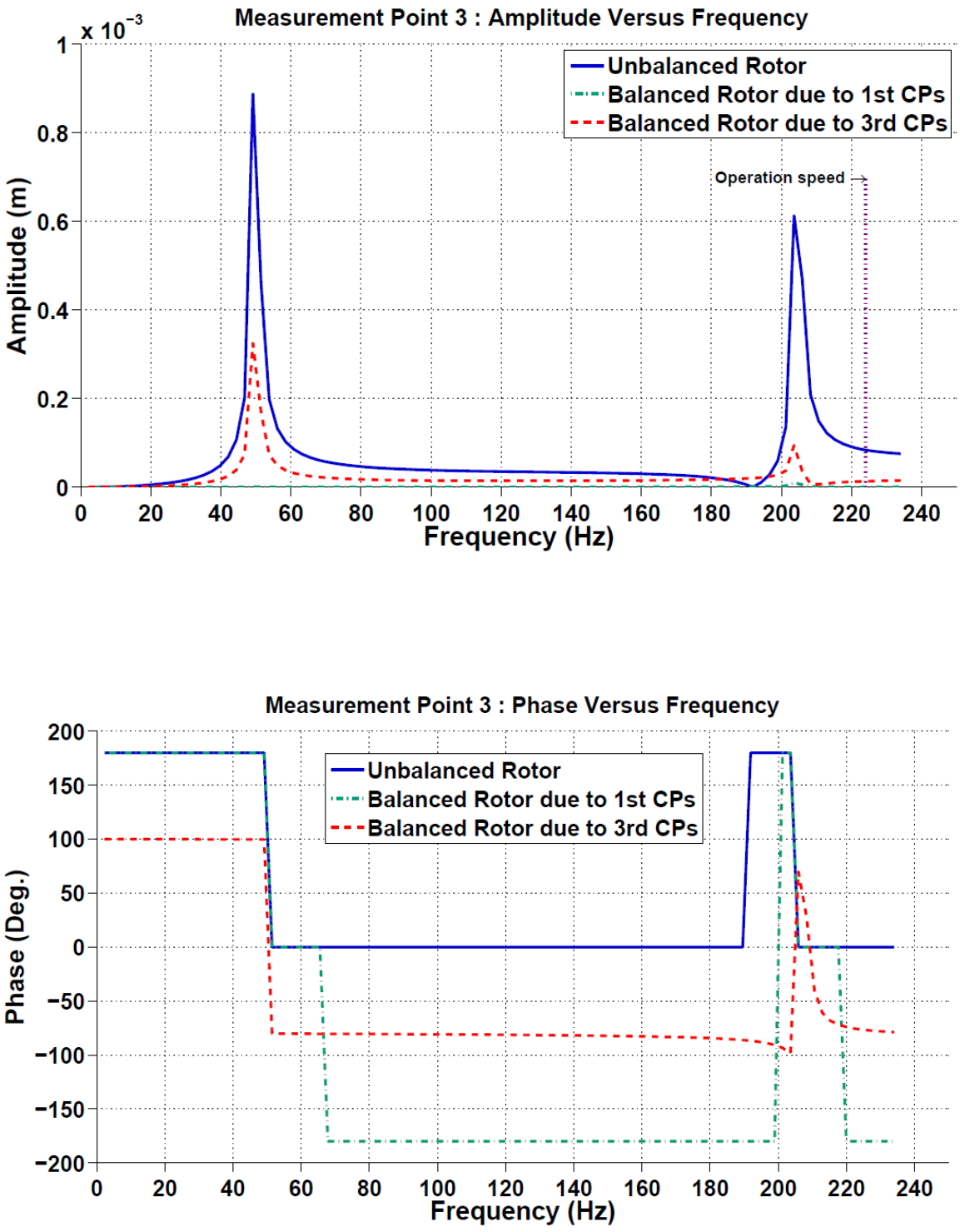

FIGURE 6.1.8: Amplitude Phase Plots (Y-Direction) at Speed above Operation Speed: at ***Measurement Point 3***

(3) Amplitude-phase Plots in Z- Direction at Speed above the Operation Speed

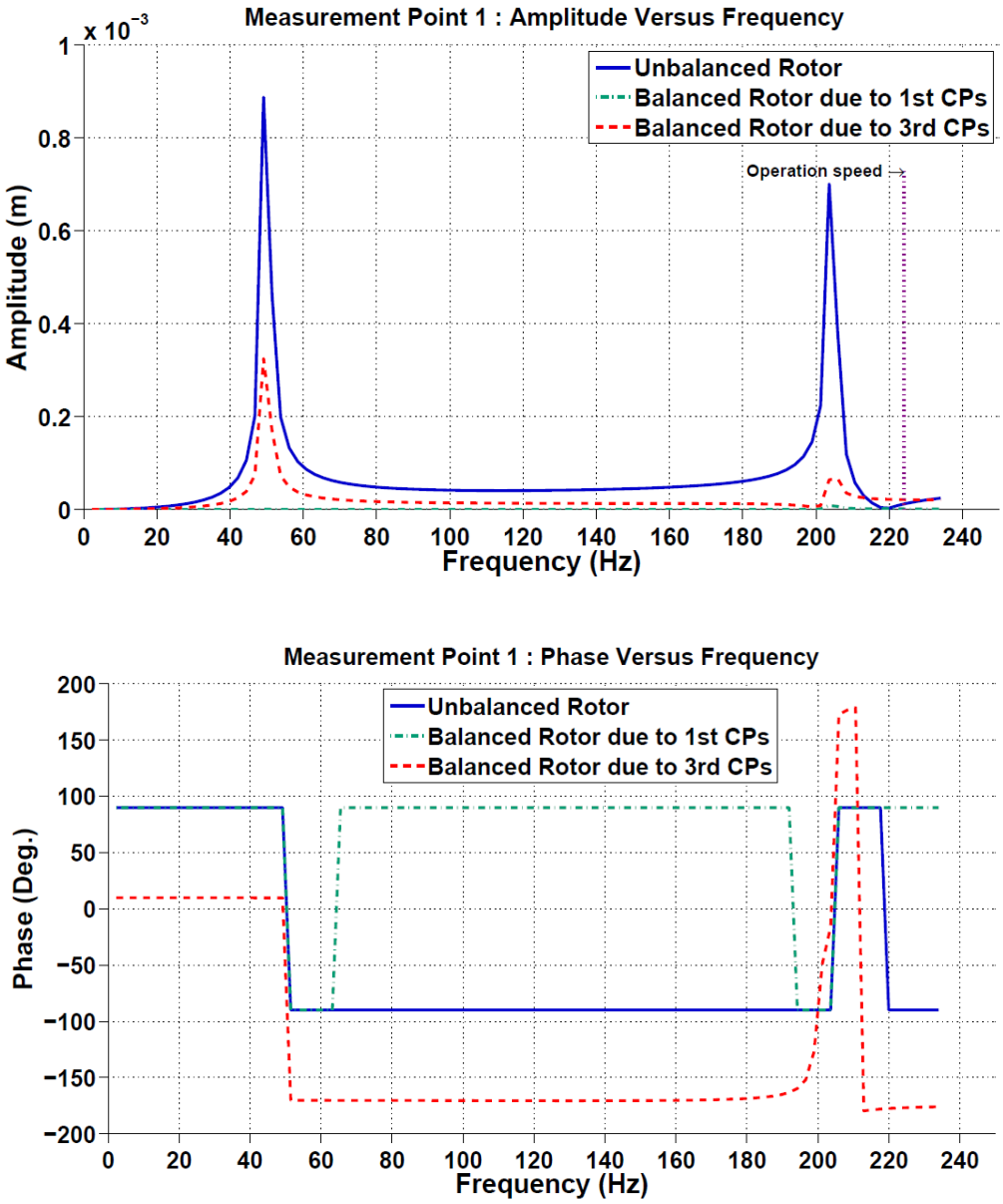

FIGURE 6.1.9: Amplitude Phase Plots (Z-Direction) at Speed above Operation Speed: at ***Measurement Point 1***

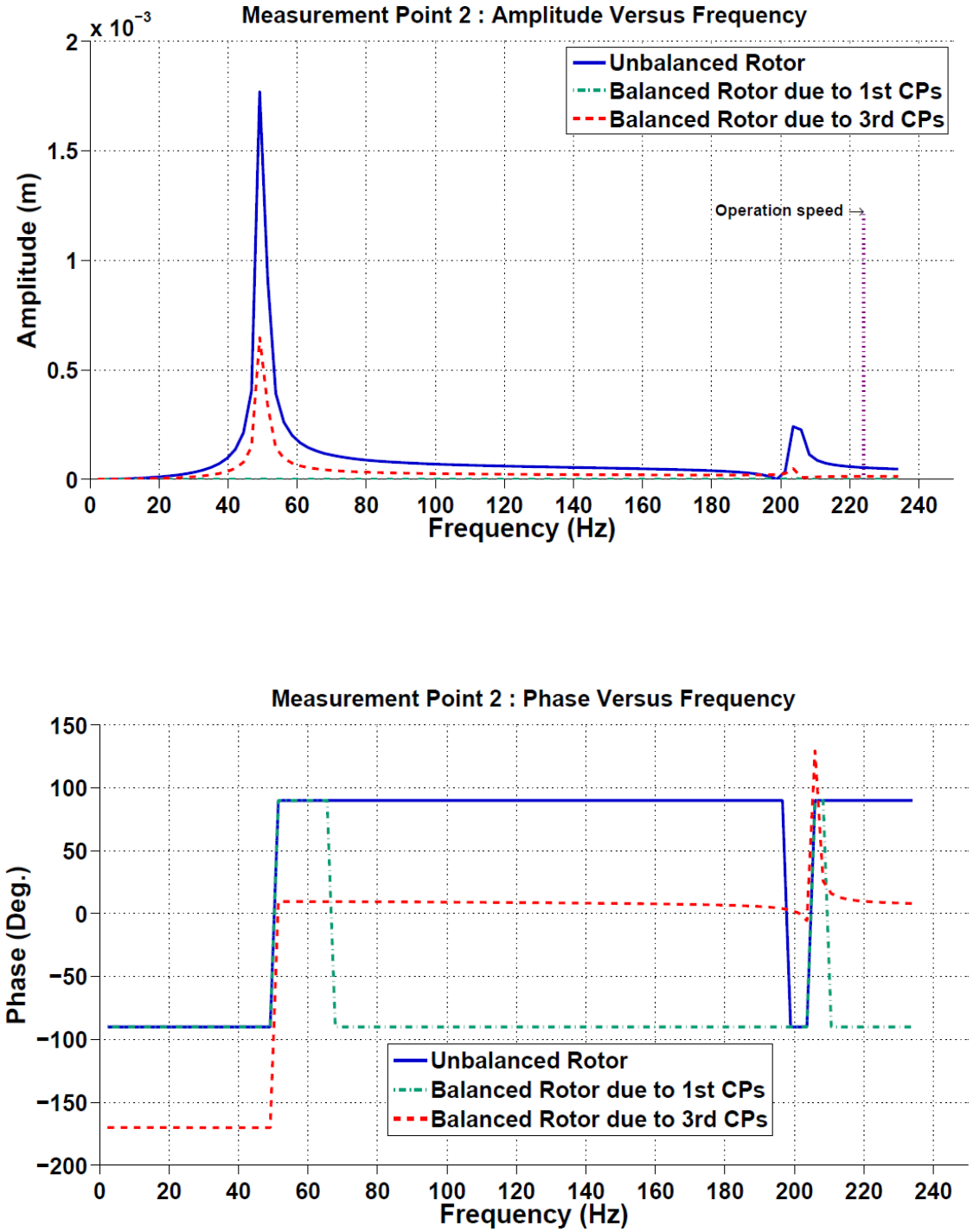

FIGURE 6.1.9: Amplitude Phase Plots (Z-Direction) at Speed above Operation Speed: at ***Measurement Point 2***

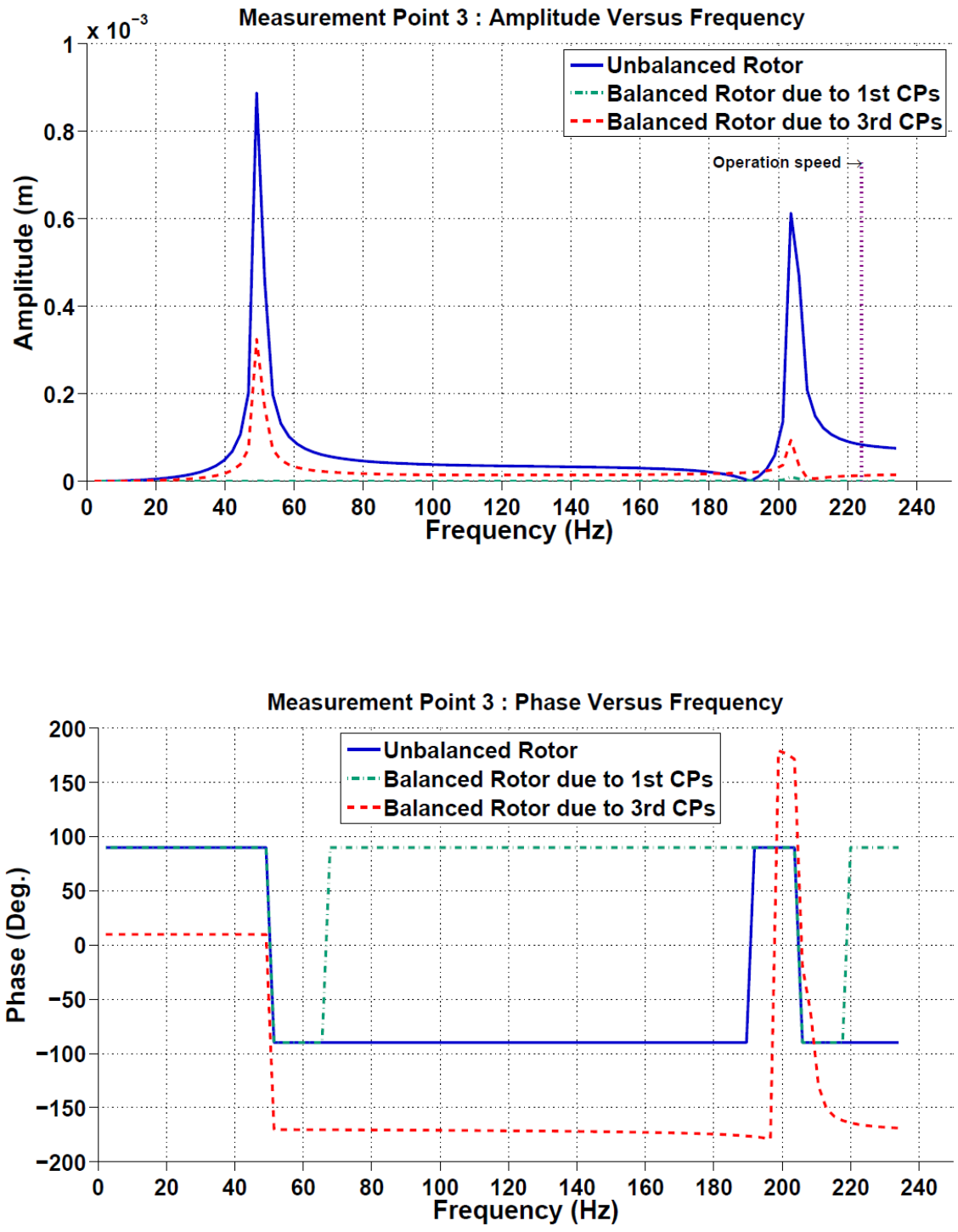

FIGURE 6.1.9: Amplitude Phase Plots (Z-Direction) at Speed above Operation Speed: at ***Measurement Point 3***

6.1.4.3 Percentage Unbalance Reduction

In order to assess the effectiveness of the developed low-speed balancing scheme, the percentage unbalance reduction is calculated. This can be used as an appropriate measure for judging the method, rather than using the balancing quality grade criteria which may not be meaningful of such an experimental rotor. There are reductions at all measuring points after the rotor has been balanced. The calculations were performed for the responses at the two critical speeds and at another speed above the operation speed. The percentage reductions of responses in Figure 6.1.8 are tabulated in the Table 6.1.6. The smallest reduction is 15% and this is due to the fact that the response at that point was very small initially, yet the balancing operation still reduced it by 15%. The values in Table 6.1.6 shows that the low-speed balancing method developed in this work reduced the initial unbalance responses of rotor to an appreciable level after balancing. It shows an average reduction of over 55%, which is acceptable in field applications. However, in practical situations where the percentage reduction is not sufficient, a "trim balancing" can be carried out.

In addition, the Table 6.1.6 is applicable to Figure 6.1.9 too. This is true because when the rotor is running on the rigid bearings, the response at any point will be the same along all other directions except the axis of rotation.

TABLE 6.1.6: Percentage Unbalance Reduction at Measurement Points

	Percentage Reduction at		
Measurement Point No	1st Critical Speed	2nd Critical Speed	Speed above Op. Speed (14,040 rpm)
	%	%	%
1	63	91	15
2	63	85	72
3	63	85	80
Average	63	87	56

6.2 Three-Disk Rotor with Rigid Bearings (2)

The rotor in section 6.1 shown in Figure 6.1.1 was reconsidered again with aim of improving the last correction parameters and average reductions obtained. The unbalance quantity, correction planes, trial parameters and operation speed were changed. The operation speed considered was 13, 440 rpm and speed above operation speed at which balanced rotor was tested was 13,690rpm. The initial responses obtained at balancing speed and the responses obtained during the low-speed balancing processes are shown in Tables 6.2.1 and 6.2.2. The correction parameters obtained from these two tables are shown in Table 6.2.3. The new correction parameters obtained in this section also balanced the rotor at balancing and operation speed as well as speed above its operation speed. Also, the average reductions are shown in Table 6.2.4 and there were improvement as we hoped for. It shows an average reduction of over 85%, which is more than hoped for in field applications. The amplitude plots for the correction parameters in Table 6.2.3 are shown in section 6.6.

TABLE 6.2.1: Initial Responses at Balancing Speed (2,000 rpm)

Initial Measuremets					
Measurement Point 1 (Node 8)		Measurement Point 2 (Node 20)		Measurement Point 3 (Node 30)	
Max Amplitude	Phase (Deg.)	Max Amplitude	Phase (Deg.)	Max Amplitude	Phase (Deg.)
1.21E-05	-4.46567	1.85E-05	-4.94786	1.10E-05	174.949

TABLE 6.2.2: Trial Parameters, Amplitudes and Phases at each Measurement Point

Trial S/N	Trial Parameters							Measurements Due to Trial Parametrs					
								Measurement Point 1		Measurement Point 2		Measurement Point 3	
	Correction Planes		Mass (kg)	Radius r (m)	mr (kg.m)	Angle (Deg.)		Max Amplitude (m)	Phase (Deg.)	Max Amplitude (m)	Phase (Deg.)	Max Amplitude (m)	Phase (Deg.)
1	1	Node 10	0.010	0.022	2.20E-04	175		1.00E-05	-6.51022	1.57E-05	-6.7090	9.40E-06	173.221
	2	Node 16	0.015	0.045	6.75E-04	0		1.98E-05	-2.73755	3.02E-05	-3.0176	1.80E-05	176.908
	3	Node 22	0.008	0.024	1.92E-04	195		1.08E-05	-3.16644	1.62E-05	-3.4973	9.55E-06	176.481
2	1	Node 10	0.010	0.022	2.20E-04	0		1.43E-05	-3.78875	2.12E-05	-4.2976	1.26E-05	175.598
	2	Node 16	0.015	0.045	6.75E-04	0		1.98E-05	-2.73755	3.02E-05	-3.0176	1.80E-05	176.908
	3	Node 22	0.008	0.024	1.92E-04	200		1.09E-05	-2.56745	1.62E-05	-2.7962	9.58E-06	177.229
3	1	Node 10	0.010	0.022	2.20E-04	180		9.98E-06	-5.43621	1.57E-05	-5.8291	9.38E-06	174.075
	2	Node 16	0.015	0.045	6.75E-04	180		4.54E-06	-12.0242	6.77E-06	-13.6034	4.10E-06	166.334
	3	Node 22	0.008	0.024	1.92E-04	200		1.09E-05	-2.56745	1.62E-05	-2.7962	9.58E-06	177.229
4	1	Node 10	0.010	0.022	2.20E-04	175		1.00E-05	-6.51022	1.57E-05	-6.7090	9.40E-06	173.221
	2	Node 16	0.015	0.045	6.75E-04	180		4.54E-06	-12.0242	6.77E-06	-13.6034	4.10E-06	166.334
	3	Node 22	0.008	0.024	1.92E-04	197		1.08E-05	-2.92484	1.62E-05	-3.2145	9.56E-06	176.783

TABLE 6.2.3: Correction Parameters and Final Amplitudes and Phases at each Measurement Point

Trial S/N	Calculated Correction Parameters				Final Measurement (Residual Unbalance)					
					Measurement Point 1		Measurement Point 2		Measurement Point3	
	Masses (kg)	Angles (Deg.)	mr (kg.m)		Max Amplitude (m)	Phase (Deg.)	Max Amplitude (m)	Phase (Deg.)	Max Amplitude (m)	Phase (Deg.)
1	0.0116	175.4891	2.55E-04		1.36E-06	-88.3441	2.06E-06	-87.9863	1.20E-06	92.2385
	0.0153	173.9383	6.89E-04							
	0.0112	-161.1844	2.69E-04							
2	0.0116	-174.4588	2.55E-04		6.49E-07	-74.1551	1.02E-06	-72.2711	5.77E-07	109.973
	0.0153	173.9046	6.89E-04							
	0.0112	-151.1130	2.69E-04							
3	0.0116	-174.5936	2.55E-04		6.47E-07	-74.5839	1.02E-06	-72.7093	5.75E-07	109.492
	0.0153	174.0002	6.89E-04							
	0.0112	-151.326	2.69E-04							
4	0.0116	175.4372	2.55E-04		1.24E-06	-86.1022	1.85E-06	-85.3192	1.07E-06	95.18
	0.0153	173.9775	6.89E-04							
	0.0112	-157.2747	2.69E-04							

TABLE 6.2.4: Percentage Unbalance Reduction at Measurement Points

	Percentage Reduction at		
Measurement Point No	1st Critical Speed	2nd Critical Speed	Speed above Op. Speed (13,690 rpm)
	%	%	%
1	89	93	67
2	89	92	96
3	89	92	94
Average	89	92	86

6.3 Low-speed vs. Two-plane balancing Methods

In this section, the low-speeed balncing is compared to traditional two-plane balancing for the same flexible high-speed rotor. Here, the unbalance of 100E-3kg at radius of 0.07m (and an angle 0^0 in the middle disk) was considered and the rotor operating speed was 22,200 rpm. The balancing speed for both methods was 2,000 rpm and the procedure for the two-plane balancing method is explained.

6.3.1 Mode Shapes from Harmonic Response Analysis

The harmonic response analysis was performed on the unbalance rotor (Figure 6.1.3) at operation speed. The mode shapes corresponding to each critical speed are obtained. Since the rotor is operating above 2nd critical speed, only the 1st and 2nd natural frequencies mode shapes were available. The operation speed is below the 3rd critical speed since operation speed has not reached 3rd critical speed. Its operation deflection shape (ODS) is utilized to serve as the mode shape of 3rd critical speed. The normal mode shapes are plotted in Figure 6.3.1, and the selected two correction planes and two measurement points are also shown in the figure.

6.3.2 Conditions for Two-Plane Balancing

The conditions required for two-plane balancing method of rotor, are defined by the following parameters:

a) The balancing speed Ω is 2,000 rpm

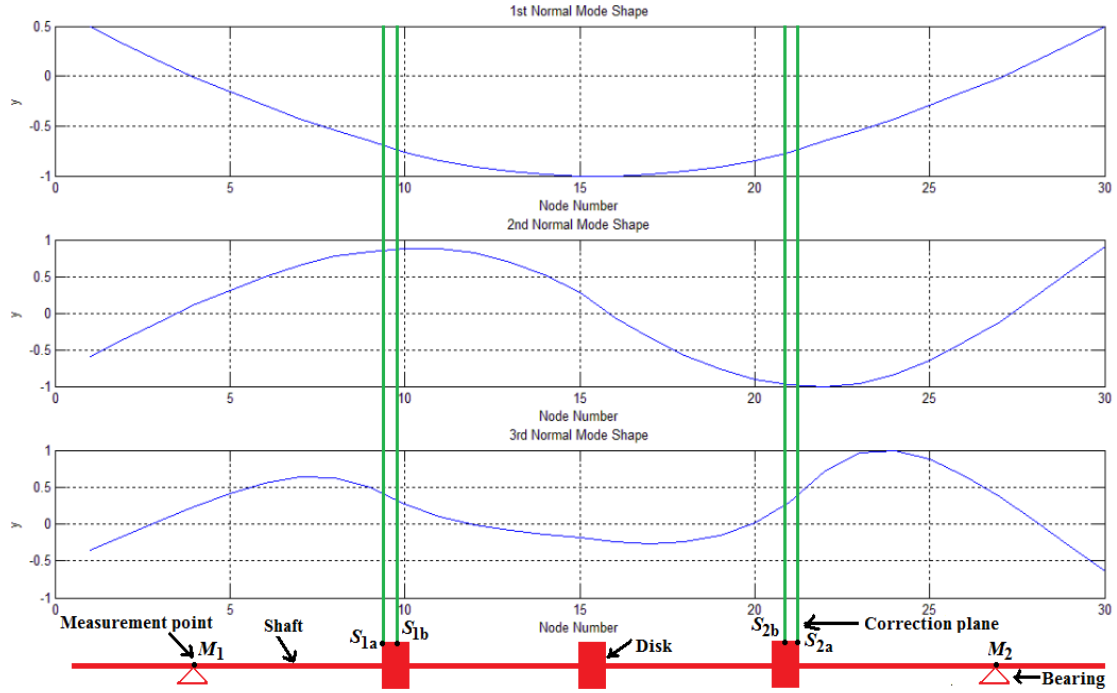

FIGURE 6.3.1: First and Second Normal Mode Shapes and ODS Versus Nodes Number

b) The measurements are taken at the two bearings.

c) The two correction planes required are S_{1a} and S_{2a} or S_{1b} and S_{2b} and the two measurement points are M_1 and M_2 were located as shown in Figure 6.3.1.

6.3.3 Two-Plane Balancing Processes

6.3.3.1 Measured Responses at Measurement Points

Harmonic analysis was performed on the unbalanced rotor shown in Figure 6.1.3 at operation and balancing speeds; while the initial responses at the two measurement points (bearing nodes) are acquired. The initial responses at balancing speed are shown in Table 6.3.1.

In addition, the balancing operation proceeds by adding trial weights to the unbalanced rotor disk at selected correction planes, one after the other. A number of different sets of trial weights were carried out using influence coefficient balancing method at balancing speed. The results obtained for three different trials are summarized in the Table 6.3.1.

6.3.4: Results and Discussions

The correction parameters are determined by utilizing data of Tables 6.3.1 and 6.3.2 and using the formula for two-plane balancing method of rotor and they were tested at both balancing and operation speeds. The correction parameters obtained and the

TABLE 6.3.1: Initial Responses at Balancing Speed (2, 000 rpm)

Initial Measuremets			
Measurement Point 1 (Node 4)		Measurement Point 2 (Node 27)	
Max Amplitude	Phase (Deg.)	Max Amplitude	Phase (Deg.)
2.97E-06	0	3.09E-06	0

TABLE 6.3.2: Trial Parameters, Amplitudes and Phases at each Measurement Point

							Measurement Point 1		Measurement Point 2	
Trial S/N	Correction Planes		m(kg)	Radius r	Teta		Max Amplitude	Phase	Max Amplitude	Phase
1	1	Node 9	1.1	0.12	0		6.69E-05	0	3.44E-05	0
	2	Node 22	1.1	0.12	0		3.43E-05	0.00E+00	6.70E-05	0
2	1	Node 9	1.3	0.12	0		7.85E-05	0	4.01E-05	0
	2	Node 22	1.3	0.12	180		3.40E-05	-180	7.24E-05	-180
3	1	Node 71	1.11	0.12	180		6.16E-05	-180	3.15E-05	-180
	2	Node 78	1.11	0.12	180		3.16E-05	-180	6.15E-05	-180

TABLE 6.3.3: Correction Parameters and Final Amplitudes and Phases at each Measurement Point

	Calculated Correction Parameters			Final Measurement			
				Measurement Point 1		Measurement Point 2	
	Masses (kg)	Angles (Deg.)		Max Amplitude (m)	Phase (Deg.)	Max Amplitude (m)	Phase (Deg.)
1	0.033	180		1.01E-07	-180	1.03E-07	-180
	0.0371	180					
2	0.033	180		1.01E-07	-180	1.03E-07	-180
	0.0371	180					
3	0.03172	180		8.25E-08	-180	8.30E-08	-180
	0.03616	180					

responses at measurement points when each set of the correction parameters is applied to the rotor at balancing speed are shown in the Table 6.3.3.

Moreover, when the three correction parameters (in Table 6.3.3) are applied to the rotor one after the other, the test-runs at balancing and operation speeds, demonstrate that the rotor was balanced at the balancing speed. Yet, the rotor became unbalanced once again at when the rotor is run at its operating speed. The amplitude plot of the initial responses due to unbalance and final responses obtained when the 1st and 3rd correction parameters were applied to the rotor at both balancing and operation speeds are shown in the subsection 6.3.4.1 for each measurement point.

It can be seen from Figures 6.3.4 to 6.3.5 that the flexible rotor can only remain balanced within the balancing speed employed when two-plane balancing method is used. Hence, it can be concluded that the low-speed balancing method developed in the present work can balance the rotor both at balancing and operating speeds; while the traditional two-plane balancing method fails at the higher operating speed.

6.3.4.1 Amplitude plots

The amplitude plots, that is, amplitude versus frequency for two-plane and low-speed balancing methods of rotor under consideration are plotted here for test-runs at both balancing and operation speeds for all measurement points. These are shown in the Figures 6.3.2 to 6.3.5 for all measurement points. The Figures 6.3.2 and 6.3.3 show the rotor responses at the all measuring points when the rotor is unbalanced and after it has been balanced at balancing speed. It can be seen that at all measuring points, the final responses are decreased appreciably when compare to initial responses.

(1)Amplitude in Y- Direction at Balancing Speed

(1.1)Two-Plane Balancing Method

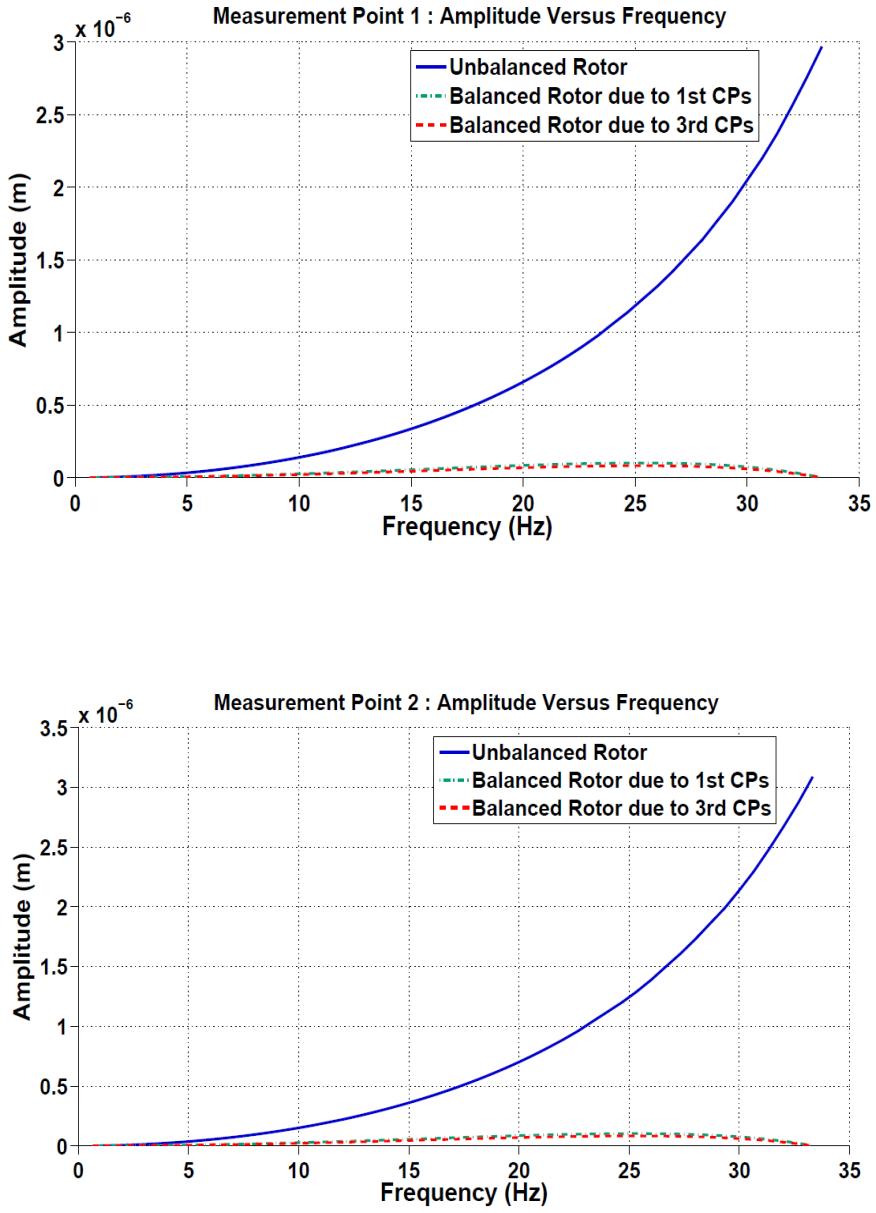

FIGURE 6.3.2: Amplitude Plots due to Correction Parameters and Initial Responses at Balancing Speed for Two-Plane Balancing Method

(1.2)Low Speed Balancing Method

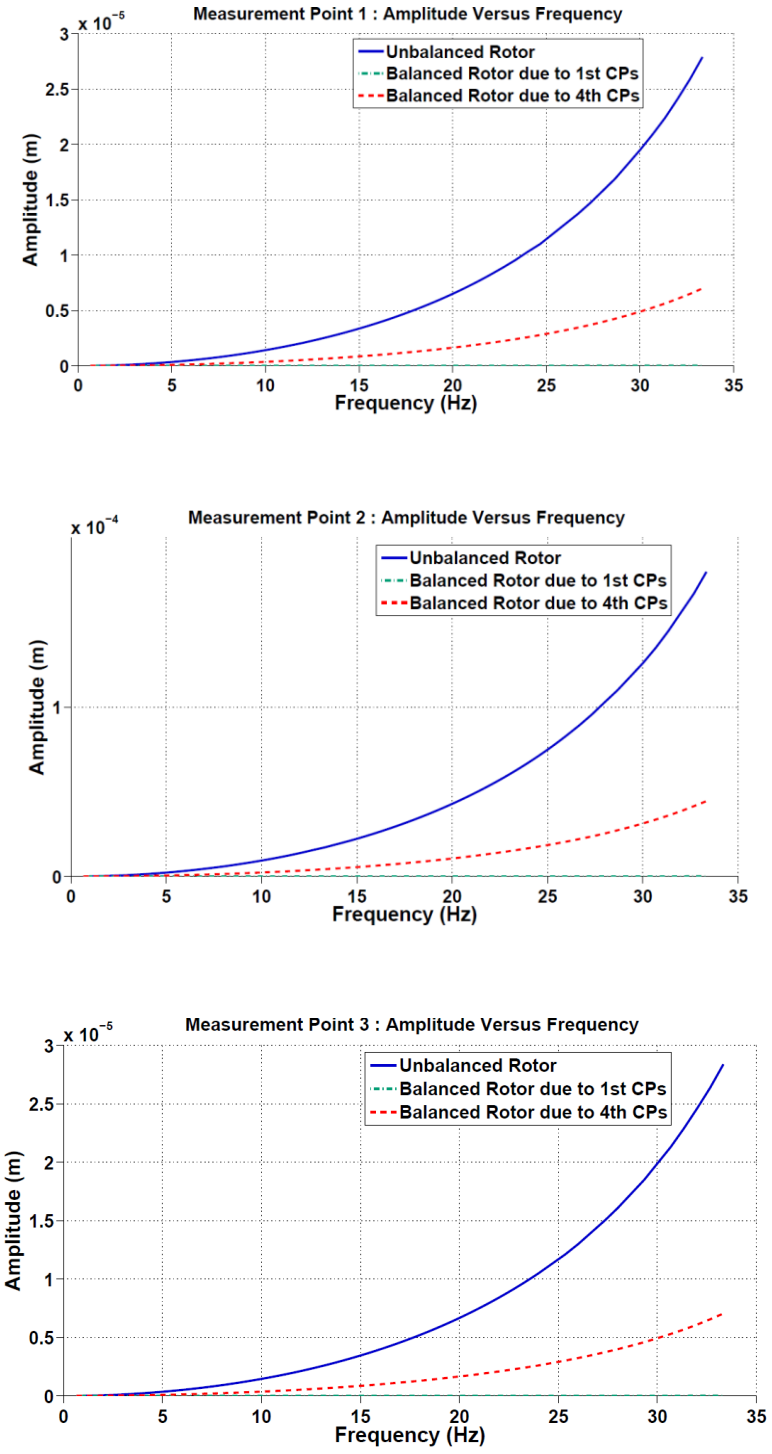

FIGURE 6.3.3: Amplitude Plots due to Correction Parameters and Initial Responses at Balancing Speed for Low –Speed Balancing Method

(2)Amplitude-phase Plots in Y- Direction at Operation Speed

(2.1)Two Plane Balancing Method

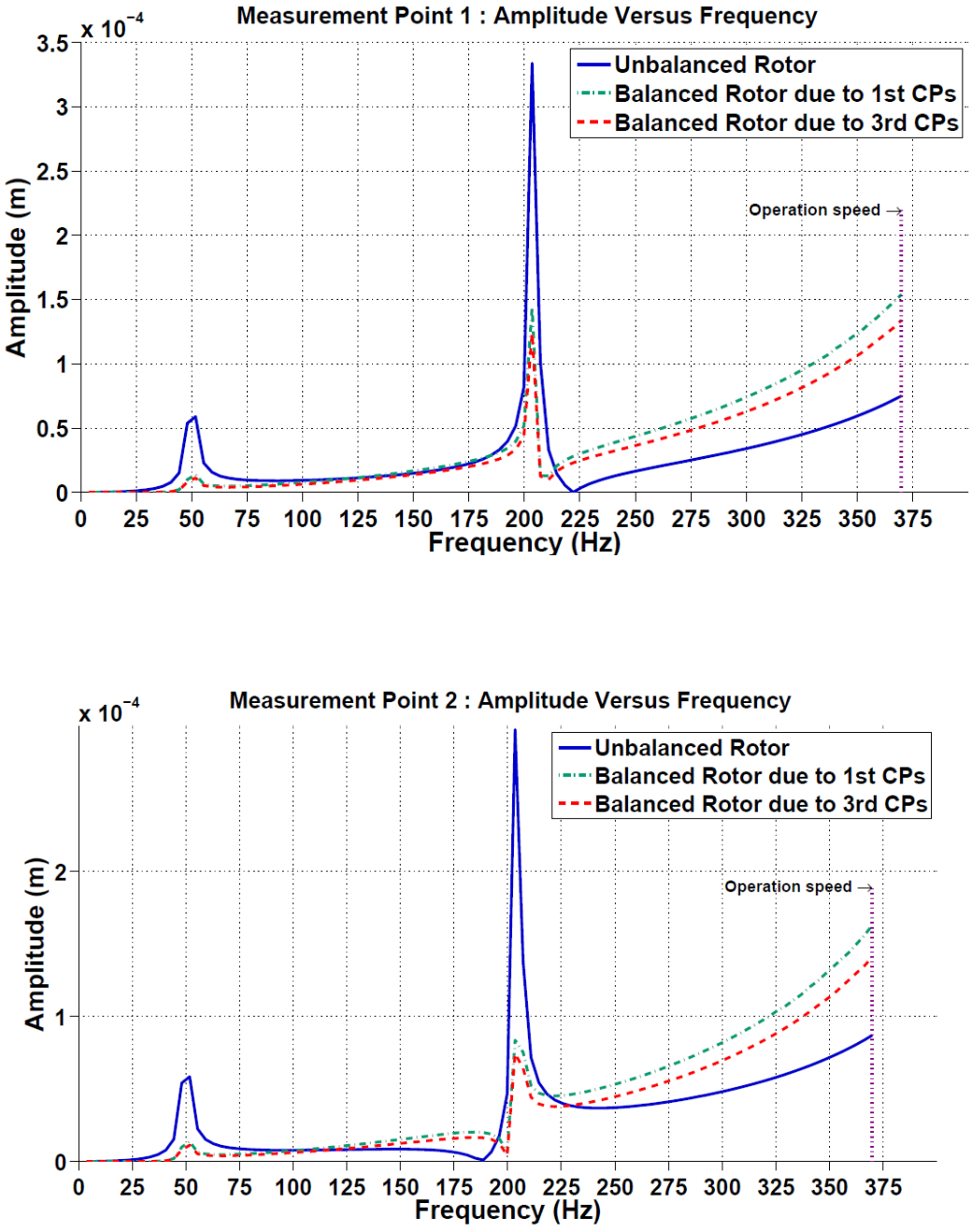

FIGURE 6.3.4: Amplitude Plots due to the Correction Parameters and Initial Responses at Operation Speed for Two-Plane Balancing Methods

(2.2)Low Speed Balancing Method

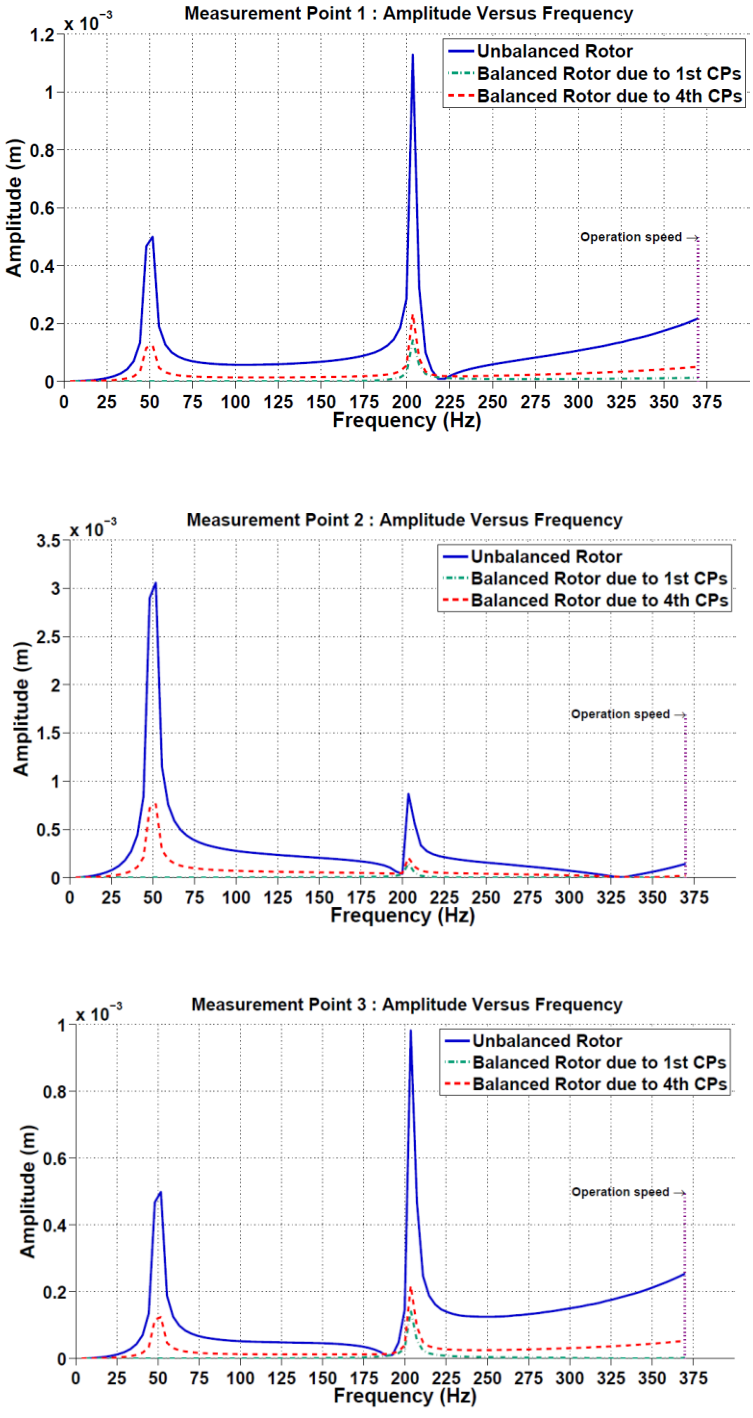

FIGURE 6.3.5: Amplitude Plots due to the Correction Parameters and Initial Responses at Operation Speed for Low-Speed Balancing Methods

6.3.4.2 Percentage Unbalance Increment and Reduction

Figures 6.3.4 and 6.3.5 show the rotor responses at all measuring points when it is being tested at its operation speed. The initial responses that have been obtained from unbalanced rotor were plotted against the responses of balanced rotor. While the rotor (Figure 6.3.5) balanced by low-speed balancing method developed in this work remained balanced at operation speed, the rotor (Figures 6.3.4) balanced by the two-plane balancing method becomes unbalance at operation speed. The percentage unbalance reductions or increments are shown in the table for each method.

TABLE 6.3.4: Percentage Unbalance Increment/Reduction at Measurement Points

		Percentage			
		Reduction at			**Increment at**
Balancing Method	Measurement Point No	1st Critical Speed	2nd Critical Speed	Operation Speed (22,200 rpm)	Operation Speed (22,200 rpm)
		%	%	%	%
Two plane Method	1	81	63	0	78
	2	81	75	0	62
Low-Speed Balancing Method	1	100	87	94	0
	2	99	83	99	0
	3	100	96	99	0

It is concluded from this result that the low-speed balancing method developed in this work is capable to balancing the rotor not only at balancing speed but also at operation speed or even at some marginal speeds above the operation speed.

6.4 Multi Stage Turbine with Rigid Bearings

In this scetion, an industrial large-scale turbine rotor Figure 6.4.1 similar to that studied in [35] will be considerd and the geometry data are as stated in their work. In this work, the multi stage turbine is operating at 16,200 rpm and there are two unbalances located on the turbine at stations 12 and 21 with quantities of 0.5 oz-in at 0^o and 1.5 oz-in at 90^o (or 3.6E-04kg-m at 0^o and 1.08E-03 kg-m at 90^o where radii are 0.2802 and 0.2675m) respectively. The turbine is running on the two bearings (with $K_{yy} = K_{zz} = 1.0E08$ N/m while cross coupling stiffness and dampers are zeros) and the objective is to balance the turbine at low speed.

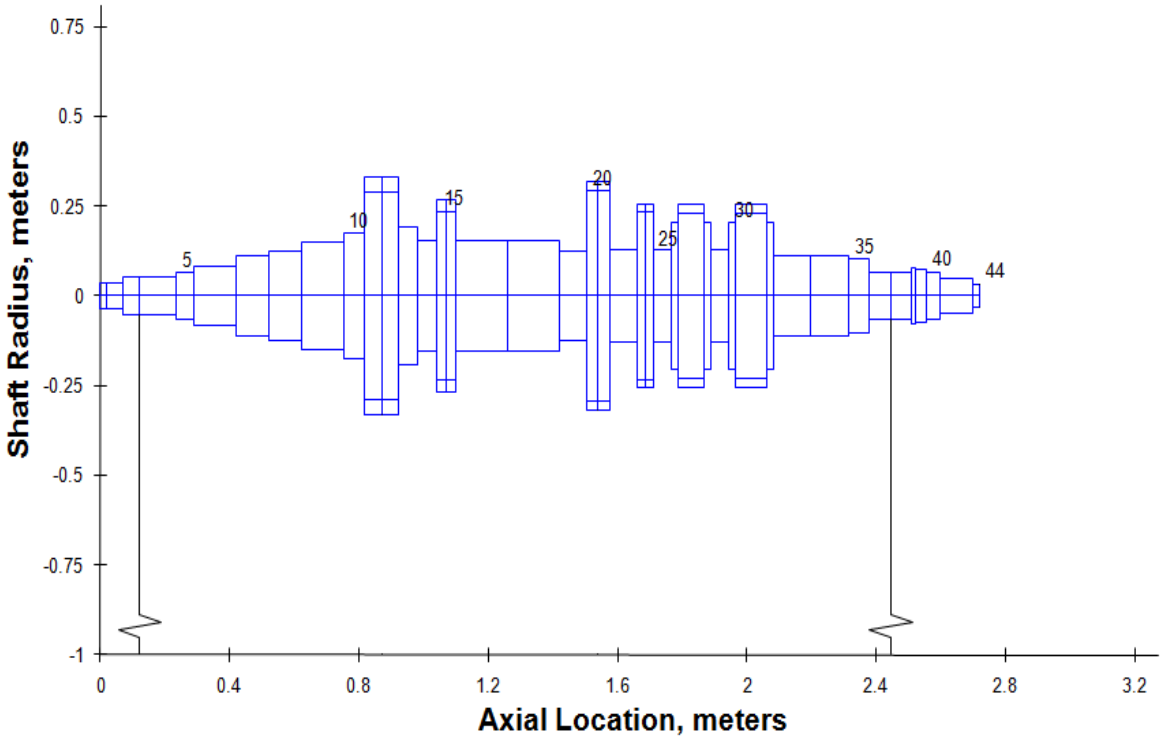

FIGURE 6.4.1: Multi Stage Turbine [35]

6.4.1 Turbine Modeling

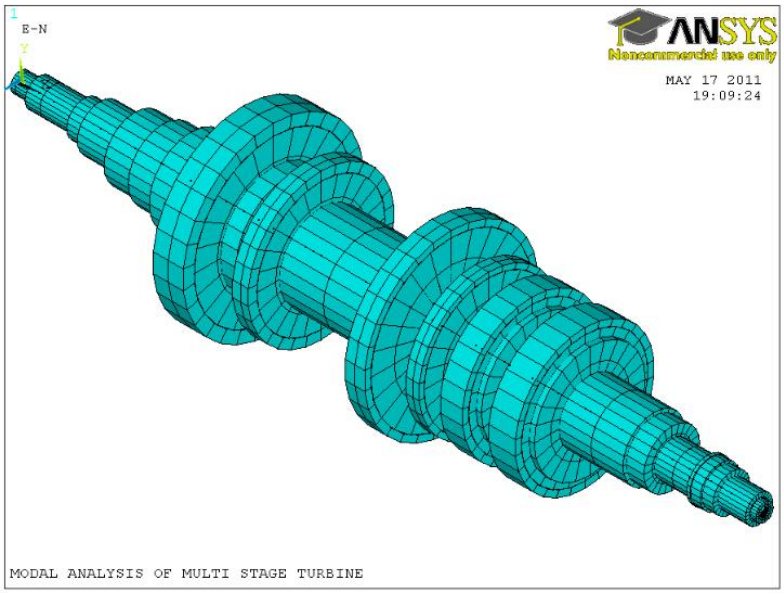

(a)Isometric View

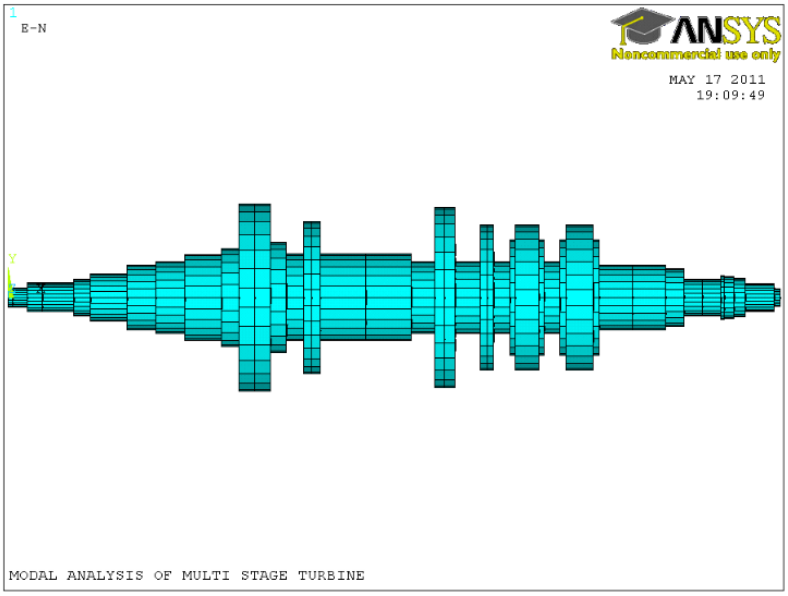

(b) Front View

FIGURE 6.4.2: Multi Stage Turbine Modeling

6.4.2 Modal Analysis of the Turbine

The modal analysis was carried out on the above model at its operation speed and the first three natural frequencies of the system are listed in Table 6.4.1.

TABLE 6.4.1: Natural Frequencies of Multi Stage Turbine

Mode Number	Damped Frequency (Hz)		Undamped Frequency (HZ)
	Real	Complex	
1	0	44.352	44.553
	0	-44.352	
2	0	44.74	44.553
	0	-44.74	
3	0	92.671	104.49
	0	-92.671	
4	0	117.79	104.49
	0	-117.79	
5	0	276.41	310.57
	0	-276.41	
6	0	347.63	310.57
	0	-347.63	

6.4.3 Rotor Balancing

6.4.3.1 Operation Conditions

1.) The natural frequencies recorded above indicate that the turbine is operating between the second critical speed (104.49 Hz or 6,264.4 rpm) and third critical speeds (310.57HZ or 18,634.2 rpm).

2.) The operating speed Ω_{op} is 270 Hz (16,200 rpm)

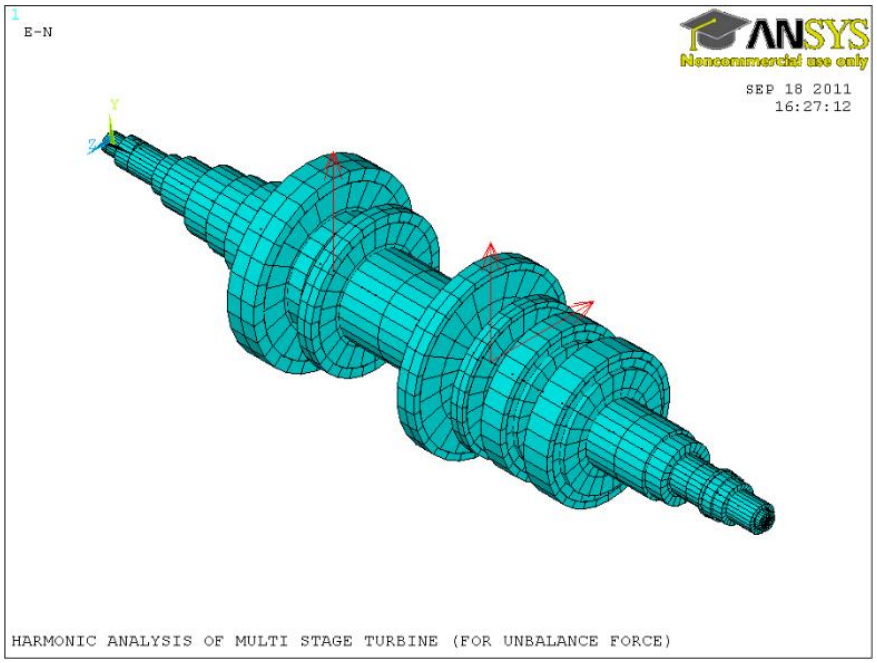

FIGURE 6.4.3: Unbalance Multi Stage Turbine

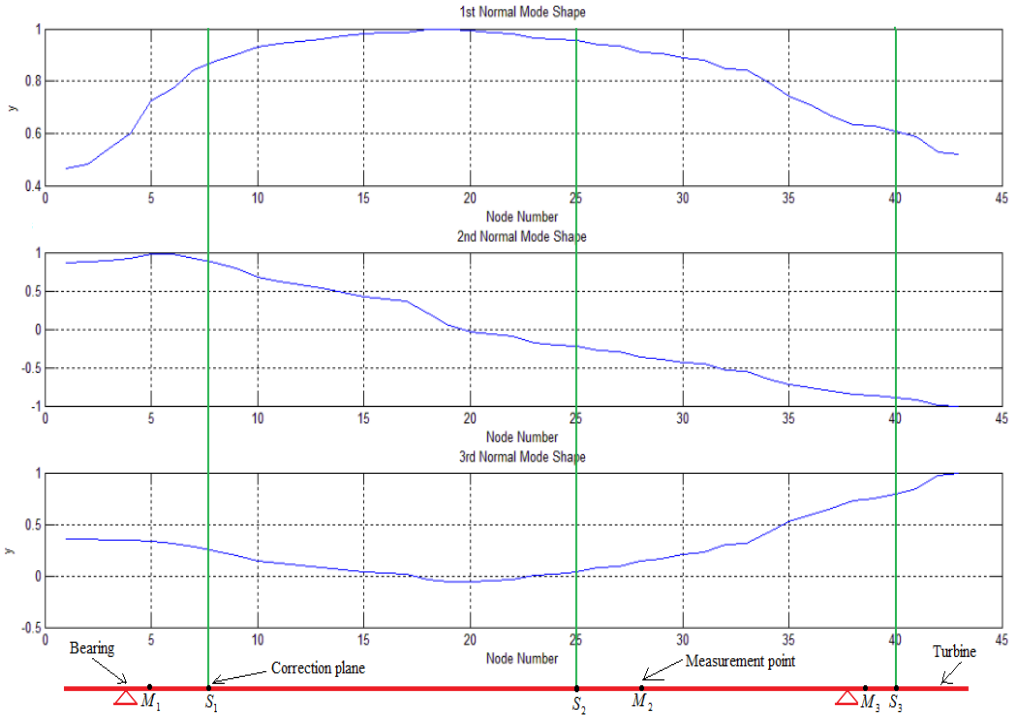

FIGURE 6.4.4: First, Second and ODS Normal Mode Shapes Versus Nodes Numbers

6.4.3.2 Mode Shapes from Harmonic Response Analysis

Based on the available parameters, the unbalance was created on the turbine as shown in the Figure 6.4.3 and the harmonic response analysis was performed on the unbalanced turbine at operation speed (16,200 rpm).The mode shape corresponding to each critical speed were then obtained. Since turbine is operating above the second critical speed, only the first and second natural mode shapes are needed. The turbine's operational deflection shape (ODS) is used to serve as mode shape of 3rd critical speed. The normal mode shapes shown in the Figure 6.4.4 are plotted, while the correction planes and measurement points are selected as shown in the Figure 6.4.4.

6.4.3.3 Low-Speed Balancing Conditions

In order to satisfy the conditions required for low-speed balancing procedures described in section 5.2, the following parameters were used:

1.) Balancing speed Ω is 2,000 rpm which is well below the first critical speed.
2.) Since turbine is operating above the second critical speed, then $N = 3$ and three correction planes plus three measurement points are required.
3.) The three correction planes are S_1, S_2 and S_3 and the three measurement points are M_1, M_2 and M_3 which are located as shown in Figure 6.4.4

6.4.3.4 Low Speed Turbine Balancing Processes

6.4.3.4.1 Initial Responses depicted at Measurement Points

The Harmonic analysis was carried out for the unbalanced turbine shown in the Figure 6.4.3 at operation speed (16,200 rpm) and at balancing speeds in order to obtain the initial responses. The initial responses at the three measurement points (three nodes) are then acquired. The initial responses at balancing speed are shown in Table 6.4.2. Now, having obtained the initial responses of the turbine, the balancing operation proceeds by adding trial weights to the unbalanced turbine at the selected correction planes, one after the other. Several trial sessions are carried out using the low-speed balancing procedure described in section 5.2 at balancing speed. In this context, we have tested four different sets of trial weights. The results obtained from the four different trials sessions are summarized in the Table 6.4.3.

6.4.4 Results

In this section, the correction parameters are determined by utilizing the data in Tables 6.4.2 and 6.4.3 together with the equation of the low-speed balancing procedure described in section 5.2. The balanced turbine (i.e. after adding correction masses) is tested at both balancing and operation speeds as well as at its operation speed. The acquired correction parameters and the responses at measurement points when each of the correction parameters was applied to the turbine at balancing speed are shown in Table 6.4.4.

TABLE 6.4.2: Initial Responses at Balancing Speed (2, 000 rpm)

Initial Measuremets					
Measurement Point 1 (Node 5)		Measurement Point 2 (Node 28)		Measurement Point 3 (Node 38)	
Max Amplitude	Phase (Deg.)	Max Amplitude	Phase (Deg.)	Max Amplitude	Phase (Deg.)
6.281E-07	-67.38	8.7997E-07	-73.7285	6.216E-07	-76.199

TABLE 6.4.3: Trial Parameters, Amplitudes and Phases at each Measurement Point

Trial Parameters							Measurement Point 1		Measurement Point 2		Measurement Point 3	
Trial S/N	Correction Planes		Mass (kg)	Radius r (m)	Angle (Deg.)		Max Amplitude	Phase	Max Amplitude	Phase	Max Amplitude	Phase
1	1	Node 7	0.68	0.1131	10		5.64E-05	-10.5375	4.19E-05	-11.0787	2.11E-05	-11.5468
	2	Node 25	0.68	0.127	270		4.23E-05	89.6729	6.64E-05	89.7874	4.96E-05	89.8288
	3	Node 40	0.68	0.0667	90		8.86E-06	-88.438	2.75E-05	-89.4871	3.23E-05	-89.737
2	1	Node 7	0.68	0.1131	30		5.66E-05	-30.3863	4.22E-05	-30.8267	2.12E-05	-31.21
	2	Node 25	0.68	0.127	90		4.35E-05	-89.6816	6.81E-05	-89.7927	5.08E-05	-89.8329
	3	Node 40	0.68	0.0667	120		8.67E-06	-116.702	2.73E-05	-118.666	3.22E-05	-119.233
3	1	Node 7	0.68	0.1131	20		5.65E-05	-20.4689	4.20E-05	-20.9669	2.12E-05	-21.3986
	2	Node 25	0.68	0.127	270		4.23E-05	89.6729	6.64E-05	89.7874	4.96E-05	89.8288
	3	Node 40	0.68	0.0667	240		7.66E-06	120.604	2.58E-05	120.463	3.11E-05	120.319
4	1	Node 7	0.68	0.1131	30		5.66E-05	-30.3863	4.22E-05	-30.8267	2.12E-05	-31.21
	2	Node 25	0.68	0.127	90		4.35E-05	-89.6816	6.81E-05	-89.7927	5.08E-05	-89.8329
	3	Node 40	0.68	0.0667	240		7.66E-06	120.604	2.58E-05	120.463	3.11E-05	120.319

TABLE 6.4.4: Correction Parameters and Final Amplitudes and Phases at each Measurement Point

	Calculated Correction Parameters			Final Measurement (Residual Unbalance)					
				Measurement Point 1		Measurement Point 2		Measurement Point3	
	Masses (kg)	Angles		Max Amplitude	Phase	Max Amplitude	Phase	Max Amplitude	Phase
	0.0019	179.739							
1	0.0087	-79.387		1.87E-07	-16.4162	2.71E-07	-7.88873	1.85E-07	-5.45352
	0.0011	117.9236							
	0.0019	-140.2601							
2	0.0087	-79.3868		2.17E-07	15.8343	2.83E-07	15.1836	1.82E-07	20.344
	0.0011	177.9226							
	0.0019	-160.2612							
3	0.0087	-79.3867		2.02E-07	0.320847	3.19E-07	0.720883	2.39E-07	0.993802
	0.0011	57.9261							
	0.0019	-140.2603							
4	0.0087	-79.3866		2.34E-07	11.909	3.41E-07	6.56476	2.50E-07	4.97385
	0.0011	57.9255							

It is noted that, when the four sets of correction parameters (in Table 6.4.4) were applied to the turbine one after the other, the turbine was balanced not only at balancing speed but also at operation speed. The amplitude-phase plot of the initial responses due to unbalance and final responses acquired when turbine was balanced using the 3^{rd} and 4^{th} correction parameters at both balancing and operation speeds are shown, for each measurement point in subsection 6.4.4.2.

Accordingly, it is concluded from Figures 6.4.6 to 6.4.8 that the turbine could be balanced at low speed (a speed less than the first critical speed).

6.4.4 .1 3D Plots of Critical Mode shapes of the Turbine

Since turbine is operating above second critical speed, the 3D plots of the first two critical mode shapes of the turbine at operation speed (before and after balancing) are shown in Figures 6.4.5. It is imperative to know that these mode shapes are obtained through the harmonic analysis at excitation frequency equivalent or close to each of the two critical speeds of normal rotor. The figures show the difference in turbine mode shapes before and after balancing.

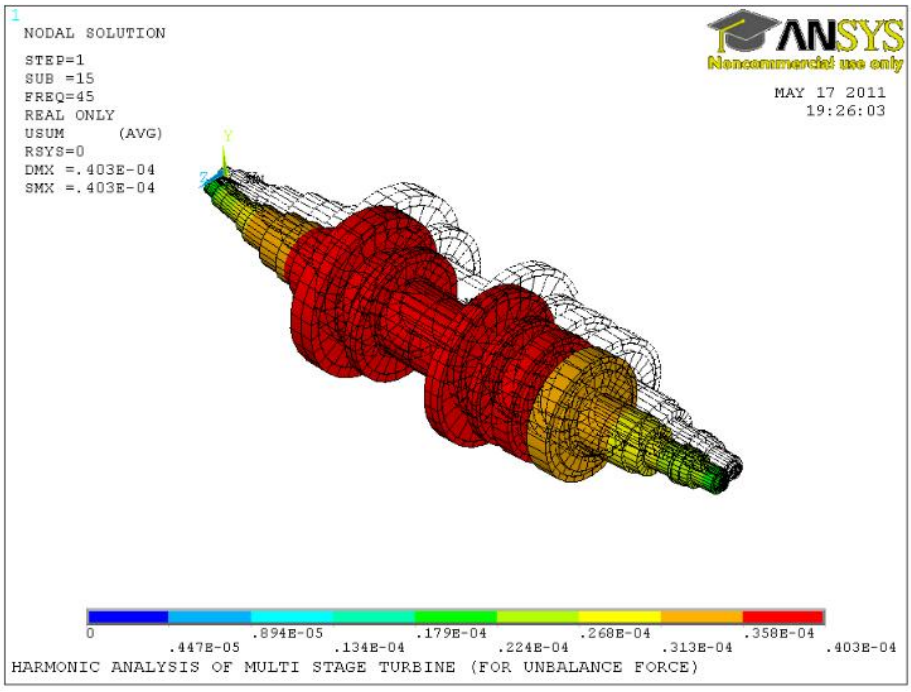

(a1): First Critical Mode Shape Before Balancing

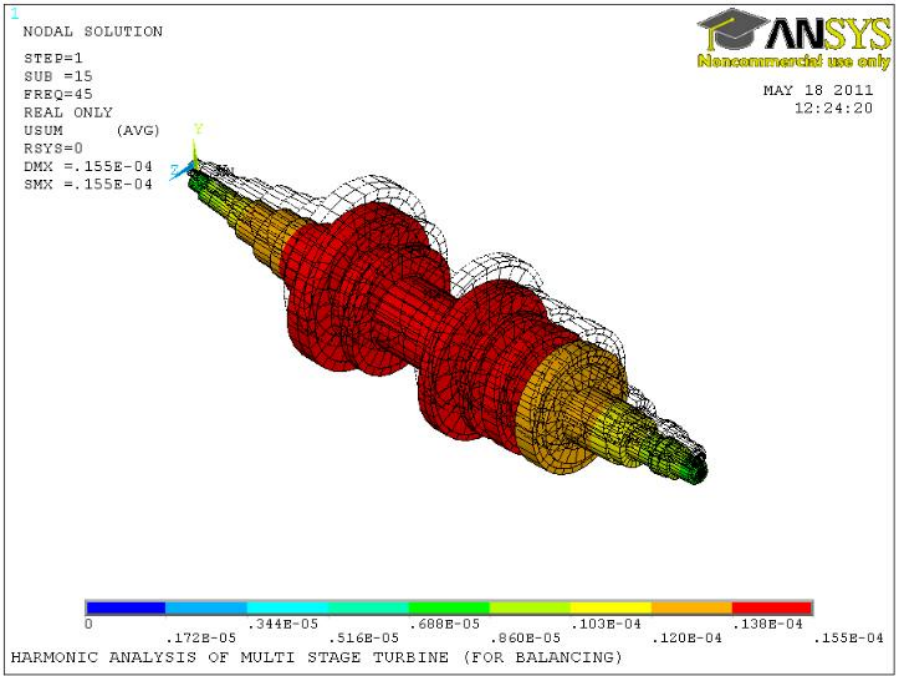

(a2): First Critical Mode Shape After Balancing

FIGURE 6.4.5(a): Multi Stage Turbine Mode Shapes before and after balancing

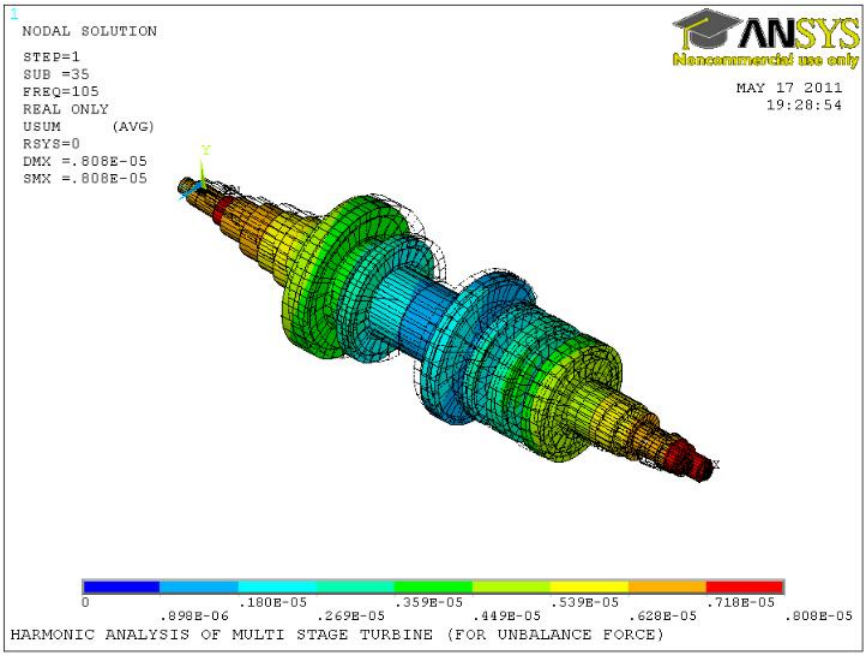

(b1): Second Critical Mode Shape Before Balancing

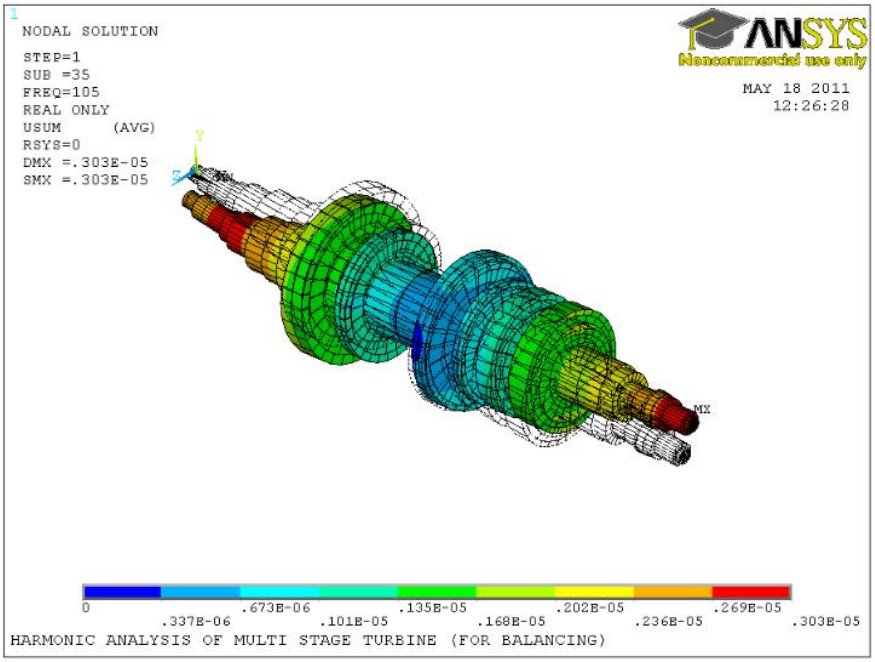

(b2): Second Critical Mode Shape After Balancing

FIGURE 6.4.5(b): Multi Stage Turbine Mode Shapes Before and After balancing

6.4.4.2 Amplitude–phase plot (Bode Plot)

When the correction parameters (in Table 6.4.4) are applied to the turbine one after the other during the test-run at balancing and operation speeds, the amplitude phase plots are made from the responses obtained. The amplitude-phase plot is made up of two parts, which include the amplitude versus frequency and the phase versus frequency. These are shown in Figures 6.4.6 to 6.4.8 for all measurement points. Such figures demonstrate clearly how the low-speed balancing scheme reduced the initial unbalance to an acceptable level; as explained hereunder.

Figures 6.4.6 shows the turbine responses at three measuring points; before and after balancing. It can be seen that at all measuring points, the final responses are decreased drastically when compared to initial response at balancing speed. Also, Figures 6.4.7 and 6.4.8 show the turbine responses (in y and z directions) at all measuring points when it is being tested at its operation speed. The initial responses that have been obtained from unbalanced turbine were plotted against the responses of balanced turbine. The vertical dashed line indicates the actual turbine operation speed. Turbine was run to its operation speed in order to observe its balanced state.

(1)Amplitude in Y- Direction at balancing Speed

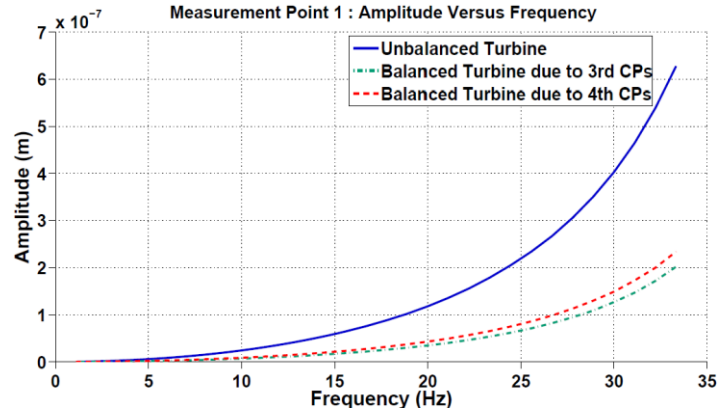

(a)Measurement point 1

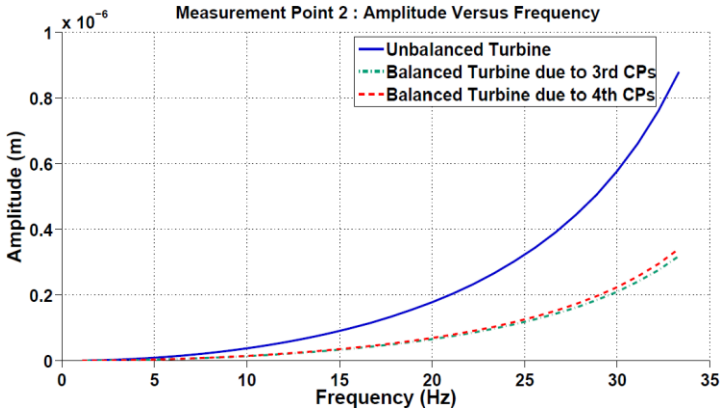

(b) Measurement point 2

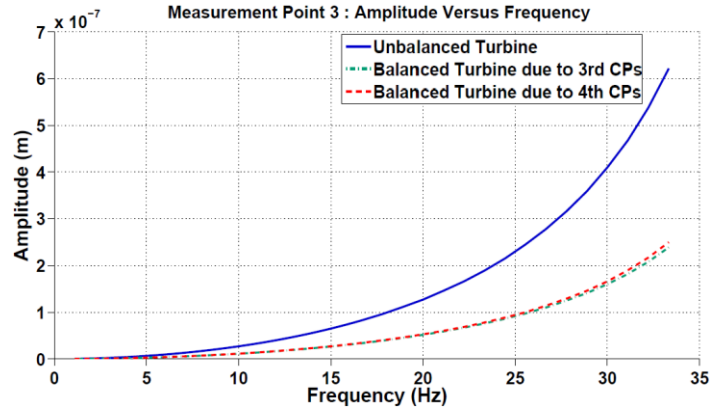

(c) Measurement point 3

FIGURE 6.4.6: Amplitude Plots due to the Correction Parameters and Initial Responses at Balancing Speed at Three Measurement Points

(2) *Amplitude-phase Plots* in Y- Direction at Operation speeds

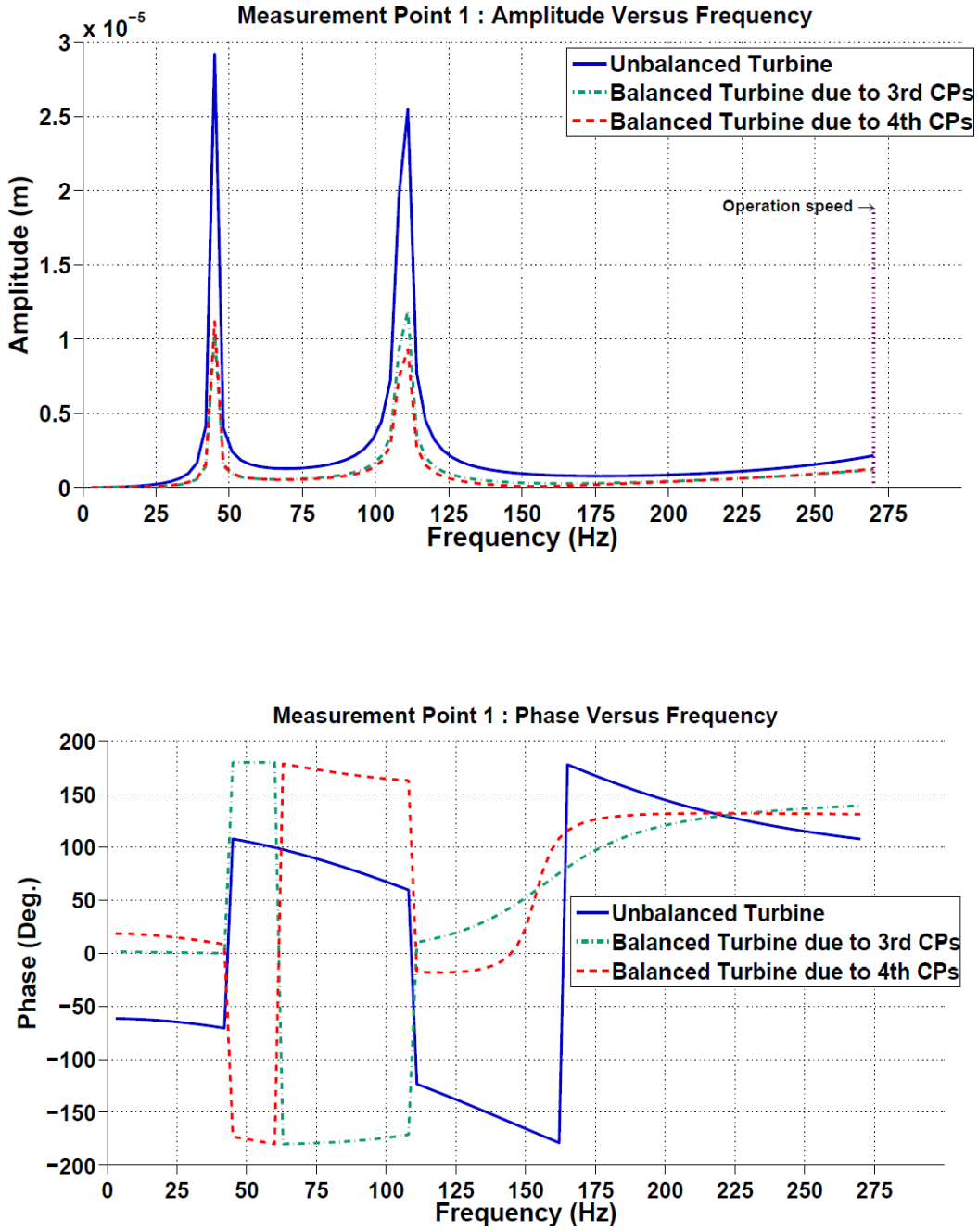

FIGURE 6.4.7: Amplitude-Phase Plot (Y-Direction) at Operation Speed: at ***Measurement Point 1***

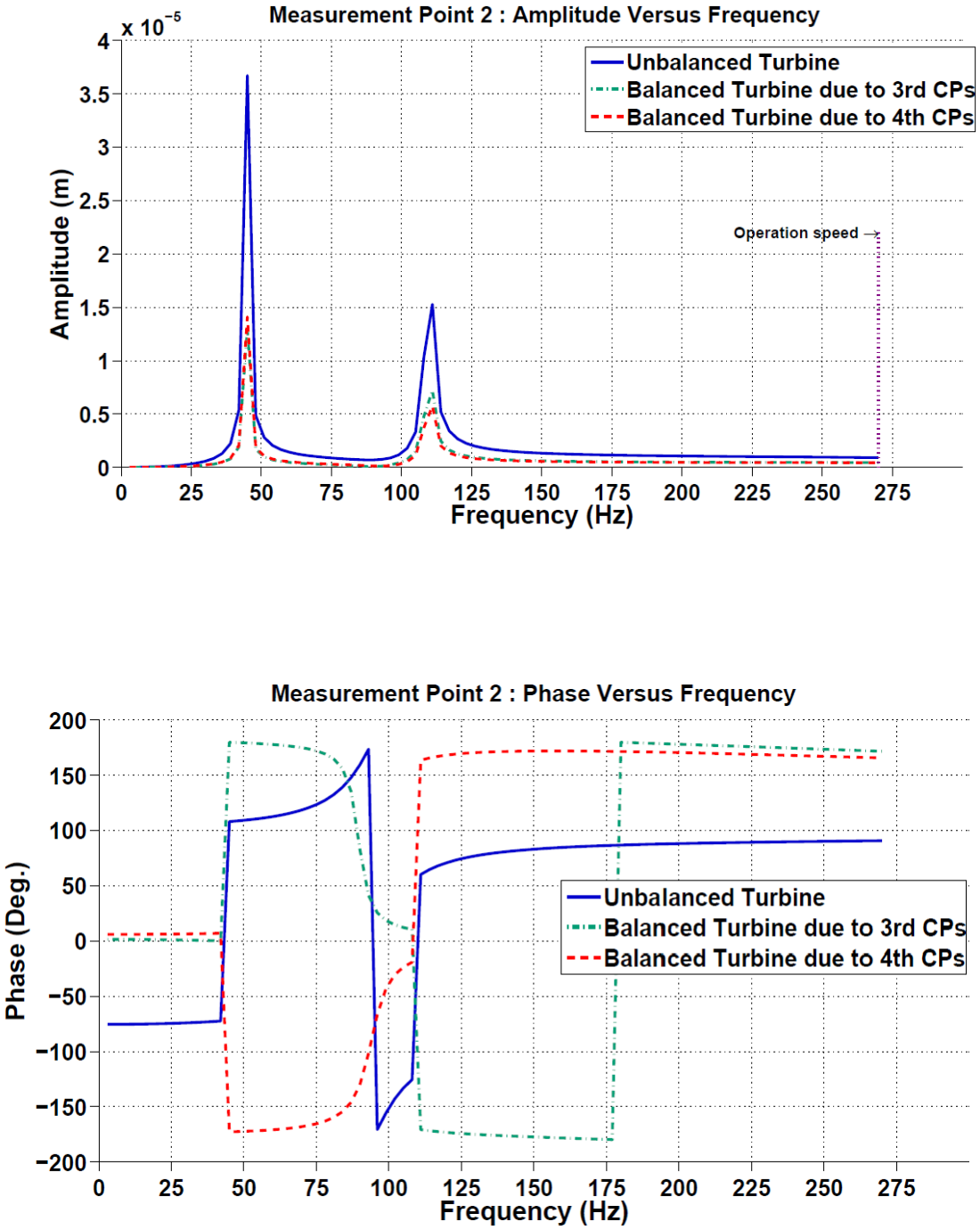

FIGURE 6.4.7: Amplitude-Phase Plot (Y-Direction) at Operation Speed: at ***Measurement Point 2***

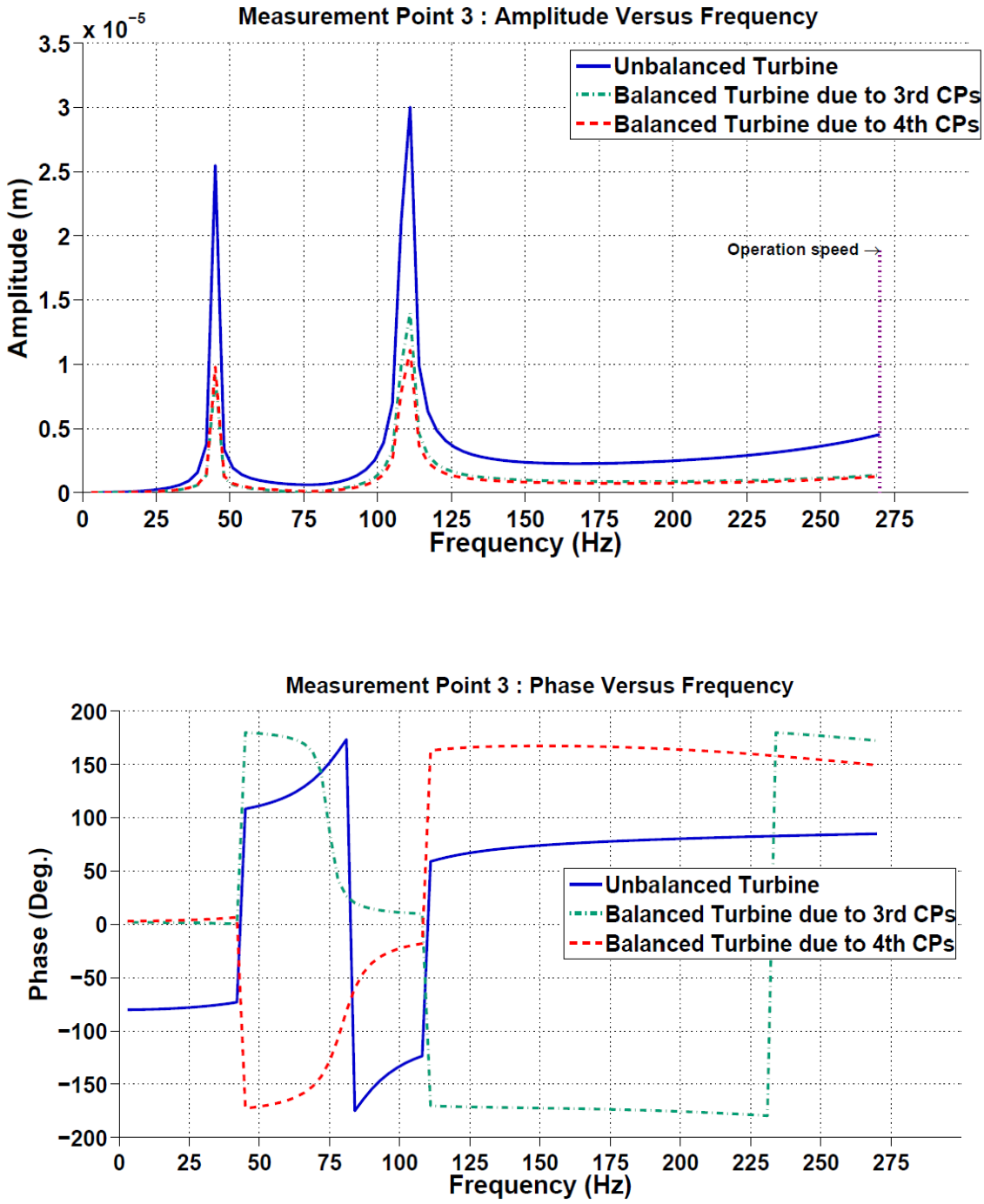

FIGURE 6.4.7: Amplitude-Phase Plot (Y-Direction) at Operation Speed: at ***Measurement Point 3***

(3)Amplitude in Z- Direction at Operation speeds

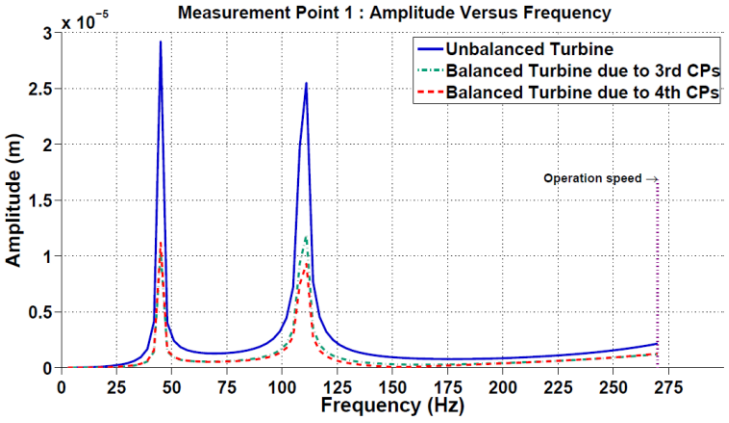

(a) Measurement point 1

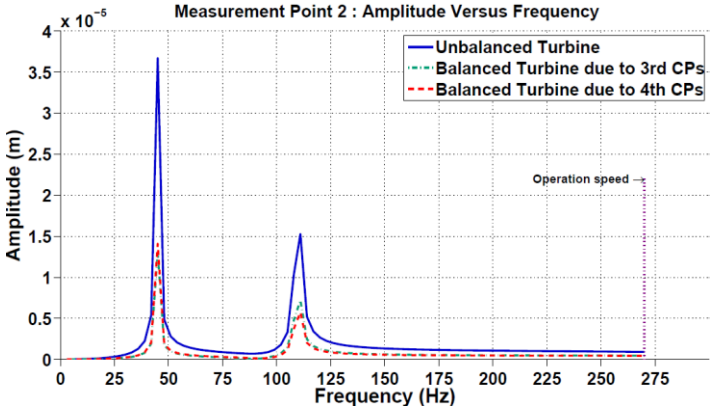

(b) Measurement point 2

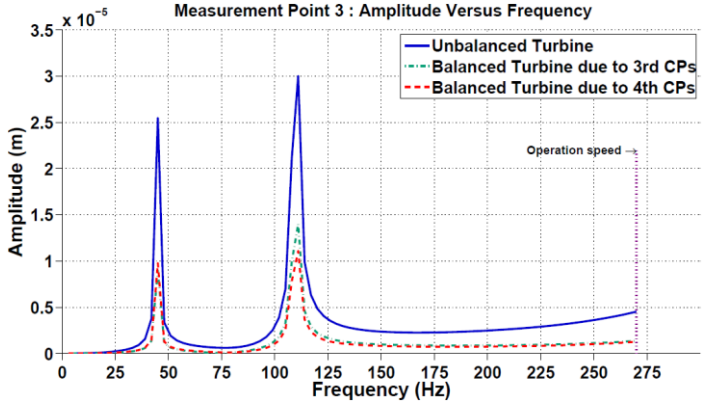

(c) Measurement point 3

FIGURE 6.4.8: Amplitude Plots (Z-Direction) at Operation Speed at Three Measurement Points

6.4.4.3 Percentage Unbalance Reduction

In order to assess the effectiveness of the developed low-speed balancing scheme, the percentage unbalance reduction is calculated. This can be used as an appropriate measure for judging the method, rather than using the balancing quality grade criteria which may not be meaningful of such an experimental turbine. There are reductions at all measuring points after the turbine has been balanced. The calculations were performed for the responses at the two critical speeds and at operation speed. The percentage reductions of responses in Figure 6.4.7 are tabulated in Table 6.4.5. The values in Table 6.4.5 show that the low-speed balancing method developed in this work reduced the initial unbalance responses of turbine to an appreciable level after balancing. It shows an average reduction of 55% minimum, which is acceptable in field applications. However, in practical situations where the percentage reduction is not sufficient, a "trim balancing" can be carried out.

TABLE 6.4.5: Percentage Unbalance Reduction at Measurement Points

	Percentage Reduction at		
Measurement Point No	1st Critical Speed	2nd Critical Speed	Operation Speed (16,200 rpm)
	%	%	%
1	62	64	42
2	62	62	51
3	61	63	72
Average	62	63	55

In addition, this table is applicable to Figure 6.4.8 too. This is true because when the turbine is running on the rigid bearings, the response at a point will be the same along all other axes except the axis of rotation.

6.4.4 .4 Orbit Plot

The orbits for the first two critical speeds from modal analysis (when turbine contained no unbalance) were obtained while the orbits of the excitation frequencies corresponding to the first two critical speeds were also obtained from harmonic analysis (when turbine was unbalance and balanced using 4th correction parameter). These orbits were as shown in the Figures 6.4.9 and 6.4.10 and it can be observed that Figures B_1 and B_2 (for unbalanced) and C_1 and C_2 (after balancing) were similar to A_1 and A_2 (Normal Turbine). Hence, only Figures C_1 and C_2 were closer to Figures A_1 and A_2. This shows that the correction paramter brought the unbalanced turbine close to initial turbine which was perfectly balance.

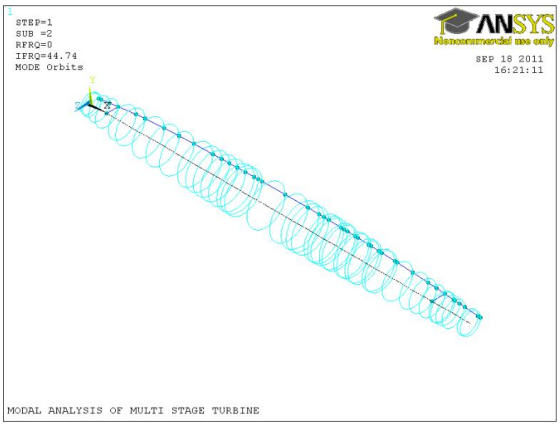

(A_1) Orbit plot for the first critical speed of normal turbine

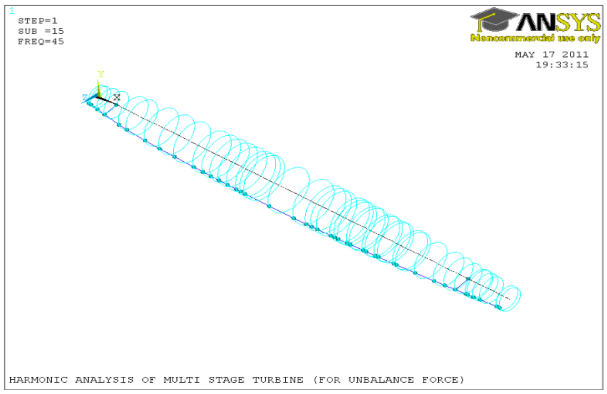

(B_1) Orbit plot for the excitation frequency (45Hz) of unbalanced turbine

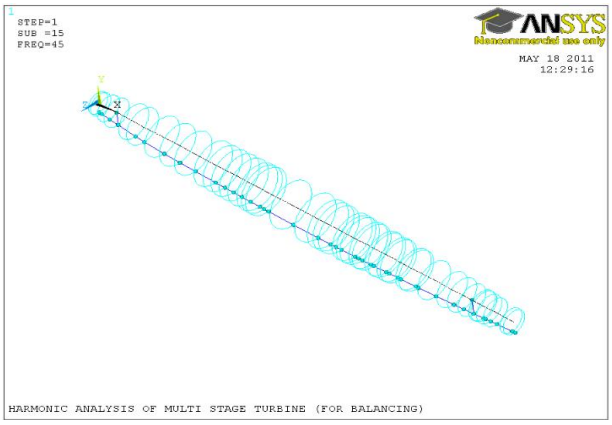

(C_1) Orbit plot for the excitation frequency (45Hz) of balanced turbine.

FIGURE 6.4.9 (A_1-C_1): Comparison between Orbit Plots from Normal, Unbalanced and Balanced Turbines at First Critical Speed

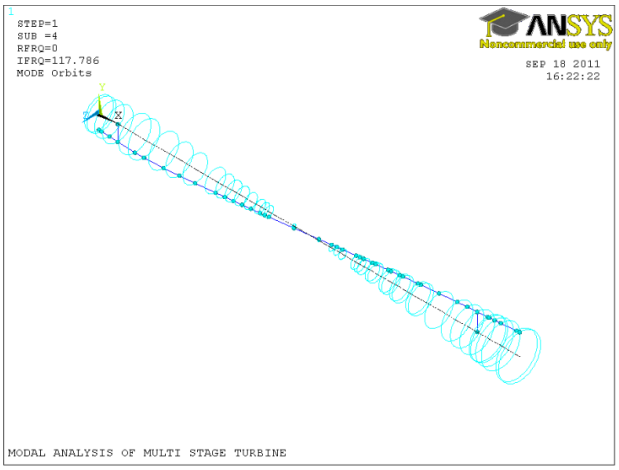

(A_2) Orbit plot for the second critical speed of normal turbine

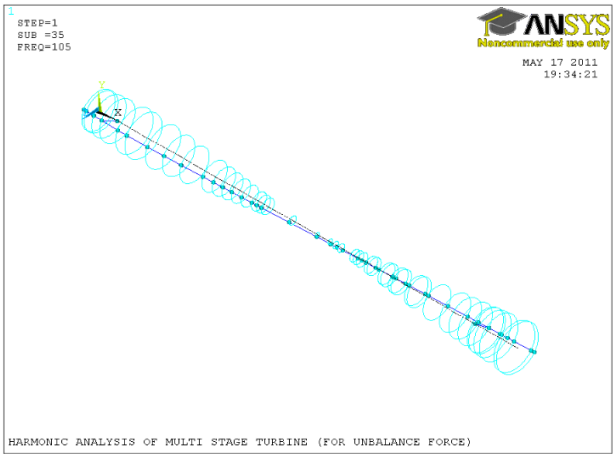

(B_2) Orbit plot for the excitation frequency (105Hz) of unbalanced turbine

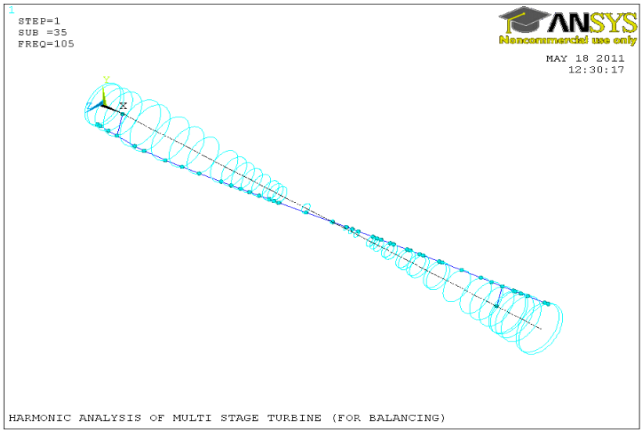

(C_2) Orbit plot for the excitation frequency (105Hz) of balanced turbine

FIGURE 6.4.10 (A_2-C_2): Comparison between Orbit Plots from Normal, Unbalanced and Balanced Turbine at Second Critical Speed

6.5 Multi Stage Turbine with Elastic Bearings

In this section, an industrial large-scale turbine rotor Figure 6.5.1 similar to that studied in section 6.4 (from [35]) will be considered again but with elastic bearings. The multi stage turbine is operating at a speed of 5,000 rpm (with bearing parameters:

$K_{zz} = 7.91E+07, K_{zy} = 1.51E+07, K_{yz} = -2.01E+08, K_{yy} = 4.04E+08$ N/m and

$C_{zz} = 162{,}997, C_{zy} = -66{,}463, C_{yz} = -65{,}932, C_{yy} = 603{,}928$ N-s/m) and there are two unbalances located on the turbine at stations 12 and 21 with quantities of 10E-3 kg.m at 0^o and 10E-3 kg.m at 90^o (where radii are 0.2802 and 0.2675 m) respectively. The turbine is running on the two bearings and the objective is to balance the turbine at low speed.

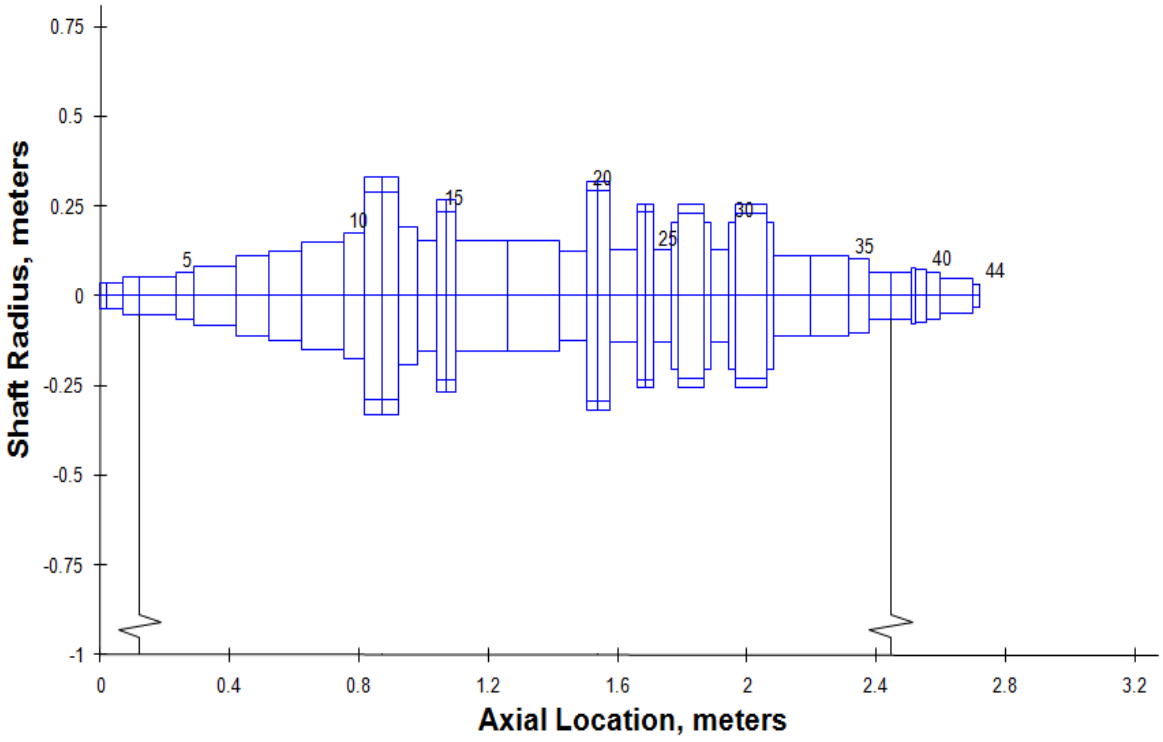

FIGURE 6.5.1: Multi Stage Turbine [35]

6.5.2 Turbine Modeling

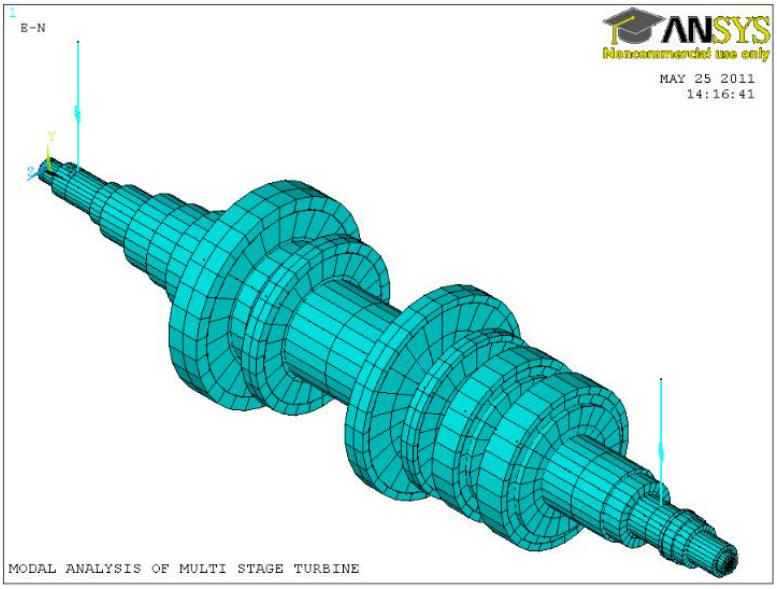

(a)Isometric View

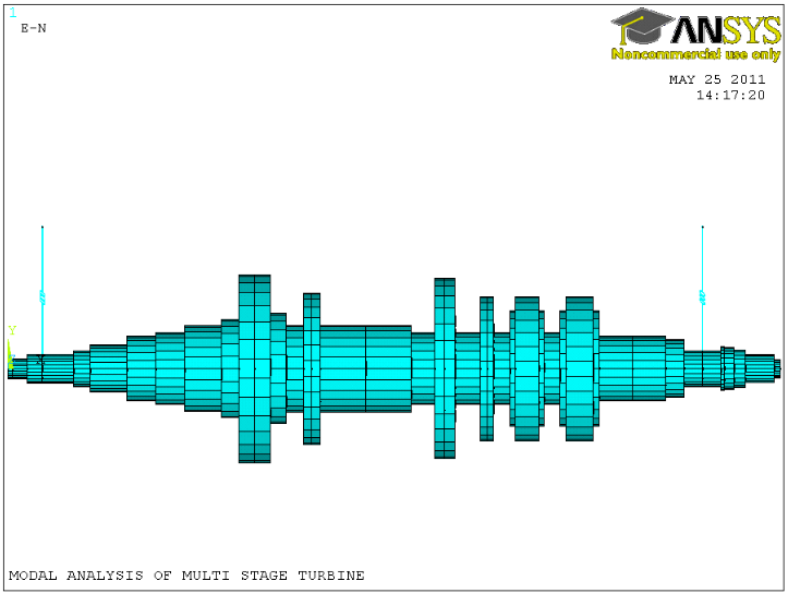

(b) Front View

FIGURE 6.5.2: Multi Stage Turbine Modeling

6.5.2 Modal Analysis of the turbine

The modal analysis was carried out on the above turbine model at its operation speed and the first five natural frequencies of the system are listed in Table 6.5.1.

TABLE 6.5.1: Natural Frequencies of Multi Stage Turbine

Mode Number	Damped Frequency (Hz)		Undamped Frequency (HZ)
	Real	Complex	
1	-6.9424	42.07	41.016
	-6.9424	-42.07	
2	-7.1427	62.846	63.394
	-7.1427	-62.846	
3	-37.454	86.431	94.537
	-37.454	-86.431	
4	-93.559	151.27	173.22
	-93.559	-151.27	
5	-108.88	276.35	303.48
	-108.88	-276.35	

6.5.3 Turbine Balancing

6.5.3.1 Operation Conditions

1.) The natural frequencies recorded above indicate that the turbine is operating between the second critical speed (63.394 Hz or 3,803.64 rpm) and third critical speed (94.537Hz or 5,672.22 rpm).

2.) The operating speed Ω_{op} is 83.33 Hz (5,000 rpm)

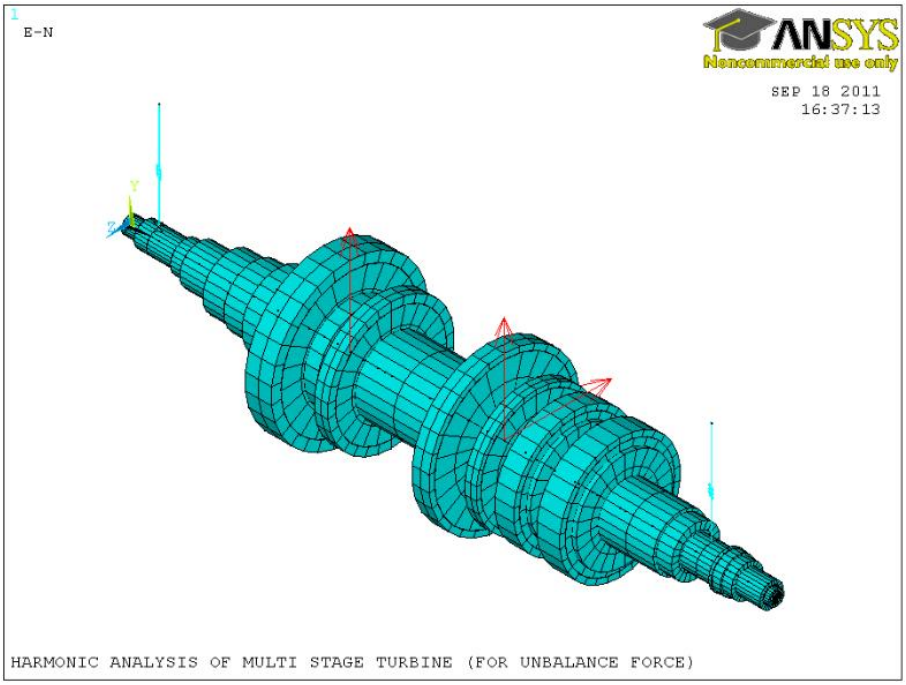

FIGURE 6.5.3: Unbalanced Multi Stage Turbine

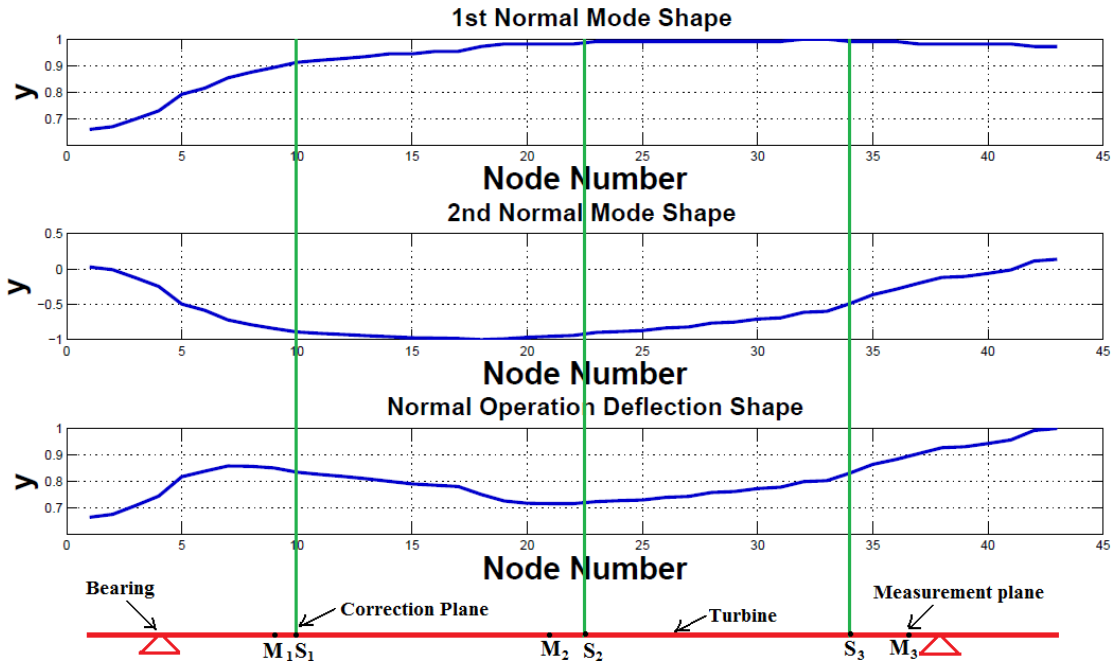

FIGURE 6.5.4: First and Second Normal Mode Shapes and ODS of Turbine Versus Nodes Number

6.5.3.2 Mode Shapes from Harmonic Response Analysis

Based on the available parameters, the unbalance was created on the turbine as shown in Figure 6.5.3 and the harmonic response analysis was performed on the unbalanced turbine at operation speed (5,000 rpm).The mode shape corresponding to each critical speed were then obtained. Since the turbine is operating above the second critical speed, only the first and second natural mode shapes are needed. The rotor's operational deflection shape (ODS) is used to serve as mode shape of 3rd critical speed. The normal mode shapes shown in Figure 6.5.4 are plotted, while the correction planes and measurement points are selected as shown in Figure 6.5.4.

6.5.3.3 Low Speed Balancing Conditions

In order to satisfy the conditions required for low-speed balancing procedures described in section 5.2, the following parameters were used:

1.) Balancing speed Ω is 2,000 rpm which is well below the first critical speed.
2.) Since turbine is operating above the second critical speed, then $N = 3$ and three correction planes plus three measurement points are required.
3.) The three correction planes are S_1, S_2 and S_3 and the three measurement points are M_1, M_2 and M_2 which are located as shown in Figure 6.5.4.

6.5.3.4 Low-Speed Turbine Balancing Processes

6.5.3.4.1 Initial Responses depicted at Measurement Points

The Harmonic analysis was carried out for the unbalance turbine shown in Figure 6.5.3 at speed (6,000 rpm) which is above the operation speed (5,000 rpm) and at balancing speeds in order to obtain the initial responses. The initial responses at the three measurement points (three nodes) are then acquired. The initial responses at balancing speed are shown in Figure 6.5.2.

Now, having obtained the initial responses of the turbine, the balancing operation proceeds by adding trial weights to the unbalanced turbine at the selected correction planes, one after the other. Several trial sessions are carried out using the low-speed balancing procedure described in section 5.2 at balancing speed. In this context, we have tested four different sets of trial weights. The results obtained from the four different trials sessions are summarized in Figure 6.5.3.

6.5.4 Results

In this section, the correction parameters are determined by utilizing the data in Tables 6.5.2 and 6.5.3 together with the equation of the low-speed balancing procedure described in section 5.2. The balanced turbine (i.e. after adding correction masses) is tested at both balancing and operation speeds as well as at a speed above the operation speed. The acquired correction parameters and the responses at measurement points when each of the correction parameters was applied to the turbine at balancing speed are shown in Tables 6.5.4.

TABLE 6.5.2: Initial Responses at Balancing Speed (2, 000 rpm)

Initial Measuremets					
Measurement Point 1 (Node 9)		Measurement Point 2 (Node 21)		Measurement Point 3 (Node 36)	
Max Amplitude	Phase (Deg.)	Max Amplitude	Phase (Deg.)	Max Amplitude	Phase (Deg.)
3.58E-06	-142.13	3.96E-06	-144.209	4.11E-06	-175.595

TABLE 6.5.3: Trial Parameters, Amplitudes and Phases at each Measurement Point

Trial S/N	Trial Parameters							Measurements Due to Trial Parametrs					
								Measurement Point 1		Measurement Point 2		Measurement Point 3	
	Correction Planes		Mass (kg)	Radius r (m)	mr (kg.m)	Angle (Deg.)		Max Amplitude (m)	Phase (Deg.)	Max Amplitude (m)	Phase (Deg.)	Max Amplitude (m)	Phase (Deg.)
1	1	Node 10	0.020	0.17305	0.003461	4		4.39E-06	-133.626	4.70E-06	-137.374	4.72E-06	-169.413
	2	Node 23	0.015	0.254	0.00381	255		2.92E-06	-130.223	3.06E-06	-134.222	3.03E-06	-167.498
	3	Node 34	0.025	0.1131	0.002828	100		3.71E-06	-151.511	4.31E-06	-154.689	4.85E-06	176.612
2	1	Node 10	0.020	0.17305	0.003461	4		4.39E-06	-133.626	4.70E-06	-137.374	4.72E-06	-169.413
	2	Node 23	0.015	0.254	0.00381	257		2.94E-06	-129.835	3.09E-06	-133.687	3.05E-06	-166.822
	3	Node 34	0.025	0.1131	0.002828	100		3.71E-06	-151.511	4.31E-06	-154.689	4.85E-06	176.612
3	1	Node 10	0.020	0.17305	0.003461	0		4.35E-06	-132.858	4.67E-06	-136.732	4.69E-06	-168.881
	2	Node 23	0.015	0.254	0.00381	257		2.94E-06	-129.835	3.09E-06	-133.687	3.05E-06	-166.822
	3	Node 34	0.025	0.1131	0.002828	100		3.71E-06	-151.511	4.31E-06	-154.689	4.85E-06	176.612
4	1	Node 10	0.020	0.17305	0.003461	0		4.35E-06	-132.858	4.67E-06	-136.732	4.69E-06	-168.881
	2	Node 23	0.015	0.254	0.00381	260		2.98E-06	-129.301	3.13E-06	-132.932	3.08E-06	-165.853
	3	Node 34	0.025	0.1131	0.002828	95		3.76E-06	-151.24	4.37E-06	-154.181	4.89E-06	177.431

TABLE 6.5.4: Correction Parameters and Final Amplitudes and Phases at each Measurement Point

Trial S/N	Calculated Correction Parameters				Final Measurement (Residual Unbalance)					
					Measurement Point 1		Measurement Point 2		Measurement Point3	
	Masses (kg)	Angles (Deg.)	mr (kg.m)		Max Amplitude (m)	Phase (Deg.)	Max Amplitude (m)	Phase (Deg.)	Max Amplitude (m)	Phase (Deg.)
1	0.0449	-173.326	0.0078		5.37E-07	9.9518	6.24E-07	23.2783	5.53E-07	23.1978
	0.0440	-102.9546	0.0112							
	0.0122	152.0791	0.0014							
2	0.0449	-173.3247	0.0078		5.18E-07	-10.9638	5.83E-07	2.44502	4.23E-07	-1.39993
	0.0440	-98.956	0.0112							
	0.0122	152.0932	0.0014							
3	0.0449	178.6755	0.0078		2.04E-07	-11.7063	3.24E-07	17.024	2.91E-07	32.5895
	0.0440	-98.949	0.0112							
	0.0122	152.0956	0.0014							
4	0.0449	178.6747	0.0078		3.36E-07	-73.9861	3.34E-07	-47.8284	1.78E-07	-88.1057
	0.0440	-92.9515	0.0112							
	0.0122	142.0817	0.0014							

It is noted that, when the four sets of correction parameters (in Tables 6.5.4) were applied to the turbine one after the other, the turbine was balanced not only at balancing speed but also at operation speed. The amplitude-phase plot of the initial responses due to unbalance and final responses acquired when turbine was balanced using the 3rd and 4th correction parameters at both balancing and operation speeds are shown, for each measurement point in subsection 6.5.4.2.

Accordingly, it is concluded from Figures 6.5.7 to 6.5.9 that the turbine could be balanced at low speed (a speed less than the first critical speed).

6.5.4 .1 3D Plots of Critical Mode shapes of the Turbine

Since turbine is operating above second critical speed, the 3D plots of the first two critical mode shapes of the turbine at operation speed (before and after balancing) are shown in Figures 6.5.5 (a and b). It is imperative to know that these mode shapes are obtained through the harmonic analysis at excitation frequency equivalent or close to each of the two critical speeds of normal turbine. The figures show the difference in turbine mode shapes before and after balancing.

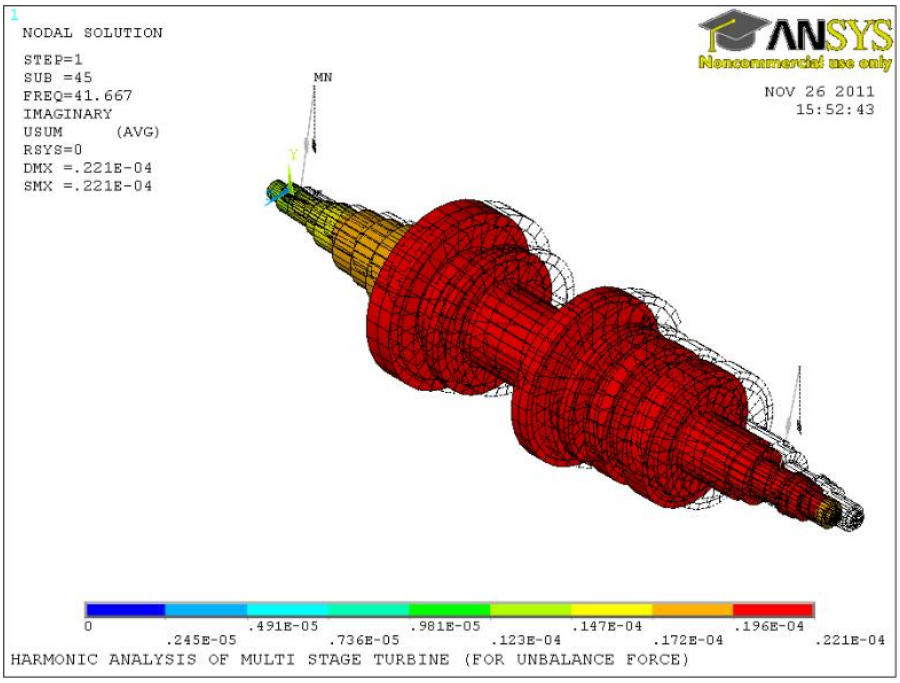

(a_1): Mode Shape at excitation frequency of 41.667 Hz before balancing

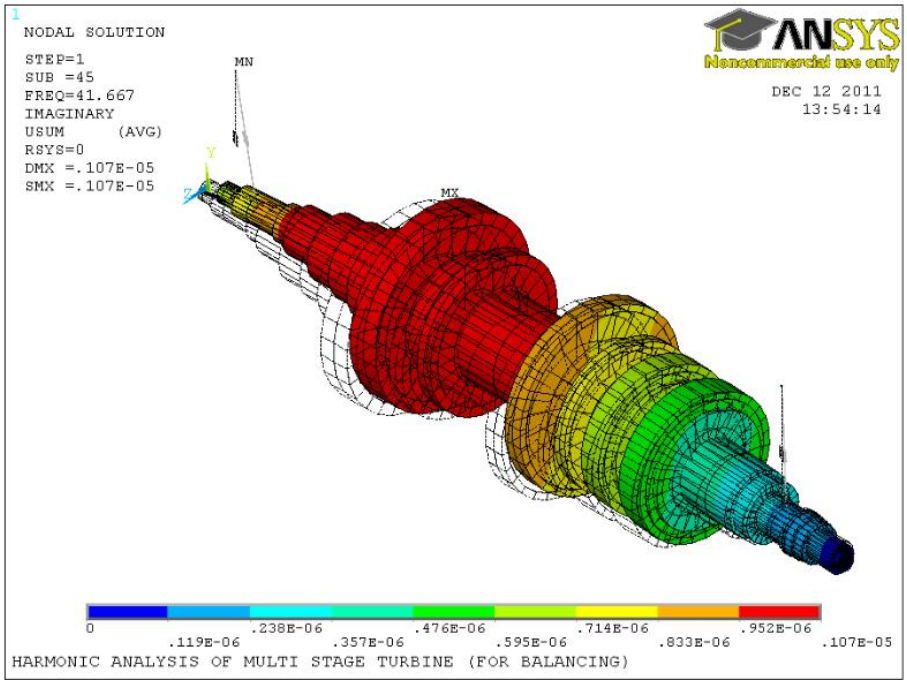

(a_2): Mode Shape at excitation frequency of 41.667 Hz after balancing

FIGURE 6.5.5 (a): Multi Stage Turbine Mode Shapes Before and After Balancing

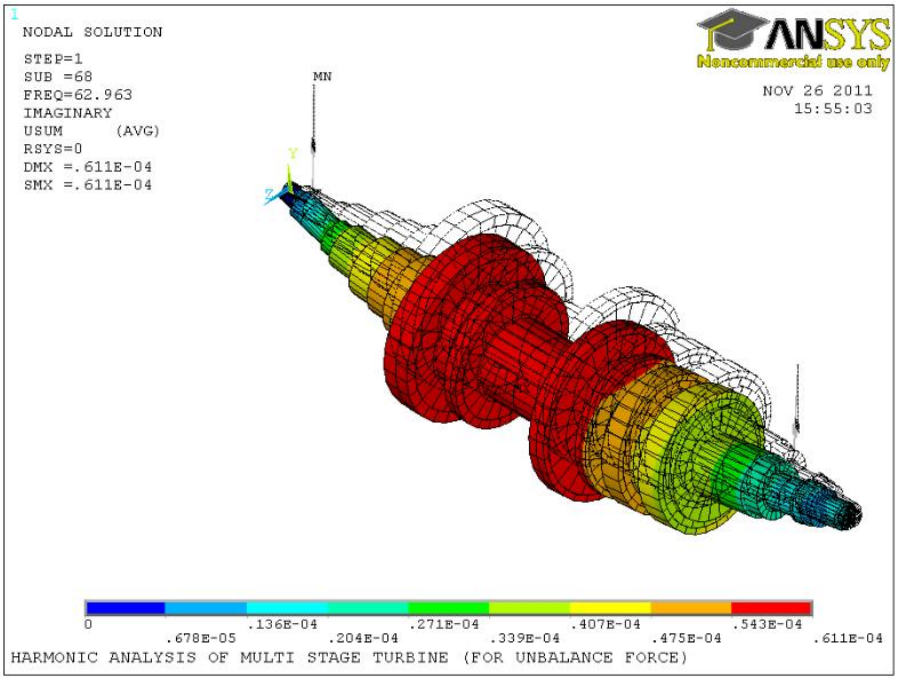

(b_1): Mode Shape at excitation frequency of 62.963 Hz before balancing

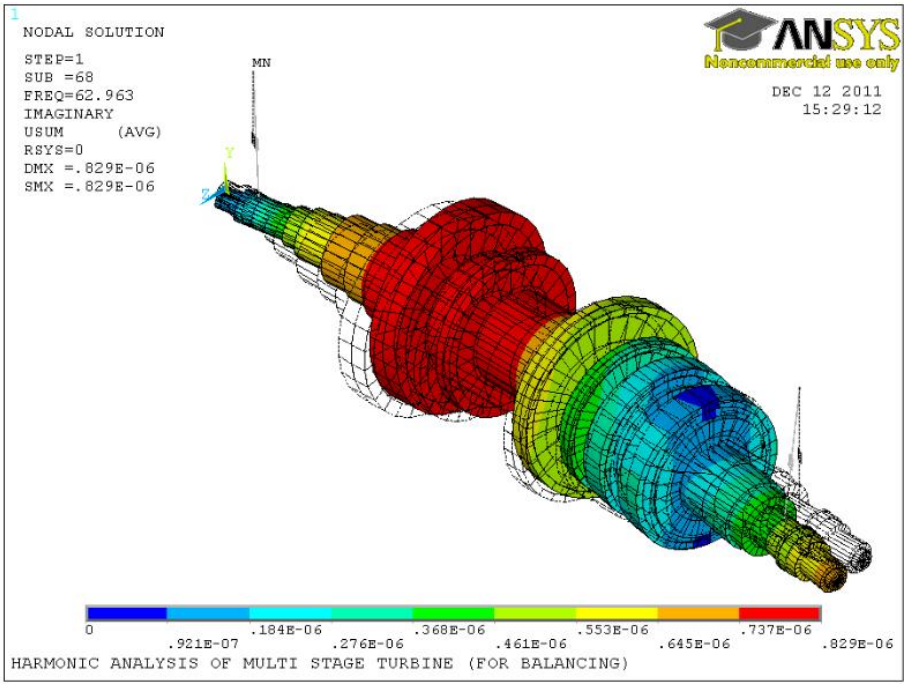

(b_2): Mode Shape at excitation frequency of 62.963 Hz after balancing

FIGURE 6.5.5 (b): Multi Stage Turbine Mode Shapes Before and After Balancing

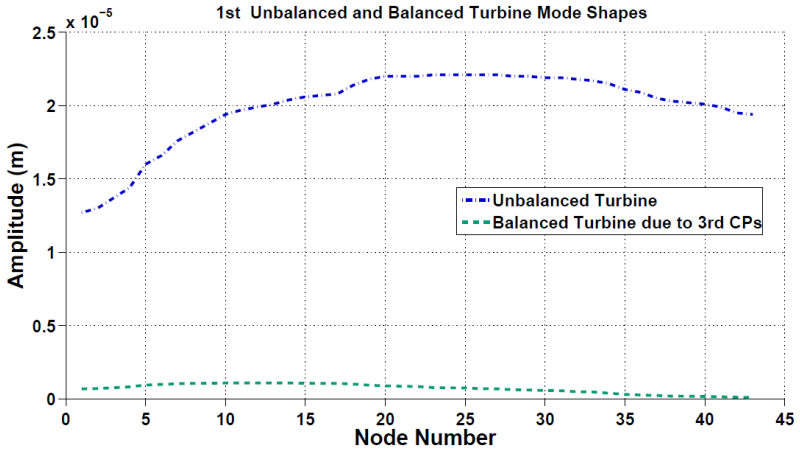

(a) First Mode

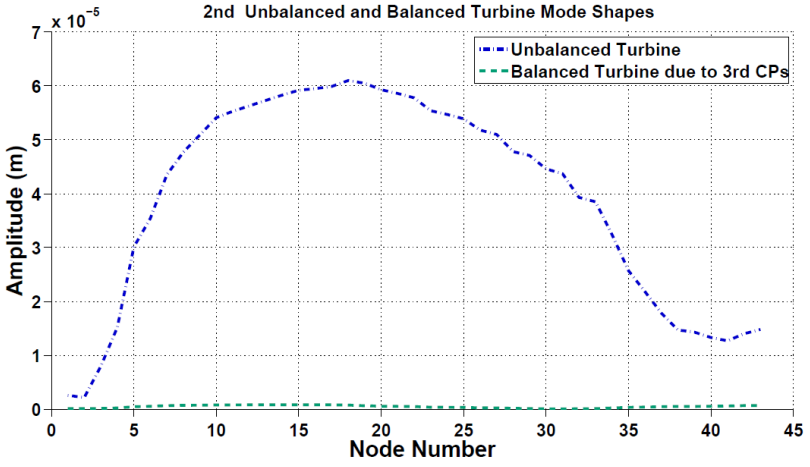

(b) Second Mode

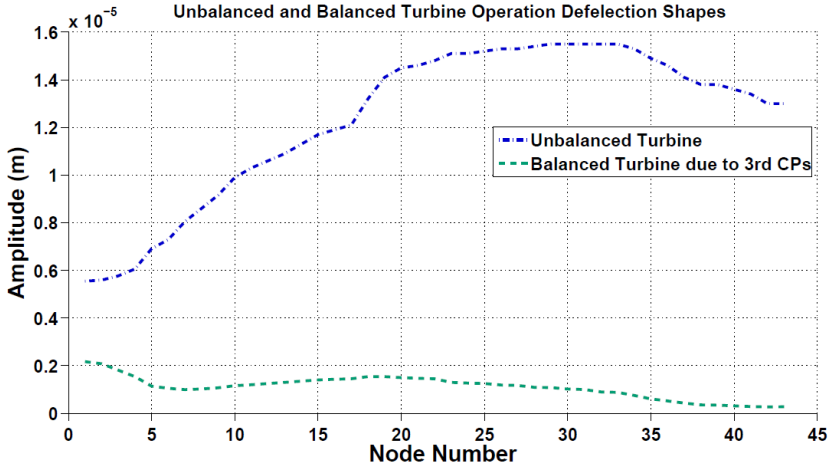

(c) ODS

FIGURE 6.5.6: Multi Stage Turbine Unbalanced and Balanced Mode Shapes

Similarly, despite the fact that the differences in mode shapes are shown in three-diemnsional configuration in Figures 6.5.5 for unbalanced and balanced turbine, these differences were corroborated further in Figures 6.5.6 (a, b and c). Both Figures 6.5.5 and 6.5.6 are obtained by using USUM. It can been seen in these figures that modes of the turbine have been reduced drastically after the turbine was balanced.

6.5.4 .2 Amplitude–phase plot (Bode Plot)

When the correction parameters (in Table 6.5.4) are applied to the turbine one after the other during the test-run at balancing and operation speeds, the amplitude phase plots are made from the responses obtained. The amplitude-phase plot is made up of two parts, which include the amplitude versus frequency and the phase versus frequency. These are shown in Figures 6.5.7 to 6.5.9 for all measurement points. Such figures demonstrate clearly how the low-speed balancing scheme reduced the initial unbalance to an acceptable level; as explained hereunder.

Figure 6.5.7 shows the turbine responses at three measuring points; before and after balancing. It can be seen that at all measuring points, the final responses are decreased drastically when compared to initial response at balancing speed. Also, Figures 6.5.8 and 6.5.9 show the turbine responses (in y and z directions) at all measuring points when it is being tested at a speed above its operation speed. The initial responses that have been obtained from unbalanced turbine were plotted against the responses of balanced turbine. The vertical dashed line indicates the actual turbine operation speed. Turbine was run to a speed above its operation speed in order to observe how far the balanced turbine will be able to maintain its balanced state. This test becomes necessary;

as precautionary measure to check the likelihood that the turbine speed may drift above the operating speed, due to some unexpected operating circumstances. This test will allow one to know the safe speed that needs to be considered during all modes of operation without compromising the balancing conditions.

(1)Amplitude in Y- Direction at Balancing Speed

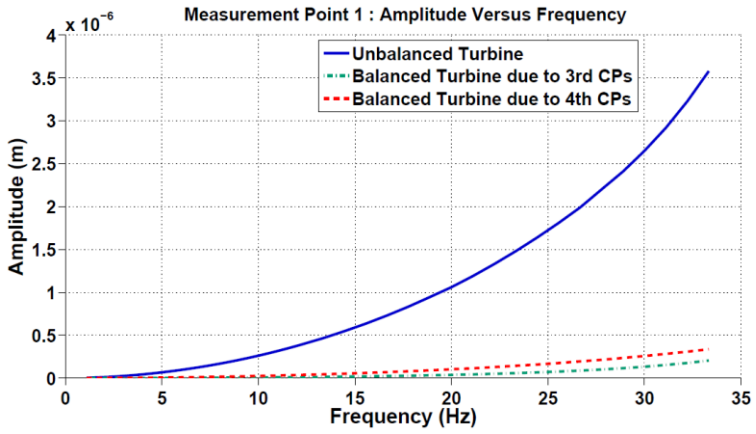

(a)Measurement point 1

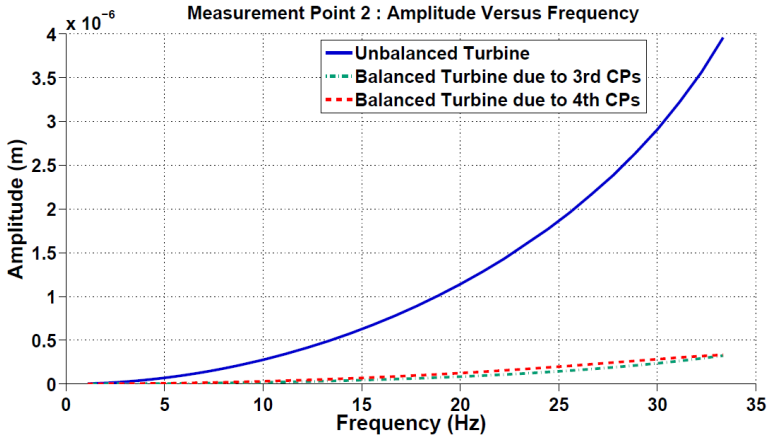

(b) Measurement point 2

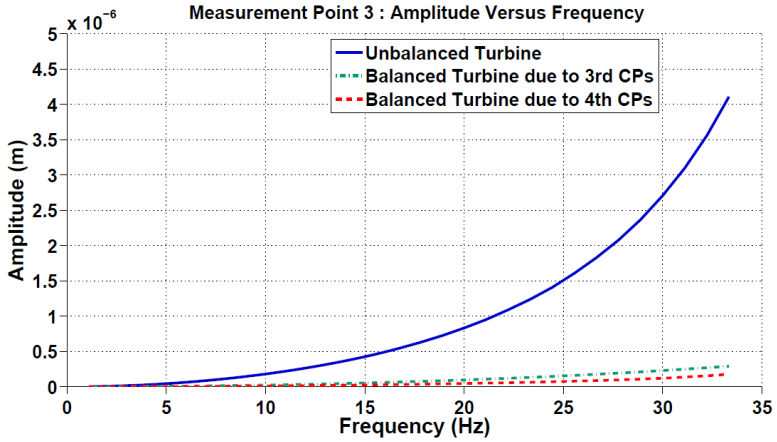

(c) Measurement point 3

FIGURE 6.5.7: Amplitude Plots due to the Correction Parameters and Initial Responses at Balancing Speed at Three Measurement Points

(2)Amplitude-phase Plots in Y- Direction at Speed above the Operation Speed

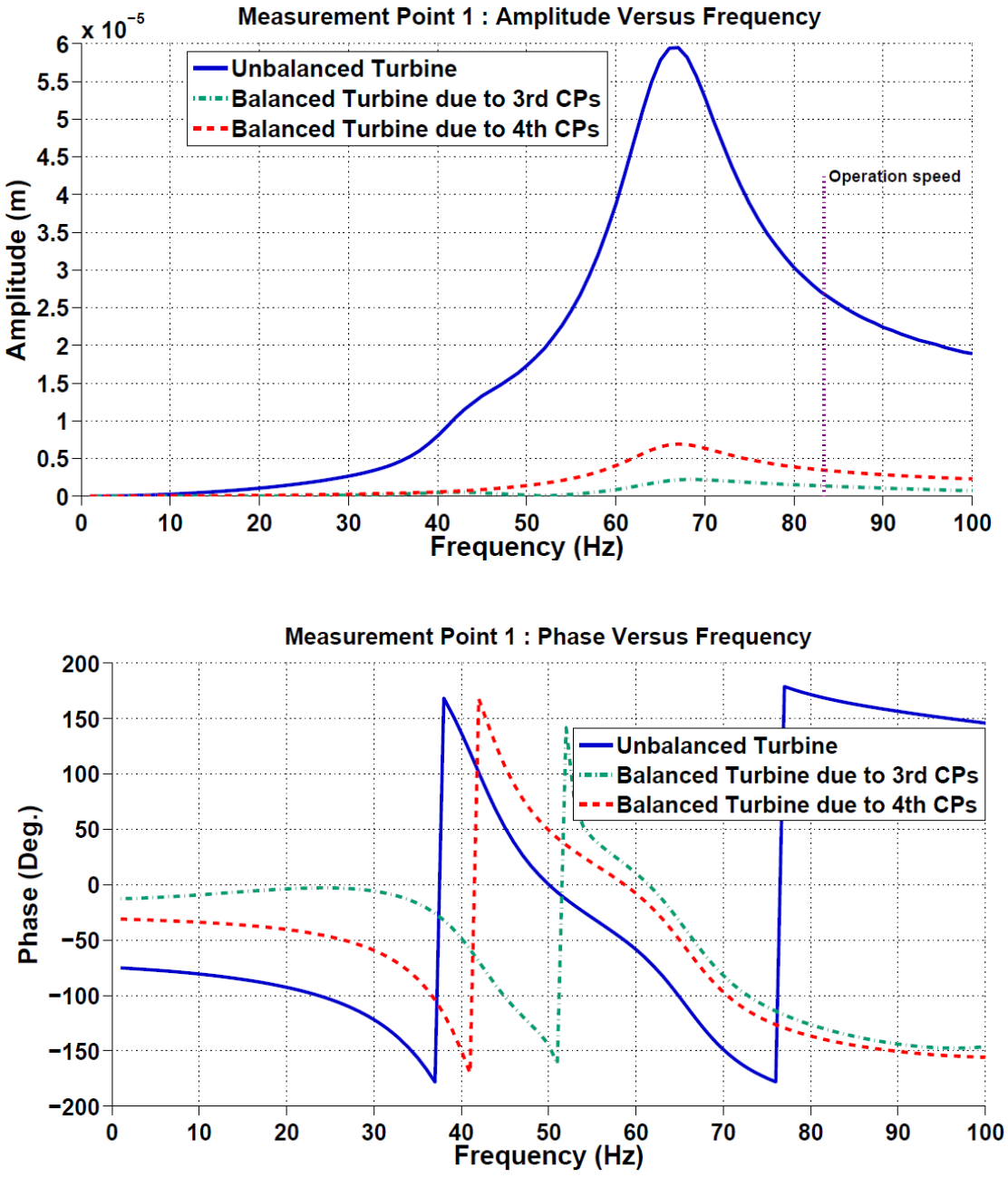

FIGURE 6.5.8: Amplitude-Phase Plots (Y-Direction) at Speed above Operation Speed: at ***Measurement Point 1***

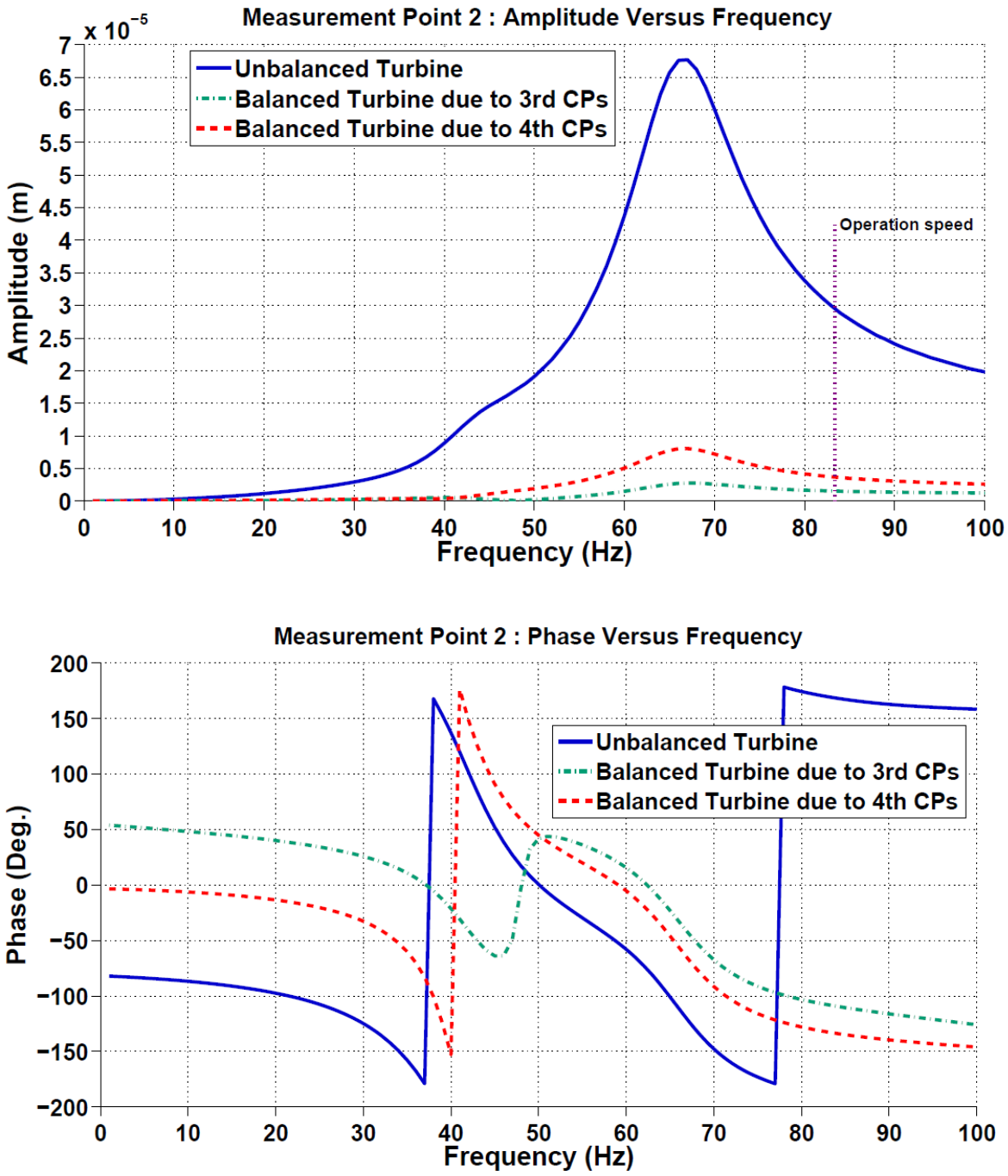

FIGURE 6.5.8: Amplitude-Phase Plots (Y-Direction) at Speed above Operation Speed: at ***Measurement Point 2***

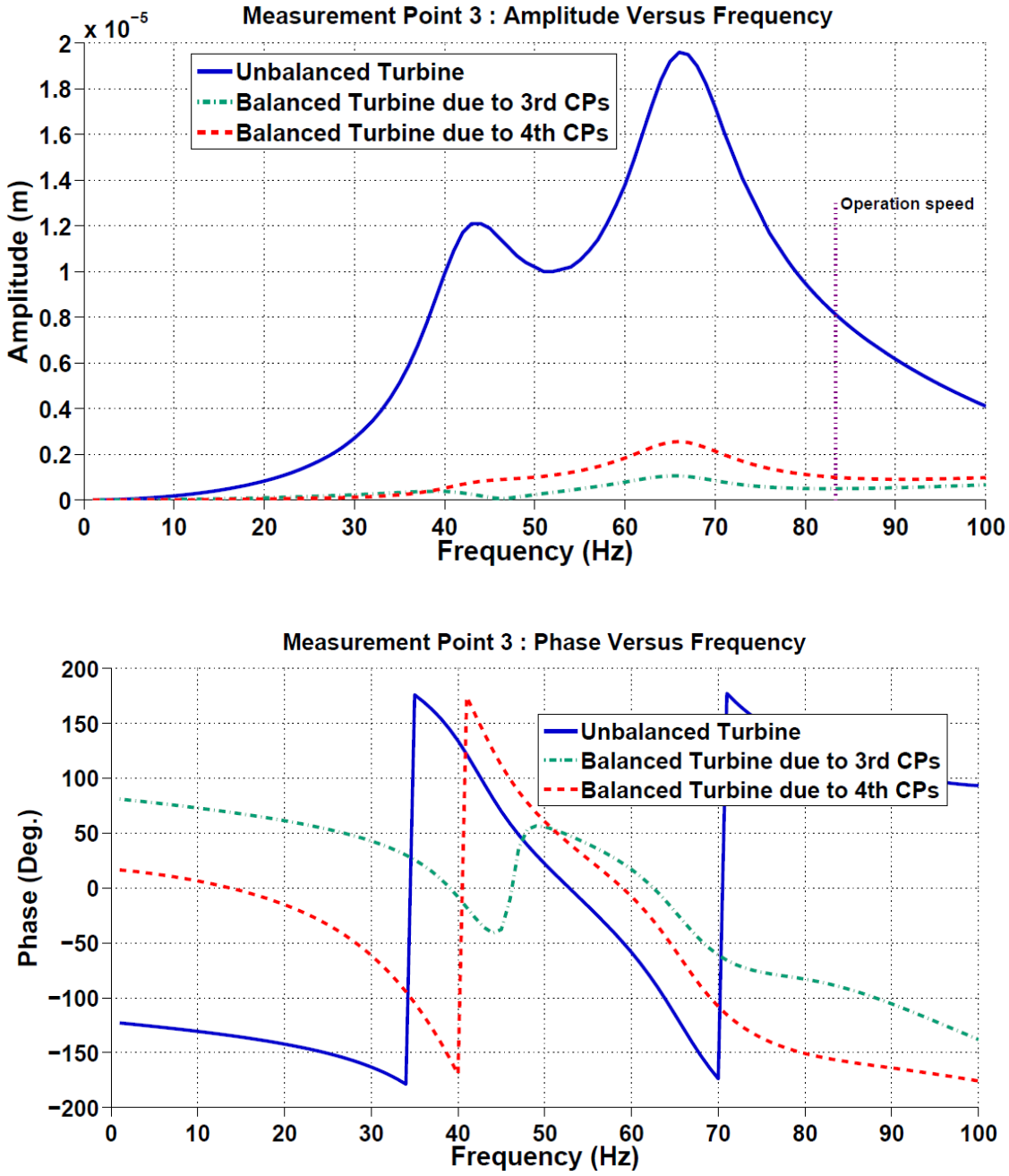

FIGURE 6.5.8: Amplitude-Phase Plots (Y-Direction) at Speed above Operation Speed: at ***Measurement Point 3***

(3) Amplitude-phase Plots in Z- Direction at Speed above the Operation Speed

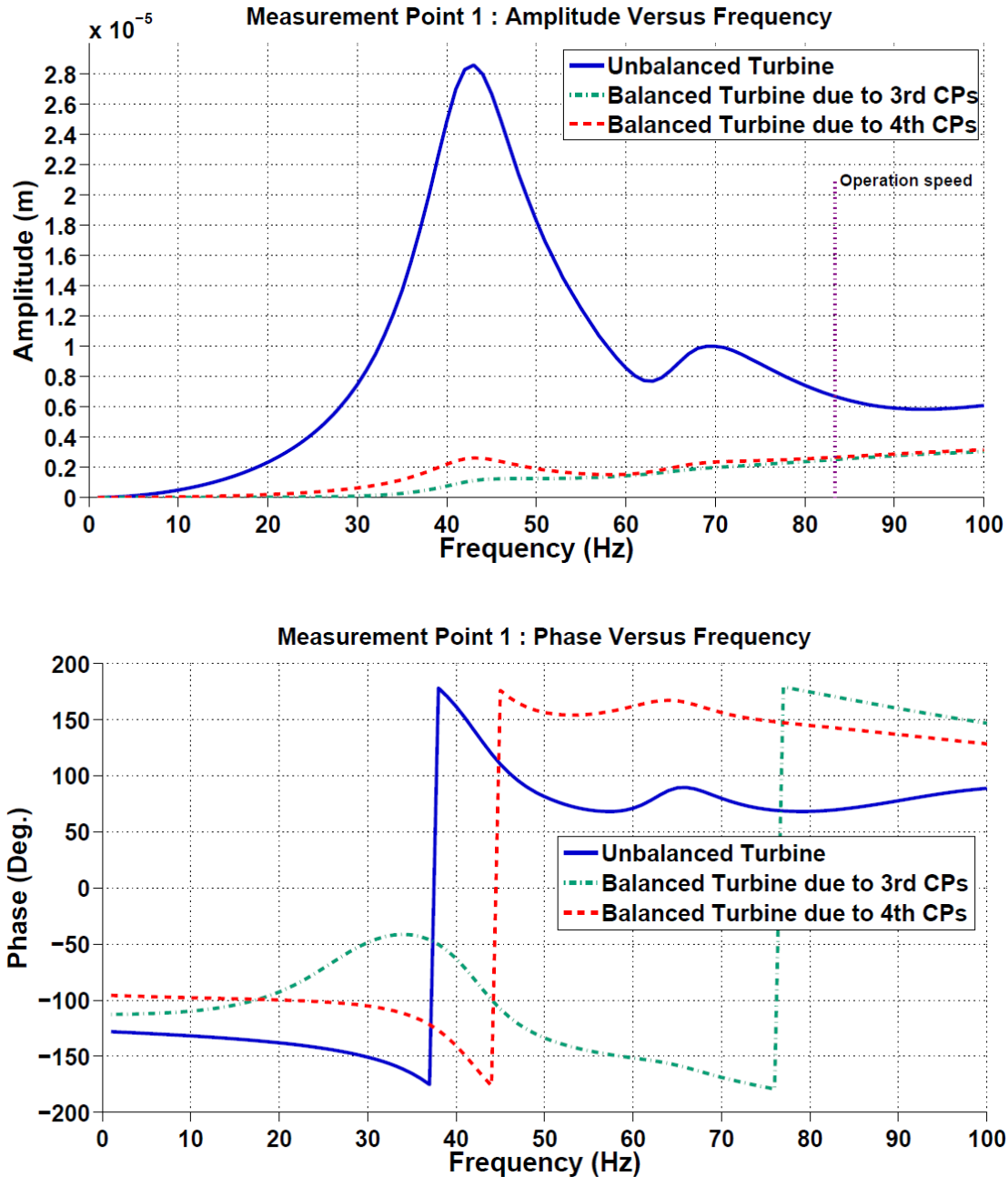

FIGURE 6.5.9: Amplitude-Phase Plots (Z-Direction) at Speed above Operation Speed: at ***Measurement Point 1***

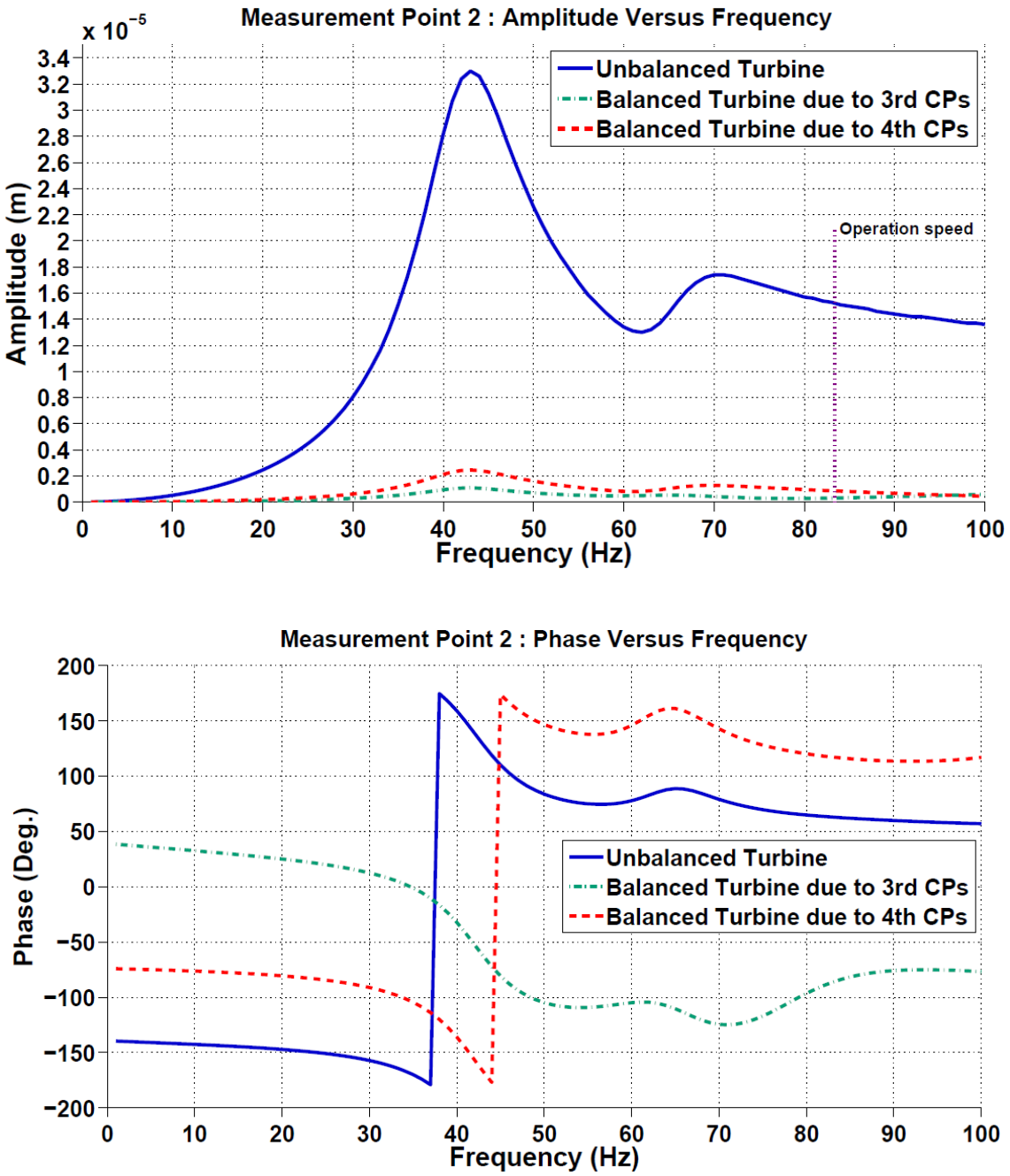

FIGURE 6.5.9: Amplitude-Phase Plots (Z-Direction) at Speed above Operation Speed: at ***Measurement Point 2***

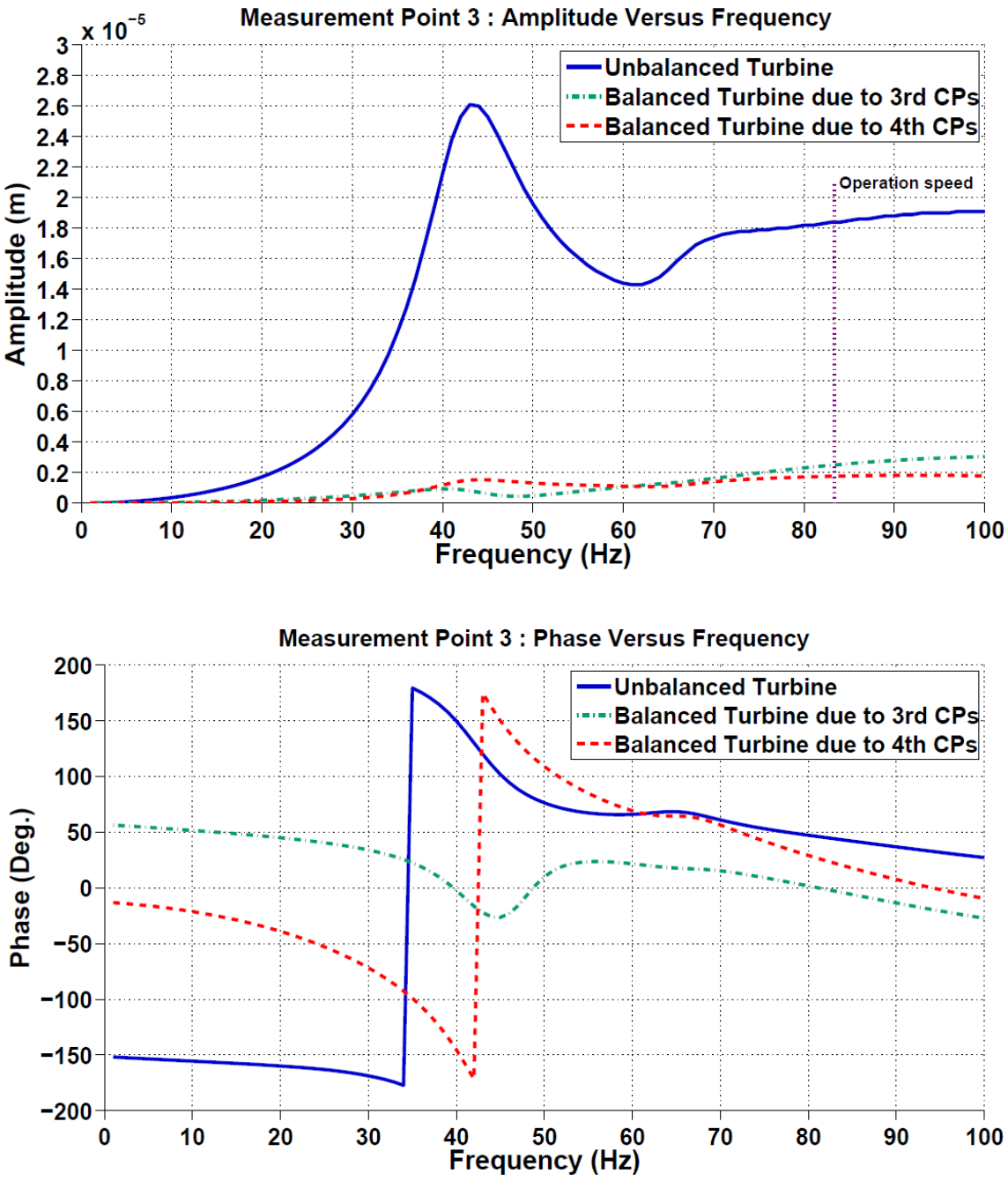

FIGURE 6.5.9: Amplitude-Phase plots (Z-direction) at speed above operation speed: at ***measurement point 3***

6.5.4.3 Percentage Unbalance Reduction

In order to assess the effectiveness of the developed low-speed balancing scheme, the percentage unbalance reduction is calculated. This can be used as an appropriate measure for judging the method, rather than using the balancing quality grade criteria which may not be meaningful of such an experimental turbine. There are reductions at all measuring points after the turbine has been balanced. The calculations were performed for the responses at the two critical speeds and at another speed above the operation speed. The percentage reductions of responses in Figure 6.5.8 are tabulated in Table 6.5.5 when 3rd correction parameter is considered. The values in Table 6.5.5 show that the low-speed balancing method developed in this work reduced the initial unbalance responses of turbine to an appreciable level after balancing. It shows an average reduction of over 90% per column, which is more than hoped for in field applications. However, in practical situations where the percentage reduction is not sufficient, a "trim balancing" can be carried out.

In addition, since this turbine is running on elastic bearings, the percentage reductions in y and z axes are no longer the same. Then, the percentage reductions for z-axis are shown in Table 6.5.6. . It shows an average reduction of over 75% per column, which is also more than hoped for in field applications.

TABLE 6.5.5: Percentage Unbalance Reduction at Measurement Points (Y-Direction)

	Percentage Reduction at		
Measurement Point No	1st Critical Speed	2nd Critical Speed	Speed above Op. Speed (6,000 rpm)
	%	%	%
1	96	96	96
2	97	96	94
3	98	95	84
Average	97	96	91

TABLE 6.5.6: Percentage Unbalance Reduction at Measurement Points (Z-Direction)

	Percentage Reduction at		
Measurement Point No	1st Critical Speed	2nd Critical Speed	Speed above Op. Speed (6,000 rpm)
	%	%	%
1	96	81	50
2	97	97	96
3	97	91	84
Average	97	90	77

6.5.5 Orbit Plot

In this section, orbit plots for the first two critical speeds from modal analysis (when turbine contained no unbalance) were obtained. Also, orbit plots for the excitation frequencies corresponding or close to these two critical speeds were also obtained from harmonic analysis for unbalanced and balanced turbines. Those orbit plots obtained for the balanced turbine were acquired when the 3rd correction parameter was considered. These orbit plots are as shown in Figures 6.5.10 and 6.5.11 for comparison at the two critical speeds. It can be observed that plots in Figures 6.5.10 (B_1) and 6.5.11 (B_2) (for unbalanced turbine) are not close to those plots in Figures 6.5.10 (A_1) and 6.5.11 (A_2) when turbine was normal. Whereas, the plots in Figures 6.5.10 (C_1) and 6.5.11 (C_2) (after balancing) are almost the same as those in Figures 6.5.10 (A_1) and 6.5.11 (A_2). The slight differences in A's and C's might probably be due to the fact that A's were obtained from damped natural frequencies while C's are acquired from values approximately equal to natural frequencies. Similarly, these differences might also be due to the insignificant differences in their frequencies values. Hence, the agreement of C's and A's demonstrates that the correction paramters brought the unbalanced turbine close to the initial turbine state, which was absolutely balanced (normal).

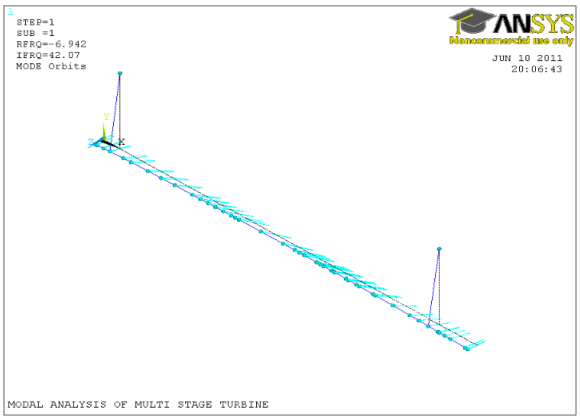

(A_1): Orbit plot for the first critical speed of normal turbine

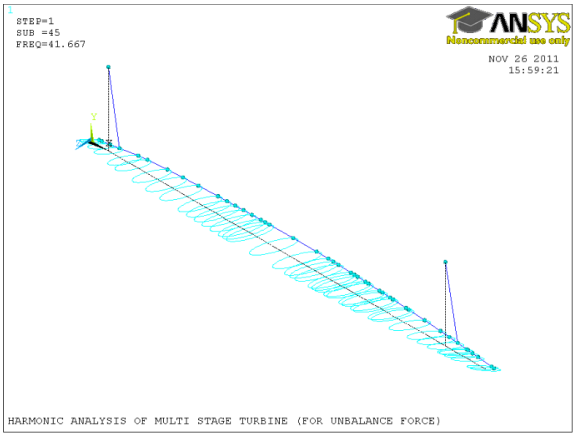

(B_1): Orbit plot for the excitation frequency (41.667 Hz) of unbalanced turbine

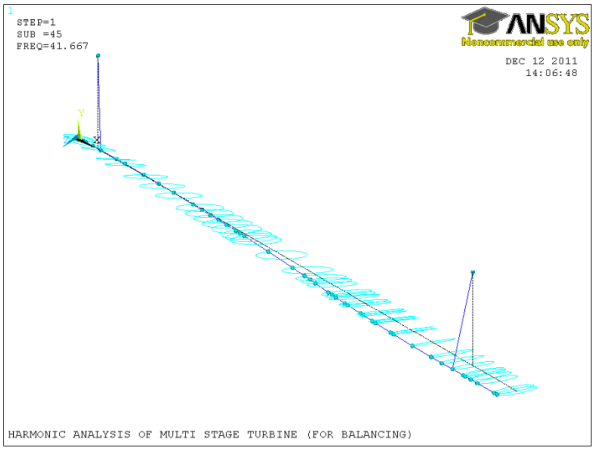

(C_1): Orbit plot for the excitation frequency (41.667 Hz) of balanced turbine

FIGURE 6.5.10 (A_1-C_1): Comparison between Orbit Plots from Normal, Unbalance and Balanced Turbine at First Critical Speed

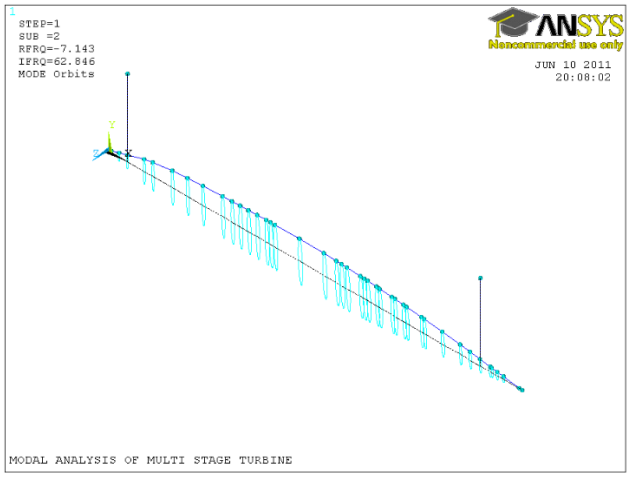

(A_2): Orbit plot for the second critical speed of normal turbine

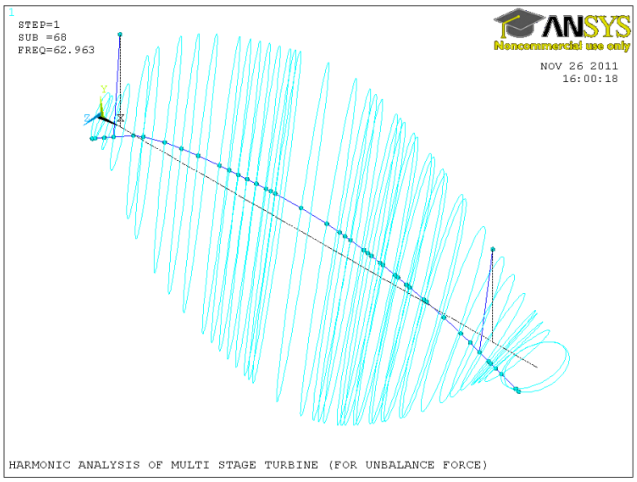

(B_2): Orbit plot for the excitation frequency (62.963 Hz) of unbalance turbine

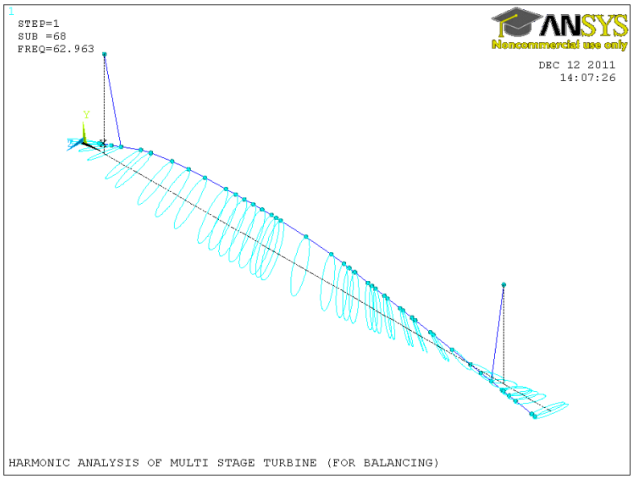

(C_2): Orbit plot for the excitation frequency (62.963 Hz) of balanced turbine

FIGURE 6.5.11 (A_2-C_2): Comparison between Orbit Plots from Normal, Unbalance and Balanced Turbine at Second Critical Speed

6.6 Performance of Balanced Rotor at High Speeds Analysis

In this section, rotor with rigid bearings (Figure 6.1.2) and multi-stage turbine with elastic bearings (Figure 6.5.2) discussed earlier were considered. The speed used for each of these systems was high speed above their operation speeds. The reasons for carrying out this analysis are as follows:

1. To observe how far the balanced systems will be able to maintain their balanced states.
2. To calculate the percentage reduction or increment in residual unbalance responses at high speed
3. As precautionary measure to check the likelihood that the rotor speed may drift above the operating speed.
4. Allow one to know the safe speed that needs to be considered during all modes of operation without compromising the balancing conditions.

6.6.1 Three-Disk Rotor with Rigid Bearings

The 1st correction parameters among the correction parameters obtained during the low-speed balancing shown in Table 6.2.3 was used here. The rotor operation speed is 13, 440 rpm and the speed considered for this analysis was 21,000 rpm. The response (amplitude) plots obtained are shown in the Figure 6.6.1.

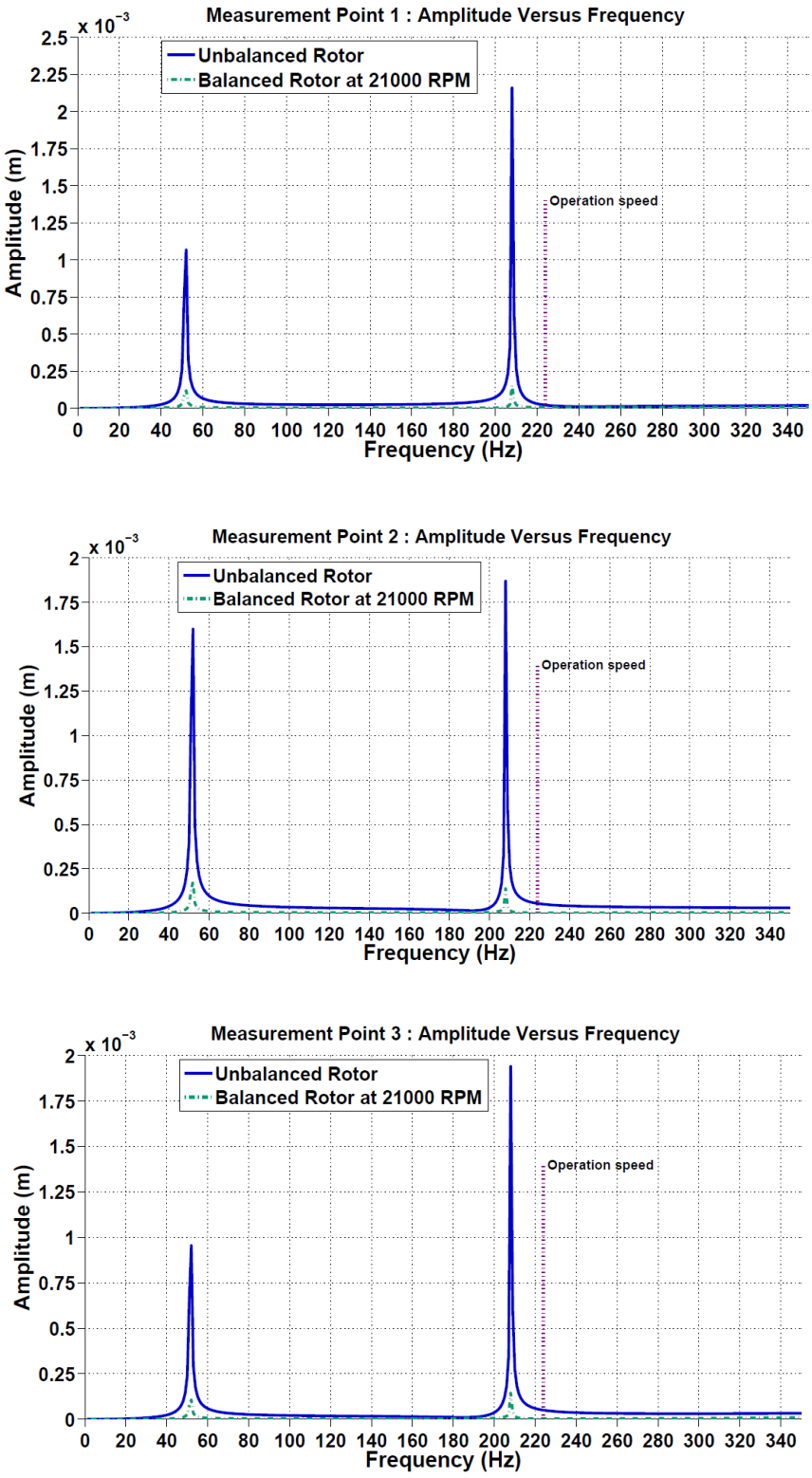

FIGURE 6.6.1: Amplitude Plots (Y- and Z-Directions) at a Speed of 21,000 rpm

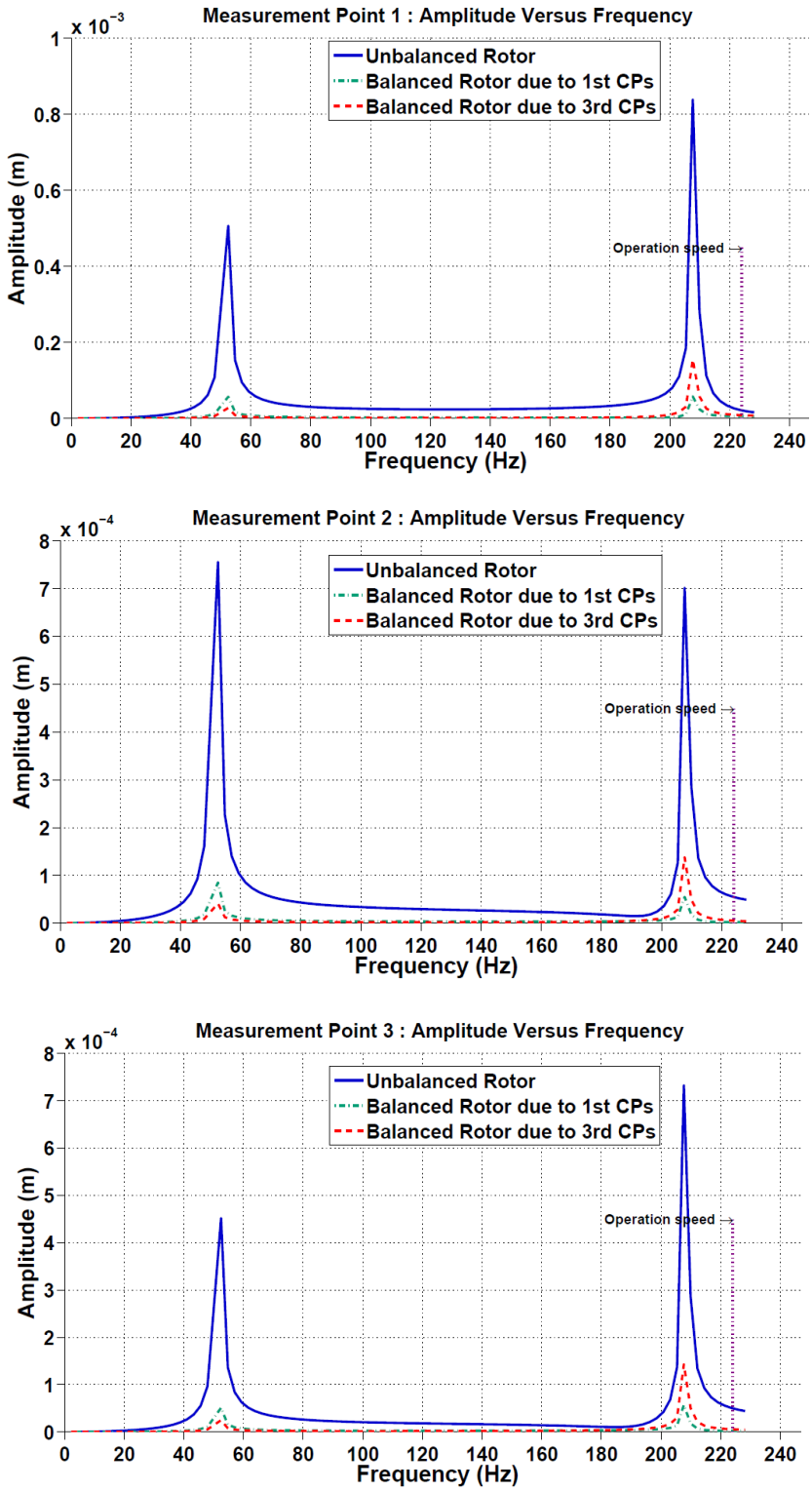

FIGURE 6.6.2: Amplitude Plots (Y- and Z-Directions) at a Speed of 13,690 rpm

The amplitude plots in Figure 6.6.2 are those plots obtained when rotor was balanced and tested at 13,690 rpm that was above the rotor operation speed (13,440 rpm). The following points can be observed when the amplitude plots in Figures 6.6.1 are look critically:

- The initial balanced state at operation speed is maintained for the entire speed.
- The entire responses for both balanced and unbalanced rotors changed at 21,000 rpm from those plots we have for a speed (13,690 rpm in Figures 6.6.1) that was also above the operation speed.
- Yet, the rotor still remained balanced at it is current state
- The percentage increments in residual unbalance at measurement points occurred. When the amplitudes at the two critical speeds in plots for 21,000 rpm compared to those plots for 13,690 rpm, the percentage increments results obtained are shown in Table 6.6.1 with average above 110%.

TABLE 6.6.1: Percentage Increment in Residual Unbalance of Rotor

	Percentage Increment at	
Measurement Point No	1st Critical Speed	2nd Critical Speed
	%	%
1	111	166
2	111	155
3	111	156
Average	111	159

6.6.2 Multi Stage Turbine with Elastic Bearings

The 3rd correction parameters among the correction parameters obtained during the low-speed balancing shown in Table 6.5.4 was used here. The turbine operation speed is 5,000 rpm and the speed considered for this analysis was 10, 020 rpm. The response (amplitude) plots obtained are shown in Figures 6.6.3 and 6.6.4. The following points can be observed when the amplitude plots in Figures 6.6.3 and 6.6.4 are look critically:

- The initial residual unbalance responses at operation speed are maintained or changed for some ranges of speeds or the entire speeds.
- After the ranges at which residual unbalance responses are maintained, the residual unbalance responses began to increase linearly but at very small percentage.
- At certain speed ranges, the already increased residual unbalance responses for range of speeds began to decrease again.
- In all plots, the turbine preserved its balanced state at high speed

However, we can compare the plots in Figure 6.6.3 to those in Figure 6.5.8 or compare the plots in Figure 6.6.4 to those in Figure 6.5.9. We observed that the responses at a speed up to 6,000 rpm in Figures 6.5.8 and 6.6.3 are alike and the responses in Figures 6.5.9 and 6.6.4 are also similar. It should be remembered that Figures 6.5.8 and 6.5.9 are obtained when balanced turbine that is operating at 5,000 rpm was tested at 6,000 rpm.

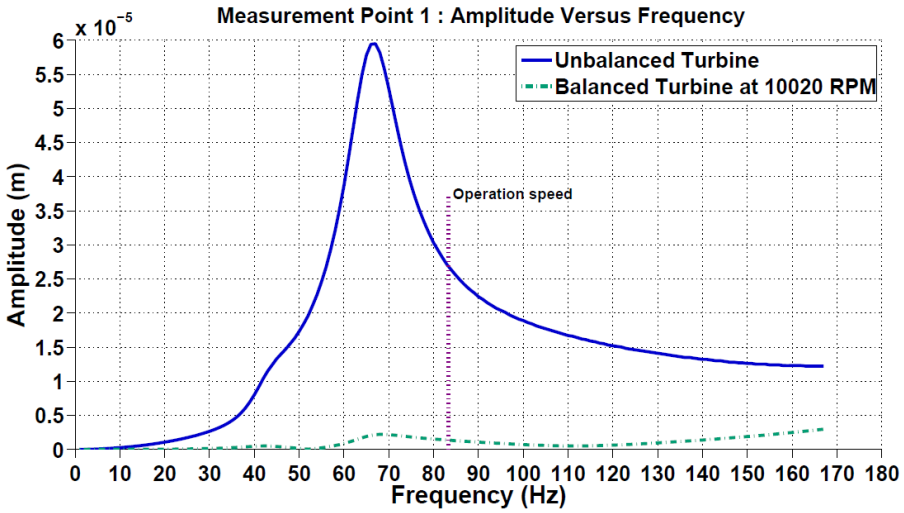

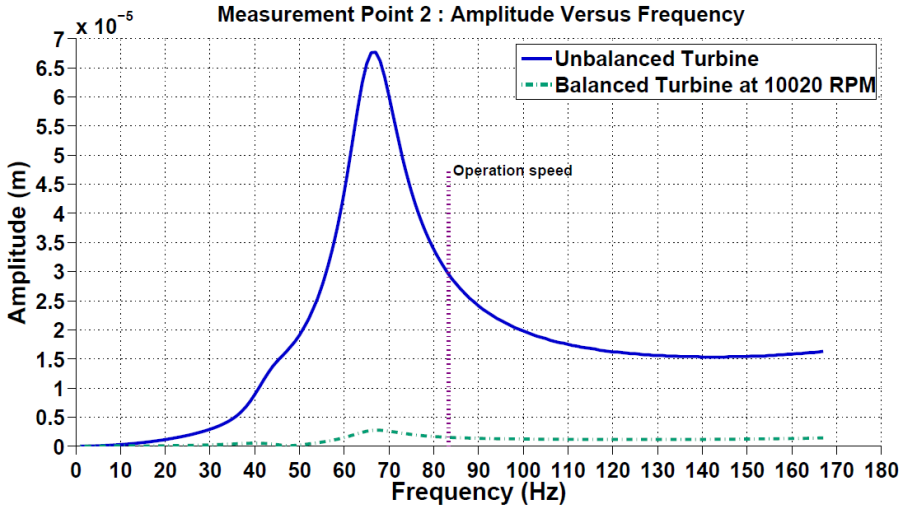

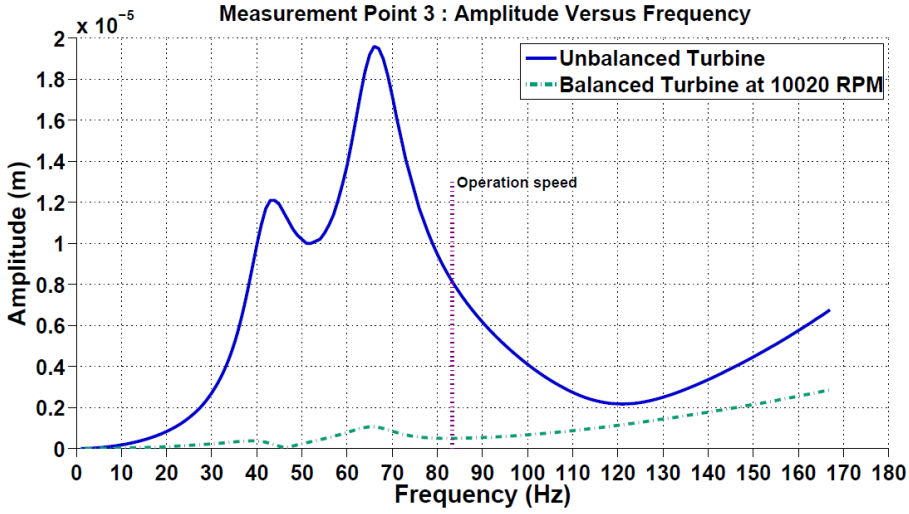

FIGURE 6.6.3: Amplitude Plots (Y-Direction) at a Speed of 10,020 rpm

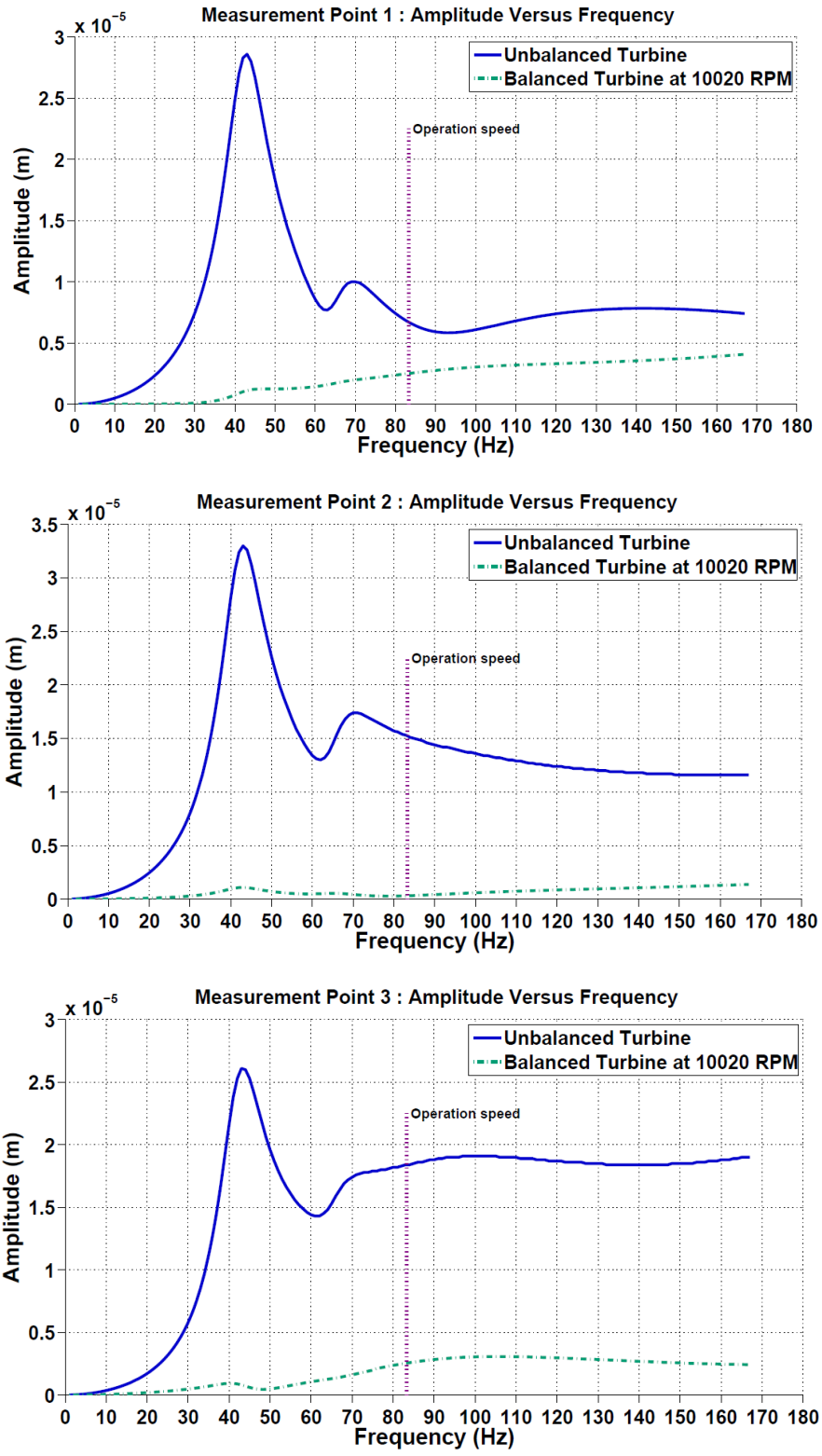

FIGURE 6.6.4: Amplitude Plots (Z-Direction) at a Speed of 10,020 rpm

CHAPTER 7

CONCLUSIONS AND RECOMMENDATIONS

The objectives of this research are to devise a method for balancing flexible rotor at low speed and to numerically investigate the developed technique in order to ascertain its applicability and efficiency. An elastodynamic rotor model based on the finite element method that accounts for rotary inertia, gyroscopic and shear effects is presented. The FEM rotor model was used to revise the theory postulated by Tan and Wang [28] for low speed balancing of flexible high-speed rotors, and to arrive at a feasible procedure of low-speed balancing.

The low-speed balancing method developed in this research study is primarily dependent on knowledge of modal characteristics of the rotor. In addition, measurements may only be taken in one direction only in all measurements planes, one run for each correction plane, the rotor is satisfactorily balanced at all directions, at both the balancing and operation speeds. The rotor sustained its state of balancing even at speeds above the operation speed. Hence, the simulation results showed that flexible rotor can be balanced successfully at low speeds using the modally-tuned influence coefficient method. It is noteworthy to mention that the application of this method to real-life rotors would require acquisition of modal characteristics by means of experiential and operational modal analysis.

Currently, high speed flexible rotors need to be balanced at a high-speed balancing facility, which requires the rotor to be shipped to such specialized facilities. It was also

noted that there is no high-speed balancing facility in the Kingdom, which stands in the forefront of turbomachinery users in the world. Accordingly, carrying the developed low-speed balancing scheme to the implementation stage would save the high cost of shipping such rotors abroad for balancing. The numerical testing results of the developed low-speed balancing scheme are encouraging. In order to investigate the applicability of the developed method to field applications, the method needs to be tested experimentally on an actual rotor. The experimental investigation of this low-speed balancing procedure is currently underway by Khulief and Mohiuddin [18].

APPENDIX

Bearing Element: COMBIN214

If COMBIN214 is element 1 and it is in YZ plane (let Y and Z implies 1 and 2) then, the characteristics can be defined as [23]

r,1, K_{11} K_{22}, K_{12},$K_{21,}$ C_{11}, C_{22}

rmore, $C_{12,}$ C_{21}

The third node is for orientation and applies to nonlinear analyses only. The element has the following KEYOPTs:

The KEYOPT(2) = 0 through 2 options define the element plane. The element operates in the nodal coordinate system.

The KEYOPT(3) = 0 and 1 options specify whether or not the element is symmetric. The cross-coupling terms in stiffness and damping coefficients will be equaled (K_{12} = K_{21} and C_{12}= C_{21}) when it is symmetric.

Similarly, COMBIN14 element is defined by two nodes and its properties include a spring constant (K), damping coefficients (C_v) ($C_v = C_{v1} + C_{v2}$ where C_{v1} and C_{v2} are damping and nonlinear damping coefficients), initial length and initial force

REFERENCES

[1] Al-Bahkali, E. and ElMadany, M.**,** **"**Dynamic Analysis of Rotating Machinery Using Computer Aided Design Approach", Department of Mechanical Engineering, King Saud University.

[2] ANSYS Mechanical Manual, Release 12.1.

[3] "ANSYS Structural Analysis Guide", ANSYS release 10.0, ANSYS, lnc. and ANSYS Europe Ltd., 00124 August 2005.

[4] Brüel & Kjær Vibro Seminar on Rotor Balancing, available at http://www.nvms.net/safety-condition-monitoring/pdf/series40/, accessed on 03/04/2011.

[5] Caughey, T.K. and O'Kelly, M.E., "Effect of Damping on the Natural Frequencies of Linear Dynamic Systems", Journal of the Acoustical Society of America Volume 33(11), 1458-1461, November, 1961.

[6] Darlow, M.S., "Balancing of High-speed Machinery: Theory, Methods and Experimental Results", Mechanical Systems and Signal Processing l(l), 105-134, 1987.

[7] Das, A.S., Nighil, M.C., Dutt, J.K. and Irretier, H., "Vibration Control and Stability Analysis of Rotor-shaft System with Electromagnetic Exciters", Mechanism and Machine Theory, 43, 1295–1316, 2008.

[8] Feese, T.D. and Grazier, P.E., "Balance This!: Case Histories From Difficult Balance Jobs", 33rd Turbomachinery Symposium, September 2004.

[9] Goodwin, M.J., "Dynamics of Rotor-Bearing Systems", Unwin hyman ltd, London, 1989.

[10] Harker, R.J., "Generalized Method of Vibration analysis", John Wiley & Sons, Inc., Canada, 1983.

[11] Herbert, R.G., "When to High-speed Balance Large Turbine Generator Rotors", National Power Plc, Swindow, UK (Seventh International Conference On Vibrations in Rotating Machinery, Professional Engineering Publishing, 2000).

[12] IRD Balancing Technical Paper 1, "Balance Quality Requirements of Rigid Rotors: The Practical Application of ISO 1940/1", IRD P/N E51267 Rev 2, March 2009.

[13] Kang, Y., Lin, T., Chang, Y.J., Chang, Y.P., and Wang, C., "Optimal balancing of flexible rotors by minimizing the condition number of influence coefficients", Mechanism and Machine Theory, 43, 891–908, 2008.

[14] Khulief, Y.A. and Mohiuddin, M.A., "Modal characteristics of Rotors using a conical shaft Finite Element", Comput. Methods Appl. Mech. Engrg., 115, 125-144, 1994.

[15] Khulief, Y.A. and Mohiuddin, M.A., "On the Dynamic Analysis of Rotors using Modal Reduction", Finite Elements in Analysis and Design, 26, 41-55, 1997.

[16] Khulief, Y.A. and Mohiuddin, M.A., "Modal Characteristics Of Cracked Rotors Using a Conical Shaft Finite Element", Comput. Methods Appl. Mech. Engrg., 162, 223-247, 1998.

[17] Khulief, Y.A. and Mohiuddin, M.A., "Coupled Bendin Torsional Vibration Of Rotors Using Finite Element", Journal of Sound and Vibration, 223(2), 297-316, 1999.

[18] Khulief, Y.A. and Mohiuddin, M.A., "Modally-Tuned Influence Coefficients For Low-Speed Balancing Of Flexible Rotors", Paper No. DETC2011- 47150, ASME Design Engineering Technical Conference, Washington DC, August 2011.

[19] Khulief, Y.A. Mohiuddin, M.A. and Bettayeb, M., "Dynamic Analysis and reduced order Modelling of Flexible Rotor-bearing Systems", Computers and Structures, 69, 349-359, 1998.

[20] Kikuchi, K., "Analysis of Unbalance Vibration of Rotating Shaft System with Many Bearings and Disks", The Japan Society of Mechanical Engineers, 13(61), 864-872, 1970.

[21] Kumar, M.S., "Rotor Dynamic Analysis Using ANSYS", K.G Gupta(ed.), IUTAM Symposium on Emerging Trends in Rotor Dynamics, IUTAM Bookseries 25, DOI 10.1007/978-94-007-0020-8_14, Spring Science+Busineness Media B.V.2011.

[22] Lalanne, M. and Ferraris, G., "Rotor Dynamics Prediction in Engineering", second edition, John Willy and Sons, New York, 1998.

[23] Lee, C., "Balancing of Rotors", Mechanical Engineering Department, KAIST, 2010.

[24] Lei, S. and Palazzolo, A., "Control of flexible rotor systems with active magnetic bearings", Journal of Sound and Vibration, 314, 19–38, 2008.

[25] Liu, S., “A modified low-speed balancing method for flexible rotors based on holospectrum”, Mechanical Systems and Signal Processing, 21, 348–364, 2007.

[26] Liu, S., and Qu, L., “A new field balancing method of rotor systems based on holospectrum and genetic algorithm”, Applied Soft Computing, 8, 446–455, 2008.

[27] Pettinato, J.D., “Development of Effective Balancing Procedure for CT Scanner”, MS Thesis Report, Cleveland State University, 2008.

[28] Pilkey, W.D., “Formulas for Stress, Strain, and Structural Matrices”, Second Edition, John Wiley & Sons, Inc., Hoboken, New Jersey, 2005.

[29] Regener, M. and Huebner, L., “Balancing Flexible Rotors of Large Electrical Machines”, Copyright Material IEEE, Paper No. PCIC-2010-10.

[30] Ruddy A. V., “Interactive Analysis of Bearing Influenced Rotor Dynamics”, Paper No.19, Symposium April 6th-9th, 1986.

[31] “Rotordynamic Analysis Guide”, Release 12.0, ANSYS, lnc., Southpointe, April 2009.

[32] Swanson, E., Powell, C.D. and Weissman, S., “A Practical Review of Rotating Machinery Critical Speeds and Modes”, Sound and Vibration, May 2005.

[33] Tan, S.G. and Wang, X.X., “A Theoretical Introduction to Low Speed Balancing of Flexible Rotors: Unification and Development of the Modal Balancing and Influence Coefficient Techniques”, Journal of sound and vibration, 168(3), 385-394, 1993.

[34] Thieffry, P., “Turning to Rotordynamics: Tools from ANSYS work together to optimize rotating parts”, ANSYS, Inc., 2010.

[35] Vance, J.M., Murphy, B.T. and Tripp, H.A., “Critical Speeds of Turbomachinery Computer Predictions vs. Experimental Measurements PART I: The Rotor Mass-Elastic Model”; Journal of Vibration, Acoustics, Stress, and Reliability in Design, 109(1), 1-7, January 1987.

[36] Wowk, V., “Machinery Vibration: Balancing”, McGraw-Hill, Inc, USA, 1995.

[37] Xu, B., Qu, L., and Sun, R., “The Optimization Technique-Based Balancing Of Flexible Rotors without Test Runs”, Journal of Sound and Vibration, 238(5), 877-892, 2000.

[38] Yamamoto, T. and Ishida, Y., “Linear and Nonlinear Rotordynamics: A modern Treatment with Applications”, John Wiley & Sons, inc., New York, 2001.

VITA

Name: Oke, Wasiu Adeyemi

Nationality: Nigerian

Date of Birth: March 23, 1976

Present Address: KFUPM, P. O. Box 8611, King Fahd University of Petroleum and Mineral, Dhahran-31261, Saudi Arabia

Permanent Address: Ikolaba Compound, Off Ado-Awaye Road, Malete, Iseyin, Oyo State, Nigeria

Email Address: wasiuad@kfupm.edu.sa, wasiuad@yahoo.com

Educational Qualification:

MS Mechanical Engineering (December, 2011)

King Fahd University of Petroleum & Minerals,

Dhahran, Saudi Arabia.

B.Sc. Mechanical Engineering (March, 2005)

University of Ibadan, Nigeria.

National Diploma Mechanical Engineering (May, 1998)

The Federal Polytechnic Bida, Nigeria.